Characterising the Higgs Boson

You, Tiann-Tevong

Awarding institution:
King's College London

Characterising the Higgs Boson

AUTHOR:
Tevong You

SUPERVISOR:
Prof. John Ellis CBE FRS

Theoretical Particle Physics and Cosmology Group, Physics Department,
King's College London, London WC2R 2LS, UK

A thesis submitted for the degree of
Doctor of Philosophy

September 2015

Abstract

On July 2012 the ATLAS and CMS collaborations announced the historic discovery of a Higgs boson at the CERN Large Hadron Collider. A remarkable century exploring Nature's sub-atomic constituents led to the Standard Model (SM) of particle physics with the Higgs as the last missing piece. In this thesis we review the construction of this theory and its experimental successes, focusing on the Higgs sector responsible for electroweak symmetry breaking and providing mass to matter and force particles. The defining signature of a Higgs particle is that of a scalar coupling proportionally to mass. We show how early data suggests indirectly that the observed particle has spin zero, and propose a method for directly measuring the spin using an invariant mass distribution of the Higgs produced in association with a vector boson. We also perform a global analysis of its couplings before and after the discovery, testing the expected mass-proportionality and constraining models in which the Higgs may be composite or even another scalar entirely, such as a pseudo-dilaton. In the absence of any significant deviations from the properties of the SM Higgs boson, the SM is then treated as an effective field theory (EFT) assuming new physics beyond the SM (BSM) is decoupled at higher energies. The leading lepton-number-conserving operators arise at the dimension-6 level, parametrised by their Wilson coefficients. These are constrained by their effects in Higgs physics, triple-gauge coupling measurements, and electroweak precision tests. The coefficients may also be calculated in a specific BSM theory by integrating out heavy particles. We illustrate this in the case of stops and sbottoms in the minimally supersymmetric SM, using the covariant derivative expansion method and generalising the universal one-loop effective Lagrangian in the process. Finally the potential for discovering BSM physics at future colliders is investigated. We conclude with a summary and outlook on prospects for the future.

Declaration of Authorship

I, Tevong You, declare that this thesis, titled "Characterising the Higgs Boson", is the result of work undertaken between October 2012 and September 2015 under the supervision of Prof. John Ellis. I confirm that:

- This work was done wholly while in candidature for a research degree at this university.
- Where any part of this thesis has previously been submitted for a degree or any other qualification at this university of any other institution, this has been clearly stated.
- Where I have consulted the published work of others, this is always clearly attributed.

King's College London — Tevong You
October 2015

Acknowledgements

I would like to thank John Ellis for his supervision and support throughout my doctoral studies. It has been an inspiration to witness the breadth and depth of his knowledge, his clear writing and thinking, together with his humour and generosity in physics research and outreach.

I am grateful to all my collaborators for many interesting projects and the opportunity to learn from our interactions, in particular to Verónica Sanz who has been like a second advisor during this period. I have also benefited greatly from the intellectual and social environment of the Theoretical Particle Physics and Cosmology group at King's College London where I have made many friends. Many thanks to the wonderful group of faculty, staff, postdocs and students here.

This thesis is dedicated to my mother and the memory of my father, both of whom always believed in the power of education and encouraged me to pursue my dreams. None of this would have been possible without their hard work and the sacrifices they have made to ensure my future.

Contents

1 Introduction

1.1 The Context of the Higgs Boson Discovery

The aim of theoretical particle physics is to build a quantitative description of Nature's fundamental building blocks, an endeavour which has led to the Standard Model (SM) of particle physics. This seminal theory traces its development back to Newton in the 17th century, who was the first to provide a mathematical framework for describing fundamental laws governing the motion of particles. It encompasses Maxwell's 19th century equations describing electromagnetism and light, as well as concepts discovered in the early 20th century that require these fundamental laws to obey the principles of relativity in a quantum framework. This is the quantum field theory (QFT) framework. The choice of symmetries and particle content of the QFT then determines the particular model, with numerous experiments from the last half of the 20th century confirming the gauge symmetries associated with the electroweak and strong force and the existence of all the degrees of freedom in the SM except that of the Higgs boson.

The Higgs boson, first postulated explicitly in 1964 [1], is of special importance in the SM. It is a consequence of the Brout-Englert-Higgs-Guralnik-Hagen-Kibble mechanism [1–4], often simply called the Higgs mechanism, that is necessary to give mass to the vector bosons that mediate the weak force. As such it is a direct probe of the electroweak symmetry breaking sector, in much the same way that the discovery of weak vector bosons directly confirms the non-abelian gauge symmetry realisation. Moreover it is the only fundamental scalar particle in the SM, which could make it uniquely sensitive to beyond the SM (BSM) physics. The Higgs boson discovery [5] in 2012 by the ATLAS and CMS collaborations at the CERN laboratory's Large Hadron Collider (LHC) is therefore more than merely completing a set of expected particles in the elementary spectrum - it represents our first direct look into how electroweak symmetry breaking is actually realised in Nature.

There are many ways of implementing the Higgs mechanism to break electroweak symmetry, of which the SM realisation is just one minimal possibility. In the SM a single fundamental scalar develops a non-vanishing vacuum expectation value that breaks the electroweak symmetry, but in other models the Higgs boson might be a composite scalar

that originates from a new strongly-coupled sector [6]. There could be more than a single scalar involved, or even no Higgs at all if the strongly-coupled sector is directly responsible for the electroweak symmetry-breaking dynamics [7]. Indeed QCD itself would have broken electroweak symmetry on its own when it condenses, albeit at a much lower scale than required to make the weak vector bosons massive enough. This goes to show that in principle Nature had many tricks up her sleeve to hide the electroweak symmetry at low energies.

The motivation behind these theories, and much model-building activity over the last few decades, is a serious problem associated with fundamental scalars when there is a large hierarchy of scales in the theory. Unlike fermions and bosons, quantum fluctuations drive the masses of these scalars up to the highest energy scale involved, a correction which has to be added to the bare mass parameter. Thus a relatively light scalar can only be obtained by putting in the value of the bare parameter by hand in such a way that it just happens to cancel most of the quantum correction with the overall light mass left over. The larger the hierarchy between the light and heavy scales the more arbitrary and un-natural this fine-tuning appears. Since the heaviest scale we expect is 17 orders of magnitude above the weak scale, known as the Planck mass associated to quantum gravity, this is severely fine-tuned indeed.

While the naturalness problem is not an inconsistency of the theory in itself (unlike say infinite divergences when calculating physical quantities), nevertheless such a coincidence of two unrelated contributions accidentally cancelling each other so finely strongly suggests that there must be an underlying structure to avoid this unpalatable situation. Some new mechanism surely exists to protect the Higgs mass so that it can be naturally light without having to fix such large numbers by hand. It just so happens that the only non-trivial way to extend the internal and Poincare symmetries of a four-dimensional QFT [9] also controls quantum corrections to light scalar masses. This generalisation of the Lie algebra to include a new kind of symmetry adds spin-1/2 generators relating bosons and fermions and goes under the name of "supersymmetry" [10]. In supersymmetric theories there must be at least two Higgs doublets and a heavier superpartner for each SM particle, some of which cannot lie too far above the weak scale to avoid fine-tuning. The Higgs boson is then expected to be accompanied by other BSM particles,

in particular the scalar partner of the top quark that contributes the largest quantum correction to the Higgs mass [11].

Composite models are an alternative way of avoiding fine-tuning, with the motivation that it doesn't require one to postulate any new principles beyond what we already know is realised in Nature. The original suggestion was to scale up what happens in QCD by adding a new strong sector that condenses at higher energies, breaking electroweak symmetry and giving mass to gauge bosons without a Higgs. Such "techni-color" models [7] were disfavoured early on from indirect constraints by electroweak precision measurements, though various incarnations could still be built to avoid these [8]. If the techni-color sector breaks an approximate scale invariance it may also yield a scalar pseudo-dilaton particle [12] that acts as a Higgs impostor if its couplings are arranged to be sufficiently similar to the Higgs boson. Alternatively a more popular scenario is to have the Higgs doublet emerge as a pseudo-Goldstone boson from the strong dynamics which are now decoupled from the electroweak symmetry breaking that happens in the usual way when the Higgs obtains a vacuum expectation value [13]. A pseudo-Goldstone boson is protected by a shift symmetry that makes it naturally light, and in this case one also expects the Higgs to be accompanied by BSM resonances from the composite sector.

Given that these theories could well have been discovered early on in experiments, either directly or indirectly, it is remarkable that all measurements are so far compatible with SM predictions. In Section 1.2 we will briefly go through the developments that led to the Standard Model whose mathematical structure is described in Section 1.3, where we focus on how the Higgs mechanism is implemented in this special case. Then in Section 1.5 we take a step back from the SM Higgs mechanism to describe a non-linear effective Lagrangian that characterises a general Higgs sector. Finally Section 1.6 presents the SM as a (linearly-realised) effective field theory for capturing the effects of decoupled new physics in a consistent framework. The publications for this thesis are summarised in Section 1.7.

1.2 Historical Overview of the Standard Model

Quantum field theory (QFT) emerged in the 1930s as a continuation of the development of quantum mechanics in an attempt to reconcile it with the principles of relativity

and to quantise the classical field theory of electromagnetism. The result was quantum electrodynamics (QED). After issues involving infinite divergences in calculating physical quantities were resolved in the 1940s, the success of QED as a QFT with local $U(1)$ gauge invariance naturally led Yang and Mills [14], and independently Shaw [15], in the 1950s to consider generalising the gauge principle from abelian symmetry groups to non-abelian ones. This describes forces with several mediating vector bosons but non-abelian gauge theories were unpopular at the time as gauge invariance seemingly forbid adding mass terms for the gauge bosons. It apparently contradicted observations since a massless gauge boson would mediate a long-range force just like electromagnetism[1]. Non-abelian gauge theories thus seemed to be missing a crucial ingredient for generating gauge boson masses without violating the gauge symmetry.

Around the same time condensed matter theorists were investigating the phenomena of spontaneously broken symmetries in superconductivity [16, 17] which Nambu realised could also be of importance in particle physics [18]. Symmetries of the Lagrangian do not have to be respected by states in the theory. The ground state in particular could minimise the potential energy at a non-vanishing field value which appears to break the symmetry so that it is hidden from an observer at that point. Nambu suggested that a spontaneous breaking of the chiral symmetry was responsible for the pion that would be massless in the exact chiral symmetry limit of equal up and down quark masses [18]. A theorem by Goldstone, Salam and Weinberg [19] showed that a spontaneously broken symmetry necessarily comes with such a massless scalar particle, a Goldstone boson [20].

In the 1960s came the discovery that the problem of massless bosons in non-abelian gauge theories could be solved by the massless Goldstone bosons [21]. This was known to happen in condensed matter systems where Anderson demonstrated mathematically how the photon acquires an effective mass inside a superconductor [17]. Anderson, as well as Klein and Lee [22], argued that it would be possible to implement this relativistically, but Gilbert argued it would be impossible to do this in a fully relativistic theory [23]. A fully relativistic theory of massive gauge bosons from spontaneous symmetry breaking was finally formulated in 1964 by Brout and Englert [2], independently followed by Higgs [1, 3, 24] then Guralnik, Hagen and Kibble [4, 25], and soon after Migdal and Polyakov [26].

[1]We now know that massless gauge bosons in non-abelian gauge theories don't always give rise to long-range forces, but the possibility of confinement had not yet been discovered back then.

The paper by Higgs specifically pointed out the signature of a massive scalar in the physical spectrum [1].

Everything was then in place to describe the weak force as a non-abelian gauge theory, which contained a neutral boson that was tempting to unify with the photon of electromagnetism, as Glashow had done earlier using the $SU(2) \times U(1)$ symmetry group [27]. In 1967 Weinberg [28] and Salam [29] put this together with the spontaneous symmetry breaking mechanism to describe the weak and electromagnetic interactions in a unified theory. Weinberg furthermore realised that the Higgs boson could provide mass to fermions through Yukawa couplings [28]. The Glashow-Weinberg-Salam model now forms the entire leptonic sector of the SM.

The full triumph of non-abelian gauge theories came about in the 1970s when the description of the strong force as an $SU(3)$ gauge symmetry and phenomena such as confinement and asymptotic freedom [30] were established. This period also saw the proof of renormalisability for spontaneously broken non-abelian gauge theories by 't Hooft and Veltman [31] which led to theoretical acceptance of the SM, followed soon after by indirect experimental validation in the discovery of neutral currents [32] and the charm quark [33] predicted by the GIM mechanism [34]. Even before the discovery of charm the phenomenological properties of the Higgs boson had been studied in anticipation of its eventual importance for completing the SM [35]. The $W^{\pm}$ and Z bosons were directly discovered in 1983 [36]. With the tau lepton appearing from 1974 [37] and the bottom quark produced in 1977 [38] the top quark was expected to complete the three-generations structure of the SM and it was indeed found in 1995 [39]. Mixing between the three flavours in the SM is encoded in the KM matrix that predicts a CP-violating phase [40]. Only the Higgs boson remained, the last missing piece of the SM, which was finally announced announced in 2012 [5].

	$SU(3)_c$	$SU(2)_L$	$U(1)_Y$
Q_L	**3**	**2**	$\frac{1}{6}$
q_R^u	**3**	**1**	$\frac{2}{3}$
q_R^d	**3**	**1**	$-\frac{1}{3}$
L_L	**1**	**2**	$-\frac{1}{2}$
l_R	**1**	**1**	-1
ϕ	**1**	**2**	$\frac{1}{2}$

Table 1: *Table of scalar (last row) and fermions (all other rows) that make up the SM listed with their charges under $SU(3)_c \times SU(2)_L \times U(1)_Y$. The electromagnetic charge is given by $Q \equiv T^3 + Y$.*

1.3 The Standard Model Higgs Mechanism

The SM is defined by the field content listed in Table 1 and their charges under the $SU(3)_c \times SU(2)_L \times U(1)_Y$ gauge symmetries. Each field comes in three generations,

$$\begin{aligned} Q_L &\equiv \begin{pmatrix} u_L \\ d_L \end{pmatrix}, \begin{pmatrix} c_L \\ s_L \end{pmatrix}, \begin{pmatrix} t_L \\ b_L \end{pmatrix} \quad , \quad q_R^u \equiv u_R, c_R, t_R \quad , \quad q_R^d \equiv d_R, s_R, b_R \quad , \\ L_L &\equiv \begin{pmatrix} \nu_L^e \\ e_L \end{pmatrix}, \begin{pmatrix} \nu_L^\mu \\ \mu_L \end{pmatrix}, \begin{pmatrix} \nu_L^\tau \\ \tau_L \end{pmatrix} \quad , \quad l_R \equiv e_R, \mu_R, \tau_R \qquad . \end{aligned}$$

All terms in the SM Lagrangian are then fixed by the possible renormalizable and Lorentz-invariant combinations of fields. We will focus on the electroweak sector given by

$$\mathcal{L}_{SM} = \mathcal{L}_m + \mathcal{L}_g + \mathcal{L}_h + \mathcal{L}_y \qquad , \tag{1.1}$$

$$\begin{aligned} \mathcal{L}_m &= \bar{Q}_L i\gamma^\mu D_\mu^L Q_L + \bar{q}_R i\gamma^\mu D_\mu^R q_R + \bar{L}_L i\gamma^\mu D_\mu^L L_L + \bar{l}_R i\gamma^\mu D_\mu^R l_R \\ \mathcal{L}_g &= -\frac{1}{4} B_{\mu\nu} B^{\mu\nu} - \frac{1}{4} W_{\mu\nu}^a W^{a\mu\nu} \\ \mathcal{L}_h &= (D_\mu^L \phi)^\dagger (D^{L\mu} \phi) - V(\phi) \\ \mathcal{L}_y &= y_d \bar{Q}_L \phi q_R^d + y_u \bar{Q}_L \phi^c q_R^u + y_L \bar{L}_L \phi l_R + \text{h.c.} \qquad . \end{aligned}$$

The Dirac, flavour and gauge indices are kept implicit for clarity. We defined $\phi^c \equiv \epsilon \phi^*$ where $\epsilon_{2,1} = -1$ is the 2×2 antisymmetric matrix in $SU(2)_L$ space. The subscripts L and R on the Dirac fermions denote the left and right-handed fields projected out by the $P_{R,L} \equiv \frac{1}{2}(1 \pm \gamma_5)$ operators. The covariant derivatives and Higgs potential are normalised

as

$$D_\mu^L = \partial_\mu - igW_\mu^a T^a - iYg'B_\mu \quad , \quad D_\mu^R = \partial_\mu - iYg'B_\mu \quad ,$$
$$V(\phi) = -\mu^2\phi^2 + \lambda\phi^4 \qquad ,$$

and the field strength tensors are given by

$$W_{\mu\nu}^a = \partial_\mu W_\nu^a - \partial_\nu W_\mu^a - g\epsilon^{abc}W_\mu^b W_\nu^c$$
$$B_{\mu\nu} = \partial_\mu B_\nu - \partial_\nu B_\mu \quad .$$

g and g' denote the $SU(2)_L$ and $U(1)_Y$ couplings respectively and Y is the $U(1)_Y$ weak hypercharge. The matrices $T^a \equiv \sigma^a/2$ are the $SU(2)_L$ generators of the weak isospin algebra, with σ^a the usual Pauli matrices. They may be used to raise and lower eigenstates of weak isospin T^3 by defining the ladder operators

$$T^\pm \equiv T^1 \pm iT^2 \quad ,$$

such that they obey the following commutation relations,

$$[T^3, T^\pm] = \pm T^\pm$$
$$[T^+, T^-] = 2T^3 \quad .$$

We can write the weak gauge bosons as the isospin triplet

$$W_\mu^a T^a = \frac{1}{\sqrt{2}}W_\mu^+ T^+ + \frac{1}{\sqrt{2}}W_\mu^- T^- + W_\mu^3 T^3 \quad , \tag{1.2}$$
$$W_\mu^\pm = \frac{1}{\sqrt{2}}(W_\mu^1 \mp iW_\mu^2) \quad . \tag{1.3}$$

These must acquire mass as the weak interactions are short-ranged, which happens via the Higgs mechanism. Writing out explicitly the relevant part of the Higgs Lagrangian we obtain

$$\mathcal{L}_{\text{Higgs}} = (\partial_\mu\phi^\dagger + igW^\mu\cdot T\phi^\dagger + \frac{1}{2}ig'B^\mu\phi^\dagger)(\partial_\mu\phi - igW_\mu\cdot T\phi - \frac{1}{2}ig'B_\mu\phi) + \lambda(\phi^\dagger\phi)^2 - \mu^2\phi^\dagger\phi \quad , \tag{1.4}$$

For $\lambda, \mu^2 > 0$ the form of the potential is the famous "Mexican hat", shown in Fig. 1, where the ground state energy is minimised along a degenerate circle where the Higgs field takes a non-vanishing vacuum expectation value

$$|\phi| = \frac{v}{\sqrt{2}} \quad , \quad v \equiv \sqrt{\frac{\mu^2}{\lambda}} \quad .$$

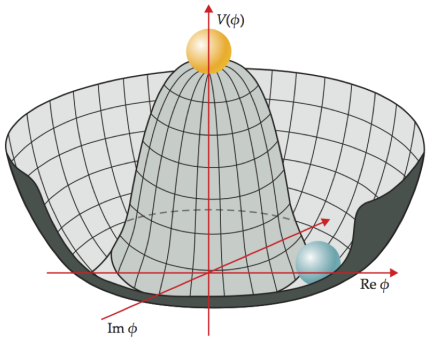

Figure 1: *The "Mexican hat" potential of a Higgs field, with the non-zero minimum at the location of the blue ball lying along a degenerate circle.*

Without loss of generality we may choose the minimum to lie along the direction,

$$\langle\phi\rangle = \frac{1}{\sqrt{2}}\begin{pmatrix} 0 \\ v \end{pmatrix} \quad .$$

We see that $\langle\phi\rangle$ remains invariant under the $U(1)_{\rm EM}$ generator $Q \equiv T^3 + Y$ associated with electric charge. We may better appreciate the physical content of the theory by a field redefinition with h parametrising the radial direction of the mexican hat and the three remaining degrees of freedom parametrised as ϵ in a local transformation U,

$$\phi = U^{-1}(\varepsilon)\begin{pmatrix} 0 \\ \frac{1}{\sqrt{2}}(h+v) \end{pmatrix} \quad , \quad U(\varepsilon) = e^{-\frac{iT\cdot\varepsilon}{v}} \quad .$$

We may then perform a gauge transformation to work in the so-called unitary gauge,

$$\begin{aligned} \phi &\longrightarrow U(\varepsilon)\phi \\ W^\mu \cdot T &\longrightarrow UW^\mu \cdot TU^{-1} + \frac{i}{g}U^{-1}\partial^\mu U \quad . \end{aligned}$$

The ϵ degrees of freedom form the longitudinal components of the gauge bosons, as required of massive vector bosons. Writing out the Higgs Lagrangian in the unitary gauge, defining the unit vector $\chi^\dagger \equiv (0,1)$ as the direction along the minimum, we may see explicitly how the gauge bosons acquire mass,

$$\begin{aligned} \mathcal{L}_{\rm Higgs} &= \left(\frac{1}{\sqrt{2}}\partial_\mu h\chi^\dagger + igW^\mu\cdot T\chi^\dagger\frac{1}{\sqrt{2}}(h+v) + \frac{1}{2}ig'B^\mu\chi^\dagger\frac{1}{\sqrt{2}}(h+v)\right)\times \\ &\left(\frac{1}{\sqrt{2}}\partial_\mu h\chi - igW_\mu\cdot T\chi\frac{1}{\sqrt{2}}(h+v) - \frac{1}{2}ig'B^\mu\chi\frac{1}{\sqrt{2}}(H+v)\right) - V\left(\frac{1}{2}(h+v)^2\right) \\ &= \frac{1}{2}\partial_\mu h\partial^\mu h - V\left(\frac{1}{2}(h+v)^2\right) + \frac{(h+v)^2}{8}\chi^\dagger\left(2gW^\mu\cdot T + g'B^\mu\right)\left(2gW_\mu\cdot T + g'B_\mu\right)\chi \quad . \end{aligned}$$

Writing the gauge bosons in the form (1.3) and substituting in the Pauli matrices

$$T^3 = \begin{pmatrix} \frac{1}{2} & 0 \\ 0 & -\frac{1}{2} \end{pmatrix} \quad T^+ = \begin{pmatrix} 0 & 1 \\ 0 & 0 \end{pmatrix} \quad T^- = \begin{pmatrix} 0 & 0 \\ 1 & 0 \end{pmatrix}$$

we obtain

$$\mathcal{L}_{\rm M} = \frac{v^2}{8}\chi^\dagger(2gW_\mu \cdot T + g'B_\mu)(2gW^\mu \cdot T + g'B^\mu)\chi \tag{1.5}$$

$$= \frac{v^2}{8}\left[(gW^3_\mu - g'B_\mu)(gW^{3\mu} - g'B^\mu) + 2g^2 W^-_\mu W^{+\mu}\right] \quad . \tag{1.6}$$

We see that the $W^\pm$ bosons now have a mass $M_W = \frac{1}{2}gv$. Diagonalising the electrically neutral gauge bosons into physical mass eigenstates gives

$$\frac{v^2}{8}(W^3_\mu, B_\mu)\begin{pmatrix} g^2 & -gg' \\ -gg' & g'^2 \end{pmatrix}\begin{pmatrix} W^3_\mu \\ B_\mu \end{pmatrix} = \frac{1}{2}(Z_\mu, A_\mu)\begin{pmatrix} M_Z^2 & 0 \\ 0 & 0 \end{pmatrix}\begin{pmatrix} Z_\mu \\ A_\mu \end{pmatrix}$$

where we may define the Glashow-Weinberg angle θ_W,

$$\begin{pmatrix} W^3_\mu \\ B_\mu \end{pmatrix} = \begin{pmatrix} \cos\theta_W & \sin\theta_W \\ -\sin\theta_W & \cos\theta_W \end{pmatrix}\begin{pmatrix} Z_\mu \\ A_\mu \end{pmatrix} \quad , \quad \tan\theta_W = \frac{g'}{g} \quad ,$$

and we see explicitly that the photon A_μ is massless and the Z boson acquires a mass

$$M_Z^2 = \frac{v^2}{4}(g^2 + g'^2) \quad ,$$

so that the ratio of the $W^\pm$ and Z gauge boson masses obeys at tree-level the relation

$$\frac{M_W^2}{M_Z^2} = \cos^2\theta_W \, .$$

The Feynman diagrams for the couplings of the Higgs to the $W^\pm, Z$ gauge bosons and fermions is shown in Fig. 2 together with their corresponding Feynman rules. The Yukawa couplings of the Higgs to the SM fermions also gives them mass,

$$M_f = \frac{1}{\sqrt{2}}y_f v \quad .$$

The defining characteristic of the Higgs is therefore that of a scalar whose coupling strength is proportional to the mass of the SM fermions and gauge bosons.

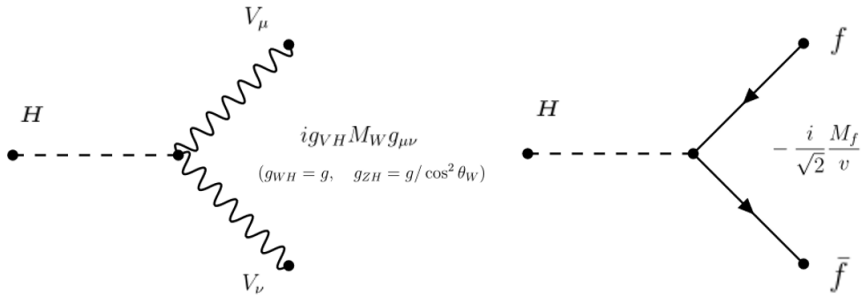

Figure 2: *Feynman diagrams and associated Feynman rules for the Higgs couplings to the $V = W^\pm, Z$ gauge bosons and fermions f.*

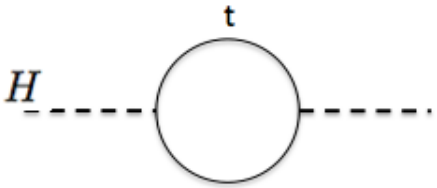

Figure 3: *Feynman diagram of a one-loop quantum correction to the Higgs mass from a top quark.*

1.4 The Hierarchy Problem

A major aesthetic problem of the SM Higgs is the unnatural cancellation between the bare value of its mass and large quantum corrections. The mass squared of the Higgs at tree-level in the SM is given by

$$M_h^2 = 2\lambda v^2 \,.$$

Feynman diagrams involving loops of SM fermions, gauge bosons, or Higgs self-interactions, are responsible for the quadratic sensitivity to the cut-off $\Lambda_{\rm UV}$ of the theory. For example the top quark loop depicted in Fig. 3 gives a contribution of the form

$$\delta M_h^2 = -\frac{y_t^2}{8\pi^2}\Lambda_{\rm UV}^2 \,,$$

where $\Lambda_{\rm UV}$ could be many orders of magnitude above the weak scale, if not at the Planck scale $M_{\rm pl} \sim 10^{19}$ GeV.

One might argue that this is an artefact of choosing a momentum cut-off to regularise the infinite divergence when evaluating the momentum loop integral. After all had we chosen to use dimensional regularisation and renormalised by absorbing infinities into

counterterms the usual way then there appears to be no problem. This would indeed be true if there exists nothing else other than the SM, which would then be a complete renormalisable theory of everything. However this cannot be the case as we know at the very least that gravity and its associated degrees of freedom at the Planck scale must be incorporated into the picture. The UV cut-off is then physical and the conclusion holds.

A simple example makes this clear. Consider a toy model of a single light fundamental scalar ϕ with a Yukawa coupling to a heavy fermion ψ,

$$\mathcal{L} = i\bar{\psi}\gamma^\mu\partial_\mu\psi - M\bar{\psi}\psi + \frac{1}{2}(\partial_\mu\phi)^2 - \frac{1}{2}m^2\phi^2 - y\bar{\psi}\psi\phi\,.$$

Integrating out the heavy fermion at one-loop using dimensional regularisation with the $\bar{\text{MS}}$ renormalisation scheme gives the following mass term in the low-energy effective theory,

$$\mathcal{L}_{\text{EFT}} \supset -\frac{1}{2}\left[m^2 + \frac{y^2}{4\pi^2}\left(1 - 3\log\frac{M^2}{\mu^2}\right)M^2\right]\phi^2\,.$$

Therefore even if we start out with $m^2 \ll M^2$ we see that quantum corrections proportional to M^2 will make the scalar as heavy as the heaviest particle in the theory. This is not the case for fermions or gauge bosons which are protected by a chiral and gauge symmetry respectively, in the sense that if the mass parameter vanishes the theory gains this additional symmetry. This means that any quantum corrections that violates the symmetry must be proportional to this mass parameter, since the theory regains the symmetry as the parameter goes to zero, so a light fermion or gauge boson mass will remain light and receive at most a logarithmic dependence on the heavy cut-off. This is the criteria for "technical naturalness" where relatively small numbers for parameters are protected and can be put in by hand without fine-tuning [41]. The definition of naturalness can be used in many other senses, for example having to set a parameter to be extremely tiny can seem un-natural even if it is protected, or excessive model-building may be natural in a technical sense but appear contrived in a harder to quantify way.

1.5 A Non-Linear Effective Lagrangian for Electroweak Symmetry Breaking

The SM Higgs sector has an accidental $SO(4)$ global symmetry, spontaneously broken to $O(3)$, which is responsible for the observed ratio between the W and Z boson mass

parametrised by

$$\rho \equiv \frac{M_W^2}{M_Z^2 \cos^2 \theta_W} \,.$$

Experimentally the prediction that $\rho \sim 1$ has been verified beyond percent level accuracy when radiative corrections are included [42].

In the SM this accidental symmetry is a consequence of the fact that gauge and Lorentz invariance enforces the form of the Higgs potential to be a function of

$$H^\dagger H = h_1^2 + h_2^2 + h_3^2 + h_4^2 \,,$$

where h_i are the components of the complex Higgs doublet. This is manifestly symmetric under $SO(4)$, and when the Higgs gets a vacuum expectation value the residual $O(3)$ symmetry in the limit $g' \to 0$ is responsible for the relation

$$W_\mu^1 W^{\mu 1} + W_\mu^2 W^{\mu 2} + W_\mu^3 W^{\mu 3} = 2 W_\mu^+ W^{\mu -} + W_\mu^3 W^{\mu 3}$$

between the gauge boson masses. This "custodial" symmetry is broken explicitly at tree-level by g' which introduces the Glashow-Weinberg angle dependence in the ρ parameter, as well as radiative corrections from the fermion sector.

In the SM the custodial symmetry is an accidental consequence of other more fundamental symmetries, but in other theories it could be a deeper sign of the underlying structure of the Higgs sector. For example in composite Higgs models the Higgs arises as a pseudo-Goldstone boson from a new strong sector [6, 13]. The strong dynamics spontaneously break a global symmetry to an unbroken one, and this unbroken group then acts as the custodial symmetry. In models with two Higgs doublets or additional resonances one needs to ensure that custodial-violating effects are within experimental bounds on the ρ parameter.

Given the wide variety of ways of breaking electroweak symmetry discussed in Section 1.1, including the possibility of scalars that are not necessarily responsible for electroweak symmetry breaking, we can use the global symmetry breaking pattern to write down a low energy effective theory containing only the Goldstone degrees of freedom that form the longitudinal components of the massive gauge bosons [43]. Assuming a global symmetry breaking pattern of $SO(4) \cong SU(2)_L \times SU(2)_R$ spontaneously broken to its $SU(2)_V$ vectorial subgroup we may write the non-linear effective Lagrangian as

$$\mathcal{L}_{\rm NL} = \frac{v^2}{4} Tr D_\mu \Sigma^\dagger D^\mu \Sigma - M_{f_i} \bar{\psi}_L^i \Sigma \psi_R^i + \text{h.c.} \,, \tag{1.7}$$

where Σ is a unitary 2×2 matrix containing the Goldstones π^a that can be parametrised as

$$\Sigma \equiv \exp\left(\frac{i\sigma^a\pi^a}{v}\right) .$$

It is well known that scattering amplitudes diverge at higher energies in such a theory and violates unitarity around the TeV scale [44]. In the SM the Higgs restores unitarity in the scattering amplitudes[2], while in Higgsless models a tower of resonances does the job. A composite Higgs can partially restore unitarity before resonances enter at higher energies. Either way something physically must happen when particles collide at such energies, which guaranteed the observation of some new phenomena at the LHC and strongly motivated its construction.

The low-energy effective theory can capture this partial or complete restoration of unitarity at higher energies by adding to Eq. 1.7 a singlet scalar h with general couplings to the SM gauge bosons and fermions,

$$\begin{aligned}\mathcal{L}_{\rm NL} = &\frac{v^2}{4} Tr D_\mu \Sigma^\dagger D^\mu \Sigma \left(1 + 2a\frac{h}{v} + b\frac{h^2}{v^2} + ...\right) - M_{f_i}\bar{\psi}^i_L \Sigma \left(1 + c_{f_i}\frac{h}{v} + ...\right)\psi^i_R + \text{h.c.} \\ &+ \frac{1}{2}(\partial_\mu h)^2 + \frac{1}{2}M_h^2 h^2 + d_3\frac{1}{6}\left(\frac{3M_h^2}{v}\right)h^3 + d_4\frac{1}{24}\left(\frac{3M_h^2}{v^2}\right)h^4 + \dots . \end{aligned} \tag{1.8}$$

The coefficients are normalised in such a way that when the coupling rescaling factors $a, b, c_{f_i}, d_i = 1$ the SM is recovered. We will usually assume that the rescaling of the coupling to the gauge bosons, a, is the same for W and Z except in cases where it is motivated to consider models that violate this. As a simplification we will also often take $c_{f_i} = c$ as a universal rescaling for all fermions before allowing more freedom in the fit for specific scenarios. In this framework particular values of the coupling rescaling factors would then correspond to different variations of the Higgs boson, and in Higgsless models the scalar could even be the pseudo-dilaton. This forms a motivated approach for probing the electroweak symmetry breaking sector and characterising a new scalar resonance from a phenomenological perspective. Following the Higgs boson discovery the ATLAS and CMS experimental collaborations adopted such a formalism using κ_V, κ_f as rescaling factors for the Higgs couplings to gauge bosons and fermions respectively, and their Higgs couplings results have recently been combined in Ref. [46].

[2]In fact starting from the Fermi theory one can recover the SM Lagrangian just by requiring couplings to be fixed in such a way that amplitudes remain finite [45].

1.6 The Standard Model as an Effective Field Theory

In this Section we outline the motivation for an alternative framework for characterising BSM physics. The non-linear effective theory presented in Section 1.5 is appropriate for a general approach to electroweak symmetry breaking and characterising the properties of the newly-discovered resonance. Here we simply assume that it is a SM Higgs and interpret any possible deviations of the measured couplings as due to the indirect effects of BSM resonances at higher energies.

The effects of decoupled new physics are captured by higher-dimensional operators in the effective field theory of the Standard Model [47]. The most general Lagrangian consistent with the symmetries of the Standard Model has the form

$$\mathcal{L}_{\text{SMEFT}} = \sum_{d=0}^{\infty} \sum_{i=1}^{\infty} \frac{(c_d)_i}{\Lambda^{d-4}} (\mathcal{O}_d)_i \,,$$

where d is the operator mass dimension, Λ is the UV cut-off scale and $(c_d)_i$ is a dimensionless Wilson coefficient. When referring to the Standard Model we usually mean implicitly the theory as defined by the renormalisable Lagrangian up to $d \leq 4$ in operator mass dimension d, but the effective field theory viewpoint requires the $d > 4$ operators to also be present. Since the coefficients of these higher-dimensional operators are inversely proportional to the cut-off scale Λ their effects are suppressed at lower energies.

The attraction of working in the SM EFT aproach is then the possibility of a systematic classification of all possible effects of decoupled new physics on observables. It is encouraging that the unique lepton-number-violating dimension-5 operator gives neutrinos Majorana masses when the Higgs gets a vacuum expectation value [48]. The leading effects that conserve lepton number are parametrised by $d = 6$ operators, and we shall be concerned with the phenomenology of the following Lagrangian,

$$\mathcal{L}_{\text{SMEFT}} = \mathcal{L}_{\text{SM}} + \sum_{i=1}^{i=2499} \frac{c_i}{\Lambda^2} \mathcal{O}_i \,,$$

where $\mathcal{O}_i$ are dimension-6 operators. There are 2499 [49] possible combinations of SM fields forming an independent basis of operators unrelated by equations of motion, field redefinitions or integration by parts [50]. If we assume a flavour-blind structure of the operators this reduces to a more manageable 59 operators [51]. The dimension-6 operators

were first classified in the 80s [47], while a complete non-redundant basis of operators was performed only relatively recently [51].

EWPTs	Higgs Physics	TGCs
$\mathcal{O}_W = \frac{ig}{2}\left(H^\dagger\sigma^a \overleftrightarrow{D^\mu} H\right) D^\nu W^a_{\mu\nu}$		
$\mathcal{O}_B = \frac{ig'}{2}\left(H^\dagger \overleftrightarrow{D^\mu} H\right)\partial^\nu B_{\mu\nu}$		$\mathcal{O}_{3W} = g\frac{\epsilon_{abc}}{3!}W^{a\,\nu}_{\mu} W^b_{\nu\rho} W^{c\,\rho\mu}$
$\mathcal{O}_T = \frac{1}{2}\left(H^\dagger \overleftrightarrow{D}_\mu H\right)^2$	$\mathcal{O}_{HW} = ig(D^\mu H)^\dagger\sigma^a(D^\nu H)W^a_{\mu\nu}$	
$\mathcal{O}_{LL}^{(3)\,l} = (\bar{L}_L\sigma^a\gamma^\mu L_L)(\bar{L}_L\sigma^a\gamma_\mu L_L)$	$\mathcal{O}_{HB} = ig'(D^\mu H)^\dagger(D^\nu H)B_{\mu\nu}$	
$\mathcal{O}_R^e = (iH^\dagger \overleftrightarrow{D}_\mu H)(\bar{e}_R\gamma^\mu e_R)$	$\mathcal{O}_g = g_s^2\lvert H\rvert^2 G^A_{\mu\nu}G^{A\mu\nu}$	
$\mathcal{O}_R^u = (iH^\dagger \overleftrightarrow{D}_\mu H)(\bar{u}_R\gamma^\mu u_R)$	$\mathcal{O}_\gamma = g'^2\lvert H\rvert^2 B_{\mu\nu}B^{\mu\nu}$	
$\mathcal{O}_R^d = (iH^\dagger \overleftrightarrow{D}_\mu H)(\bar{d}_R\gamma^\mu d_R)$	$\mathcal{O}_H = \frac{1}{2}(\partial^\mu\lvert H\rvert^2)^2$	
$\mathcal{O}_L^{(3)\,q} = (iH^\dagger\sigma^a \overleftrightarrow{D}_\mu H)(\bar{Q}_L\sigma^a\gamma^\mu Q_L)$	$\mathcal{O}_f = y_f\lvert H\rvert^2\bar{F}_L H^{(c)} f_R + \text{h.c.}$	
$\mathcal{O}_L^q = (iH^\dagger \overleftrightarrow{D}_\mu H)(\bar{Q}_L\gamma^\mu Q_L)$	$\mathcal{O}_6 = \lambda\lvert H\rvert^6$	

Table 2: *List of CP-even dimension-6 operators in our chosen basis and the dominant category of observables that places the strongest constraints on the operators or their linear combinations.*

Most of the 59 operators are four-fermion operators that are constrained independently from those affecting Higgs physics, triple-gauge couplings and EWPTs, assuming the contributions from dimension-6 operators enter only at tree-level. We will also focus on CP-even operators throughout this thesis. In the complete basis of Ref. [52] that we adopt the relevant operators for these three categories of observables are listed in Table 2. For operators across several categories we have different linear combinations affecting each category independently. Operators (or their linear combinations) that are strongly constrained by EWPTs are taken to be effectively zero for Higgs physics and triple-gauge couplings.

1.7 Summary of Selected Publications

This thesis is formally submitted as a "Thesis Incorporating Publications". As required by the guidelines the papers are bound in as published and selected to form a focused theme of research. The author list is alphabetical as is conventional in the field of high energy particle physics but by the standards of the discipline the author of this thesis

meets the criteria for being a principal investigator of the publications included. Thus all the requirements 1-8 of the official *"Guidelines on Submitting a Thesis Incorporating Publications"* document have been met.

Section 2 was published in the *Journal of High Energy Physics* and co-authored with John Ellis [53]. We analyse the couplings of the Higgs boson in a non-linear effective Lagrangian framework with an added singlet scalar by performing a global fit of experimental data to assess the compatibility of various possibilities for the Higgs sector, from SM-like to minimal composite models. We also propose a test of the mass-proportional couplings expected of a scalar that gives mass through its vacuum expectation value. Model-dependent limits on the total Higgs decay width are placed, as well as constraints on possible new physics from their contributions to loop-induced Higgs couplings or through invisible Higgs decays. My personal contribution was to produce the plots and write part of the sections.

Section 3 was published in the *Conference Proceedings of the 25th Rencontres de Blois* [54]. It summarises work with John Ellis, Dae Sung Hwang, and Verónica Sanz on probing the spin-parity of the Higgs in the associated production channel. This can be done both indirectly, using the different energy dependence of associated production for different spin-parity, or directly by measuring the invariant mass differential distribution. The latter method formed the basis for the spin-parity analyses by D0 and CDF at the Tevatron collider. I wrote the conference proceeding. My contribution to the work on which it was based involved running numerical simulations together with Veronica Sanz and estimating the statistical significance.

Sections 4 and 5 were published in the *Journal of High Energy Physics* and co-authored with John Ellis and Verónica Sanz [55, 56]. After spin measurements excluded alternatives to the expected scalar assignment for the newly-discovered particle and its couplings appeared SM-like to a first approximation it became increasingly motivated to assume the SM degrees of freedom as established with new physics decoupled at higher energy scales. The effects are then captured in an EFT framework where one includes the leading effects parametrised by dimension-6 operators. We performed a global fit to the Higgs sector, triple-gauge-couplings and electroweak precision tests in this SM EFT approach, indicating the sensitivity to new physics in each of these measurements and their

complementarity for complete coverage of a full dimension-6 operator basis. I produced most of the plots and wrote the fit to estimate the global constraints. I also contributed to the writing of the paper.

Finally the work in Section 6 was also published in the *Journal of High Energy Physics*, co-authored with Aleksandra Drozd, John Ellis and Jérémie Quevillon [57]. We used the covariant derivative method (CDE) to calculate the effects of decoupled new physics affecting the loop-induced couplings of the Higgs to gluons and photons in the SM EFT, and generalised the universal results for these particular dimension-6 operators to the case of a non-degenerate mass matrix of the heavy particles being integrated out. This applies in particular to stops which we use to illustrate this approach. Limits are placed on the masses of non-degenerate stops from current and future measurements. I calculated the results in parallel with my collaborators and produced some of the plots that appear in the paper.

References

[1] P. W. Higgs, Phys. Rev. Lett. **13** (1964) 508.

[2] F. Englert and R. Brout, Phys. Rev. Lett. **13** (1964) 321

[3] P. W. Higgs, Phys. Lett. **12** (1964) 132.

[4] G. S. Guralnik, C. R. Hagen and T. W. B. Kibble, Phys. Rev. Lett. **13** (1964) 585.

[5] G. Aad *et al.* [ATLAS Collaboration], Phys. Lett. B **716** (2012) 1 [arXiv:1207.7214 [hep-ex]]. S. Chatrchyan *et al.* [CMS Collaboration], Phys. Lett. B **716** (2012) 30 [arXiv:1207.7235 [hep-ex]].

[6] D. B. Kaplan, H. Georgi and S. Dimopoulos, Phys. Lett. B **136** (1984) 187. D. B. Kaplan and H. Georgi, Phys. Lett. B **136** (1984) 183. H. Georgi and D. B. Kaplan, Phys. Lett. B **145** (1984) 216.

[7] S. Weinberg, Phys. Rev. D **13** (1976) 974; Phys. Rev. D **19** (1979) 1277; L. Susskind, Phys. Rev. D **20** (1979) 2619.

[8] C. Csaki, C. Grojean and J. Terning, arXiv:1512.00468 [hep-ph].

[9] S. R. Coleman and J. Mandula, Phys. Rev. **159** (1967) 1251. R. Haag, J. T. Lopuszanski and M. Sohnius, Nucl. Phys. B **88** (1975) 257.

[10] J. Wess and B. Zumino, Phys. Lett. B **49** (1974) 52; Nucl. Phys. B 70 (1974) 39.

[11] J. R. Ellis, G. Ridol and F. Zwirner, Phys. Lett. B **257** (1991) 83; H. E. Haber and R. Hempfling, Phys. Rev. Lett. **66** (1991) 1815; Y. Okada, M. Yamaguchi and T. Yanagida, Prog. Theor. Phys. **85** (1991) 1.

[12] A. Salam and J. A. Strathdee, Phys. Rev. **184** (1969) 1760. J. R. Ellis, Nucl. Phys. B **22** (1970) 478.

[13] R. Contino, Y. Nomura and A. Pomarol, Nucl. Phys. B **671** (2003) 148 [hep-ph/0306259]. K. Agashe, R. Contino and A. Pomarol, Nucl. Phys. B **719** (2005) 165 [hep-ph/0412089]. K. Agashe and R. Contino, Nucl. Phys. B **742** (2006) 59 [hep-ph/0510164].

[14] C. N. Yang and R. Mills, Phys. Rev. **96** (1954) 191.

[15] R. Shaw, PhD thesis, University of Cambridge, 1955.

[16] J. Bardeen, L. N. Cooper and J. R. Schrieer, Phys. Rev. **106** (1957) 162; V. L. Ginzburg and L. D. Landau, Zh. Eksp. Teor. Fiz. **20** (1950) 1064; Phys. Rev. **108** (1957) 1175; L. N. Cooper, Phys. Rev. **104** (1956) 1189; Y. Nambu, Phys. Rev. **117** (1960) 648.

[17] P. W. Anderson, Phys. Rev. **130** (1963) 439;

[18] Y. Nambu, Phys. Rev. Lett. **4** (1960) 380.

[19] J. Goldstone, A. Salam and S. Weinberg, Phys. Rev. **127** (1962) 965.

[20] J. Goldstone, Nuovo Cim. **19** (1961) 154;

[21] J. Ellis, M. K. Gaillard and D. V. Nanopoulos, arXiv:1201.6045 [hep-ph]; arXiv:1504.07217 [hep-ph].

[22] A. Klein and B. W. Lee, Phys. Rev. Lett. **12** (1964) 266.

[23] W. Gilbert, Phys. Rev. Lett. **12** (1964) 713.

[24] P. W. Higgs, Phys. Rev. **145** (1966) 1156.

[25] T. W. B. Kibble, Phys. Rev. **155** (1967) 1554.

[26] A. A. Migdal and A. M. Polyakov, J. Exptl. Theoret. Physics (U.S.S.R.) **51** (1966) 135.

[27] S. L. Glashow, Nucl. Phys. **22** (1961) 579.

[28] S. Weinberg, Phys. Rev. Lett. **19**, 1264 (1967).

[29] A. Salam, Proceedings of 8th Nobel Symposium, Lerum, Sweden, 19-25 May 1968, pp 367-377.

[30] H. D. Politzer, Phys. Rev. Lett. **30** (1973) 1346. D. J. Gross and F. Wilczek, Phys. Rev. Lett. **30** (1973) 1343.

[31] G. t Hooft, Nucl. Phys. B 35, **167** (1971); G. t Hooft and M. J. G. Veltman, Nucl. Phys. B **44** (1972) 189.

[32] Gargamelle Neutrino Collaboration, F. Hasert et al., Phys.Lett. **B46** (1973) 138140.

[33] E598 Collaboration, J. Aubert et al., Phys.Rev.Lett. **33** (1974) 14041406.

[34] S.L. Glashow, J. Iliopoulos, L. Maiani, Phys. Rev. D **2** (1970) 1285.

[35] J. R. Ellis, M. K. Gaillard and D. V. Nanopoulos, CERN preprint Nov. 1975, published in Nucl. Phys. B **106** (1976) 292.

[36] G. Arnison *et al.* [UA1 Collaboration], Phys. Lett. B **122** (1983) 103; M. Banner *et al.* [UA2 Collaboration], Phys. Lett. B **122** (1983) 476; G. Arnison *et al.* [UA1 Collaboration], Phys. Lett. B **126** (1983) 398; P. Bagnaia *et al.* [UA2 Collaboration], Phys. Lett. B **129** (1983) 120.

[37] M. L. Perl, G. Abrams, A. Boyarski, M. Breidenbach, D. Briggs, et al., Phys.Rev.Lett. **35** (1975) 14891492.

[38] S. Herb, D. Hom, L. Lederman, J. Sens, H. Snyder, et al., Phys.Rev.Lett. **39** (1977) 252255.

[39] CDF Collaboration, F. Abe et al., Phys.Rev.Lett. **74** (1995) 26262631, [hep-ex/9503002]; D0 Collaboration, S. Abachi et al., Phys.Rev.Lett. **74** (1995) 26322637, [hep-ex/9503003].

[40] M. Kobayashi and T. Maskawa, Prog.Theor.Phys. **49** (1973) 652657.

[41] G. 't Hooft, NATO Sci. Ser. B **59** (1980) 135.

[42] M. E. Peskin, T. Takeuchi, Phys. Rev. D, **46**, no. 1, (1992)

[43] S. R. Coleman, J. Wess and B. Zumino, Phys. Rev. **177** (1969) 2239; C. Callan, S. Coleman, J. Wess, B. Zumino, Phys. Rev., **177**, no. 5, (1969)

[44] C. E. Vayonakis, Print-77-0432 (ATHENS); M. J. G. Veltman, Phys. Lett. B **70** (1977) 253; B. W. Lee, C. Quigg and H. B. Thacker, Phys. Rev. Lett. **38** (1977) 883; Phys. Rev. D **16** (1977) 1519.

[45] C. H. Llewellyn Smith, Phys,. Lett. **46B** (1973) 233; S. Joglekar, Ann. Phys. (NY) **83** (1974) 427.

[46] ATLAS Collaboration, ATLAS-CONF-2015-044 (2015)

[47] W. Buchmuller and D. Wyler, Nucl. Phys. B **268** (1986) 621.

[48] S. Weinberg, Phys. Rev. Lett. **43** (1979) 1566

[49] R. Alonso, E. E. Jenkins, A. V. Manohar and M. Trott, JHEP **1404** (2014) 159 [arXiv:1312.2014 [hep-ph]].

[50] H. D. Politzer, Nucl. Phys. B 172 (1980) 349; H. Kluberg-Stern and J. B. Zuber, Phys. Rev. D 12 (1975) 3159; C. Grosse-Knetter, Phys. Rev. D 49 (1994) 6709 [hep-ph/9306321]; C. Arzt, Phys. Lett. B 342 (1995) 189 [hep-ph/9304230]; H. Simma, Z. Phys. C 61 (1994) 67 [hep-ph/9307274]; J. Wudka, Int. J. Mod. Phys. A 9 (1994) 2301 [hep-ph/9406205].

[51] B. Grzadkowski, M. Iskrzynski, M. Misiak and J. Rosiek, JHEP **1010**, 085 (2010) [arXiv:1008.4884 [hep-ph]].

[52] A. Pomarol and F. Riva, JHEP **1401** (2014) 151 [arXiv:1308.2803 [hep-ph]].

[53] J. Ellis and T. You, JHEP **1306** (2013) 103 [arXiv:1303.3879 [hep-ph]].

[54] T. You, arXiv:1309.6619 [hep-ph].

[55] J. Ellis, V. Sanz and T. You, JHEP **1407** (2014) 036 [arXiv:1404.3667 [hep-ph]].

[56] J. Ellis, V. Sanz and T. You, JHEP **1503** (2015) 157 [arXiv:1410.7703 [hep-ph]].

[57] A. Drozd, J. Ellis, J. Quevillon and T. You, JHEP **1506** (2015) 028 [arXiv:1504.02409 [hep-ph]].

2 Updated Global Analysis of Higgs Couplings

Published for SISSA by Springer

Received: *April 3, 2013*
Accepted: *May 31, 2013*
Published: *June 26, 2013*

Updated global analysis of Higgs couplings

John Ellis[a,b] **and Tevong You**[a]

[a] *Theoretical Particle Physics and Cosmology Group, Physics Department, King's College London, London WC2R 2LS, U.K.*
[b] *TH Division, Physics Department, CERN, CH-1211 Geneva 23, Switzerland*

E-mail: john.ellis@cern.ch, tevong.you@kcl.ac.uk

Abstract: There are many indirect and direct experimental indications that the new particle H discovered by the ATLAS and CMS Collaborations has spin zero and (mostly) positive parity, and that its couplings to other particles are correlated with their masses. To a high degree of confidence, it is a Higgs boson, and here we examine the extent to which its couplings resemble those of the single Higgs boson of the Standard Model. Our global analysis of its couplings to fermions and massive bosons determines that they have the same relative sign as in the Standard Model. We also show directly that these couplings are highly consistent with a dependence on particle masses that is linear to within a few %, and scaled by the conventional electroweak symmetry-breaking scale to within 10%. We also give constraints on loop-induced couplings, on the total Higgs decay width, and on possible invisible decays of the Higgs boson under various assumptions.

Keywords: Higgs Physics, Technicolor and Composite Models, Standard Model

ArXiv ePrint: 1303.3879

Open Access

doi:10.1007/JHEP06(2013)103

JHEP06(2013)103

Contents

JHEP06(2013)103

1 Introduction and summary

It has now been established with a high degree of confidence that the new particle H with mass $\sim 126\,\text{GeV}$ discovered by the ATLAS [1, 2] and CMS [3, 4] has spin zero and (mainly) positive-parity couplings, as expected for a Higgs boson [5, 6]. Minimal spin-two alternatives with graviton-like couplings have been disfavoured by measurements of the H couplings to vector bosons [7], and quite strongly excluded by constraints on the energy dependence of H production [8]. The graviton-like spin-two hypothesis has also been disfavoured strongly by analyses of H decays into $\gamma\gamma$ [9], ZZ^* and WW^* final states [10, 11], and the positive-parity assignment is favoured by decays into ZZ^* [12], in particular.[1] To a high degree of confidence, the H particle is a Higgs boson.

In this paper we make updated global fits to the H couplings to other particles with the aim of characterizing the extent to which they resemble those of the Higgs boson of the Standard Model. There has been considerable progress since our previous analysis of H couplings [59], including updates at the Hadron Collider Physics conference in November 2012 [17], the CERN Council in December 2013 [18, 19], the Moriond Electroweak Conference [20] and the Aspen 'Higgs Quo Vadis' Meeting in March 2013 [21], and most recently an update of the CMS $H \to \gamma\gamma$ data at the Moriond QCD session [22].

There have been many analyses of the H couplings [23–59], some also including the Moriond 2013 data [60, 61].[2] Many of these analyses, including those made by the different experimental Collaborations, assume simple parameterizations in which the couplings of the Standard Model Higgs boson to bosons and fermions are rescaled by factors a_V and c_f, respectively (or equivalently by factors $\kappa_{V,f}$) [64]. Fits with non-minimal couplings to

[1] It is also impressive that the mass of the H particle coincides with the best fit for the mass of the Higgs boson found in a global fit to precision electroweak data taking account of pre-LHC searches at LEP and the TeVatron [13], and is also highly consistent with low-energy supersymmetry [14–16].

[2] After this work was completed ATLAS and CMS have made public their couplings analyses [62, 63].

massive vector bosons have also been considered, as have fits in which the loop-induced couplings to gluons and photons deviate by factors $c_{g,\gamma}$ from the values predicted in the Standard Model. The latter have been of interest in view of the possible excess of $H \to \gamma\gamma$ decays relative to the Standard Model prediction, particularly as reported by the ATLAS Collaboration [9]. Since the $H\gamma\gamma$ coupling could in principle receive contributions from new massive charged particles, and the Hgg coupling from new massive coloured particles, these are particularly sensitive to new physics beyond the Standard Model. In this paper we make updated global fits to the H couplings within such common phenomenological frameworks.

We also revisit parameterizations of the H couplings to fermions and bosons that were first considered in [59], which are designed specifically to probe the dependence of the H couplings on particle masses. Namely, we consider parameterizations of the H couplings to fermions λ_f and massive bosons g_V of the form

$$\lambda_f \;=\; \sqrt{2}\left(\frac{m_f}{M}\right)^{1+\epsilon}, \; g_V \;=\; 2\left(\frac{m_V^{2(1+\epsilon)}}{M^{1+2\epsilon}}\right), \tag{1.1}$$

which reduce to the couplings of the Standard Model Higgs boson in the double limit $\epsilon \to 0, M \to v = 246\,\text{GeV}$. This parameterization addresses explicitly the question the extent to which the H particle resembles a quantum excitation [5, 6] of the Englert-Brout-Higgs field that is thought to give masses to the particles of the Standard Model [5, 6, 65–67].

We find that, in the absence of contributions from any particles beyond the Standard Model, a combination of the Higgs signal strengths measured in different channels is now very close to the Standard Model value, within 13% at the 68% CL. We also find, for the first time, a strong preference for the couplings to bosons and fermions to have the same sign, also as expected in the Standard Model, driven largely by the new CMS result on $H \to \gamma\gamma$ decay. This also means that there is no significant evidence of additional loop contributions to the $H\gamma\gamma$ beyond those due to the top quark and the W boson. Using the parameterization (1.1), we find that the dependence of the Higgs couplings to different particle species is within a few % of a linear dependence of their masses. Within the parameterization (1.1), or marginalizing over the H couplings to Standard Model bosons and fermions, we find that the total Higgs decay rate lies within 20% of the Standard Model value at the 68% CL. If the couplings of the Higgs Boson to Standard Model particles have their Standard Model values and there are no non-standard contributions to the Hgg and $H\gamma\gamma$ amplitudes, the upper limit on invisible Higgs decays is 10% of the total Higgs decay rate.

2 Summary of the data

The analysis of this paper is based mainly on the material presented by the LHC and Tevatron experimental Collaborations at the March 2013 Moriond Conferences in La Thuile [20, 22]. The following are some of the main features of interest among the new results:

- The $H \to \bar{b}b$ signal strength reported by the TeVatron experiments has reduced from 2.0 ± 0.7 to 1.6 ± 0.75 times the Standard Model value.

JHEP06(2013)103

- A new $H \to \tau^+\tau^-$ result of 1.1 ± 0.4 has been reported by CMS, improving on the previous value of 0.7 ± 0.5.

- The $H \to \gamma\gamma$ signal strength reported by ATLAS has reduced somewhat from $1.80^{+0.4}_{-0.36}$ to $1.65^{+0.34}_{-0.30}$ times the Standard Model value. Most importantly, CMS has reported a new result of $0.78^{+0.28}_{-0.26}$ for the signal strength using an MVA approach.

- The $H \to WW^*$ signal strength reported by ATLAS has reduced from 1.5 ± 0.6 to 1.01 ± 0.31 times the Standard Model value.

All the latest available results from ATLAS, CMS and TeVatron are incorporated into our global fit. The experimental data are used to reconstruct the likelihood in a combination of three possible ways according to the available information: 1) using the official best-fit central value of μ with its 1-σ error bars, 2) using the given number of signal, background and observed events with their respective errors, or 3) reconstructing the central value of μ from the 95% CL expected and observed μ. Specifically, the data inputs are as follows:

- The TeVatron $H \to \bar{b}b, \tau^+\tau^-, WW^*, \gamma\gamma$ combined best-fit μ and 1-σ error bars from [68].

- The likelihood for the CMS 8 TeV WW^* 0,1-jet analysis is reconstructed from the numbers of events given in table 4 of [69]. The WW^* 2-jet event numbers are instead taken from table 3 of [70]. In addition, we use the fit values from [71] for the 7-TeV CMS WW^* data. The ATLAS Collaboration provides 0,1-jet and 2-jet μ central values and 1-σ ranges for a combination of 7- and 8-TeV, which we treat effectively as 8 TeV. The percentages of the vector-boson fusion (VBF) production mode contributions to the signals in the 0,1 and 2-jet channels are taken to be 2%, 12% and 81%, respectively [72].

- For $H \to b\bar{b}$ in CMS we used the 7- and 8-TeV best-fit values from [71] and [73], while for ATLAS the likelihood was reconstructed from the 95% CL expected and observed values of μ at 7 and 8 TeV given in [74].

- The CMS $H \to \tau^+\tau^-$ and ZZ^* and ZZ^* dijet rates were taken from the central values given in [10]. Since no separate 7- and 8-TeV numbers are given for these, we treat them effectively as 8 TeV. Numbers of events for the ATLAS $H \to ZZ^*$ 7- and 8-TeV analyses are provided separately in [10], while the ATLAS $H \to \tau^+\tau^-$ likelihood is reconstructed using the 95% expected and observed values of μ given in [75]. The VBF $\tau^+\tau^-$ efficiencies are taken from [76].

- The CMS $\gamma\gamma$ central values are given for six (five) different subchannels at 8 (7) TeV in [10], along with the percentage contributions from all production mechanisms in table 2 in [77]. The same information can be found for ATLAS at 7 TeV in [1, 2] and at 8 TeV in [10], broken down into eleven subchannels including two VBF-dominated ones. The CMS update is reported for a cut-based and MVA analysis; we use the MVA result, which has the greater sensitivity.

JHEP06(2013)103

The likelihood is assumed to have a Gaussian distribution, which is in practice a good approximation for a substantial number of events $\gtrsim 10$. In cases where asymmetric errors are reported, the larger of the two is conservatively taken to be the symmetric 1σ error. Due to the limited experimental information available, we ignore correlation effects and any marginalization over nuisance parameters, which is not expected to affect our results outside the $\sim 10\%$ current level of accuracy. For each individual experiment we have checked that our combinations of the likelihoods for the various subchannels agree with official combinations with only slight exceptions, for example the CMS 7-TeV $\gamma\gamma$ analysis ($\mu = 1.58^{+0.60}_{-0.61}$ instead of the official value of $1.69^{+0.65}_{-0.59}$). When combined with the CMS 8-TeV data (for which we reproduce the official central value) we calculate for the combined CMS $\gamma\gamma$ data a value of $\mu = 0.72^{+0.24}_{-0.26}$ (to be compared with the official value of $0.78^{+0.28}_{-0.26}$). This difference of a fraction of the quoted error does not impact significantly our overall results.

As a preliminary to our analysis, we compile in figure 1 the overall signal strengths in the principal channels, as calculated by combining the data from the different experiments. Thus, for example, in the first line we report the $V + (H \to \bar{b}b)$ signal strength found by combining the data on associated $V + H$ production from the TeVatron and LHC. As can be seen in the second line, so far there is no significant indication of associated $\bar{t}t + H$ production. The third line in figure 1 combines the experimental information on the $H \to \bar{b}b$ signal strengths in these two channels. Signals for $H \to \tau^+\tau^-$ decay have now been reported in various production channels, as reported in the next three lines of figure 1, and the combined signal strength is given in the following line. As we have discussed, data are available on $H \to \gamma\gamma$ final states following production in gluon-gluon collisions and via vector-boson fusion. The central values of the corresponding signal strengths are now only slightly larger than the Standard Model predictions, and we return later to a discussion of the significance of these measurements. The signal strengths in the $H \to WW^*$ and ZZ^* final states are very much in line with the predictions of the Standard Model. These dominate the determination of the combined signal strength reported in the last line of figure 1, together with the $\gamma\gamma$ final state. It is striking that the available data already constrain the combined Higgs signal strength to be very close to the Standard Model value:

$$\mu \;=\; 1.02^{+0.11}_{-0.12}\,. \tag{2.1}$$

We present separately the combined signal strength in the VBF and VH channels without the loop-induced $\gamma\gamma$ final state, which lies slightly (but not significantly) above the Standard Model value. To the extent that a signal with direct Higgs couplings in both the initial and final state is established, this combination disfavours models that predict a universal suppression of the Higgs couplings.[3]

[3]We address later in a full fit of the effective couplings of the Higgs to photons and gluons the question whether an enhancement of the loop-induced gluon fusion production could compemsate for this by contaminating the VBF cut selection.

JHEP06(2013)103

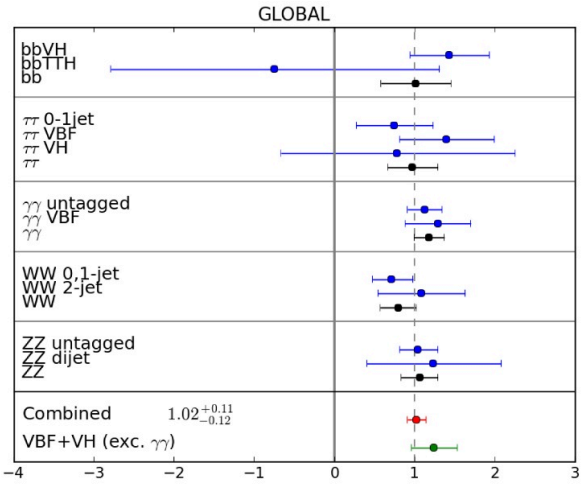

Figure 1. A compilation of the Higgs signal strengths measured by the ATLAS, CDF, D0 and CMS Collaborations in the $\bar{b}b$, $\tau^+\tau^-$, $\gamma\gamma$, WW^* and ZZ^* final states. We display the combinations of the different channels for each final state, and also the combination of all these measurements, with the result for the VBF and VH channels (excluding the $\gamma\gamma$ final state) shown separately in the bottom line.

3 Higgs couplings to bosons and fermions

Our first step in analyzing the implications of these data uses the following effective low-energy nonlinear Lagrangian for the electroweak symmetry-breaking sector [78–81]:

$$\begin{aligned}\mathcal{L}_{\rm eff} &= \frac{v^2}{4}\mathrm{Tr}\left(D_\mu U D^\mu U^\dagger\right)\times\left[1+2a\frac{H}{v}+\dots\right]\\ &\quad -\frac{v}{\sqrt{2}}\Sigma_f \bar{f}_L\lambda_f f_R\left[1+c_f\frac{H}{v}+\dots\right]+h.c.\,,\end{aligned}\tag{3.1}$$

where U is a unitary 2×2 matrix parametrizing the three Nambu-Goldstone fields that give masses to the $W^\pm$ and Z^0 bosons, H is the physical Higgs boson field and $v\sim 246\,\mathrm{GeV}$ is the conventional electroweak symmetry-breaking scale. The coefficients λ_f are the Standard Model Yukawa couplings of the fermion flavours f, and the factors a and c_f characterize the deviations from the Standard Model Higgs boson couplings of the H couplings to massive vector bosons and the fermions f, respectively. The couplings of the Higgs boson to massless boson pairs gg and $\gamma\gamma$ are described by the following dimension-5 loop-induced couplings:

$$\mathcal{L}_\Delta = -\left[\frac{\alpha_s}{8\pi}c_g b_g G_{a\mu\nu}G_a^{\mu\nu}+\frac{\alpha_{em}}{8\pi}c_\gamma b_\gamma F_{\mu\nu}F^{\mu\nu}\right]\left(\frac{H}{V}\right),\tag{3.2}$$

where the coefficients $b_{g,\gamma}$ are those found in the Standard Model, and the factors $c_{g,\gamma}$ characterize the deviations from the Standard Model predictions for the H couplings to massless vector bosons.

JHEP06(2013)103

One specific model for a common rescaling factor of all fermion and vector boson Higgs couplings is a minimal composite Higgs scenario [78–81], the MCHM4, in which the compositeness scale f is related to (a, c) by

$$a = c = \sqrt{1 - \left(\frac{v}{f}\right)^2} \, .$$

A similar universal suppression is found in pseudo-dilaton models. A variant of this minimal model with a different embedding of the Standard Model fermions in SO(5) representations of the new strong sector, the MCHM5, has separate vector and fermion rescalings:

$$a = \sqrt{1 - \left(\frac{v}{f}\right)^2} \quad , \quad c = \frac{1 - 2\left(\frac{v}{f}\right)^2}{\sqrt{1 - \left(\frac{v}{f}\right)^2}} \, .$$

In the following we confront the data with these specific models, as well as an 'anti-dilaton' scenario in which $c = -a$.

Figure 2 compiles the constraints imposed by the data summarized in figure 1 on the factors (a, c) in the effective Lagrangian (3.1), assuming universality in the fermion factors $c_f \equiv c$, and assuming that no non-Standard-Model particles contribute to the anomaly factors $c_{g,\gamma}$, which therefore are determined by a combination of the factors $c_t = c$ and $a_W = a$. In each panel of figure 2 and similar subsequent figures, the more likely regions of parameter space have lighter shading, and the 68, 95 and 99% CL contours are indicated by dotted, dashed and solid lines, respectively.

We see again in the top row of panels of figure 2 that the data on $H \to \bar{b}b$ decays (left) and $\tau^+\tau^-$ decays (right) are entirely consistent with the Standard Model predictions $(a, c) = (1, 1)$. The region of the (a, c) plane favoured by the $\bar{b}b$ data manifests a correlation between a and c that arises because the dominant production mechanism is associated $V+X$ production, which is $\propto a^2$. On the other hand, the region of the (a, c) plane favoured by the $\tau^+\tau^-$ data exhibits a weaker correlation between a and c, reflecting the importance of data on production via gluon fusion in this case. As was to be expected from the compilation in figure 1, the $\gamma\gamma$ data displayed in the middle left panel of figure 2 are now compatible with the Standard Model prediction $(a, c) = (1, 1)$, following inclusion of the latest CMS result. The data on $H \to WW^*$ (middle right panel of figure 2) and ZZ^* decays (bottom left panel) are also entirely consistent with $(a, c) = (1, 1)$.

We draw attention to the importance of the 2-jet analyses, which select a VBF-enriched sample, in disfavouring bands of the plots around $c \sim 0$. This effect is very visible in the $\gamma\gamma$ and WW^* results displayed in the middle plots. On the other hand, in the ZZ^* case the CMS dijet analysis is less powerful, so there is a weaker suppression of the likelihood around $c \sim 0$.

All the above information is combined in the bottom right panel of figure 2, assuming that there are no virtual non-Standard-Model particles contributing to $H \to \gamma\gamma$ decay or the Hgg coupling. We note that the global fit is not symmetric between the two possibilities for the sign of c relative to a, a feature visible in the middle left panel of figure 2, and

JHEP06(2013)103

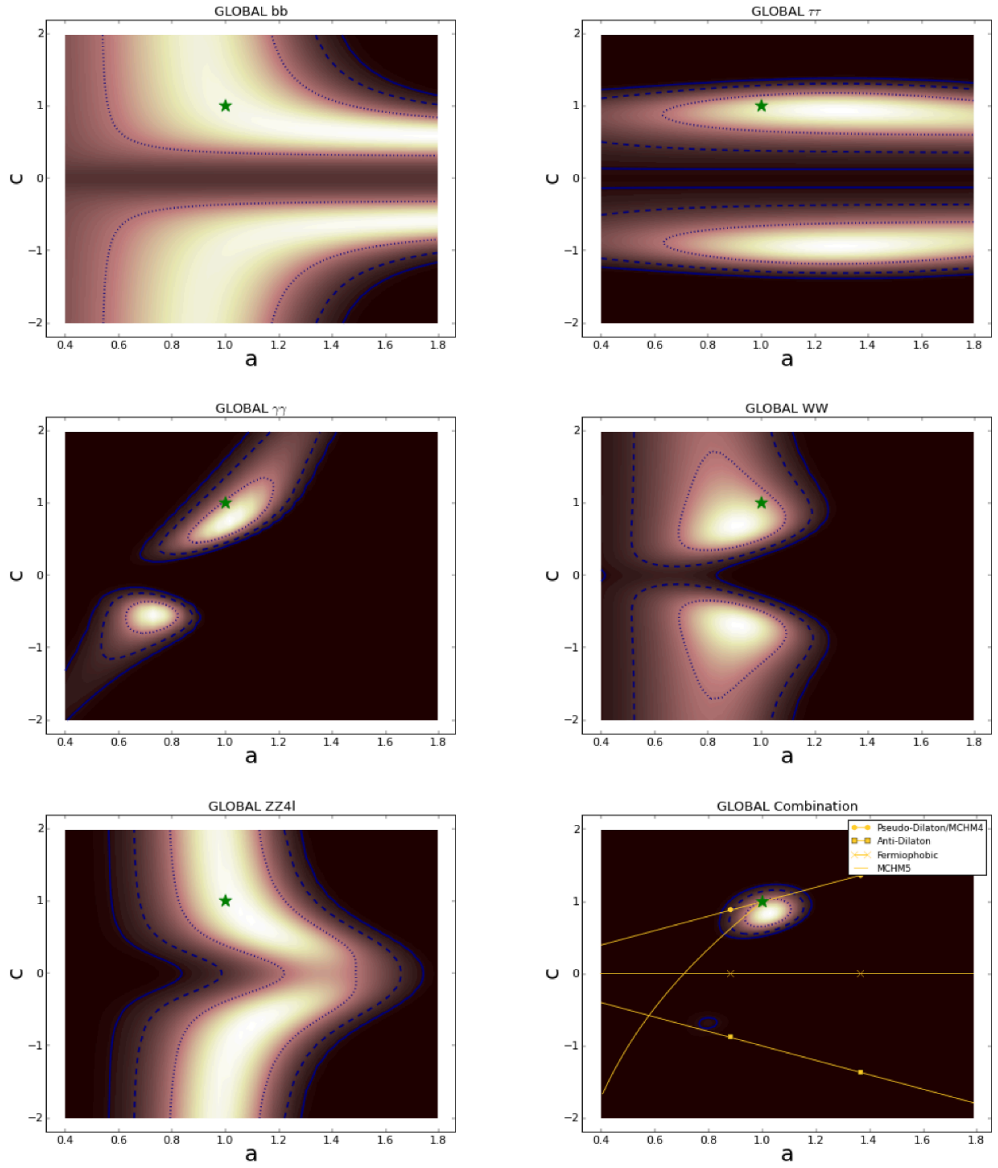

Figure 2. The constraints in the (a, c) plane imposed by the measurements in figure 1 in the $\bar{b}b$ final state (top left), in the $\tau^+\tau^-$ final state (top right), in the $\gamma\gamma$ final state (middle left), in the WW^* final state (middle right) and in the ZZ^* final state (bottom left). The combination of all these constraints is shown in the bottom right panel.

traceable to the interference between the t quark and W boson loops contributing to the $H \to \gamma\gamma$ decay amplitude. In the past it has been a common feature of such global fits that they have exhibited two local minima of the likelihood function with opposite signs of c that, because of this asymmetry, were not equivalent but had similar likelihoods [82, 83]. We see in the bottom right panel of figure 2, for the first time a clear preference for the

JHEP06(2013)103

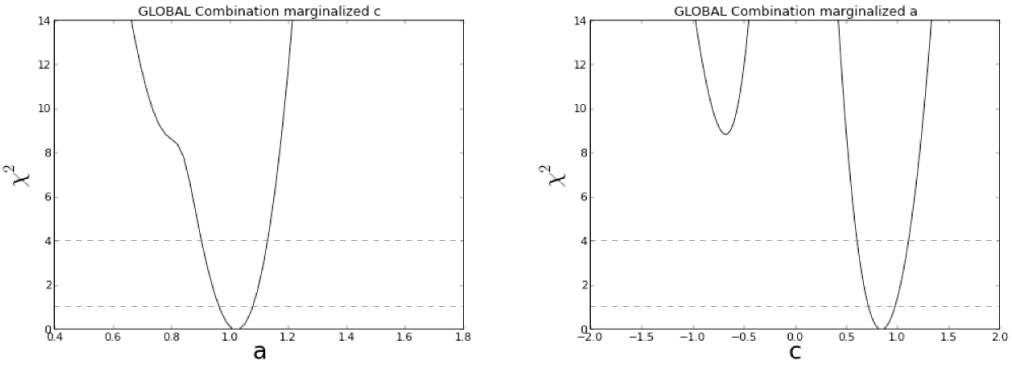

Figure 3. The one-dimensional likelihood functions for the boson coupling parameter a (left panel) and the fermion coupling parameter c (right panel), as obtained by marginalizing over the other parameter in the bottom right panel of figure 2.

minimum with $c > 0$, i.e., the same sign as in the Standard Model.

This feature is also seen clearly in figure 3, where we display in the left panel the one-dimensional likelihood function χ^2 for the boson coupling parameter a obtained by marginalizing over the fermion coupling parameter c, and in the right panel the one-dimensional likelihood function for c obtained by marginalizing over a. We see that the fit with $c > 0$ is strongly favoured over that with $c < 0$, with $\Delta\chi^2 \sim 9$. The parameters of the global minimum of the χ^2 function and their 68% CL ranges are as follows:

$$a \;=\; 1.03 \pm 0.06 \;,\; c \;=\; 0.84 \pm 0.15 \,. \tag{3.3}$$

This preference for $c > 0$ is largely driven by the recently-released CMS $\gamma\gamma$ data.

The yellow lines in the bottom right panel of figure 2 correspond to various alternatives to the Standard Model, as discussed above. We see that fermiophobic models (the horizontal line) are very strongly excluded, as are anti-dilaton models in which $c = -a$. On the other hand, dilaton/MCHM4 models with $a = c$ are compatible with the data as long as their common value is close to unity. Likewise, MCHM5 models lying along the curved line are also compatible with the data if their parameters are chosen to give predictions close to the Standard Model.

The fact that, whereas all the direct measurements of H couplings to fermions and massive vector bosons are very compatible with the Standard Model, the coupling to $\gamma\gamma$ was formerly less compatible, has given rise to much speculation that additional virtual particles may be contributing to the factor c_γ in (3.2). However, the motivation for this speculation has been largely removed by the recent re-evaluation of the $H \to \gamma\gamma$ decay rate by the CMS Collaboration, which is quite compatible with the Standard Model prediction. The left panel of figure 4 shows the results of a global fit to the anomaly factors (c_γ, c_g), assuming the Standard Model values $(a, c) = (1, 1)$ for the tree-level couplings to massive bosons and fermions. Under this hypothesis, any deviation from $(c_\gamma, c_g) = (1, 1)$ would be due to new particles beyond the Standard Model. We see explicitly in figure 4 that, while

JHEP06(2013)103

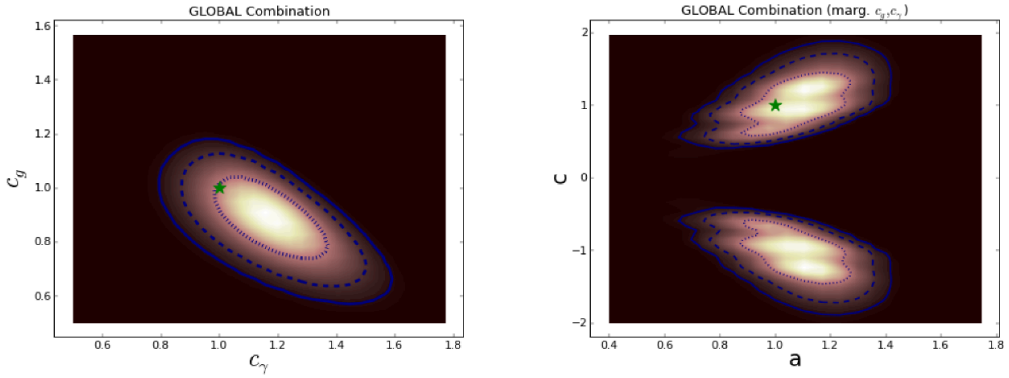

Figure 4. Left: The constraints in the (c_γ, c_g) plane imposed by the measurements in figure 1, assuming the Standard Model values for the tree-level couplings to massive bosons and fermions, i.e., $a = c = 1$. Right: The constraints in the (a, c) plane when marginalizing over c_γ and c_g.

there may still be a hint that $c_\gamma > 1$, the value of c_g is completely compatible with the Standard Model. Thus, any set of new particles contributing to c_γ should be constructed so as not to contribute significantly to c_g.

The right panel of figure 4 is complementary, showing the constraints in the (a, c) plane after marginalizing over (c_γ, c_g). Thus it represents the constraints on a and c if no assumption is made about the absence of new particle contributions to the loop amplitudes. In this case, the symmetry between the solutions with $c > 0$ and < 0 is restored, as the $H \to \gamma\gamma$ decay rate no longer discriminates between them. In this case, the Standard Model values $a = c = 1$ are well inside the most favoured region of the (a, c) plane.

We display in the left panel of figure 5 the one-dimensional likelihood function χ^2 for the factor c_γ obtained by marginalizing over c_g, and in the right panel the one-dimensional likelihood function for c_g obtained by marginalizing over c_γ. The central values and the 68% CL ranges of c_γ and c_g are as follows:

$$c_\gamma \;=\; 1.18 \pm 0.12\,,\; c_g \;=\; 0.88 \pm 0.11\,, \tag{3.4}$$

and the likelihood price for $c_\gamma = 1$ is $\Delta\chi^2 = 2$, whereas the price for $c_g = 1$ is $\Delta\chi^2 = 1$.

4 Probing the mass dependence of Higgs couplings

We now turn to the results of a global fit using the (M, ϵ) parameterization (1.1) that probes directly the extent to which the current measurements constrain the H couplings to other particles to be approximately linear: $\epsilon \sim 0$, and the extent to which the mass scaling parameter $M \sim v$. In this limit the Standard Model is recovered in the tree-level approximation. The left panel of figure 6 shows the result of combining the measurements shown in figure 1 in the (M, ϵ) plane. The horizontal and vertical yellow lines correspond to $\epsilon = 0$ and $M = v$, respectively, and the data are quite compatible with these values. The central values and the 68% CL ranges of M and ϵ are as follows:

$$M \;=\; 244^{+20}_{-10}\ \text{GeV}\,,\; \epsilon \;=\; -0.022^{+0.042}_{-0.021}\,, \tag{4.1}$$

JHEP06(2013)103

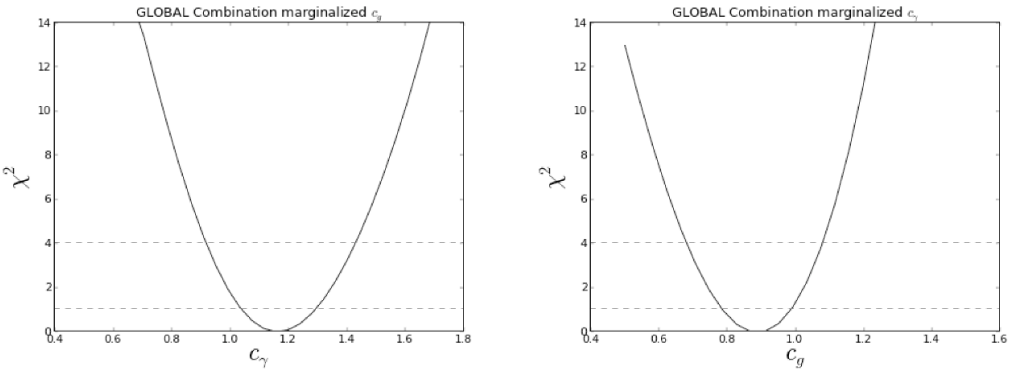

Figure 5. The one-dimensional likelihood functions for c_γ (left panel) and c_g (right panel), as obtained by marginalizing over the other variable in the bottom right panel of figure 4, assuming the Standard Model values for the tree-level couplings to massive bosons and fermions.

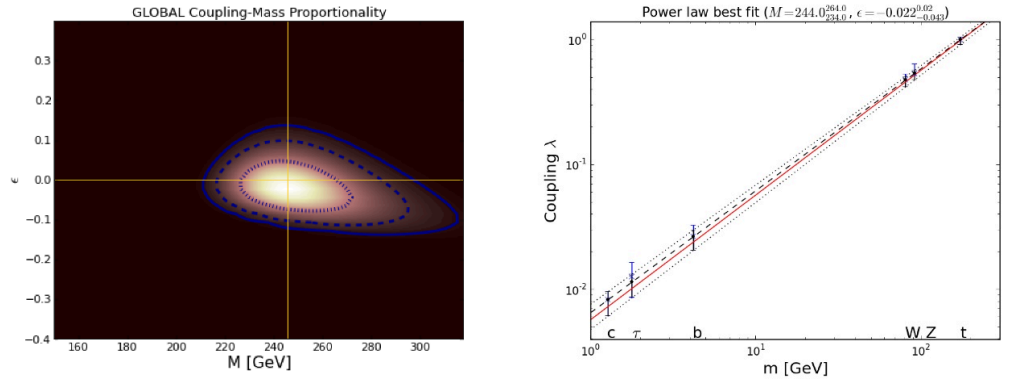

Figure 6. The constraints in the (M, ϵ) plane imposed by the measurements in figure 1 (left panel) and the strengths of the couplings to different fermion flavours and massive bosons predicted by this two-parameter (M, ϵ) fit (right panel). In the latter, the red line is the Standard Model prediction, the black dashed line is the best fit, and the dotted lines are the 68% CL ranges. For each particle species, the black error bar shows the range predicted by the global fit, and the blue error bar shows the range predicted for that coupling if its measurement is omitted from the global fit.

and the likelihood price for $M = 246\,\text{GeV}$ and $\epsilon = 0$ is $\Delta\chi^2 = 0.12$. It is remarkable that the data already constrain the mass dependence of the H couplings to other particles to be linear in their masses to within a few %, and that the mass scaling parameter M is within 10% of the Standard Model value $v = 246\,\text{GeV}$. We display in the left panel of figure 7 the one-dimensional likelihood function χ^2 for the factor ϵ obtained by marginalizing over M, and in the right panel the one-dimensional likelihood function for M obtained by marginalizing over ϵ.

The right panel of figure 6 displays the mass dependence of the H couplings in a different way, exhibiting explicitly the constraints on the couplings of H to other particles within the parameterization (1.1). The solid red line is the prediction of the Standard

JHEP06(2013)103

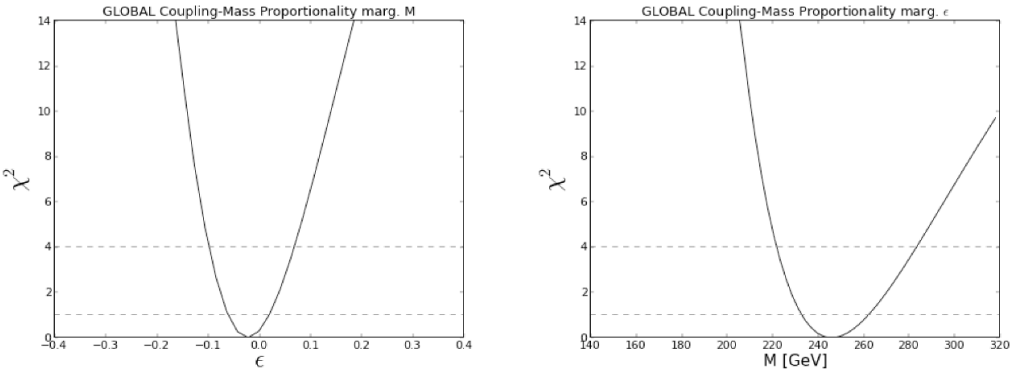

Figure 7. The one-dimensional likelihood functions for ϵ (left panel) and M (right panel), as obtained by marginalizing over the other variable in the left panel of figure 6.

Model, $\epsilon = 0$ and $M = v$, the black dashed line corresponds to the best-fit values in (4.1), and the dotted lines correspond to their 68% CL ranges. The black points and vertical error bars are the predictions of the (M, ϵ) fit for the couplings of H to each of the other particle species: the points lie on the best-fit dashed line and the error bars end on the upper and lower dotted lines. Also shown (in blue) for each particle species is the prediction for its coupling to H if the data on that particular species are omitted from the global fit. In other words, the blue points and error bars represent the predictions for the H coupling to that particle, as derived from the couplings to other particles.

5 The total Higgs decay rate

We now discuss the total Higgs decay rate in the two classes of global fit discussed above, assuming that the Higgs has no other decays beyond those in the Standard Model [84, 85]. The left panel of figure 8 displays contours of the Higgs decay rate relative to the Standard Model prediction in the (a, c) plane discussed in section 3. The local χ^2 minimum with $c > 0$ corresponds to a Higgs decay rate very close to the Standard Model value, whereas the disfavoured 'echo' solution with $c < 0$ has a somewhat smaller decay rate. The right panel of figure 8 displays contours of the Higgs decay rate in the (M, ϵ) plane, where we again see that the best fit has a total decay rate very close to the Standard Model value. We display in figure 9 the one-dimensional likelihood function for the total Higgs decay width relative to its Standard Model value assuming no contributions from non-Standard-Model particles. The solid line is obtained assuming that $a = c$ (or, equivalently, that $\epsilon = 0$ but M is free), the dashed line is obtained marginalizing over (a, c), and the dot-dashed line is obtained by marginalizing over (M, ϵ).

One may also use the current Higgs measurements to constrain the branching ratio for Higgs decays into invisible particles, BR_{inv} [86, 87]. This invisible branching ratio factors out of the total decay width as

$$\Gamma_{\rm Tot} = \Gamma_{\rm Vis} + \Gamma_{\rm Inv} = \left(\frac{R_{\rm Vis}}{1 - BR_{\rm Inv}}\right) \Gamma^{\rm SM}_{\rm Tot} \quad , \tag{5.1}$$

JHEP06(2013)103

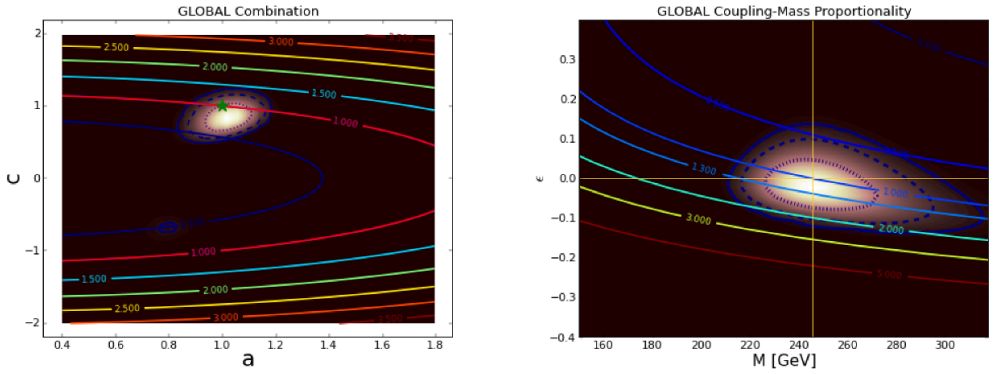

Figure 8. Contours of the total Higgs decay rate relative to the Standard Model prediction in the (a, c) plane shown in the bottom right panel of Fig 2 (left) and the (M, ϵ) plane shown in the left panel of figure 6 (right).

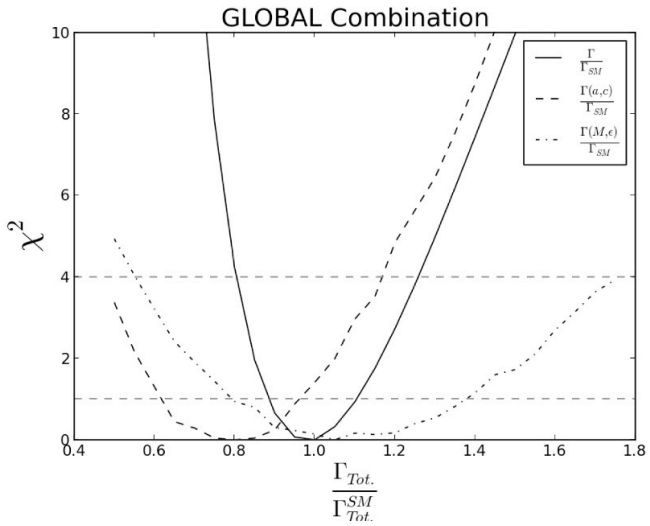

Figure 9. The one-dimensional likelihood function for the total Higgs decay width relative to its value in the Standard Model, $R \equiv \Gamma/\Gamma_{SM}$, assuming decays into Standard Model particles alone and assuming $a = c$ or equivalently $\epsilon = 0$ (solid line), marginalizing over (a, c) (dashed line) and marginalizing over (M, ϵ) (dot-dashed line).

where $R_{\rm Vis} = \Gamma_{\rm Vis}/\Gamma^{\rm SM}_{\rm Tot}$ is the rescaling factor of the total decay width in the absence of an invisible contribution. Thus we see that an invisible branching ratio acts as a general suppression of all other branching ratios, which could be compensated by non-standard visible Higgs decays.

The left panel of figure 10 displays the χ^2 function for BR_{inv} under various assumptions. The solid line was obtained assuming the Standard Model couplings for visible particles, i.e., $(a, c) = (1, 1)$ or equivalently $(M, \epsilon) = (v, 0)$. We see that the best fit has

JHEP06(2013)103

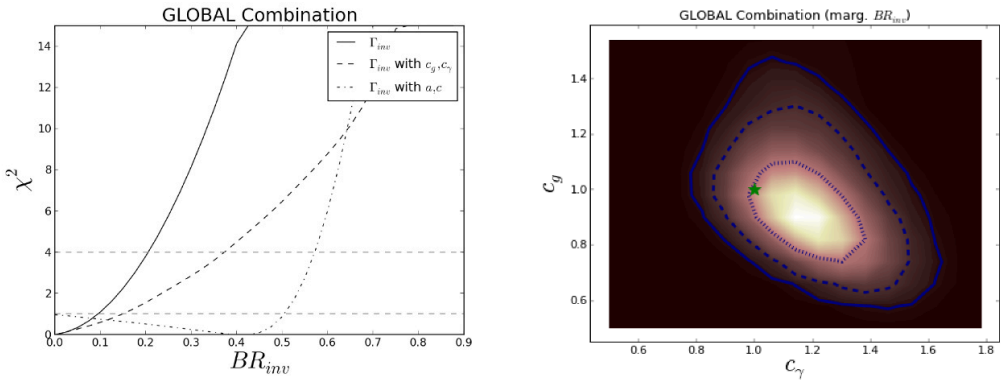

Figure 10. Left: The branching ratio for Higgs decay into invisible particles obtained assuming the Standard Model decay rates for all the visible Higgs decays (solid), marginalizing over (c_γ, c_g) (dashed) and (a,c) (dot-dashed). Right: The constraints in the (c_γ, c_g) plane when marginalizing over the invisible branching ration BR_{inv}.

$BR_{inv} = 0$, and that the 68 and 95% CL limits are 0.09 and 0.21, respectively. The dot-dashed line was obtained by marginalizing over (a, c), where the shallow minimum at $BR_{inv} \sim 0.4$ would require $a > 1$.[4] Finally, the dashed line was obtained fixing $(a, c) = (1, 1)$ (or equivalently $(M, \epsilon) = (v, 0)$), but marginalizing over the loop factors (c_γ, c_g). Conversely, the right panel of figure 10 displays the constraint in the (c_γ, c_g) plane obtained by marginalizing over BR_{inv}.

6 Conclusions

The recent installments of data from the LHC experiments announced in March 2013 impose strong new constraints on the properties and couplings of the H particle, which is a Higgs boson to a high confidence level. The data now constrain this particle to have couplings that differ by only some % from those of the Higgs boson of the Standard Model. In particular, the relative sign of its couplings to bosons and fermions is fixed for the first time, its couplings to other particles are very close to being linear in their masses, and strong upper limits on invisible Higgs decays can be derived.

The data now impose severe constraints on composite alternatives to the elementary Higgs boson of the Standard Model. However, they do not yet challenge the predictions of supersymmetric models, which typically make predictions much closer to the Standard Model values. We therefore infer that the Higgs coupling measurements, as well as its mass, provide circumstantial support to supersymmetry as opposed to these minimal composite alternatives, though this inference is not conclusive.

It is likely that the first LHC run at 7 and 8 TeV has now yielded most of its Higgs secrets, and we look forward to the next LHC run at higher energy, and its later runs at

[4]Constraining $a \leq 1$, as expected in most BSM models, can also lead to interesting upper limits on the invisible Higgs decays [85–87].

JHEP06(2013)103

significantly higher luminosity. These will provide significant new information about the H particle and constrain further its couplings, as well as providing opportunities to probe directly for other new physics. The LHC will be a hard act to follow.

Acknowledgments

The work of JE was supported partly by the London Centre for Terauniverse Studies (LCTS), using funding from the European Research Council via the Advanced Investigator Grant 267352. The work of TY was supported by a Graduate Teaching Assistantship from King's College London. JE thanks CERN for kind hospitality.

References

[1] ATLAS collaboration, *Observation of a new particle in the search for the Standard Model Higgs boson with the ATLAS detector at the LHC*, *Phys. Lett.* **B 716** (2012) 1 [arXiv:1207.7214] [INSPIRE].

[2] https://twiki.cern.ch/twiki/bin/view/AtlasPublic/HiggsPublicResults.

[3] CMS collaboration, *Observation of a new boson at a mass of 125 GeV with the CMS experiment at the LHC*, *Phys. Lett.* **B 716** (2012) 30 [arXiv:1207.7235] [INSPIRE].

[4] http://cms.web.cern.ch/org/cms-papers-and-results.

[5] P.W. Higgs, *Broken Symmetries and the Masses of Gauge Bosons*, *Phys. Rev. Lett.* **13** (1964) 508 [INSPIRE].

[6] P.W. Higgs, *Spontaneous Symmetry Breakdown without Massless Bosons*, *Phys. Rev.* **145** (1966) 1156 [INSPIRE].

[7] J. Ellis, V. Sanz and T. You, *Prima Facie Evidence against Spin-Two Higgs Impostors*, arXiv:1211.3068 [INSPIRE].

[8] J. Ellis, V. Sanz and T. You, *Associated Production Evidence against Higgs Impostors and Anomalous Couplings*, arXiv:1303.0208 [INSPIRE].

[9] ATLAS collaboration, *Study of the spin of the Higgs-like boson in the two photon decay channel using 20.7 fb^{-1} of pp collisions collected at $\sqrt{s}$ = 8 TeV with the ATLAS detector*, ATLAS-CONF-2013-029 (2013).

[10] M. Chen on behalf of the CMS collaboration, *Combination and Standard Model Scalar Boson Properties in CMS*, talk given at the Rencontres de Moriond Electroweak Session (2013), https://indico.in2p3.fr/getFile.py/access?contribId=15&sessionId=6&resId=0&materialId=slides&confId=7411.

[11] T. Adye on behalf of the ATLAS collaboration, *Measurement of Higgs Boson Properties in ATLAS*, Talk given at the Rencontres de Moriond Electroweak Session (2013), http://moriond.in2p3.fr/QCD/2013/ThursdayMorning/Adye.pdf.

JHEP06(2013)103

[12] CMS collaboration, S. Chatrchyan et al., *On the mass and spin-parity of the Higgs boson candidate via its decays to Z boson pairs*, *Phys. Rev. Lett.* **110** (2013) 081803 [arXiv:1212.6639] [INSPIRE].

[13] M. Baak et al., *Updated Status of the Global Electroweak Fit and Constraints on New Physics*, *Eur. Phys. J.* **C 72** (2012) 2003 [arXiv:1107.0975] [INSPIRE].

[14] J.R. Ellis, G. Ridolfi and F. Zwirner, *Radiative corrections to the masses of supersymmetric Higgs bosons*, *Phys. Lett.* **B 257** (1991) 83 [INSPIRE].

[15] Y. Okada, M. Yamaguchi and T. Yanagida, *Renormalization group analysis on the Higgs mass in the softly broken supersymmetric standard model*, *Phys. Lett.* **B 262** (1991) 54 [INSPIRE].

[16] H.E. Haber and R. Hempfling, *Can the mass of the lightest Higgs boson of the minimal supersymmetric model be larger than m(Z)?*, *Phys. Rev. Lett.* **66** (1991) 1815 [INSPIRE].

[17] Hadron Collider Physics Symposium 2012, http://www.icepp.s.u-tokyo.ac.jp/hcp2012/.

[18] M. Kado on behalf of the ATLAS collaboration, *Physics Jamboree at CERN*, Dec. 13th, 2012, http://indico.cern.ch/getFile.py/access?resId=0&materialId=slides&contribId=0&sessionId=0&subContId=3&confId=218449.

[19] S. Bolognesi on behalf of the CMS collaboration, *Physics Jamboree at CERN*, Dec. 13th, 2012, http://indico.cern.ch/getFile.py/access?resId=0&materialId=slides&contribId=0&sessionId=0&subContId=2&confId=218449.

[20] Rencontres de Moriond 2013 Electroweak Session, https://indico.in2p3.fr/conferenceDisplay.py?confId=7411.

[21] Aspen 2013 - Higgs Quo Vadis, http://indico.cern.ch/conferenceDisplay.py?confId=202554.

[22] Rencontres de Moriond 2013 QCD Session, http://moriond.in2p3.fr/QCD/2013/MorQCD13Prog.html.

[23] D. Carmi, A. Falkowski, E. Kuflik and T. Volansky, *Interpreting LHC Higgs Results from Natural New Physics Perspective*, *JHEP* **07** (2012) 136 [arXiv:1202.3144] [INSPIRE].

[24] A. Azatov, R. Contino and J. Galloway, *Model-Independent Bounds on a Light Higgs*, *JHEP* **04** (2012) 127 [*Erratum ibid.* **1304** (2013) 140] [arXiv:1202.3415] [INSPIRE].

[25] J. Espinosa, C. Grojean, M. Muhlleitner and M. Trott, *Fingerprinting Higgs Suspects at the LHC*, *JHEP* **05** (2012) 097 [arXiv:1202.3697] [INSPIRE].

[26] P.P. Giardino, K. Kannike, M. Raidal and A. Strumia, *Reconstructing Higgs boson properties from the LHC and Tevatron data*, *JHEP* **06** (2012) 117 [arXiv:1203.4254] [INSPIRE].

[27] T. Li, X. Wan, Y.-k. Wang and S.-h. Zhu, *Constraints on the Universal Varying Yukawa Couplings: from SM-like to Fermiophobic*, *JHEP* **09** (2012) 086 [arXiv:1203.5083] [INSPIRE].

[28] M. Rauch, *Determination of Higgs-boson couplings (SFitter)*, arXiv:1203.6826 [INSPIRE].

[29] J. Ellis and T. You, *Global Analysis of Experimental Constraints on a Possible Higgs-Like Particle with Mass* ~ 125 *GeV*, *JHEP* **06** (2012) 140 [arXiv:1204.0464] [INSPIRE].

[30] A. Azatov et al., *Determining Higgs couplings with a model-independent analysis of* $h \to \gamma\gamma$, *JHEP* **06** (2012) 134 [arXiv:1204.4817] [INSPIRE].

JHEP06(2013)103

[31] M. Klute, R. Lafaye, T. Plehn, M. Rauch and D. Zerwas, *Measuring Higgs Couplings from LHC Data*, *Phys. Rev. Lett.* **109** (2012) 101801 [arXiv:1205.2699] [INSPIRE].

[32] L. Wang and X.-F. Han, *The recent Higgs boson data and Higgs triplet model with vector-like quark*, *Phys. Rev.* **D 86** (2012) 095007 [arXiv:1206.1673] [INSPIRE].

[33] D. Carmi, A. Falkowski, E. Kuflik and T. Volansky, *Interpreting the Higgs*, arXiv:1206.4201 [INSPIRE].

[34] M.J. Dolan, C. Englert and M. Spannowsky, *Higgs self-coupling measurements at the LHC*, *JHEP* **10** (2012) 112 [arXiv:1206.5001] [INSPIRE].

[35] J. Chang, K. Cheung, P.-Y. Tseng and T.-C. Yuan, *Distinguishing Various Models of the 125 GeV Boson in Vector Boson Fusion*, *JHEP* **12** (2012) 058 [arXiv:1206.5853] [INSPIRE].

[36] S. Chang, C.A. Newby, N. Raj and C. Wanotayaroj, *Revisiting Theories with Enhanced Higgs Couplings to Weak Gauge Bosons*, *Phys. Rev.* **D 86** (2012) 095015 [arXiv:1207.0493] [INSPIRE].

[37] I. Low, J. Lykken and G. Shaughnessy, *Have We Observed the Higgs (Imposter)?*, *Phys. Rev.* **D 86** (2012) 093012 [arXiv:1207.1093] [INSPIRE].

[38] T. Corbett, O. Eboli, J. Gonzalez-Fraile and M. Gonzalez-Garcia, *Constraining anomalous Higgs interactions*, *Phys. Rev.* **D 86** (2012) 075013 [arXiv:1207.1344] [INSPIRE].

[39] P.P. Giardino, K. Kannike, M. Raidal and A. Strumia, *Is the resonance at 125 GeV the Higgs boson?*, *Phys. Lett.* **B 718** (2012) 469 [arXiv:1207.1347] [INSPIRE].

[40] M. Montull and F. Riva, *Higgs discovery: the beginning or the end of natural EWSB?*, *JHEP* **11** (2012) 018 [arXiv:1207.1716] [INSPIRE].

[41] J. Espinosa, C. Grojean, M. Muhlleitner and M. Trott, *First Glimpses at Higgs' face*, *JHEP* **12** (2012) 045 [arXiv:1207.1717] [INSPIRE].

[42] D. Carmi, A. Falkowski, E. Kuflik, T. Volansky and J. Zupan, *Higgs After the Discovery: A Status Report*, *JHEP* **10** (2012) 196 [arXiv:1207.1718] [INSPIRE].

[43] S. Banerjee, S. Mukhopadhyay and B. Mukhopadhyaya, *New Higgs interactions and recent data from the LHC and the Tevatron*, *JHEP* **10** (2012) 062 [arXiv:1207.3588] [INSPIRE].

[44] F. Bonnet, T. Ota, M. Rauch and W. Winter, *Interpretation of precision tests in the Higgs sector in terms of physics beyond the Standard Model*, *Phys. Rev.* **D 86** (2012) 093014 [arXiv:1207.4599] [INSPIRE].

[45] T. Plehn and M. Rauch, *Higgs Couplings after the Discovery*, *Europhys. Lett.* **100** (2012) 11002 [arXiv:1207.6108] [INSPIRE].

[46] A. Djouadi, *Precision Higgs coupling measurements at the LHC through ratios of production cross sections*, arXiv:1208.3436 [INSPIRE].

[47] B. Batell, S. Gori and L.T. Wang, *Higgs couplings and precision electroweak data*, arXiv:1209.6832.

[48] G. Moreau, *Constraining extra-fermion(s) from the Higgs boson data*, *Phys. Rev.* **D 87** (2013) 015027 [arXiv:1210.3977] [INSPIRE].

[49] G. Cacciapaglia, A. Deandrea, G.D. La Rochelle and J.-B. Flament, *Higgs couplings beyond the Standard Model*, *JHEP* **03** (2013) 029 [arXiv:1210.8120] [INSPIRE].

[50] E. Masso and V. Sanz, *Limits on Anomalous Couplings of the Higgs to Electroweak Gauge Bosons from LEP and LHC*, *Phys. Rev.* **D 87** (2013) 033001 [arXiv:1211.1320] [INSPIRE].

JHEP06(2013)103

[51] T. Corbett, O. Eboli, J. Gonzalez-Fraile and M. Gonzalez-Garcia, *Robust Determination of the Higgs Couplings: Power to the Data*, *Phys. Rev.* **D 87** (2013) 015022 [arXiv:1211.4580] [INSPIRE].

[52] R.T. D'Agnolo, E. Kuflik and M. Zanetti, *Fitting the Higgs to Natural SUSY*, *JHEP* **03** (2013) 043 [arXiv:1212.1165] [INSPIRE].

[53] A. Azatov and J. Galloway, *Electroweak Symmetry Breaking and the Higgs Boson: Confronting Theories at Colliders*, *Int. J. Mod. Phys.* **A 28** (2013) 1330004 [arXiv:1212.1380] [INSPIRE].

[54] G. Bhattacharyya, D. Das and P.B. Pal, *Modified Higgs couplings and unitarity violation*, *Phys. Rev.* **D 87** (2013) 011702 [arXiv:1212.4651] [INSPIRE].

[55] D. Choudhury, R. Islam, A. Kundu and B. Mukhopadhyaya, *Anomalous Higgs Couplings as a Window to New Physics*, arXiv:1212.4652 [INSPIRE].

[56] R.S. Gupta, M. Montull and F. Riva, *SUSY Faces its Higgs Couplings*, *JHEP* **04** (2013) 132 [arXiv:1212.5240] [INSPIRE].

[57] G. Bélanger, B. Dumont, U. Ellwanger, J. Gunion and S. Kraml, *Higgs Couplings at the End of 2012*, *JHEP* **02** (2013) 053 [arXiv:1212.5244] [INSPIRE].

[58] K. Cheung, J.S. Lee and P.-Y. Tseng, *Higgs Precision (Higgcision) Era begins*, *JHEP* **05** (2013) 134 [arXiv:1302.3794] [INSPIRE].

[59] J. Ellis and T. You, *Global Analysis of the Higgs Candidate with Mass ∼ 125 GeV*, *JHEP* **09** (2012) 123 [arXiv:1207.1693] [INSPIRE].

[60] A. Falkowski, F. Riva and A. Urbano, *Higgs at Last*, arXiv:1303:1812.

[61] P.P. Giardino, K. Kannike, I. Masina, M. Raidal and A. Strumia, *The universal Higgs fit*, arXiv:1303.3570 [INSPIRE].

[62] ATLAS collaboration, *Combined coupling measurements of the Higgs-like boson with the ATLAS detector using up to 25 fb^{-1} of proton-proton collision data*, ATLAS-CONF-2013-034 (2013).

[63] CMS collaboration, *CMS Physics Analysis Summary*, HIG-13-005-pas http://cds.cern.ch/record/1542387/files/HIG-13-005-pas.pdf.

[64] LHC. Higgs Cross section Working Group, *LHC HXSWG interim recommendations to explore the coupling structure of a Higgs-like particle*, arXiv:1209.0040 [INSPIRE].

[65] F. Englert and R. Brout, *Broken Symmetry and the Mass of Gauge Vector Mesons*, *Phys. Rev. Lett.* **13** (1964) 321 [INSPIRE].

[66] P.W. Higgs, *Broken symmetries, massless particles and gauge fields*, *Phys. Lett.* **12** (1964) 132 [INSPIRE].

[67] G. Guralnik, C. Hagen and T. Kibble, *Global Conservation Laws and Massless Particles*, *Phys. Rev. Lett.* **13** (1964) 585 [INSPIRE].

[68] W. Yao on behalf of the TeVatron collaboration, *Tevatron Combination and BEH properties*, Talk given at the Rencontres de Moriond Electroweak Session (2013), https://indico.in2p3.fr/getFile.py/access?contribId=69&sessionId=6&resId=0&materialId=slides&confId=7411.

[69] CMS collaboration, *Update on the search for the standard model Higgs boson in pp collisions at the LHC decaying to W+W? in the fully leptonic final state*, http://cds.cern.ch/record/1449158/files/HIG-12-003-pas.pdf.

JHEP06(2013)103

[70] CMS collaboration, *Evidence for a particle decaying to W+W? in the fully leptonic final state in a standard model Higgs boson search in pp collisions at the LHC*, http://cds.cern.ch/record/1493602/files/HIG-12-042-pas.pdf.

[71] CMS collaboration, *Observation of a new boson with a mass near 125 GeV*, http://cds.cern.ch/record/1460438/files/HIG-12-020-pas.pdf.

[72] ATLAS collaboration, *Measurements of the properties of the Higgs-like boson in the $WW^{(*)} \to \ell\nu\ell\nu$ decay channel with the ATLAS detector using 25 fb^{-1} of proton-proton collision data*, ATLAS-CONF-2013-030 (2013).

[73] CMS collaboration, *Combination of standard model Higgs boson searches and measurements of the properties of the new boson with a mass near 125 GeV*, http://cds.cern.ch/record/1494149/files/HIG-12-045-pas.pdf.

[74] ATLAS collaboration, *Search for the Standard Model Higgs boson in produced in association with a vector boson and decaying to bottom quarks with the ATLAS detector*, ATLAS-CONF-2012-161 (2012).

[75] ATLAS collaboration, *Search for the Standard Model Higgs boson in $H \to \tau^+\tau^-$ decays in proton-proton collisions with the ATLAS detector*, ATLAS-CONF-2012-160 (2012).

[76] CMS collaboration, *Search for the standard model Higgs boson decaying to tau pairs*, http://cds.cern.ch/record/1493615/files/HIG-12-043-pas.pdf.

[77] CMS collaboration, *Evidence for a new state decaying into two photons in the search for the standard model Higgs boson in pp collisions*, http://cds.cern.ch/record/1460419/files/HIG-12-015-pas.pdf.

[78] G. Giudice, C. Grojean, A. Pomarol and R. Rattazzi, *The Strongly-Interacting Light Higgs*, *JHEP* **06** (2007) 045 [hep-ph/0703164] [INSPIRE].

[79] R. Contino, C. Grojean, M. Moretti, F. Piccinini and R. Rattazzi, *Strong Double Higgs Production at the LHC*, *JHEP* **05** (2010) 089 [arXiv:1002.1011] [INSPIRE].

[80] R. Contino, *The Higgs as a Composite Nambu-Goldstone Boson*, arXiv:1005.4269 [INSPIRE].

[81] R. Grober and M. Muhlleitner, *Composite Higgs Boson Pair Production at the LHC*, *JHEP* **06** (2011) 020 [arXiv:1012.1562] [INSPIRE].

[82] S. Biswas, E. Gabrielli and B. Mele, *Single top and Higgs associated production as a probe of the Htt coupling sign at the LHC*, *JHEP* **01** (2013) 088 [arXiv:1211.0499] [INSPIRE].

[83] M. Farina, C. Grojean, F. Maltoni, E. Salvioni and A. Thamm, *Lifting degeneracies in Higgs couplings using single top production in association with a Higgs boson*, *JHEP* **05** (2013) 022 [arXiv:1211.3736] [INSPIRE].

[84] V. Barger, M. Ishida and W.-Y. Keung, *Total Width of 125 GeV Higgs Boson*, *Phys. Rev. Lett.* **108** (2012) 261801 [arXiv:1203.3456] [INSPIRE].

[85] B.A. Dobrescu and J.D. Lykken, *Coupling spans of the Higgs-like boson*, *JHEP* **02** (2013) 073 [arXiv:1210.3342] [INSPIRE].

[86] J.R. Espinosa, M. Muhlleitner, C. Grojean and M. Trott, *Probing for Invisible Higgs Decays with Global Fits*, *JHEP* **09** (2012) 126 [arXiv:1205.6790] [INSPIRE].

[87] G. Bélanger, B. Dumont, U. Ellwanger, J. Gunion and S. Kraml, *Status of invisible Higgs decays*, *Phys. Lett.* **B 723** (2013) 340 [arXiv:1302.5694] [INSPIRE].

JHEP06(2013)103

3 Constraining Higgs Properties in Associated Production

KCL-PH-TH/2013-31

Constraining Higgs Properties in Associated Production[a]

Tevong You
Theoretical Particle Physics and Cosmology Group, Physics Department,
King's College London, London WC2R 2LS, UK

The Higgs boson H produced in association with a vector boson $V = W^{\pm}, Z$ is the main production mechanism for searches at the Tevatron and forms an important part of Higgs analyses at the LHC. We show here that the $V+H$ invariant mass distribution and the energy dependence of associated production provide powerful ways of constraining Higgs properties, such as its spin-parity and dimension-6 operator coefficients.

1 Introduction

Following the historic discovery of a Higgs boson at the LHC [1], accompanied by strong evidence from the Tevatron [2], attention now turns towards the question whether it is indeed *the* Higgs particle of the Standard Model (SM). The question is: to what extent does the current data allow us to infer that this is a spin-zero elementary scalar with even parity responsible for breaking the electroweak symmetry?

It was first noted by Miller et al. [3] that the $e^+e^- \to V + X$ reaction would be sensitive to the spin-parity of the X due to the different threshold behaviour of the $V + X$ invariant mass distribution. In Section 2 we consider this process at hadron colliders and find that the discriminating power of associated production remains after simulating typical cuts at the LHC and Tevatron. In particular the D0 experiment at the latter is already able to exclude a spin two hypothesis at 99.9% CL using this method in the $H \to b\bar{b}$ channel alone [4]. In Section 3 the point is made that the observation of a signal at the Tevatron and LHC already strongly exclude spin two, as well as placing competitive limits on dimension-6 operator coefficients. This is due to the different energy dependence of associated production for the various hypotheses. We conclude in Section 4.

The work on which this contribution to the conference proceedings was based on can be found in Ellis et al. [5] [6].

2 $V + X$ Invariant Mass Distribution

On Fig. 1 the different $Z + X$ invariant mass distribution at the parton level for J^P spin-parity hypotheses $0^+, 0^-$ and 2^+ is plotted in solid black, dotted pink and dashed blue lines respectively. The simulation was performed in MadGraph, with more information and details of the model implementation in Ellis et al. [5]. The figure clearly shows a difference between the scenarios at both the LHC and Tevatron, which can be understood by the production being an s-wave process for the 0^+ case, whereas for 0^- this is p-wave and 2^+ contains d-wave contributions. This difference survives the experimental cuts as illustrated for example in Fig. 2 for the 2-lepton channel at D0 and CMS, with the the background from $Z + b\bar{b}$ in green.

[a] Talk given on May 2013 at the 25^{th} *Rencontres de Blois*.

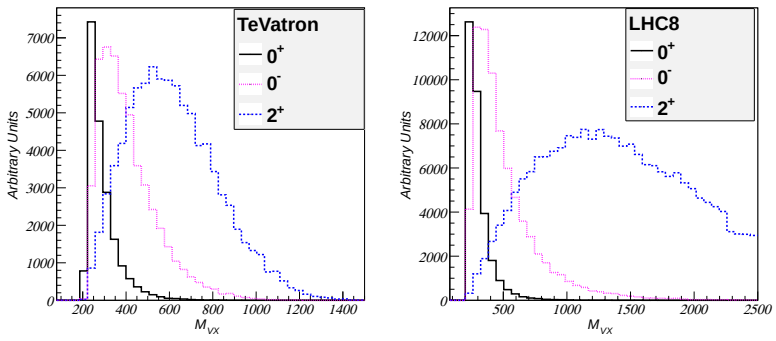

Figure 1: *Parton-level distribution of the $Z + X$ invariant mass for the $J^P = 0^+, 0^-, 2^+$ hypotheses in solid black, dotted pink and dashed blue lines respectively, at the Tevatron on the left and LHC at 8 TeV on the right.*

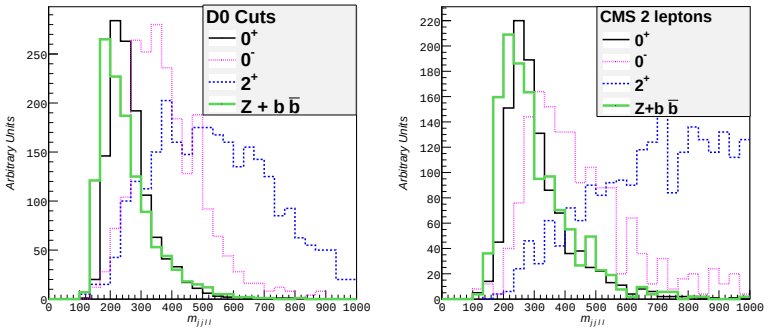

Figure 2: *Distribution after cuts of the $Z + X$ invariant mass in the 2-lepton channel for the $J^P = 0^+, 0^-, 2^+$ hypotheses in solid black, dotted pink and dashed blue lines respectively, for D0 on the left and CMS at 8 TeV on the right. The $Z + b\bar{b}$ background is shown in green.*

The 0-,1- and 2-lepton channels at D0, CDF, CMS and ATLAS are simulated with experimental cuts (assuming no backgrounds) with the separation significance between two hypotheses A and B quantified by a log-likelihood ratio

$$\Lambda = -2ln\left(\frac{\mathcal{L}_A}{\mathcal{L}_B}\right) \quad , \tag{1}$$

where the likelihood for a spin hypothesis s is obtained by multiplying the probability distribution function

$$\mathcal{L}_s = \prod_i pdf_s(x_i) \tag{2}$$

for each event x_i in a 'toy' simulation. Running a set of toys for the number of events after cuts expected for each experimental analysis generates a distribution in our test statistic Λ. Quantifying the separation significance between the two distributions in numbers of σ, we list in Table 1 the results for the various hypotheses in each search category, as well as their combination.

Note that this is for the ideal case of a perfectly clean extracted signal, since we are assuming no backgrounds. However the s/b ratio at the Tevatron in the $H \to b\bar{b}$ channel is low enough to expect good sensitivity, and indeed a recent analysis of the invariant mass distribution by the D0 collaboration has excluded the spin 2^+ hypothesis with graviton-like couplings with 3.1σ significance [4].

Experiment	Category	Hypothesis A	Hypothesis B	Significance in σ
CDF	0l	0^+	$2^+(0^-)$	3.7 (1.3)
	1l	0^+	$2^+(0^-)$	2.5 (1.0)
	2l	0^+	$2^+(0^-)$	1.4 (0.78)
	Combined	0^+	$2^+(0^-)$	4.8 (1.6)
D0	0l	0^+	$2^+(0^-)$	3.5 (1.2)
	2l	0^+	$2^+(0^-)$	1.8 (1.2)
	Combined	0^+	$2^+(0^-)$	4.0 (1.6)
ATLAS	2l	0^+	$2^+(0^-)$	2.4 (1.1)
CMS	2l	0^+	$2^+(0^-)$	2.3 (0.70)

Table 1: *Estimated separation significance between different J^P hypotheses at the Tevatron and LHC.*

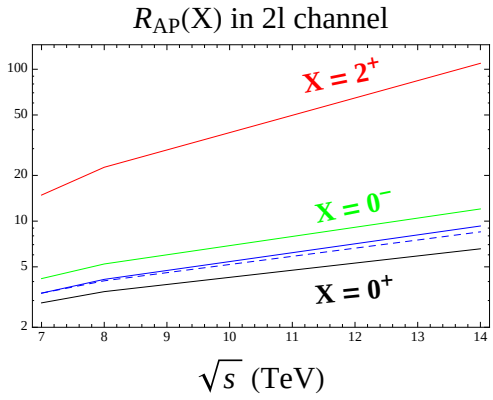

Figure 3: *Ratio of the LHC signal strength relative to the Tevatron vs LHC energy for associated production $Z+X$ in the 2-lepton channel, after experimental cuts. The solid black, green and red line denote $J^P = 0^+, 0^-$ and 2^+ respectively, while the solid blue line is the dimension-6 contribution with $\epsilon_W = 1$.*

3 Energy Dependence of Associated Production

More information can be teased out of the fact that the Tevatron and LHC see a signal at different energies. The couplings of a pseudoscalar A or graviton-like particle $G^{\mu\nu}$ have a different energy dependence to a SM Higgs due to their derivative couplings

$$\mathcal{L}_{0^-} \sim A F_{\mu\nu}\tilde{F}^{\mu\nu} \quad , \quad \mathcal{L}_{2^+} \sim G^{\mu\nu} T_{\mu\nu} \quad . \tag{3}$$

The ratio of the signal strength in the 2-lepton channel at the LHC relative to the Tevatron is shown in Fig. 3 as a function of LHC energy for the $0^+, 0^-$ and 2^+ hypotheses in black, green and red respectively. Note that this is including experimental cuts, with the 0-,1-lepton cases exhibiting an even stronger energy dependence. We refer the reader to Ellis et al. [6] for more details of the calculation. The signal expected at the LHC for a 2^+ particle would be an order of magnitude larger than that of the Higgs. Since the observed signal strength is close to SM expectation within errors, this immediately provides evidence disfavouring such an interpretation.

For example at the 8 TeV LHC the ratio of the signal strength at the LHC relative to the Tevatron for the spin 2^+ hypothesis divided by the same ratio for the SM 0^+ hypothesis gives a double ratio of $\mathcal{R}_{2^+/0^+} = 7.4$. The observed double ratio extracted from the measured signal strength data yields $\mathcal{R}_{data} = 0.47 \pm 0.58$..

This same method allows us to constrain the SM as an effective theory, in which higher-dimensional operators involving the Higgs contribute to measurable processes. In this case the

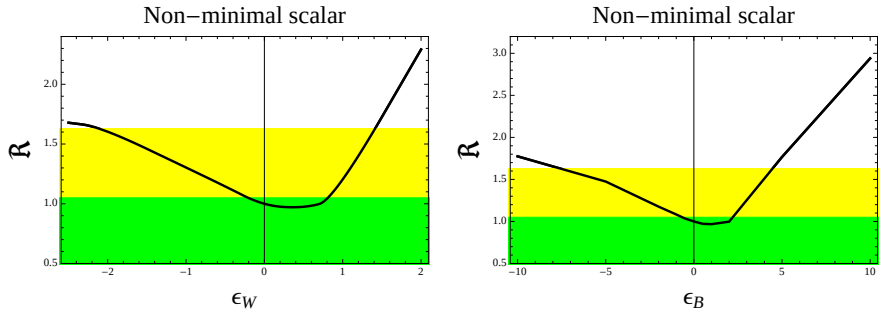

Figure 4: *Double ratio $\mathcal{R}$ of the energy growth for dimension-6 operator contributions relative to that of a SM Higgs as a function ofϵ_W on the left and ϵ_B on the right. The experimental one and two sigma limits are shown as green and yellow bands.*

derivative couplings of the Higgs doublet Φ in the operators

$$\mathcal{O}_W = (D_\mu \Phi)^\dagger \widehat{W}^{\mu\nu} (D_\nu \Phi) \quad , \quad \mathcal{O}_B = (D_\mu \Phi)^\dagger (D_\nu \Phi) \widehat{B}^{\mu\nu} \quad , \tag{4}$$

are responsible for the energy dependence. Fig. 4 plots the double ratio $\mathcal{R}$ as a function of the operator coefficients $\epsilon_{W,B} \equiv f_{W,B} \frac{v^2}{\Lambda^2}$, with the experimental 1- and 2-σ bands shown in green and yellow. The 95% CL limits on $\epsilon_{W,B}$ can be read off as

$$\epsilon_W \in [-2.2, 1.4] \quad , \quad \epsilon_B \in [-7.5, 4.4] \quad . \tag{5}$$

4 Conclusion

The invariant mass distribution of the $V + H$ associated production mechanism provides a good discriminating variable to investigate further the properties of the newly-discovered particle. We have seen that this provides another handle on spin-parity measurements, with the D0 experiment at the Tevatron able to use this method to exclude spin 2^+ at 99.9% CL. We also showed how the energy dependence of this mode gives a complementary way of disfavouring a graviton-like particle or a pseudoscalar. Limits were placed on the coefficients of dimension-6 operators with derivative couplings that affect this energy dependence.

Acknowledgments

The author thanks the organisers of the 25th Rencontres de Blois for the invitation to talk at an enjoyable and stimulating meeting, as well as John Ellis, Dae Sung Hwang and Veronica Sanz, with whom this work was carried out.

References

1. G. Aad *et al.* [ATLAS Collaboration], Phys. Lett. B **716** (2012) 1 [arXiv:1207.7214 [hep-ex]]; S. Chatrchyan *et al.* [CMS Collaboration], Phys. Lett. B **716** (2012) 30 [arXiv:1207.7235 [hep-ex]].
2. T. Aaltonen *et al.* [CDF and D0 Collaborations], Phys. Rev. Lett. **109** (2012) 071804 [arXiv:1207.6436 [hep-ex]].
3. D. J. Miller, S. Y. Choi, B. Eberle, M. M. Muhlleitner and P. M. Zerwas, *Measuring the spin of the Higgs boson,* Phys. Lett. B **505** (2001) 149 [hep-ph/0102023].
4. The D0 Collaboration, CONF-6387 (2013).
5. J. Ellis, D. S. Hwang, V. Sanz and T. You, JHEP **1211** (2012) 134 [arXiv:1208.6002 [hep-ph]].
6. J. Ellis, V. Sanz and T. You, Eur. Phys. J. C **73** (2013) 2507 [arXiv:1303.0208 [hep-ph]].

4 Complete Higgs Sector Constraints on Dimension-6 Operators

Published for SISSA by Springer

Received: April 24, 2014
Revised: May 20, 2014
Accepted: May 21, 2014
Published: July 8, 2014

Complete Higgs sector constraints on dimension-6 operators

John Ellis,[a,b] **Verónica Sanz**[c] **and Tevong You**[a]

[a] *Theoretical Particle Physics and Cosmology Group, Physics Department, King's College London, London WC2R 2LS, U.K.*
[b] *TH Division, Physics Department, CERN, CH-1211 Geneva 23, Switzerland*
[c] *Department of Physics and Astronomy, University of Sussex, Brighton BN1 9QH, U.K.*

E-mail: john.ellis@cern.ch, v.sanz@sussex.ac.uk, tevong.you@kcl.ac.uk

Abstract: Constraints on the full set of Standard Model dimension-6 operators have previously used triple-gauge couplings to complement the constraints obtainable from Higgs signal strengths. Here we extend previous analyses of the Higgs sector constraints by including information from the associated production of Higgs and massive vector bosons (H+V production), which excludes a direction of limited sensitivity allowed by partial cancellations in the triple-gauge sector measured at LEP. Kinematic distributions in H+V production provide improved sensitivity to dimension-6 operators, as we illustrate here with simulations of the invariant mass and p_T distributions measured by D0 and ATLAS, respectively. We provide bounds from a global fit to a complete set of CP-conserving operators affecting Higgs physics.

Keywords: Higgs Physics, Beyond Standard Model, Standard Model

ArXiv ePrint: 1404.3667

doi:10.1007/JHEP07(2014)036

JHEP07(2014)036

Contents

1 Introduction

The investigation of the properties of the recently-discovered Higgs boson [1, 2] proceeded initially by characterizing its signal strength relative to the Standard Model (SM) expectation [3, 4], with many studies refining this picture to constrain deviations in the Higgs couplings under various assumptions [5–44]. Although the signal strengths and pattern of couplings provided some information about the spin and parity of the Higgs boson [45], it was through the use of differential kinematic distributions that different Lorentz structures could be probed most thoroughly [46–70]. The evidence now indicates convincingly [71–73] that we are dealing with a spin-zero, positive-parity particle, as expected for the Higgs boson responsible for electroweak symmetry breaking.

Moreover, there is no significant indication of any deviation of the dimension-4 couplings of this particle from those expected in the SM. Studies of these couplings continue, and are being supplemented by searches for anomalous couplings that could arise from new physics in the electroweak sector. If this new physics is decoupled at some heavy scale, then the effects of these interactions are cohesively captured by supplementing the SM Lagrangian with higher-dimensional operators involving multiple fields and/or derivative interactions in an effective field theory (EFT) framework[1] [74–78].

[1] For a recent short review, see [79].

JHEP07(2014)036

Constraints on these operators have been placed for subsets of operators [80–89] and in full global fits both before [90] and after [91–93] the Higgs discovery.[2] Many strong constraints come from electroweak precision tests (EWPT) [94–96] at LEP, and from triple-gauge coupling (TGC) [91, 92, 97] measurements at LEP and the LHC. In the case of Higgs observables, aside from operators contributing to couplings that are absent at tree-level in the SM, only weaker limits are available so far. Some combinations of these operators enter into EWPT and TGC, but the presence of a poorly constrained direction [98] in measurements of the latter means that constraints on dimension-6 operators from Higgs physics are complementary and not redundant within the EFT framework. Constraints from EWPT on operators that contribute at loop level rely on assuming no unnatural cancellations [99–105], with unambiguous bounds being far weaker [106, 107]. Thus, it is desirable to refine as much as possible the analysis of the Higgs sector [108].

We illustrate here the power of associated $H + V$ production and its differential kinematic distributions to constrain CP-conserving dimension-6 operators within the EFT framework. In particular, we note that the distribution of the $H + V$ invariant mass, m_{VH}, measured by D0 [109] and the vector-boson transverse momentum, p_T^V, distribution measured by ATLAS [110] in the associated production channel $V + H \to V\bar{b}b$ have very low backgrounds in the higher mass and p_T bins, respectively, where higher-dimension operators would contribute. These searches are, therefore, ideal for constraining the boosted signature of new physics that could arise from dimension-6 operators, despite the large uncertainties in the total signal strength [111, 112]. Moreover, we find that the inclusion of associated production at D0 and ATLAS removes certain degeneracies in a complete fit to the full set of operators affecting Higgs physics.

In the following section we introduce the CP-even dimension-6 operators that affect Higgs physics. In section 3.1 we constrain one operator using the m_{VH} distribution of $VH \to V\bar{b}b$ in the $V \to$ 0-, 1- and 2-lepton sub-channels used in the D0 search, quantifying the improvement obtained by using differential information, and we do the same using the ATLAS p_T^V distribution in section 3.2. In section 4 we combine these channels and make a multi-parameter fit to obtain global constraints from the Higgs sector. Section 5 summarizes our conclusions. Details of the analysis implementations for D0 and ATLAS can be found in the appendices.

2 Dimension-6 operators in the Higgs sector

In the basis of [113–116], the CP-even dimension-6 Lagrangian involving Higgs doublets may be written as

$$\mathcal{L} \supset \frac{\bar{c}_H}{2v^2}\partial^\mu\left[\Phi^\dagger\Phi\right]\partial_\mu\left[\Phi^\dagger\Phi\right] + \frac{g'^2\,\bar{c}_\gamma}{m_W^2}\Phi^\dagger\Phi B_{\mu\nu}B^{\mu\nu} + \frac{g_s^2\,\bar{c}_g}{m_W^2}\Phi^\dagger\Phi G^a_{\mu\nu}G_a^{\mu\nu}$$
$$+\frac{2ig\,\bar{c}_{HW}}{m_W^2}\left[D^\mu\Phi^\dagger T_{2k}D^\nu\Phi\right]W^k_{\mu\nu} + \frac{ig'\,\bar{c}_{HB}}{m_W^2}\left[D^\mu\Phi^\dagger D^\nu\Phi\right]B_{\mu\nu}$$

[2] Ref. [93] in particular includes a full set of operators in the EWPT sector.

JHEP07(2014)036

$$+\frac{ig\ \bar{c}_W}{m_W^2}\left[\Phi^\dagger T_{2k}\overleftrightarrow{D}^\mu\Phi\right]D^\nu W^k_{\mu\nu}+\frac{ig'\ \bar{c}_B}{2m_W^2}\left[\Phi^\dagger\overleftrightarrow{D}^\mu\Phi\right]\partial^\nu B_{\mu\nu}$$
$$+\frac{\bar{c}_t}{v^2}y_t\Phi^\dagger\Phi\ \Phi^\dagger\cdot\bar{Q}_L t_R+\frac{\bar{c}_b}{v^2}y_b\Phi^\dagger\Phi\ \Phi\cdot\bar{Q}_L b_R+\frac{\bar{c}_\tau}{v^2}y_\tau\ \Phi^\dagger\Phi\ \Phi\cdot\bar{L}_L\tau_R\,. \tag{2.1}$$

We note that $\bar{c}_T$ corresponds to the $\hat{T}$ parameter, which is constrained at the per-mille level by EWPT, and $\bar{c}_6$ only affects the Higgs self-coupling, so we drop these from our analysis. The linear combination $\bar{c}_W+\bar{c}_B$ is related to the $\hat{S}$ parameter, which is also bounded at the per-mille level, so we set $\bar{c}_B=-\bar{c}_W$. The independent set of parameters affecting Higgs physics is thereby reduced to

$$\bar{c}_i\equiv\{\bar{c}_H,\bar{c}_{t,b,\tau},\bar{c}_W,\bar{c}_{HW},\bar{c}_{HB},\bar{c}_\gamma,\bar{c}_g\}\,. \tag{2.2}$$

The other dimension-6 operators enter either in EWPT or TGC observables, but do not affect the Higgs sector. For an analysis of the above operators and TGCs, see ref. [91, 92, 97].

A more phenomenological and experimentally transparent approach is often used in the form of an effective Lagrangian with anomalous Higgs couplings. Experimental bounds expressed in terms of anomalous couplings may then be related to other more theoretically-motivated effective theories or models, which has proven to be a useful approach for EWPT and TGCs. For example, following ref. [117], the relevant subset of the Higgs anomalous couplings in the mass basis and unitary gauge includes

$$\begin{aligned}\mathcal{L}\supset\ &-\frac{1}{4}g^{(1)}_{HZZ}Z_{\mu\nu}Z^{\mu\nu}h-g^{(2)}_{HZZ}Z_\nu\partial_\mu Z^{\mu\nu}h\\&-\frac{1}{2}g^{(1)}_{HWW}W^{\mu\nu}W^\dagger_{\mu\nu}h-\left[g^{(2)}_{HWW}W^\nu\partial^\mu W^\dagger_{\mu\nu}h+\text{h.c.}\right],\end{aligned} \tag{2.3}$$

with the relation between these anomalous coupling coefficients and the dimension-6 coefficients in our basis given by

$$\begin{aligned}g^{(1)}_{hzz}&=\frac{2g}{c_W^2m_W}\left[\bar{c}_{HB}s_W^2-4\bar{c}_\gamma s_W^4+c_W^2\bar{c}_{HW}\right]\\g^{(2)}_{hzz}&=\frac{2g}{c_W^2m_W}\left[(\bar{c}_{HW}+\bar{c}_W)c_W^2+(\bar{c}_{HB}+\bar{c}_B)s_W^2\right]\\g^{(1)}_{hww}&=\frac{2g}{m_W}\bar{c}_{HW}\\g^{(2)}_{hww}&=\frac{g}{m_W}(\bar{c}_W+\bar{c}_{HW})\,.\end{aligned} \tag{2.4}$$

We refer the reader to ref. [117] for more details and a complete list of Higgs anomalous couplings.

We calculate the effects of the dimension-6 operators on $V+H$ associated production by Monte-Carlo (MC) simulations using `MadGraph5 v2.1.0` [118] interfaced with `Pythia` [119] and `Delphes v3` [120], combined with the dimension-6 model implementation developed in [117]. We start with $\bar{c}_W$ as an illustrative example, switching off all other coefficients, before considering briefly $\bar{c}_{HW}$ and then the full set of coefficients (2.2) in a global fit.

JHEP07(2014)036

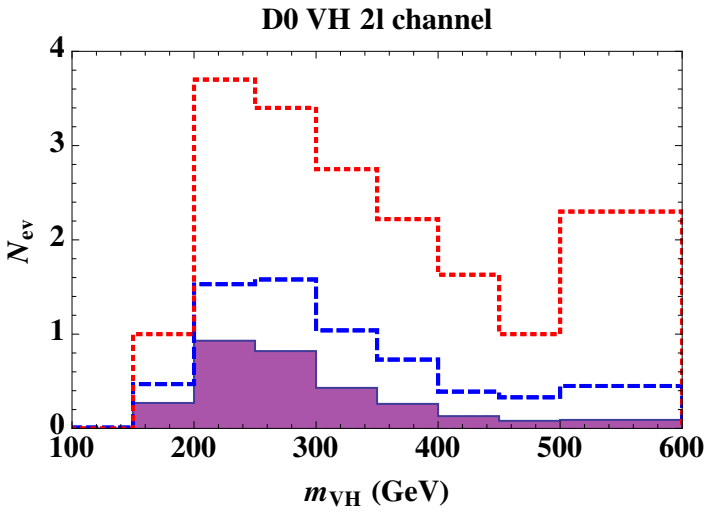

Figure 1. Simulation of the m_{VH} distribution in $(V \to 2\ell) + (H \to \bar{b}b)$ events at the Tevatron after implementing D0 cuts, obtained using `MadGraph v2.1.0` interfaced with `Pythia` and `Delphes v3`, combined with the dimension-6 model implementation developed in [117]. The solid distribution is the SM expectation, while the red-dotted and blue-dashed lines correspond to the distributions with $\bar{c}_W$ =0.1 and 0.035, respectively.

3 Kinematic distributions in $H + V$ production

3.1 The $H + V$ invariant mass distribution measured by D0

It was pointed out in [121], see also [111, 112], that the invariant mass distribution in $H + V$ events could be used to discriminate between minimally-coupled $J^P = 0^+, 0^-$ and graviton-like 2^+ spin-parity assignments for the H particle. Subsequently, the D0 Collaboration has made available the observed $H + V$ invariant mass distribution as well as those expected in these scenarios [109]. Here we use their background distribution and simulate the signal events for a SM Higgs including the effects of non-zero dimension-6 coefficients, considering separately the 2-, 1- and 0-lepton channels for the decays of vector bosons $V = Z, W^\pm$ produced in association with H decaying to $b\bar{b}$.

Implementation details of the simulation can be found in appendix A. Summing the cross-section times efficiency over the 0-, 1- and 2-lepton channels, we obtain the following signal strength as a function of $\bar{c}_W$ for $VH \to V\bar{b}b$ at D0,

$$\mu_{H\bar{b}b} \simeq 1 + 29\bar{c}_W ,$$

indicating a strong dependence of the signal strength on the coefficient of the dimension-6 operator, which compensates for the relatively large error bar in the D0 measurement of this channel. We find that the best-fit signal strength $\mu_{H\bar{b}b} = 1.2 \pm 1.2$ reported by D0 [109] yields the following 95% CL bounds in a χ^2 fit:

$$\bar{c}_W \in [-0.15, 0.09] .$$

More information can be obtained from the differential kinematic distribution for $H + V$ production by considering the measurements in bins in m_{VH}, which affords full sensitivity

JHEP07(2014)036

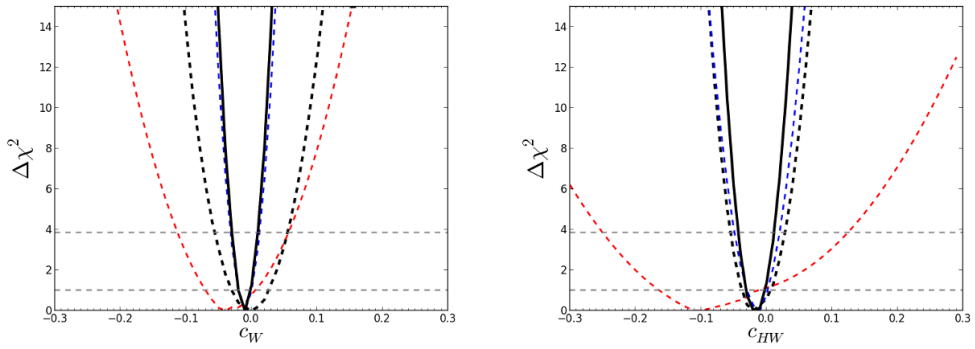

Figure 2. The one-dimensional fit to the parameter $\bar{c}_W$ (left panel) and to $\bar{c}_{HW}$ (right panel). In each panel, the dashed-red line corresponds to the constraint from the 0-, 1- and 2-lepton D0 m_{VH} distribution including all bins, the dashed-blue line to the 0-, 1- and 2-lepton ATLAS p_T^V distribution using the last bin only, the dashed-black is the combination of CMS and ATLAS signal strengths in all channels except VH, and the solid-black is the combination of all the above.

to $\bar{c}_W$ via the differential information available in the invariant mass distribution, particularly in the higher-mass bins where the signal-to-background ratio increases most rapidly. The invariant mass distribution found in our simulation is plotted for the 2-lepton case in figure 1 for various values of $\bar{c}_W$. As expected, the effect of the dimension-6 operator is to generate a larger tail at high invariant masses than in the SM.

We include the information from signal strength and differential distribution by constructing a χ^2 function with a contribution from each m_{VH} bin. We treat the errors provided as Gaussian, neglecting any correlations between bins as this information is not available. Since the sensitivity of the distribution analysis is largely driven by the last bin, the sensitivity of the limit to correlations is minimal. The resulting improved bounds are

$$\bar{c}_W \in [-0.11, 0.06]\,. \tag{3.1}$$

The χ^2 distribution from this constraint is shown as the dashed-red line in the left panel of figure 2.

This limit, using differential information, is better than the more inclusive observable μ_{HV} by 15-20 %. A better understanding of the tail in the kinematic distribution could improve considerably this limit. However, the Tevatron analysis is limited by statistics, whereas the LHC experiments benefit from increased energy, which expands the available phase space and hence enhances the effect of anomalous couplings, with the prospect also of future improvements in statistical significance. The study of constraints from Run 1 of the LHC at 8 TeV is the subject of the next section.

3.2 The vector-boson transverse-momentum distribution measured by ATLAS

The fact that dimension-6 operators generate a larger tail at higher invariant masses by modifying the production kinematics implies greater sensitivity at the LHC, where the higher energy opens up the available phase space. Since the $V + H$ invariant mass distribution is not available, we make use here of the transverse momentum of the vector boson,

JHEP07(2014)036

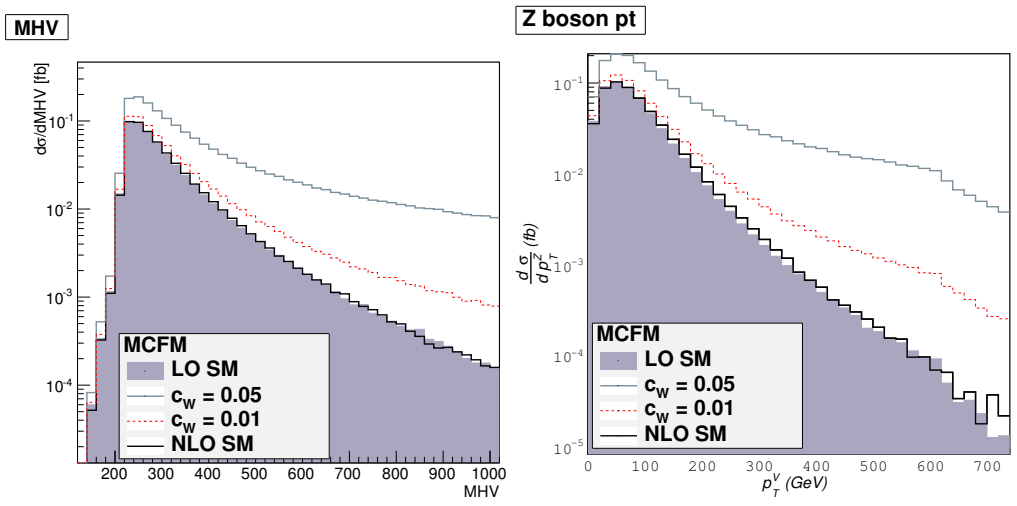

Figure 3. The invariant mass (left panel) and transverse momentum (right panel) distributions for LHC Run 1 at 8 TeV, calculated with LO and NLO QCD and compared with the effects of an effective operator.

p_T^V, measured by ATLAS. However, the p_T^V distribution is more affected by NLO QCD corrections than is the $V + H$ invariant mass distribution [122]. We present in figure 3 the results of an NLO calculation using MCFM [123–125]. Although the p_T^V distribution is more sensitive to NLO corrections, the constraint on the coefficient of an effective operator that we can obtain with LHC Run 1 data at 8 TeV is still quite insensitive to the QCD higher order corrections. However, this will be an important effect when reaching $\bar{c}_W \sim \mathcal{O}(10^{-3})$. Since such effects tend to broaden the p_T^V distribution in the SM, the inclusion of NLO would only strengthen the bounds reported here and as such will not modify our conclusions, which are reached under conservative assumptions.

Details of the cuts implemented for the 0-,1- and 2-lepton ATLAS analysis can be found in appendix B. Figure 4 is an example of the p_V^T distribution for the 2-lepton signal in the bins used by the ATLAS search, for various values of $\bar{c}_W$.

We see that the number of events in the last (overflow) bin increases rapidly with $\bar{c}_W$. Since the background overwhelms any signal in the lower bins, henceforth we focus exclusively on this overflow bin where the signal-to-background ratio is highest. A χ^2 fit to the observed data gives the 95% CL range

$$\bar{c}_W \in [-0.07, 0.07]\,,$$

which improves upon the D0 constraint (3.1), as expected. The contribution to the χ^2 function from this constraint is shown as the dashed blue line in the left panel of figure 2. For comparison, using the signal strength given for each of the 0-, 1- and 2-lepton channels, which grow with $\bar{c}_W$ as

$$\begin{aligned}\mu_{2-\text{lepton}} &\simeq 1 + 23\bar{c}_W \\ \mu_{1-\text{lepton}} &\simeq 1 + 32\bar{c}_W \\ \mu_{0-\text{lepton}} &\simeq 1 + 33\bar{c}_W\,,\end{aligned}$$

JHEP07(2014)036

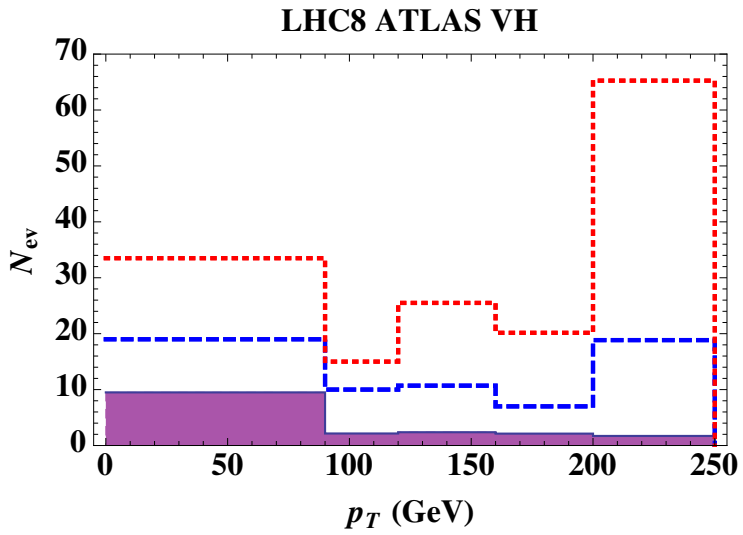

Figure 4. Simulation of the p_T^V distribution in $(V \to 2\ell) + (H \to \bar{b}b)$ events at the LHC after implementing ATLAS cuts, as obtained using `MadGraph v2.1.0` interfaced with `Pythia` and `Delphes v3`, combined with the dimension-6 model implementation developed in [117]. The solid distribution is the SM expectation, and the red-dotted and blue-dashed lines correspond to the distributions with $\bar{c}_W$ =0.1 and 0.05, respectively.

we find the 95% CL range

$$\bar{c}_W \in [-0.09, 0.03]\,,$$

which is comparable to that using only the last bin of the p_V^T differential distribution.

We emphasise that only the leading linear dependence on the dimension-6 coefficient is kept in our fit. Including the quadratic term could appear to give tighter constraints as it allows the signal to grow faster with increasing $\bar{c}_W$, but such bounds are spurious since it is not consistent to include a dependence on $\bar{c}_W^2$ without also introducing dimension-8 operators whose effects are formally of the same order. In the example given above, including the quadratic term would reduce the bounds to [-0.06 , 0.03] for the signal-strength fit and $[-0.04, 0.04]$ for the binned fit. This sensitivity to higher-order effects indicates the level to which we may trust these constraints. At the current level of precision, the differences in the bounds between the linear and quadratic fits are larger than any uncertainties in background distributions or MC simulations.

Full results of one-dimensional fits for $\bar{c}_W$ are summarized on the left plot in figure 2. In addition to the dashed red line corresponding to the analysis of the D0 m_{VH} distribution and the dashed blue line corresponding to the ATLAS p_T^V distribution discussed above, the dashed black line is the combination of CMS and ATLAS signal strengths including all channels except VH, and the solid black line is the combination of all the above. The right panel of figure 2 shows the corresponding one-dimensional constraints on $\bar{c}_{HW}$, where we see that the addition of the differential information is less important than for $\bar{c}_W$.

JHEP07(2014)036

4 Global constraints from signal strengths and differential distributions

Following these examples, we now combine the information from associated production measurements in the $H \to \bar{b}b$ final state by D0 and ATLAS together with the signal strengths in the $H \to \gamma\gamma, \gamma Z, WW, ZZ$ and $\tau\tau$ search channels measured by CMS and ATLAS. We first constrain the dimension-6 coefficients individually, setting to zero all other coefficients, and then include the full set of coefficients (2.2) in a global fit.

The decay widths for $H \to Z^* Z^{(*)} \to 4l$, $H \to W^* W^{(*)} \to l\nu l\nu$, $H \to \bar{f}f$, $H \to gg$ and $H \to \gamma\gamma$ have dependences on the dimension-6 coefficients that are given in [126, 127]. The dimension-6 operators also affect the vector boson fusion (VBF) production mode. Using the standard VBF cuts used at the LHC 8-TeV analysis, namely $m_{jj} > 400\,\text{GeV}$, $p_T^j > 20\,\text{GeV}$, $|\eta_j| < 4.5$ and $\Delta\eta_{jj} > 2.8$, we find

$$\frac{\sigma(pp \to V^*V^*jj \to hjj)}{\sigma(pp \to V^*V^*jj \to hjj)_{\text{SM}}} \simeq 1 - 8.30(\bar{c}_W + \tan^2\theta_w \bar{c}_B) - 6.9(\bar{c}_{HW} + \tan^2\theta_w \bar{c}_{HB}) - 0.26\bar{c}_\gamma\,.$$

We confront these predictions with the likelihoods for the total signal strengths μ given by ATLAS and CMS in a particularly useful form [128] as a 2-dimensional χ^2 grid of $\mu_{\text{ggF, tth}}$ vs $\mu_{\text{VBF,AP}}$. For ATLAS we use the likelihoods made publicly available for diboson final states in [129] and the 2-dimensional $H \to \tau\tau$ likelihood given in [130]. The CMS likelihoods for the $H \to \gamma\gamma, WW^*, ZZ^*$ and $\tau\tau$ channels are taken from [131]. We assume gluon fusion and VBF to be the dominant production modes in all these channels, with associated production only entering the fit through the differential distributions of the D0 and ATLAS $\bar{b}b$ final states.[3] The $H \to Z\gamma$ likelihood is reconstructed from the expected and observed 95% CL signal strength using the method of [132].

The result of the signal strength fit for all channels excluding $\bar{b}b$ at ATLAS and CMS gives the following 95% CL range for $\bar{c}_W$, setting all other coefficients to zero:

$$\bar{c}_W \in [-0.05, 0.06]\,.$$

Including the ATLAS p_V^T and D0 m_{VH} information discussed in the previous section reduces this range to

$$\bar{c}_W \in [-0.03, 0.01]\,.$$

The improvement of the limit on a single operator is significant. Furthermore the importance of using as many inputs as possible becomes clear when one includes several operators simultaneously [89]. For example, allowing the coefficient $\bar{c}_{HW}$ to vary simultaneously with $\bar{c}_W$ introduces a possible degeneracy in the fit, as shown in the upper left panel of figure 5. We see that the D0 m_{VH} data alone constrain essentially just one linear combination of $\bar{c}_W$ and $\bar{c}_{HW}$, and a similar effect occurs in the upper right panel where the result of a 2-parameter fit to just the ATLAS p_T^V data is shown. However, the correlation coefficients are somewhat different, so that combining the two sets of data breaks the degeneracy to some extent, as seen in the lower left panel of figure 5. Finally, in the lower right panel

[3] The signal strength information is also included in the differential distribution through the normalisation of the heights of each bin to the total number of signal events.

JHEP07(2014)036

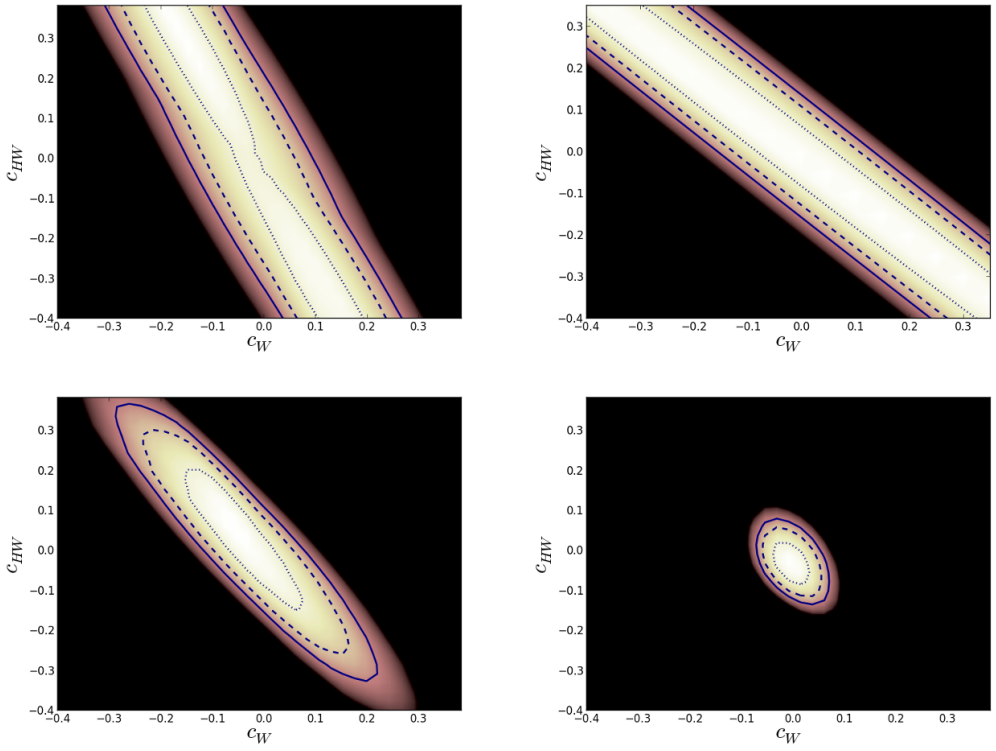

Figure 5. Regions in the $(\bar{c}_W, \bar{c}_{HW})$ planes allowed at the 68 (95) (99)% CL (in lighter shading and bounded by dotted, dashed and solid lines, respectively) in fits to the D0 m_{VH} data alone (upper left panel), the ATLAS p_T^V data alone (upper right panel), the combination of these data (lower left panel) and a global fit using also signal-strength information from CMS and ATLAS (lower right panel).

of figure 5 the degeneracy between $\bar{c}_W$ and $\bar{c}_{HW}$ is completely removed when the D0 and ATLAS associated production data are combined with the signal strength data from the other channels. This is primarily because, of the two operators considered here, only $\bar{c}_W$ enters in the $H \to \gamma\gamma$ decay width.

Finally we consider the full set of 8 dimension-6 operators listed in (2.2), setting $c_b = c_\tau \equiv c_d$, including a linear dependence on these coefficients in the ATLAS and CMS signal strengths, combined with the differential distribution information of $H + V$ associated production at ATLAS and D0 discussed in section 3. The result of a scan over the 8-dimensional parameter space is represented by the marginalized $\Delta\chi^2$ in solid black in figure 6. The blue dashed line in figure 6 is the result of the 8-parameter fit using only ATLAS and CMS signal strengths without $H + V \to V\bar{b}b$ associated production information. We see that omitting associated production yields no significant constraints on any of the operators aside from $\bar{c}_g$.[4]

[4]The bi-modal distribution of $\bar{c}_g$ is due to the linear dependence on the coefficient of the gluon production cross-section rescaling, which is not allowed to go negative and so is responsible for the two minima in the best fit.

JHEP07(2014)036

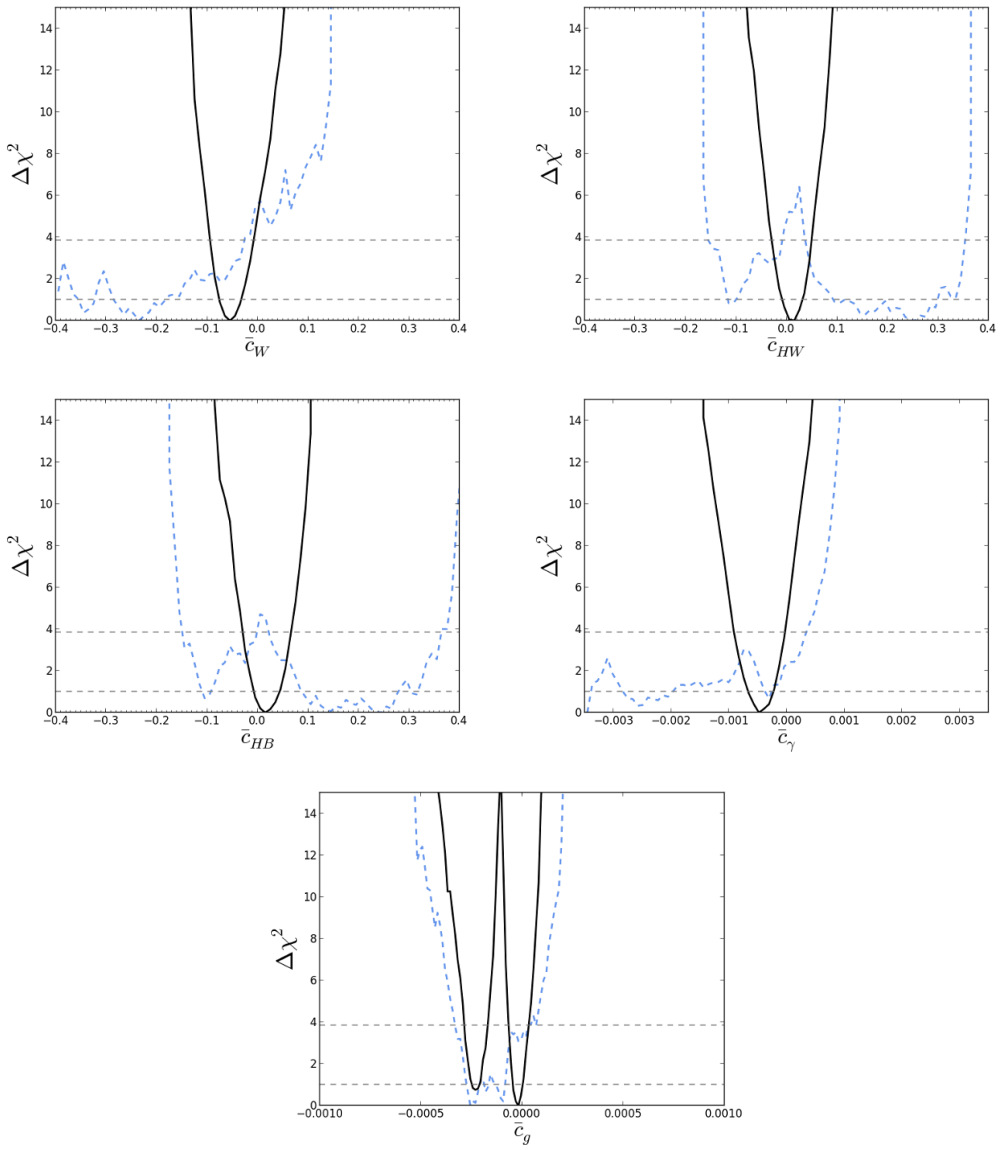

Figure 6. Marginalized $\Delta\chi^2$ from a scan over the 8-dimensional parameter space (2.2) using the differential distribution information about $H + V$ associated production from D0 and ATLAS as well as the ATLAS and CMS signal strengths (solid black line) and dropping the information from the kinematic distributions (blue dashed line).

The scan over the 8-dimensional parameter space including the kinematical information from $H + V$ production yields the 95% CL bounds summarized in the black error bars of figure 7. Also shown in green in figure 2 are the 1-dimensional constraints obtained by switching on one operator at a time with all others set to zero. We omit c_t, c_d and c_H in this and the previous figure, as no meaningful constraints are found for these coefficients.

JHEP07(2014)036

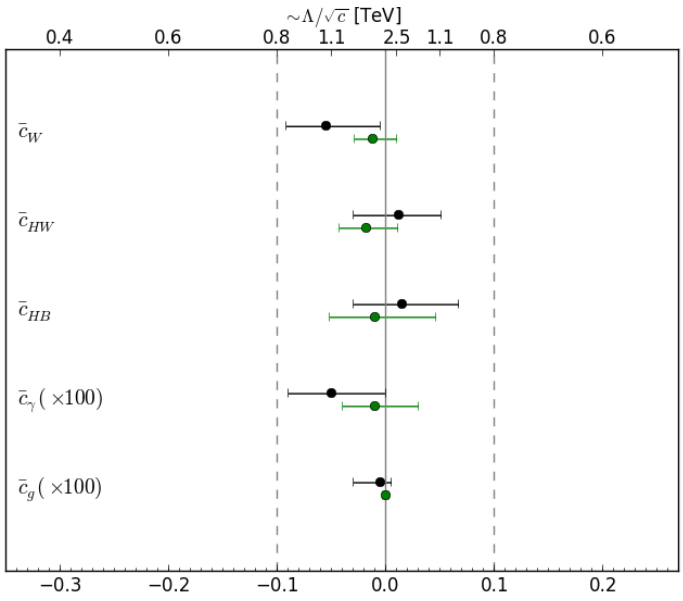

Figure 7. The 95% CL ranges allowed in a global fit to the dimension-6 operator coefficients listed in (2.2) (black), and the 95% CL ranges allowed for each operator coefficient individually, setting the others to zero (green). The upper axis is the corresponding sensitivity to the scale $\Lambda/\sqrt{c}$ in TeV where $\bar{c} \equiv c\frac{v^2}{\Lambda^2}$. Note that $\bar{c}_{\gamma,g}$ are shown ×100 for which the upper axis should therefore be read ×10.

We may also express the bounds obtained here in terms of the Higgs anomalous couplings as parametrized in (2.3). Our results are displayed in figure 8 using the same colour coding as in figure 7.

5 Conclusions

With Higgs property measurements consistent with SM expectations, and no clear sign of new physics from Run I of the LHC, it is natural to consider the SM as an effective theory supplemented by dimension-6 operators whose effects are suppressed by the scale of new physics. In this model-independent approach it is particularly interesting to consider a complete set of operators that minimizes any assumptions on the Wilson coefficients one chooses to include, thus providing truly universal bounds if one accepts the framework of the SM and decoupled new physics.

In this analysis we considered the set of CP-even operators that affect the Higgs sector at tree-level. Certain operators contain derivative interactions that modify the kinematics in $H + V$ associated production, modifying in particular the tail in the differential distribution of the $V + H$ invariant mass and the vector boson transverse momentum. We simulated the $V + H \to Vb\bar{b}$ process at D0 and found greater sensitivity to dimension-6 operators using the differential invariant mass distribution than using only signal strength information in this channel. Since the higher energies of the LHC enlarge the available

JHEP07(2014)036

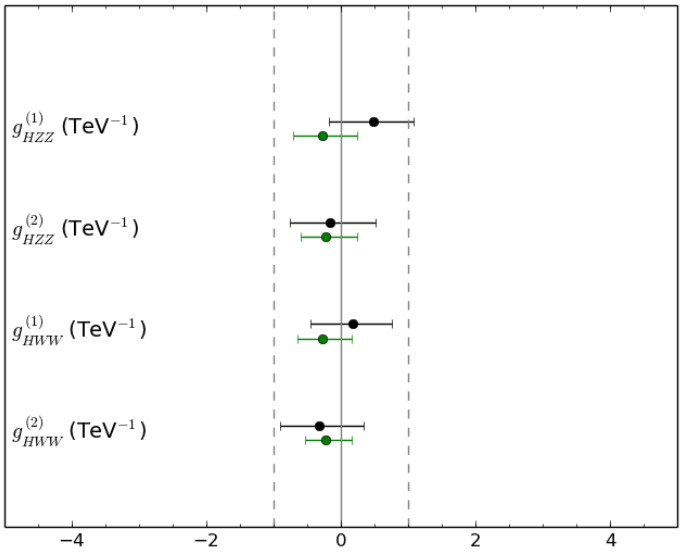

Figure 8. The 95% CL ranges allowed in a global fit to the anomalous Higgs couplings listed in (2.4) (black), and the 95% CL ranges allowed for each coupling individually, setting the others to zero (green).

phase space for boosted new physics, observations of the same process by ATLAS and CMS are expected to be more sensitive than D0 to the effects of dimension-6 operators, as we have confirmed here. Moreover, including kinematic distributions from both Tevatron and LHC can help remove degeneracies in multi-parameter fits.

Including differential distributions of associated production with the signal strength from other channels, we have performed a scan of the 8-dimensional parameter space of the CP-even dimension-6 operator coefficients and placed 95% CL bounds. Without the use of associated production information, there are degeneracies that give flat directions in the fit. These could otherwise be eliminated using measurements of TGCs. However, this may introduce model-dependent assumptions as TGCs, despite their greater sensitivity compared to Higgs measurements, also contain a poorly constrained direction due to a partial cancellation among contributions to $e^+e^- \to W^+W^-$. Thus the use of associated Higgs production complements other ingredients in global fits to a complete set of operators. As better measurements of TGCs at the LHC become available it will be interesting to fully explore this complementarity, which we intend to address in future work. This information will grow in importance when higher-energy LHC data are analyzed, since the increased phase space will further improve the sensitivity to dimension-6 operators.

Note added. We thank A. Knochel and the authors of ref. [137] for pointing out to us that the previous version of this paper underestimated the ATLAS p_V^T constraints due to a misinterpretation of the expected number of SM events in table 5 of ref. [110], which actually corresponds to a best fit signal strength of 0.2. Normalising instead to a signal

JHEP07(2014)036

strength of 1.0 yields improved constraints competitive with those of LEP, in agreement with comparable results in [137].

Acknowledgments

VS thanks Adam Falkowski, Alex Pomarol, Francesco Riva and Ciaran Williams and TY thanks Robert Hogan and Thomas Richardson for useful conversations. The authors are grateful to Jonathan Hays for providing information on the D0 analysis. The work of JE was supported partly by the London Centre for Terauniverse Studies (LCTS), using funding from the European Research Council via the Advanced Investigator Grant 267352. The work of VS is supported by the STFC grant ST/J000477/1. The work of TY was supported by a Graduate Teaching Assistantship from King's College London.

A D0 $H + V$ analysis

A.1 $p\bar{p} \to Zh \to l\bar{l}b\bar{b}$

The event selection for the 2-lepton channel is taken from [133]. The basic cuts for di-electrons are $p_T > 15$, $|\eta| < 15$ and at least one electron with $|\eta| < 1.1$, and for di-muons are $p_T > 10\,\text{GeV}$, $|\eta| < 2$ and at least one muon with $p_T > 15\text{GeV}, |\eta| < 1.5$. The muons have an isolation cut that requires them to be separated from all jets by $\Delta R = \sqrt{\Delta\eta^2 + \Delta\phi^2} > 0.5$.

The "pretag" cuts are then applied to keep only events with $70 < M_{ll} < 110\,\text{GeV}$ and at least two jets having $p_T > 20\,\text{GeV}$ and $|\eta| < 2.5$. The final selection step is b-tagging the jets according to "loose" and "tight" categories, with at least one tight and one loose b-tagged jet. We simulate this double-tagged (DT) requirement by using the efficiencies reported as a function of p_T in [134]. Fitting to figure 6a and 6b in that reference yields the following formula for the loose and tight efficiencies ϵ:

$$\epsilon_{\text{loose}} = a_{\text{loose}} e^{-\frac{p_T}{600}} \tanh(0.020 p_T + 0.77)\,,$$
$$\epsilon_{\text{tight}} = a_{\text{tight}} e^{-\frac{p_T}{360}} \tanh(0.029 p_T + 0.34)\,,$$

where the coefficients $a_{\text{loose}} = 0.79, a_{\text{tight}} = 0.70$ in the region $|\eta| < 1.5$ and $a_{\text{loose}} = 0.67, a_{\text{tight}} = 0.58$ for $|\eta| > 1.5$, the efficiency being fairly flat as a function of η in these regions.

Finally we set the `Delphes` ECAL and HCAL resolutions as functions of energy E to $0.01E + 0.2\sqrt{E} + 0.25$ and $0.050E + 0.8\sqrt{E}$ respectively. The same expression is used for the ECAL electron energy resolution.

After running our simulation we obtain the number of signal events by multiplying the cross-section given by `MadGraph` with the efficiency after cuts and reweighting by a k-factor of 1.5 as an overall normalization. We find the resulting number of pretag and DT signal events for a SM Higgs to be 8.6 and 3.1 respectively, in agreement with the numbers listed in table 3 of [133]. We have also verified that we reproduce well the distribution of $H + V$ invariant masses for the SM Higgs signal given by D0 in figure 2c of [73].

JHEP07(2014)036

A.2 $p\bar{p} \to Wh \to l\nu b\bar{b}$

We implement the cuts listed in [135] by requiring one electron (muon) with $p_T > 15$ and $|\eta| < 2.5$ (2.0), and by requiring two jets with $p_T > 20\,\text{GeV}$ and $|\eta| < 2.5$. The muon is required to be isolated from all jets by $\Delta R > 0.5$. Finally, the transverse mass M_T^W, defined as $2p_T^l \not{E}_T(1 - \cos\Delta\phi(l, \not{E}_T))$, must satisfy $M_T^W > 40\text{GeV} - 0.5\not{E}_T$. This defines the pretag events with the b-tag cut then applied as described previously. Running the simulation with the cross-section times efficiency reweighted by a k-factor of 1.7 gives good agreement with the expected numbers of pretag and final events given in table 1 of [135].

A.3 $p\bar{p} \to Zh \to \nu\bar{\nu}b\bar{b}$

Following [136], we select events containing two jets with $p_T > 20\,\text{GeV}$ and $|\eta| < 2.5$, whose opening angle is $\Delta\phi < 165°$, and apply a missing transverse energy cut $\not{E}_T > 40\,\text{GeV}$. The jets are furthermore required to have the scalar sum of the their transverse momenta larger than 80 GeV. We also reject events with an isolated muon or electron having $p_T > 15\,\text{GeV}$. We verified that the resulting numbers of events both before and after b-tag cuts agree within errors with the numbers given in table 1 of [136] without any reweighting.

B ATLAS $H + V$ analysis

The implementation of this analysis follows the cuts given in [110].

B.1 $p\bar{p} \to Zh \to l\bar{l}b\bar{b}$

We select events with exactly 2 muons (electrons) satisfying $|\eta| < 2.5\,(2.47)$ and $83 < M_{ll} < 99\,\text{GeV}$. A missing transverse energy cut of E_T^{miss} is applied. There must be only 2 b-tagged jets with the higher-p_T jet $> 45\,\text{GeV}$ and $p_T > 20\,\text{GeV}$ for the other jet, and both with $|\eta| < 2.5$. Finally we place a ΔR cut on the angle between the two jets which varies depending on the p_T^V bin (see table 2 in [110]). The transverse momentum p_T^V of the vector boson is reconstructed using the vector sum of the transverse components of the two leptons.

We simulate events at the 8 TeV LHC with the resulting distribution in the p_T^V bins used by ATLAS. We reweight the cross-section so as to normalise the number of signal events in each bin to the expected SM count from table 5 of [110].

B.2 $p\bar{p} \to Wh \to l\nu b\bar{b}$

In this sub-channel we select exactly one muon (electron) with $|\eta| < 2.5(2.47)$ and $E_T > 25\,\text{GeV}$. The missing transverse energy requirement is $E_T^{\text{miss}} > 25\,(50)$ for p_T^V less (greater) than 200 GeV. The invariant transverse mass m_T^W is required to be less than 120 GeV, and for $p_T^V < 160\,\text{GeV}$ it must also be greater than 40 GeV. The p_T^V transverse momentum is in this case the vector sum of the transverse components of the lepton and missing E_T. The jet requirements are the same as for the 2-lepton case, and we have normalised our number of events after simulation in the same way as above.

JHEP07(2014)036

B.3 $p\bar{p} \to Zh \to \nu\bar{\nu}b\bar{b}$

Here we require no leptons that pass the other criterias and a large missing transverse energy of $E_T^{\rm miss} > 120\,{\rm GeV}$ with $p_T^{\rm miss} > 30\,{\rm GeV}$ and an angle between the two of $\Delta\phi < \pi/2$. The azimuthal angle between the $E_T^{\rm miss}$ and the vector sum of the jets must be $\Delta\phi > 4.8$, as well as $\Delta\phi > 1.5$ with the nearest jet. The other jet cuts and ΔR requirements as a function of p_T^V are also the same here, with the p_T^V identified as the $E_{\rm miss}^T$. We again normalize the number of signal events to the SM expectation from table 5 of [110].

JHEP07(2014)036

References

[1] ATLAS collaboration, *Observation of a new particle in the search for the Standard Model Higgs boson with the ATLAS detector at the LHC*, *Phys. Lett.* **B 716** (2012) 1 [arXiv:1207.7214] [INSPIRE].

[2] CMS collaboration, *Observation of a new boson at a mass of 125 GeV with the CMS experiment at the LHC*, *Phys. Lett.* **B 716** (2012) 30 [arXiv:1207.7235] [INSPIRE].

[3] CMS collaboration, *Observation of a new boson with mass near 125 GeV in pp collisions at $\sqrt{s}$ = 7 and 8 TeV*, *JHEP* **06** (2013) 081 [arXiv:1303.4571] [INSPIRE].

[4] ATLAS collaboration, *Constraints on New Phenomena via Higgs Coupling Measurements with the ATLAS Detector*, ATLAS-CONF-2014-010.

[5] M. Baak, M. Goebel, J. Haller, A. Hoecker, D. Ludwig et al., *Updated Status of the Global Electroweak Fit and Constraints on New Physics*, *Eur. Phys. J.* **C 72** (2012) 2003 [arXiv:1107.0975] [INSPIRE].

[6] D. Carmi, A. Falkowski, E. Kuflik and T. Volansky, *Interpreting LHC Higgs Results from Natural New Physics Perspective*, *JHEP* **07** (2012) 136 [arXiv:1202.3144] [INSPIRE].

[7] A. Azatov, R. Contino and J. Galloway, *Model-Independent Bounds on a Light Higgs*, *JHEP* **04** (2012) 127 [*Erratum ibid.* **1304** (2013) 140] [arXiv:1202.3415] [INSPIRE].

[8] J.R. Espinosa, C. Grojean, M. Muhlleitner and M. Trott, *Fingerprinting Higgs Suspects at the LHC*, *JHEP* **05** (2012) 097 [arXiv:1202.3697] [INSPIRE].

[9] P.P. Giardino, K. Kannike, M. Raidal and A. Strumia, *Reconstructing Higgs boson properties from the LHC and Tevatron data*, *JHEP* **06** (2012) 117 [arXiv:1203.4254] [INSPIRE].

[10] T. Li, X. Wan, Y.-k. Wang and S.-h. Zhu, *Constraints on the Universal Varying Yukawa Couplings: from SM-like to Fermiophobic*, *JHEP* **09** (2012) 086 [arXiv:1203.5083] [INSPIRE].

[11] M. Rauch, *Determination of Higgs-boson couplings (SFitter)*, arXiv:1203.6826 [INSPIRE].

[12] J. Ellis and T. You, *Global Analysis of Experimental Constraints on a Possible Higgs-Like Particle with Mass 125 GeV*, *JHEP* **06** (2012) 140 [arXiv:1204.0464] [INSPIRE].

[13] A. Azatov, R. Contino, D. Del Re, J. Galloway, M. Grassi et al., *Determining Higgs couplings with a model-independent analysis of $h \to \gamma\gamma$*, *JHEP* **06** (2012) 134 [arXiv:1204.4817] [INSPIRE].

[14] M. Klute, R. Lafaye, T. Plehn, M. Rauch and D. Zerwas, *Measuring Higgs Couplings from LHC Data*, *Phys. Rev. Lett.* **109** (2012) 101801 [arXiv:1205.2699] [INSPIRE].

[15] L. Wang and X.-F. Han, *The recent Higgs boson data and Higgs triplet model with vector-like quark*, *Phys. Rev.* **D 86** (2012) 095007 [arXiv:1206.1673] [INSPIRE].

[16] D. Carmi, A. Falkowski, E. Kuflik and T. Volansky, *Interpreting the 125 GeV Higgs*, *Nuovo Cim.* **C 035** (2012) 315 [arXiv:1206.4201] [INSPIRE].

[17] M.J. Dolan, C. Englert and M. Spannowsky, *Higgs self-coupling measurements at the LHC*, *JHEP* **10** (2012) 112 [arXiv:1206.5001] [INSPIRE].

[18] J. Chang, K. Cheung, P.-Y. Tseng and T.-C. Yuan, *Distinguishing Various Models of the 125 GeV Boson in Vector Boson Fusion*, *JHEP* **12** (2012) 058 [arXiv:1206.5853] [INSPIRE].

[19] S. Chang, C.A. Newby, N. Raj and C. Wanotayaroj, *Revisiting Theories with Enhanced Higgs Couplings to Weak Gauge Bosons*, *Phys. Rev.* **D 86** (2012) 095015 [arXiv:1207.0493] [INSPIRE].

[20] I. Low, J. Lykken and G. Shaughnessy, *Have We Observed the Higgs (Imposter)?*, *Phys. Rev.* **D 86** (2012) 093012 [arXiv:1207.1093] [INSPIRE].

[21] J. Ellis and T. You, *Global Analysis of the Higgs Candidate with Mass 125 GeV*, *JHEP* **09** (2012) 123 [arXiv:1207.1693] [INSPIRE].

[22] P.P. Giardino, K. Kannike, M. Raidal and A. Strumia, *Is the resonance at 125 GeV the Higgs boson?*, *Phys. Lett.* **B 718** (2012) 469 [arXiv:1207.1347] [INSPIRE].

[23] M. Montull and F. Riva, *Higgs discovery: the beginning or the end of natural EWSB?*, *JHEP* **11** (2012) 018 [arXiv:1207.1716] [INSPIRE].

[24] J.R. Espinosa, C. Grojean, M. Muhlleitner and M. Trott, *First Glimpses at Higgs' face*, *JHEP* **12** (2012) 045 [arXiv:1207.1717] [INSPIRE].

[25] D. Carmi, A. Falkowski, E. Kuflik, T. Volansky and J. Zupan, *Higgs After the Discovery: A Status Report*, *JHEP* **10** (2012) 196 [arXiv:1207.1718] [INSPIRE].

[26] S. Banerjee, S. Mukhopadhyay and B. Mukhopadhyaya, *New Higgs interactions and recent data from the LHC and the Tevatron*, *JHEP* **10** (2012) 062 [arXiv:1207.3588] [INSPIRE].

[27] F. Bonnet, T. Ota, M. Rauch and W. Winter, *Interpretation of precision tests in the Higgs sector in terms of physics beyond the Standard Model*, *Phys. Rev.* **D 86** (2012) 093014 [arXiv:1207.4599] [INSPIRE].

[28] T. Plehn and M. Rauch, *Higgs Couplings after the Discovery*, *Europhys. Lett.* **100** (2012) 11002 [arXiv:1207.6108] [INSPIRE].

[29] A. Djouadi, *Precision Higgs coupling measurements at the LHC through ratios of production cross sections*, *Eur. Phys. J.* **C 73** (2013) 2498 [arXiv:1208.3436] [INSPIRE].

[30] B. Batell, S. Gori and L.-T. Wang, *Higgs Couplings and Precision Electroweak Data*, *JHEP* **01** (2013) 139 [arXiv:1209.6382] [INSPIRE].

[31] G. Moreau, *Constraining extra-fermion(s) from the Higgs boson data*, *Phys. Rev.* **D 87** (2013) 015027 [arXiv:1210.3977] [INSPIRE].

JHEP07(2014)036

[32] G. Cacciapaglia, A. Deandrea, G.D. La Rochelle and J.-B. Flament, *Higgs couplings beyond the Standard Model*, *JHEP* **03** (2013) 029 [arXiv:1210.8120] [INSPIRE].

[33] E. Masso and V. Sanz, *Limits on Anomalous Couplings of the Higgs to Electroweak Gauge Bosons from LEP and LHC*, *Phys. Rev.* **D 87** (2013) 033001 [arXiv:1211.1320] [INSPIRE].

[34] R.T. D'Agnolo, E. Kuflik and M. Zanetti, *Fitting the Higgs to Natural SUSY*, *JHEP* **03** (2013) 043 [arXiv:1212.1165] [INSPIRE].

[35] A. Azatov and J. Galloway, *Electroweak Symmetry Breaking and the Higgs Boson: Confronting Theories at Colliders*, *Int. J. Mod. Phys.* **A 28** (2013) 1330004 [arXiv:1212.1380] [INSPIRE].

[36] G. Bhattacharyya, D. Das and P.B. Pal, *Modified Higgs couplings and unitarity violation*, *Phys. Rev.* **D 87** (2013) 011702 [arXiv:1212.4651] [INSPIRE].

[37] D. Choudhury, R. Islam and A. Kundu, *Anomalous Higgs Couplings as a Window to New Physics*, *Phys. Rev.* **D 88** (2013) 013014 [arXiv:1212.4652] [INSPIRE].

[38] R.S. Gupta, M. Montull and F. Riva, *SUSY Faces its Higgs Couplings*, *JHEP* **04** (2013) 132 [arXiv:1212.5240] [INSPIRE].

[39] G. Bélanger, B. Dumont, U. Ellwanger, J.F. Gunion and S. Kraml, *Higgs Couplings at the End of 2012*, *JHEP* **02** (2013) 053 [arXiv:1212.5244] [INSPIRE].

[40] K. Cheung, J.S. Lee and P.-Y. Tseng, *Higgs Precision (Higgcision) Era begins*, *JHEP* **05** (2013) 134 [arXiv:1302.3794] [INSPIRE].

[41] A. Falkowski, F. Riva and A. Urbano, *Higgs at last*, *JHEP* **11** (2013) 111 [arXiv:1303.1812] [INSPIRE].

[42] P.P. Giardino, K. Kannike, I. Masina, M. Raidal and A. Strumia, *The universal Higgs fit*, *JHEP* **05** (2014) 046 [arXiv:1303.3570] [INSPIRE].

[43] J. Ellis and T. You, *Updated Global Analysis of Higgs Couplings*, *JHEP* **06** (2013) 103 [arXiv:1303.3879] [INSPIRE].

[44] S. Banerjee, S. Mukhopadhyay and B. Mukhopadhyaya, *Higher dimensional operators and LHC Higgs data : the role of modified kinematics*, *Phys. Rev.* **D 89** (2014) 053010 [arXiv:1308.4860] [INSPIRE].

[45] J. Ellis, V. Sanz and T. You, *Prima Facie Evidence against Spin-Two Higgs Impostors*, *Phys. Lett.* **B 726** (2013) 244 [arXiv:1211.3068] [INSPIRE].

[46] J. Ellis and D.S. Hwang, *Does the 'Higgs' have Spin Zero?*, *JHEP* **09** (2012) 071 [arXiv:1202.6660] [INSPIRE].

[47] A. Alves, *Is the New Resonance Spin 0 or 2? Taking a Step Forward in the Higgs Boson Discovery*, *Phys. Rev.* **D 86** (2012) 113010 [arXiv:1209.1037] [INSPIRE].

[48] J. Ellis, R. Fok, D.S. Hwang, V. Sanz and T. You, *Distinguishing 'Higgs' spin hypotheses using $\gamma\gamma$ and WW^* decays*, *Eur. Phys. J.* **C 73** (2013) 2488 [arXiv:1210.5229] [INSPIRE].

[49] Y. Gao, A.V. Gritsan, Z. Guo, K. Melnikov, M. Schulze et al., *Spin determination of single-produced resonances at hadron colliders*, *Phys. Rev.* **D 81** (2010) 075022 [arXiv:1001.3396] [INSPIRE].

[50] M.C. Kumar, P. Mathews, A.A. Pankov, N. Paver, V. Ravindran et al., *Spin-analysis of s-channel diphoton resonances at the LHC*, *Phys. Rev.* **D 84** (2011) 115008 [arXiv:1108.3764] [INSPIRE].

JHEP07(2014)036

[51] S.Y. Choi, D.J. Miller, M.M. Muhlleitner and P.M. Zerwas, *Identifying the Higgs spin and parity in decays to Z pairs*, *Phys. Lett.* **B 553** (2003) 61 [hep-ph/0210077] [INSPIRE].

[52] K. Odagiri, *On azimuthal spin correlations in Higgs plus jet events at LHC*, *JHEP* **03** (2003) 009 [hep-ph/0212215] [INSPIRE].

[53] C.P. Buszello, I. Fleck, P. Marquard and J.J. van der Bij, *Prospective analysis of spin- and CP-sensitive variables in $H \to Z\,Z \to l(1)+\,l(1)-\,l(2)+\,l(2)-$ at the LHC*, *Eur. Phys. J.* **C 32** (2004) 209 [hep-ph/0212396] [INSPIRE].

[54] A. Djouadi, *The Anatomy of electro-weak symmetry breaking. I: The Higgs boson in the standard model*, *Phys. Rept.* **457** (2008) 1 [hep-ph/0503172] [INSPIRE].

[55] C.P. Buszello and P. Marquard, *Determination of spin and CP of the Higgs boson from WBF*, hep-ph/0603209 [INSPIRE].

[56] A. Bredenstein, A. Denner, S. Dittmaier and M.M. Weber, *Precise predictions for the Higgs-boson decay $H \to WW/ZZ \to 4$ leptons*, *Phys. Rev.* **D 74** (2006) 013004 [hep-ph/0604011] [INSPIRE].

[57] P.S. Bhupal Dev, A. Djouadi, R.M. Godbole, M.M. Muhlleitner and S.D. Rindani, *Determining the CP properties of the Higgs boson*, *Phys. Rev. Lett.* **100** (2008) 051801 [arXiv:0707.2878] [INSPIRE].

[58] R.M. Godbole, D.J. Miller and M.M. Muhlleitner, *Aspects of CP-violation in the H ZZ coupling at the LHC*, *JHEP* **12** (2007) 031 [arXiv:0708.0458] [INSPIRE].

[59] K. Hagiwara, Q. Li and K. Mawatari, *Jet angular correlation in vector-boson fusion processes at hadron colliders*, *JHEP* **07** (2009) 101 [arXiv:0905.4314] [INSPIRE].

[60] A. De Rujula, J. Lykken, M. Pierini, C. Rogan and M. Spiropulu, *Higgs look-alikes at the LHC*, *Phys. Rev.* **D 82** (2010) 013003 [arXiv:1001.5300] [INSPIRE].

[61] C. Englert, C. Hackstein and M. Spannowsky, *Measuring spin and CP from semi-hadronic ZZ decays using jet substructure*, *Phys. Rev.* **D 82** (2010) 114024 [arXiv:1010.0676] [INSPIRE].

[62] U. De Sanctis, M. Fabbrichesi and A. Tonero, *Telling the spin of the 'Higgs boson' at the LHC*, *Phys. Rev.* **D 84** (2011) 015013 [arXiv:1103.1973] [INSPIRE].

[63] V. Barger and P. Huang, *Higgs boson finder and mass estimator: The Higgs boson to WW to leptons decay channel at the LHC*, *Phys. Rev.* **D 84** (2011) 093001 [arXiv:1107.4131] [INSPIRE].

[64] S. Bolognesi, Y. Gao, A.V. Gritsan, K. Melnikov, M. Schulze et al., *On the spin and parity of a single-produced resonance at the LHC*, *Phys. Rev.* **D 86** (2012) 095031 [arXiv:1208.4018] [INSPIRE].

[65] R. Boughezal, T.J. LeCompte and F. Petriello, *Single-variable asymmetries for measuring the 'Higgs' boson spin and CP properties*, arXiv:1208.4311 [INSPIRE].

[66] D. Stolarski and R. Vega-Morales, *Directly Measuring the Tensor Structure of the Scalar Coupling to Gauge Bosons*, *Phys. Rev.* **D 86** (2012) 117504 [arXiv:1208.4840] [INSPIRE].

[67] S.Y. Choi, M.M. Muhlleitner and P.M. Zerwas, *Theoretical Basis of Higgs-Spin Analysis in $H \to \gamma\gamma$ and $Z\gamma$ Decays*, *Phys. Lett.* **B 718** (2013) 1031 [arXiv:1209.5268] [INSPIRE].

[68] P. Avery, D. Bourilkov, M. Chen, T. Cheng, A. Drozdetskiy et al., *Precision studies of the Higgs boson decay channel $H \to ZZ \to 4l$ with MEKD*, *Phys. Rev.* **D 87** (2013) 055006 [arXiv:1210.0896] [INSPIRE].

JHEP07(2014)036

[69] C.-Q. Geng, D. Huang, Y. Tang and Y.-L. Wu, *Note on 125 GeV Spin-2 particle*, *Phys. Lett.* **B 719** (2013) 164 [arXiv:1210.5103] [INSPIRE].

[70] A. Menon, T. Modak, D. Sahoo, R. Sinha and H.-Y. Cheng, *Inferring the nature of the boson at 125-126 GeV*, *Phys. Rev.* **D 89** (2014) 095021 [arXiv:1301.5404] [INSPIRE].

[71] CMS collaboration, *Study of the Mass and Spin-Parity of the Higgs Boson Candidate Via Its Decays to Z Boson Pairs*, *Phys. Rev. Lett.* **110** (2013) 081803 [arXiv:1212.6639] [INSPIRE].

[72] ATLAS collaboration, *Evidence for the spin-0 nature of the Higgs boson using ATLAS data*, *Phys. Lett.* **B 726** (2013) 120 [arXiv:1307.1432] [INSPIRE].

[73] D0 collaboration, *Constraints on the $J^P = 2^+$ hypothesis for the 125 GeV boson in $W/Z + b\bar{b}$ final states at the D0 Experiment*, D0 Note 6387-CONF.

[74] W. Buchmüller and D. Wyler, *Effective Lagrangian Analysis of New Interactions and Flavor Conservation*, *Nucl. Phys.* **B 268** (1986) 621 [INSPIRE].

[75] K. Hagiwara, S. Ishihara, R. Szalapski and D. Zeppenfeld, *Low-energy effects of new interactions in the electroweak boson sector*, *Phys. Rev.* **D 48** (1993) 2182 [INSPIRE].

[76] K. Hagiwara, R. Szalapski and D. Zeppenfeld, *Anomalous Higgs boson production and decay*, *Phys. Lett.* **B 318** (1993) 155 [hep-ph/9308347] [INSPIRE].

[77] B. Grzadkowski, M. Iskrzynski, M. Misiak and J. Rosiek, *Dimension-Six Terms in the Standard Model Lagrangian*, *JHEP* **10** (2010) 085 [arXiv:1008.4884] [INSPIRE].

[78] M.B. Einhorn and J. Wudka, *The Bases of Effective Field Theories*, *Nucl. Phys.* **B 876** (2013) 556 [arXiv:1307.0478] [INSPIRE].

[79] S. Willenbrock and C. Zhang, *Effective Field Theory Beyond the Standard Model*, arXiv:1401.0470 [INSPIRE].

[80] F. Bonnet, M.B. Gavela, T. Ota and W. Winter, *Anomalous Higgs couplings at the LHC and their theoretical interpretation*, *Phys. Rev.* **D 85** (2012) 035016 [arXiv:1105.5140] [INSPIRE].

[81] T. Corbett, O.J.P. Eboli, J. Gonzalez-Fraile and M.C. Gonzalez-Garcia, *Constraining anomalous Higgs interactions*, *Phys. Rev.* **D 86** (2012) 075013 [arXiv:1207.1344] [INSPIRE].

[82] W.-F. Chang, W.-P. Pan and F. Xu, *Effective gauge-Higgs operators analysis of new physics associated with the Higgs boson*, *Phys. Rev.* **D 88** (2013) 033004 [arXiv:1303.7035] [INSPIRE].

[83] A. Hayreter and G. Valencia, *Constraints on anomalous color dipole operators from Higgs boson production at the LHC*, *Phys. Rev.* **D 88** (2013) 034033 [arXiv:1304.6976] [INSPIRE].

[84] J. Elias-Miro, J.R. Espinosa, E. Masso and A. Pomarol, *Higgs windows to new physics through $D = 6$ operators: constraints and one-loop anomalous dimensions*, *JHEP* **11** (2013) 066 [arXiv:1308.1879] [INSPIRE].

[85] S. Banerjee, S. Mukhopadhyay and B. Mukhopadhyaya, *Higher dimensional operators and LHC Higgs data: the role of modified kinematics*, *Phys. Rev.* **D 89** (2014) 053010 [arXiv:1308.4860] [INSPIRE].

[86] E. Boos, V. Bunichev, M. Dubinin and Y. Kurihara, *Higgs boson signal at complete tree level in the SM extension by dimension-six operators*, *Phys. Rev.* **D 89** (2014) 035001 [arXiv:1309.5410] [INSPIRE].

JHEP07(2014)036

[87] M. Dahiya, S. Dutta and R. Islam, *Unitarizing VV Scattering in Light Higgs Scenarios*, arXiv:1311.4523 [INSPIRE].

[88] J.S. Gainer, J. Lykken, K.T. Matchev, S. Mrenna and M. Park, *Beyond Geolocating: Constraining Higher Dimensional Operators in $H \to 4\ell$ with Off-Shell Production and More*, arXiv:1403.4951 [INSPIRE].

[89] E. Masso and V. Sanz, *Limits on Anomalous Couplings of the Higgs to Electroweak Gauge Bosons from LEP and LHC*, *Phys. Rev.* **D 87** (2013) 033001 [arXiv:1211.1320] [INSPIRE].

[90] Z. Han and W. Skiba, *Effective theory analysis of precision electroweak data*, *Phys. Rev.* **D 71** (2005) 075009 [hep-ph/0412166] [INSPIRE].

[91] T. Corbett, O.J.P. Eboli, J. Gonzalez-Fraile and M.C. Gonzalez-Garcia, *Robust Determination of the Higgs Couplings: Power to the Data*, *Phys. Rev.* **D 87** (2013) 015022 [arXiv:1211.4580] [INSPIRE].

[92] B. Dumont, S. Fichet and G. von Gersdorff, *A Bayesian view of the Higgs sector with higher dimensional operators*, *JHEP* **07** (2013) 065 [arXiv:1304.3369] [INSPIRE].

[93] A. Pomarol and F. Riva, *Towards the Ultimate SM Fit to Close in on Higgs Physics*, *JHEP* **01** (2014) 151 [arXiv:1308.2803] [INSPIRE].

[94] S. Alam, S. Dawson and R. Szalapski, *Low-energy constraints on new physics revisited*, *Phys. Rev.* **D 57** (1998) 1577 [hep-ph/9706542] [INSPIRE].

[95] A. De Rujula, M.B. Gavela, P. Hernández and E. Masso, *The Selfcouplings of vector bosons: Does LEP-1 obviate LEP-2?*, *Nucl. Phys.* **B 384** (1992) 3 [INSPIRE].

[96] H. Mebane, N. Greiner, C. Zhang and S. Willenbrock, *Constraints on Electroweak Effective Operators at One Loop*, *Phys. Rev.* **D 88** (2013) 015028 [arXiv:1306.3380] [INSPIRE].

[97] T. Corbett, O.J.P. Éboli, J. Gonzalez-Fraile and M.C. Gonzalez-Garcia, *Determining Triple Gauge Boson Couplings from Higgs Data*, *Phys. Rev. Lett.* **111** (2013) 011801 [arXiv:1304.1151] [INSPIRE].

[98] A. Falkowski, S. Fichet, K. Mohan, F. Riva and V. Sanz, *Triple gauge couplings revisited*, contribution to the Les Houches 2013 proceedings, to appear.

[99] C. Grojean, E.E. Jenkins, A.V. Manohar and M. Trott, *Renormalization Group Scaling of Higgs Operators and $\Gamma(h \to \gamma\gamma)$*, *JHEP* **04** (2013) 016 [arXiv:1301.2588] [INSPIRE].

[100] J. Elias-Miró, J.R. Espinosa, E. Masso and A. Pomarol, *Renormalization of dimension-six operators relevant for the Higgs decays $h \to \gamma\gamma, \gamma Z$*, *JHEP* **08** (2013) 033 [arXiv:1302.5661] [INSPIRE].

[101] J. Elias-Miro, J.R. Espinosa, E. Masso and A. Pomarol, *Higgs windows to new physics through $D = 6$ operators: constraints and one-loop anomalous dimensions*, *JHEP* **11** (2013) 066 [arXiv:1308.1879] [INSPIRE].

[102] E.E. Jenkins, A.V. Manohar and M. Trott, *Renormalization Group Evolution of the Standard Model Dimension Six Operators I: Formalism and lambda Dependence*, *JHEP* **10** (2013) 087 [arXiv:1308.2627] [INSPIRE].

[103] E.E. Jenkins, A.V. Manohar and M. Trott, *Renormalization Group Evolution of the Standard Model Dimension Six Operators II: Yukawa Dependence*, *JHEP* **01** (2014) 035 [arXiv:1310.4838] [INSPIRE].

JHEP07(2014)036

[104] R. Alonso, E.E. Jenkins, A.V. Manohar and M. Trott, *Renormalization Group Evolution of the Standard Model Dimension Six Operators III: Gauge Coupling Dependence and Phenomenology*, *JHEP* **04** (2014) 159 [arXiv:1312.2014] [INSPIRE].

[105] J. Elias-Miró, C. Grojean, R.S. Gupta and D. Marzocca, *Scaling and tuning of EW and Higgs observables*, *JHEP* **05** (2014) 019 [arXiv:1312.2928] [INSPIRE].

[106] C.-Y. Chen, S. Dawson and C. Zhang, *Electroweak Effective Operators and Higgs Physics*, *Phys. Rev.* **D 89** (2014) 015016 [arXiv:1311.3107] [INSPIRE].

[107] H. Mebane, N. Greiner, C. Zhang and S. Willenbrock, *Constraints on Electroweak Effective Operators at One Loop*, *Phys. Rev.* **D 88** (2013) 015028 [arXiv:1306.3380] [INSPIRE].

[108] B. Henning, X. Lu and H. Murayama, *What do precision Higgs measurements buy us?*, arXiv:1404.1058 [INSPIRE].

[109] D0 collaboration, V.M. Abazov et al., *Combined search for the standard model Higgs boson decaying to $b\bar{b}$ using the D0 Run II data set*, *Phys. Rev. Lett.* **109** (2012) 121802 [arXiv:1207.6631] [INSPIRE].

[110] ATLAS collaboration, *Search for the bb decay of the Standard Model Higgs boson in associated W/ZH production with the ATLAS detector*, ATLAS-CONF-2013-079.

[111] J. Ellis, V. Sanz and T. You, *Associated Production Evidence against Higgs Impostors and Anomalous Couplings*, *Eur. Phys. J.* **C 73** (2013) 2507 [arXiv:1303.0208] [INSPIRE].

[112] G. Isidori and M. Trott, *Higgs form factors in Associated Production*, *JHEP* **02** (2014) 082 [arXiv:1307.4051] [INSPIRE].

[113] G.F. Giudice, C. Grojean, A. Pomarol and R. Rattazzi, *The Strongly-Interacting Light Higgs*, *JHEP* **06** (2007) 045 [hep-ph/0703164] [INSPIRE].

[114] R. Contino, C. Grojean, M. Moretti, F. Piccinini and R. Rattazzi, *Strong Double Higgs Production at the LHC*, *JHEP* **05** (2010) 089 [arXiv:1002.1011] [INSPIRE].

[115] R. Contino, *The Higgs as a Composite Nambu-Goldstone Boson*, arXiv:1005.4269 [INSPIRE].

[116] R. Grober and M. Muhlleitner, *Composite Higgs Boson Pair Production at the LHC*, *JHEP* **06** (2011) 020 [arXiv:1012.1562] [INSPIRE].

[117] A. Alloul, B. Fuks and V. Sanz, *Phenomenology of the Higgs Effective Lagrangian via FeynRules*, *JHEP* **04** (2014) 110 [arXiv:1310.5150] [INSPIRE].

[118] J. Alwall, M. Herquet, F. Maltoni, O. Mattelaer and T. Stelzer, *MadGraph 5 : Going Beyond*, *JHEP* **06** (2011) 128 [arXiv:1106.0522] [INSPIRE].

[119] T. Sjöstrand, S. Mrenna and P.Z. Skands, *PYTHIA 6.4 Physics and Manual*, *JHEP* **05** (2006) 026 [hep-ph/0603175] [INSPIRE].

[120] DELPHES 3 collaboration, J. de Favereau et al., *DELPHES 3, A modular framework for fast simulation of a generic collider experiment*, *JHEP* **02** (2014) 057 [arXiv:1307.6346] [INSPIRE].

[121] J. Ellis, D.S. Hwang, V. Sanz and T. You, *A Fast Track towards the 'Higgs' Spin and Parity*, *JHEP* **11** (2012) 134 [arXiv:1208.6002] [INSPIRE].

[122] V. Sanz and C. Williams, in preparation.

JHEP07(2014)036

[123] J.M. Campbell and R.K. Ellis, *MCFM for the Tevatron and the LHC*, *Nucl. Phys. Proc. Suppl.* **205** (2010) 10 [arXiv:1007.3492] [INSPIRE].

[124] J.M. Campbell, *W/Z + B, $\bar{B}$/ jets at NLO using the Monte Carlo MCFM*, hep-ph/0105226 [INSPIRE].

[125] J.M. Campbell, R.K. Ellis and C. Williams, *Vector boson pair production at the LHC*, *JHEP* **07** (2011) 018 [arXiv:1105.0020] [INSPIRE].

[126] R. Contino, M. Ghezzi, C. Grojean, M. Muhlleitner and M. Spira, *Effective Lagrangian for a light Higgs-like scalar*, *JHEP* **07** (2013) 035 [arXiv:1303.3876] [INSPIRE].

[127] R. Contino, M. Ghezzi, C. Grojean, M. Muhlleitner and M. Spira, *eHDECAY: an Implementation of the Higgs Effective Lagrangian into HDECAY*, arXiv:1403.3381 [INSPIRE].

[128] F. Boudjema, G. Cacciapaglia, K. Cranmer, G. Dissertori, A. Deandrea et al., *On the presentation of the LHC Higgs Results*, arXiv:1307.5865 [INSPIRE].

[129] ATLAS collaboration, *Measurements of Higgs boson production and couplings in diboson final states with the ATLAS detector at the LHC*, *Phys. Lett.* **B 726** (2013) 88 [arXiv:1307.1427] [INSPIRE].

[130] ATLAS collaboration, *Combined coupling measurements of the Higgs-like boson with the ATLAS detector using up to 25 fb^{-1} of proton-proton collision data*, ATLAS-CONF-2013-034.

[131] CMS collaboration, *Combination of standard model Higgs boson searches and measurements of the properties of the new boson with a mass near 125 GeV*, CMS-PAS-HIG-13-005.

[132] A. Azatov, R. Contino and J. Galloway, *Model-Independent Bounds on a Light Higgs*, *JHEP* **04** (2012) 127 [*Erratum ibid.* **1304** (2013) 140] [arXiv:1202.3415] [INSPIRE].

[133] D0 collaboration, V.M. Abazov et al., *Search for $ZH \to \ell^+\ell^- b\bar{b}$ production in 9.7 fb^{-1} of $p\bar{p}$ collisions with the D0 detector*, *Phys. Rev.* **D 88** (2013) 052010 [arXiv:1303.3276] [INSPIRE].

[134] D0 collaboration, V.M. Abazov et al., *Improved b quark jet identification at the D0 experiment*, arXiv:1312.7623 [INSPIRE].

[135] D0 collaboration, V.M. Abazov et al., *Search for the standard model Higgs boson in $\ell\nu$ + jets final states in 9.7 fb^{-1} of $p\bar{p}$ collisions with the D0 detector*, *Phys. Rev.* **D 88** (2013) 052008 [arXiv:1301.6122] [INSPIRE].

[136] D0 collaboration, V.M. Abazov et al., *Search for the standard model Higgs boson in the $ZH \to \nu\bar{\nu}b\bar{b}$ channel in 9.5 fb^{-1} of $p\bar{p}$ collisions at $\sqrt{s} = 1.96$ TeV*, *Phys. Lett.* **B 716** (2012) 285 [arXiv:1207.5689] [INSPIRE].

[137] A. Biekoetter, A. Knochel, M. Kraemer, D. Liu and F. Riva, *Vices and Virtues of Higgs EFTs at Large Energy*, arXiv:1406.7320 [INSPIRE].

JHEP07(2014)036

5 The Effective Standard Model after LHC Run 1

Published for SISSA by Springer

Received: December 1, 2014
Revised: February 12, 2015
Accepted: March 4, 2015
Published: March 30, 2015

The effective Standard Model after LHC Run I

John Ellis,[a,b] **Verónica Sanz**[c] **and Tevong You**[a]

[a] *Theoretical Particle Physics and Cosmology Group, Physics Department, King's College London, London WC2R 2LS, U.K.*

[b] *TH Division, Physics Department, CERN, CH-1211 Geneva 23, Switzerland*

[c] *Department of Physics and Astronomy, University of Sussex, Brighton BN1 9QH, U.K.*

E-mail: john.ellis@cern.ch, v.sanz@sussex.ac.uk, tevong.you@kcl.ac.uk

Abstract: We treat the Standard Model as the low-energy limit of an effective field theory that incorporates higher-dimensional operators to capture the effects of decoupled new physics. We consider the constraints imposed on the coefficients of dimension-6 operators by electroweak precision tests (EWPTs), applying a framework for the effects of dimension-6 operators on electroweak precision tests that is more general than the standard S, T formalism, and use measurements of Higgs couplings and the kinematics of associated Higgs production at the Tevatron and LHC, as well as triple-gauge couplings at the LHC. We highlight the complementarity between EWPTs, Tevatron and LHC measurements in obtaining model-independent limits on the effective Standard Model after LHC Run 1. We illustrate the combined constraints with the example of the two-Higgs doublet model.

Keywords: Higgs Physics, Beyond Standard Model, Effective field theories

ArXiv ePrint: 1410.7703

doi:10.1007/JHEP03(2015)157

JHEP03(2015)157

Contents

JHEP03(2015)157

1 Introduction

Run 1 of the LHC has taken probes of the Standard Model to a new level, not only by the discovery of the Higgs boson $H(125)$ [1, 2] and the absence of other new particles, but also via the new constraints imposed on the couplings of vector bosons and the top quark [3–41]. Now is an appropriate time to assess the global constraints placed on possible new physics by LHC Run 1 in conjunction with the Tevatron, LEP and other experiments. In view of the kinematic reach of the LHC, it is natural to suppose that the threshold for any new physics may lie substantially above the masses of the Standard Model particles. In this case, the new physics may be analyzed in the decoupling limit [42], and its effects may be parameterized in terms of higher-dimensional operators composed of Standard Model fields [43]. Using the equations of motions reduces the number of independent operators [44–49], with a complete non-redundant set first categorised in [50].

This is the effective Standard Model approach adopted in a large number of recent papers[1] [53–83], and there have been many analyses of the constraints imposed on new physics via upper limits on the coefficients of a complete dimension-6 operator basis [84–89], in particular. Several different classes of measurements make important contributions to these constraints. LEP and other experiments contribute via electroweak precision tests (EWPTs) [90], which are often presented as constraints on the S and T parameters that are defined in terms of oblique radiative corrections due to vacuum polarization diagrams, and

[1]For earlier studies of dimension-6 operators in triple-gauge couplings and Higgs physics see for example [51, 52].

via measurements of triple-gauge couplings (TGCs). The Tevatron experiments contribute via measurements of (constraints on) production of the Higgs boson H in association with massive gauge bosons $V = W^{\pm}, Z^0$ [91]. Finally, the LHC experiments contribute via many Higgs measurements including signal strengths [92, 93], branching ratios and kinematic distributions [94], and also via TGC measurements [95–97].

We demonstrated in previous work [89] the power of the constraints provided by measurements of kinematic distributions in $V + H$ production at the Tevatron and the LHC, showing that measurements of the $V + H$ invariant mass M_{VH} at the Tevatron and the transverse momentum p_T^V at the LHC could close off a 'blind' direction in the parameter space of dimension-6 operator coefficients that had been allowed by previous analyses of LEP and LHC data [98].[2] Subsequently, new data on TGCs from LHC running at 8 TeV have been published [95–97]. In this paper we make the first complete analysis of the data from LHC Run 1 and the Tevatron, in combination with the EWPT constraints, considering only CP-even operators and assuming minimal flavour violation. We consider a complete set of operators in a non-redundant basis, and the 95% CL ranges that we find for their coefficients are listed in tables 1 and 2.

We confirm previous findings that the EWPTs place very strong constraints on certain (combinations of) operator coefficients. On the other hand, we also find that the Higgs observables (signal strengths and associated production kinematics) and the TGC measurements at the LHC also have complementary rôles to play. Some operator coefficients are better constrained by the TGC data, and some by the Higgs data. One coefficient in particular only affects TGCs and nothing else. Only their combination provides a complete picture of the constraints on the dimension-6 operator coefficients after LHC Run 1.

The outline of this paper is as follows. In section 2 we discuss the EWPTs, first reviewing a general expansion formalism for EWPTs, and then demonstrating that it reproduces the constraints on the vacuum polarization parameters S and T found in other analyses before illustrating its use in capturing the effects of a complete basis of dimension-6 operators. In section 3 we discuss the constraints imposed by measurements of Higgs couplings, associated Higgs production kinematics and TGCs at the LHC, demonstrating their complementarity. Section 4 illustrates the application of these combined constraints on the coefficients of dimension-6 operators to the two-Higgs-doublet model (2HDM). Section 5 summarizes our conclusions and assesses some future prospects, and an appendix discusses aspects of kinematics and the applicability of effective field theory in our analysis.

2 Electroweak Precision Tests at LEP

Electroweak precision tests (EWPTs), particularly those provided by LEP, are amongst the most sensitive observables for constraining new physics beyond the Standard Model. EWPTs are typically summarized via constraints on the S and T parameters [99, 100] and their generalization to include the W and Y parameters [101, 102] that are relevant for custodially-symmetric and weak isospin-preserving new physics, which characterize the

[2] Contribution to G. Brooijmans et al., *Les Houches 2013: Physics at TeV Colliders: New Physics Working Group Report*, arXiv:1405.1617.

JHEP03(2015)157

Standard Model vector boson self-energy corrections.[3] If new physics affects only the Standard Model gauge sector and does not couple directly to Standard Model fermions, this approach may be sufficient for placing bounds on such 'universal' models, but the effective Standard Model also includes fermionic operators that affect electroweak precision tests. Thus a more general framework is required to capture all the possible effects of decoupled new physics in a model-independent way.

There have been many studies considering individual or subsets of bounds for all dimension-6 operators entering in EWPTs, for example [104, 105], and full analyses including simultaneously a complete basis of dimension-6 operators affecting these EWPTs have been performed in [86–88], but a full calculation of the effects of propagation of corrections to input observables and self-energies as well as direct contributions to observables was needed in each different basis. Here we employ instead the recent expansion formalism of [106], which separates the calculation of the corrections' effects on the EWPT observables and the calculations of the contributions to the corrections from new physics. This framework facilitates any χ^2 analysis that seeks to go beyond the S, T parametrization and renders more transparent the origin of the effects from each operator.

2.1 The expansion formalism

For convenience, we briefly summarize here the analysis of [106]. The principle is that, given the Standard Model with Lagrangian parameters $p_{\rm SM} \equiv \{g, g', g_s, y_t, v, \lambda\}$, one may calculate theoretical values $\hat{\mathcal{O}}_i^{\rm th}(p_{\rm SM})$ for the observables

$$\hat{\mathcal{O}}_i \equiv \left\{ m_Z, G_F, \alpha(m_Z), m_t, \alpha_s, m_H, m_W, \Gamma_l, \Gamma_q, \sigma_{\rm had}, R_l, \sin^2\theta_{\rm eff}, A_f, A_{FB}^f, \ldots \right\}$$

that are measured by experiments with errors $\Delta\hat{\mathcal{O}}_i^{\rm exp}$. To compare the theoretical predictions $\hat{\mathcal{O}}_i^{\rm th}(p_{\rm SM})$ with the experimental measurements, $\hat{\mathcal{O}}_i^{\rm exp}$, we must first choose 6 of these observables as 'input' observables $\hat{\mathcal{O}}_{i'}$, typically the most precisely measured ones,[4] such as

$$\hat{\mathcal{O}}_{i'} \equiv \{ m_Z, G_F, \alpha(m_Z), m_t, \alpha_s, m_H \} .$$

These assign values $p_{\rm SM}^{\rm ref}$ to the Lagrangian parameters such that the $\hat{\mathcal{O}}_{i'}^{\rm th}(p_{\rm SM}^{\rm ref})$ agree well with measurements, and numerical values for the other 'output' observables can then be obtained in terms of $p_{\rm SM}^{\rm ref}$.

In the presence of new physics characterized by parameters p_α, the theoretical expressions for the observables are modified by a correction $\delta^{\rm NP}\hat{\mathcal{O}}_i(p_{\rm SM}, p_\alpha)$:

$$\hat{\mathcal{O}}_i^{\rm th}(p_{\rm SM}, p_\alpha) = \hat{\mathcal{O}}_i^{\rm SM}(p_{\rm SM}) + \delta^{\rm NP}\hat{\mathcal{O}}_i(p_{\rm SM}, p_\alpha) .$$

Since the relations between input observables and Lagrangian parameters are modified in general, a different $p_{\rm SM}^{\rm ref}$ value would normally be preferred to compensate for non-zero

[3] See also [103] for another parametrisation of EWPT fits that includes vertex corrections in a set of ϵ parameters.

[4] Another convenient choice of input observables is to use m_W instead of G_F [107].

JHEP03(2015)157

values of p_α so as to remain in agreement with experiment. This may be quantified by a χ^2 analysis that varies the parameters $(p_{\rm SM}, p_\alpha)$ so as to minimize the function

$$\chi^2(p_{\rm SM}, p_\alpha) = \sum_{i,j} \left(\hat{\mathcal{O}}_i^{\rm th} - \hat{\mathcal{O}}_i^{\rm exp}\right) (\sigma^2)_{ij}^{-1} \left(\hat{\mathcal{O}}_j^{\rm th} - \hat{\mathcal{O}}_j^{\rm exp}\right) , \qquad (\sigma^2)_{ij} = \Delta\hat{\mathcal{O}}_i^{\rm exp} \rho_{ij} \Delta\hat{\mathcal{O}}_j^{\rm exp} ,$$

where ρ_{ij} is the correlation matrix.

To avoid recomputing the full expression $\hat{\mathcal{O}}_i^{\rm th}(p_{\rm SM}, p_\alpha)$ for each value of $p_{\rm SM}$ and p_α, the expansion formalism involves expanding about the Standard Model reference values for the Lagrangian parameters:

$$\begin{aligned}\hat{\mathcal{O}}_i^{\rm SM}(p_{\rm SM}) &= \hat{\mathcal{O}}_i^{\rm SM}\left(p_{\rm SM}^{\rm ref}\right) + \sum_{p_{\rm SM}} \frac{\partial\hat{\mathcal{O}}_i^{\rm SM}}{\partial p_{\rm SM}} \left(p_{\rm SM} - p_{\rm SM}^{\rm ref}\right) + \dots \\ &\simeq \hat{\mathcal{O}}_i^{\rm ref}\left[1 + \bar{\delta}^{\rm SM}\hat{\mathcal{O}}_i(p_{\rm SM})\right] ,\end{aligned}$$

where $\hat{\mathcal{O}}_i^{\rm ref} \equiv \hat{\mathcal{O}}_i^{\rm SM}\left(p_{\rm SM}^{\rm ref}\right)$, $\bar{\delta}^{\rm SM}\hat{\mathcal{O}}_i(p_{\rm SM}) = \sum_{p_{\rm SM}} G_{ip_{\rm SM}}\bar{\delta}p_{\rm SM}$, and the quantities $G_{ik'} \equiv \frac{p_{\rm SM}^{\rm ref}}{\hat{\mathcal{O}}_i^{\rm ref}}\frac{\partial\hat{\mathcal{O}}_i^{\rm SM}}{\partial p_{\rm SM}}$ are expansion coefficients that need only to be calculated once. Here $\bar{\delta}p_{\rm SM} \equiv \left(p_{\rm SM} - p_{\rm SM}^{\rm ref}\right)/p_{\rm SM}^{\rm ref}$, and the fractional shift $\bar{\delta}$ is defined in general as $\bar{\delta}\hat{\mathcal{O}}_i \equiv \left(\hat{\mathcal{O}}_i - \hat{\mathcal{O}}_i^{\rm ref}\right)/\hat{\mathcal{O}}_i^{\rm ref}$. The reference values for the SM observables are taken from table 1 of [106], to which we refer the reader for more details on the numerical calculation including the higher-order loop corrections, which were obtained using ZFITTER [108]. This is also used for the numerical differentiation involved in evaluating the expansion coefficients, which assumes that the new physics contribution factorizes out of the SM loop expansion.

Furthermore, to emphasize that the $p_{\rm SM}$ are not directly measurable, but are determined from the input observables $\hat{\mathcal{O}}_{i'}$, we note that the Lagrangian parameters can be eliminated in favour of the input observables by inverting the relation $\bar{\delta}^{\rm SM}\hat{\mathcal{O}}_{i'} = \sum_{p_{\rm SM}} G_{i'p_{\rm SM}}\bar{\delta}p_{\rm SM}$, so that

$$\bar{\delta}^{\rm SM}\hat{\mathcal{O}}_i = \sum_{i'} G_{ip_{\rm SM}} \left(\sum_{p_{\rm SM}} \left(G^{-1}\right)_{p_{\rm SM}i'} \bar{\delta}^{\rm SM}\hat{\mathcal{O}}_{i'}\right) = \sum_{i'} d_{ii'}\bar{\delta}^{\rm SM}\hat{\mathcal{O}}_{i'} .$$

The expansion coefficients for the output observables in terms of input observables are then given by the matrix $d_{ii'} \equiv \sum_{p_{\rm SM}} G_{ip_{\rm SM}}\left(G^{-1}\right)_{p_{\rm SM}i'}$.

The theoretical predictions for the output observables can now be written as $\hat{\mathcal{O}}_i^{\rm th} = \hat{\mathcal{O}}_i^{\rm ref}\left(1 + \bar{\delta}\hat{\mathcal{O}}_i^{\rm th}\right)$, with

$$\bar{\delta}\hat{\mathcal{O}}_i^{\rm th} = \sum_{i'} d_{ii'}\bar{\delta}^{\rm SM}\hat{\mathcal{O}}_{i'} + \xi_i = \sum_{i'} d_{ii'}\left(\bar{\delta}\hat{\mathcal{O}}_{i'}^{\rm th} - \xi_{i'}\right) + \xi_i ,$$

where we used $\bar{\delta}\hat{\mathcal{O}}_{i'}^{\rm SM} = \bar{\delta}\hat{\mathcal{O}}_{i'}^{\rm th} - \xi_{i'}$ and defined $\xi_i \equiv \delta^{\rm NP}\hat{\mathcal{O}}_i/\hat{\mathcal{O}}_i^{\rm ref}$. The $d_{ii'}$ matrix is pre-calculated and encapsulates the dependence of each output observable on each input observable, so that one needs only to plug in the contribution due to new physics that affect the input observables, $\xi_{i'}$, and those that directly affect the output observables, ξ_i. We note that, for the case of vector boson self-energy corrections, the $\pi_{VV} \equiv$

JHEP03(2015)157

Operator	Coefficient	LEP Constraints	
		Individual	Marginalized
$\mathcal{O}_W = \frac{ig}{2}\left(H^\dagger\sigma^a \overleftrightarrow{D^\mu} H\right) D^\nu W^a_{\mu\nu}$ $\mathcal{O}_B = \frac{ig'}{2}\left(H^\dagger \overleftrightarrow{D^\mu} H\right)\partial^\nu B_{\mu\nu}$	$\frac{m_W^2}{\Lambda^2}(c_W + c_B)$	$(-0.00055, 0.0005)$	$(-0.0033, 0.0018)$
$\mathcal{O}_T = \frac{1}{2}\left(H^\dagger \overleftrightarrow{D}_\mu H\right)^2$	$\frac{v^2}{\Lambda^2}c_T$	$(0, 0.001)$	$(-0.0043, 0.0033)$
$\mathcal{O}_{LL}^{(3)\,l} = \left(\bar{L}_L\sigma^a\gamma^\mu L_L\right)\left(\bar{L}_L\sigma^a\gamma_\mu L_L\right)$	$\frac{v^2}{\Lambda^2}c_{LL}^{(3)l}$	$(0, 0.001)$	$(-0.0013, 0.00075)$
$\mathcal{O}_R^e = \left(iH^\dagger \overleftrightarrow{D}_\mu H\right)\left(\bar{e}_R\gamma^\mu e_R\right)$	$\frac{v^2}{\Lambda^2}c_R^e$	$(-0.0015, 0.0005)$	$(-0.0018, 0.00025)$
$\mathcal{O}_R^u = \left(iH^\dagger \overleftrightarrow{D}_\mu H\right)\left(\bar{u}_R\gamma^\mu u_R\right)$	$\frac{v^2}{\Lambda^2}c_R^u$	$(-0.0035, 0.005)$	$(-0.011, 0.011)$
$\mathcal{O}_R^d = \left(iH^\dagger \overleftrightarrow{D}_\mu H\right)\left(\bar{d}_R\gamma^\mu d_R\right)$	$\frac{v^2}{\Lambda^2}c_R^d$	$(-0.0075, 0.0035)$	$(-0.042, 0.0044)$
$\mathcal{O}_L^{(3)\,q} = \left(iH^\dagger\sigma^a \overleftrightarrow{D}_\mu H\right)\left(\bar{Q}_L\sigma^a\gamma^\mu Q_L\right)$	$\frac{v^2}{\Lambda^2}c_L^{(3)q}$	$(-0.0005, 0.001)$	$(-0.0044, 0.0044)$
$\mathcal{O}_L^q = \left(iH^\dagger \overleftrightarrow{D}_\mu H\right)\left(\bar{Q}_L\gamma^\mu Q_L\right)$	$\frac{v^2}{\Lambda^2}c_L^q$	$(-0.0015, 0.003)$	$(-0.0019, 0.0069)$

Table 1. List of operators and coefficients in our basis entering in EWPTs at LEP, together with 95% CL bounds when individual coefficients are switched on one at a time, and marginalized in a simultaneous fit. For the first four coefficients we report the constraints from the leptonic observables, while the remaining coefficients also include the hadronic observables.

$\left\{\pi_{ZZ}, \pi'_{ZZ}, \pi_{\gamma Z}, \pi'_{\gamma\gamma}, \pi_{+-}, \pi^0_{WW}\right\}$ are defined as in [106], and the contributions to output observables through $\xi_{i'}$ and ξ_i are summarized by the given $b_{i,VV}$ coefficients. We then have

$$\bar{\delta}\hat{\mathcal{O}}_i^{\rm th} = \sum_{i'} d_{ii'}\bar{\delta}\hat{\mathcal{O}}_{i'}^{\rm th} + \bar{\delta}^{\rm NP}\hat{\mathcal{O}}_i\,,$$

where

$$\bar{\delta}^{\rm NP}\hat{\mathcal{O}}_i \equiv \xi_i - \sum_{i'} d_{ii'}\xi_{i'} + \sum_{VV} b_{i,VV}\delta^{\rm NP}\pi_{VV}\,, \tag{2.1}$$

and it remains only to determine the $\xi_{i'}, \xi_i$ and $\delta^{\rm NP}\pi_{VV}$ from the dimension-6 operators in the effective Standard Model.

2.2 Dimension-6 operators in EWPTs

We begin with the familiar S, T parameters before generalizing to a complete dimension-6 operator basis. The universal parts of new physics contributions are often parametrized as oblique corrections to vector boson self-energies, which can be written in terms of gauge eigenstates as

$$\mathcal{L}_{\rm VV} = -W^{+\mu}\pi_{+-}\left(p^2\right)W_\mu^- - \frac{1}{2}W^{3\mu}\pi_{33}\left(p^2\right)W_\mu^3 - W^{3\mu}\pi_{3B}\left(p^2\right)B_\mu - \frac{1}{2}B^\mu\pi_{BB}\left(p^2\right)B_\mu\,,$$

JHEP03(2015)157

where $\pi_{VV}\left(p^2\right) = \pi_{VV}^{\rm SM}\left(p^2\right) + \delta\pi_{VV}\left(p^2\right)$. Making a Taylor expansion at the quadratic order to which dimension-6 operators can contribute:

$$\pi_{VV}\left(p^2\right) = \pi_{VV}(0) + p^2\pi'_{VV}(0) + \frac{1}{2}\left(p^2\right)^2\pi''_{VV}(0) + \dots\,,$$

the usual $\hat{S}$ and $\hat{T}$ parameters[5] can be defined as

$$\hat{S} \equiv \frac{g}{g'}\frac{\pi'_{3B}(0)}{\pi'_{+-}(0)}\,, \qquad \hat{T} \equiv \frac{\pi_{+-}(0) - \pi_{33}(0)}{\pi_{+-}(0)}\,.$$

Since $\mathrm{U}(1)_Q$ symmetry is conserved, which requires $\pi_{\gamma\gamma}(0)$ and $\pi_{\gamma Z}(0)$ to vanish by gauge invariance, the following relations must hold:

$$\begin{aligned} g'^2\pi_{33}(0) + g^2\pi_{BB}(0) + 2gg'\pi_{3B}(0) &= 0 \\ g\pi_{BB}(0) + g'\pi_{3B}(0) &= 0\,. \end{aligned}$$

After normalizing the $W^\pm$ and B fields so that the kinetic terms are canonical and $\pi_{+-}(0) = -m_W^2$, we obtain the following $\hat{S}$ and $\hat{T}$ corrections in the gauge mass eigenstates for the quantities $\delta^{\rm NP}\pi_{VV}$ defined in [106]:

$$\delta^{\rm NP}\pi_{ZZ} = -\hat{T} + 2\hat{S}\sin^2\theta_W \tag{2.2}$$

$$\delta^{\rm NP}\pi'_{ZZ} = 2\hat{S}\sin^2\theta_W \tag{2.3}$$

$$\delta^{\rm NP}\pi_{\gamma Z} = -\hat{S}\cos 2\theta_W\tan\theta_W \tag{2.4}$$

$$\delta^{\rm NP}\pi'_{\gamma\gamma} = -2\hat{S}\sin^2\theta_W\,. \tag{2.5}$$

Inserting these expressions into (2.1) and performing a χ^2 analysis in the expansion formalism, using as output observables the EWPTs at the Z peak and the W mass:

$$\hat{\mathcal{O}}_i = \left\{\Gamma_Z, \sigma^0_{\rm had}, R^0_e, R^0_\mu, R^0_\tau, A^{0,e}_{\rm FB}, \sin^2\theta^e_{\rm eff}, R^0_b, R^0_c, A^{0,b}_{\rm FB}, A^{0,c}_{\rm FB}, A_b, A_c, \sin^2\theta^b_{\rm eff}, \sin^2\theta^c_{\rm eff}, m_W\right\},$$

we obtain the 68%, 95%, and 99% CL allowed regions for S vs T shown in figure 1, denoted by dotted, dashed and solid contours respectively. We treat the observables as uncorrelated but have checked that including the correlation matrix, for example in the leptonic subset as given in [90], does not affect substantially our results, which agree reasonably closely with those of [109].

The $\hat{S}$ and $\hat{T}$ parameters are equivalent to a subset of the full set of dimension-6 operators that can affect the EWPTs. In a redundant basis those entering in oblique corrections to vector boson self-energies are

$$\mathcal{L}_{\text{dim-6}} \supset \frac{\bar{c}_{WB}}{m_W^2}\mathcal{O}_{WB} + \frac{\bar{c}_W}{m_W^2}\mathcal{O}_W + \frac{\bar{c}_B}{m_W^2}\mathcal{O}_B + \frac{\bar{c}_T}{v^2}\mathcal{O}_T + \frac{\bar{c}_{2W}}{m_W^2}\mathcal{O}_{2W} + \frac{\bar{c}_{2B}}{m_W^2}\mathcal{O}_{2B}\,,$$

[5] These are related to the S and T parameters defined in [99, 100] via $S = \frac{4\sin^2\theta_W}{\alpha(m_Z)}\hat{S} \approx 119\hat{S}$ and $T = \frac{1}{\alpha(m_Z)}\hat{T} \approx 129\hat{T}$.

JHEP03(2015)157

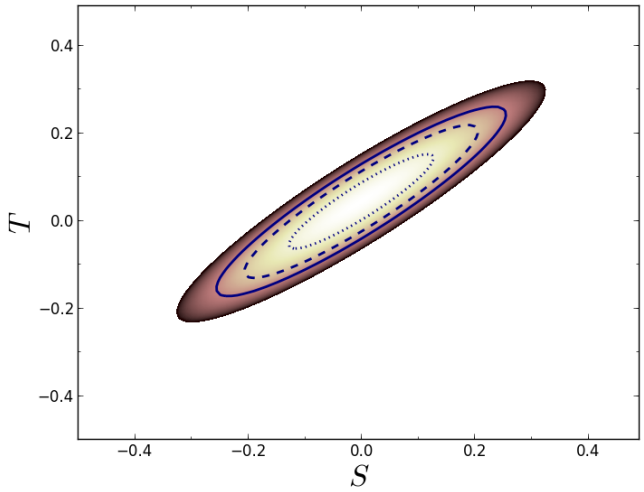

Figure 1. Results of a χ^2 analysis of ST parameters in EWPTs using the expansion formalism of [106]. The dotted, dashed and solid contours denote the regions allowed at the 68%, 95%, and 99% CL, respectively, which may be compared with those of [109].

while those that affect the leptonic and hadronic Z-pole measurements directly through modifications to the gauge boson-fermion couplings are

$$\mathcal{L}_{\text{dim-6}} \supset \sum_{f_L} \left(\frac{\bar{c}_{f_L}}{v^2} \mathcal{O}_{f_L} + \frac{\bar{c}^{(3)}_{f_L}}{v^2} \mathcal{O}^{(3)}_{f_L} \right) + \sum_{f_R} \frac{\bar{c}_{f_R}}{v^2} \mathcal{O}_{f_R} \,.$$

The sum is over the left-handed lepton and quark doublets, $f_L \equiv L_L, Q_L$, and right-handed lepton and quark singlets, $f_R \equiv e_R, u_R, d_R$, and we assume minimal flavour violation. The Fermi constant G_F defined by the muon lifetime, which we take as an input observable, is modified by $\bar{c}^{(3)}_{f_L}$ as well as the four-fermion operator $\mathcal{O}^{(3)l}_{LL}$:

$$\mathcal{L}_{\text{dim-6}} \supset \frac{\bar{c}^{(3)l}_{LL}}{v^2} \mathcal{O}^{(3)l}_{LL} \,.$$

We note that the coefficients are defined such that

$$\bar{c} \equiv c \frac{M^2}{\Lambda^2} \,, \tag{2.6}$$

where $M \equiv v, m_W$ depending on the operator normalization, and $c \sim g^2_{\text{NP}}$ is a coefficient proportional to a new physics coupling g_{NP} defined at the scale M. These are related to the coefficients at the new physics scale through RGE equations [110–117].

These operators form a redundant basis that is reducible through field redefinitions, or equivalently the equations of motion, that have no effect on the S-matrix [44–49]. Following [88], we may eliminate the operators $\mathcal{O}_{L_L}, \mathcal{O}^{(3)}_{L_L}$ that affect the left-handed leptonic Z couplings, and the operators $\mathcal{O}_{2W}, \mathcal{O}_{2B}, \mathcal{O}_{2G}$ corresponding to the Y, W and Z parameters [101, 102] in the generalization of the universal oblique parameters.[6] The coefficients

[6]The U, V and X parameters correspond to higher-dimensional operators.

JHEP03(2015)157

$\bar{c}_{WB}$ and the combination $\bar{c}_W + \bar{c}_B$ are related to the $\hat{S}$ parameter, and we eliminate the former using the identity

$$\mathcal{O}_B = \mathcal{O}_{HB} + \frac{1}{4}\mathcal{O}_{BB} + \frac{1}{4}\mathcal{O}_{WB}\,.$$

The operators $\mathcal{O}_{HB}, \mathcal{O}_{BB}$ affect Higgs physics and triple-gauge couplings, as we shall see in the next section. Finally, the $\hat{T}$ parameter is equivalent to the $\bar{c}_T$ coefficient. This choice of basis minimises the correlation of operator combinations among EWPT and LHC measurements. These operators are listed in table 1, and the remaining operators eliminated from our basis are defined in [118].

The corrections to the self-energies are then as in (2.5), with $\hat{S} = \bar{c}_W + \bar{c}_B$ and $\hat{T} = \bar{c}_T$. We also have the input observable correction

$$\xi_{G_F} = -2\bar{c}_{LL}^{(3)l}\,,$$

and direct contributions to the output observables,

$$\begin{aligned}
\xi_{\Gamma_Z} &= \frac{\Gamma_Z^l}{\Gamma_Z}\xi_{\Gamma_Z^l} + \frac{\Gamma_Z^{\rm had}}{\Gamma_Z}\xi_{\Gamma_Z^{\rm had}}\,,\\
\xi_{\sigma^0_{\rm had}} &= \xi_{\Gamma_Z^e} + \xi_{\Gamma_Z^{\rm had}} - 2\xi_{\Gamma_Z}\,,\\
\xi_{R_l} &= \xi_{\Gamma_Z^{\rm had}} - \xi_{\Gamma_Z^l}\,,\\
\xi_{R_q} &= \xi_{\Gamma_Z^q} - \xi_{\Gamma_Z^{\rm had}}\,,\\
\xi_{A_{\rm FB}^{0,f}} &= \xi_{A_e} + \xi_{A_f}\,,
\end{aligned}$$

which can be written in terms of shifts to the Z-fermion couplings,

$$\begin{aligned}
\xi_{A_f} &= \frac{4\left(g_Z^{f_L}\right)^2\left(g_Z^{f_R}\right)^2}{\left(g_Z^{f_L}\right)^4 - \left(g_Z^{f_R}\right)^4}\left(\xi_{g_Z^{f_L}} - \xi_{g_Z^{f_R}}\right)\,,\\
\xi_{\Gamma_Z^f} &= \frac{2\left(g_Z^{f_L}\right)^2}{\left(g_Z^{f_L}\right)^2 + \left(g_Z^{f_R}\right)^2}\xi_{g_Z^{f_L}} + \frac{2\left(g_Z^{f_R}\right)^2}{\left(g_Z^{f_L}\right)^2 + \left(g_Z^{f_R}\right)^2}\xi_{g_Z^{f_R}}\,,
\end{aligned}$$

where

$$\xi_{g_Z^{f_L}} = \frac{1}{g_Z^{f_L}}\left(T_f^3\bar{c}_{f_L}^{(3)} - \frac{\bar{c}_{f_L}}{2}\right)\,, \qquad \xi_{g_Z^{f_R}} = -\frac{\bar{c}_{f_R}}{2g_Z^{f_R}}\,,$$

and $g_Z^f \equiv T_f^3 - Q_f s^2_{\theta_W}$. Using these expressions and the expansion formalism in a χ^2 analysis, we obtain 95% CL limits for the operator coefficients.

The left panel of figure 2 shows our results for fits to the coefficients $\bar{c}_{LL}^{(3)l}, \bar{c}_T, \bar{c}_W + \bar{c}_B$, together with the coefficient $\bar{c}_R^e$ that affects the leptonic observables $\{\Gamma_Z, \sigma^0_{\rm had}, R_e^0, R_\mu^0, R_\tau^0, A_{\rm FB}^{0,e}, m_W\}$. The upper (green) bars indicate the ranges for each of the coefficients varied individually, assuming that the other coefficients vanish, and the lower (red) bars show the ranges for a global fit in which all the coefficients are varied simultaneously. In both fits, the coefficients are all quite compatible with zero, with ranges $\sim \pm 0.001$ in the single-coefficient analysis, increasing in the global fit up to $\sim \pm 0.004$ for the coefficient $\bar{c}_T$ in the

JHEP03(2015)157

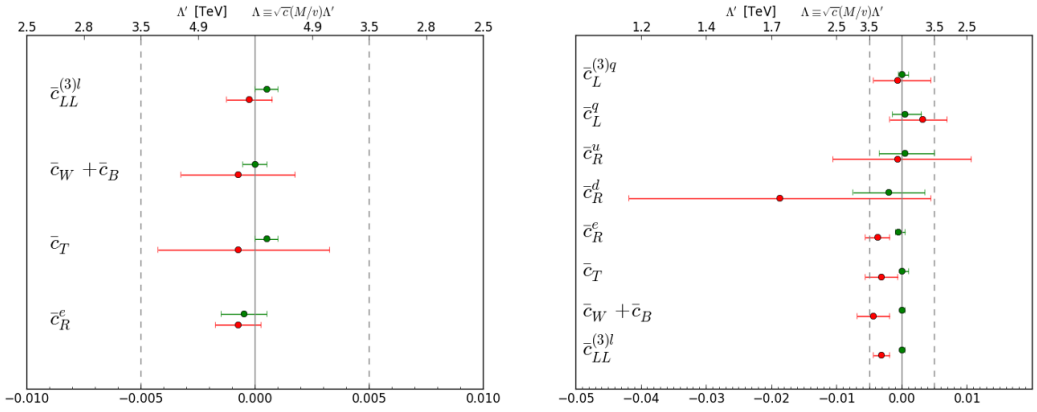

Figure 2. The 95% CL ranges found in analyses of the leptonic observables (left panel) and including also the hadronic observables (right panel). In each case, the upper (green) bars denote single-coefficient fits, and the lower (red) bars denote multi-coefficient fits. The upper-axis should be read $\times \frac{m_W}{v} \sim 1/3$ for $\bar{c}_W + \bar{c}_B$.

multi-coefficient analysis.[7] The legend at the top of the left panel of figure 2 translates the ranges of the coefficients into ranges of sensitivity to a large mass scale Λ. We see that all the sensitivities are in the multi-TeV range, including in the global analysis.

The right panel of figure 2 shows the effect of including the hadronic observables, $\{R_b^0, R_c^0, A_{\rm FB}^{0,b}, A_{\rm FB}^{0,c}, A_b, A_c\}$, and the coefficients that contribute directly to them, namely $\bar{c}_L^q, \bar{c}_L^{(3)q}, \bar{c}_R^u$ and $\bar{c}_R^d$. The ranges for the single-variable fits to $\bar{c}_{LL}^{(3)l}, \bar{c}_T, \bar{c}_W + \bar{c}_B$ and $\bar{c}_R^e$ (upper,green lines) are the same as in the left panel, but the horizontal scales are different, as seen immediately by comparing the separations of the vertical black dashed 'tramlines'. The ranges of these coefficients are altered significantly in the global 8-coefficient fit (lower, red lines) and we see significant tension with the null hypotheses for $\bar{c}_{LL}^{(3)l}, \bar{c}_T, \bar{c}_W + \bar{c}_B$ and $\bar{c}_R^e$, which reflects the well-known tension between the Standard Model and heavy-flavour measurements at the Z peak. However, values of $\bar{c}_{LL}^{(3)l}, \bar{c}_T, \bar{c}_W + \bar{c}_B$ and $\bar{c}_R^e$ between 0 and -0.01 are favoured, corresponding to $\Lambda \gtrsim 2.5\,\text{TeV}$. The ranges of $\bar{c}_L^q, \bar{c}_L^{(3)q}, \bar{c}_R^u$ and $\bar{c}_R^d$ are considerably broader in both fits, particularly in the global 8-coefficient fit, most notably $\bar{c}_R^u$ and $\bar{c}_R^d$, with values of the latter approaching -0.05 being allowed at the 95% CL.

3 Triple-gauge and Higgs couplings at the LHC

In previous work [89] we used LHC measurements of Higgs signal strengths together with differential distributions in Higgs associated production measurements by ATLAS and D0 to constrain all the dimension-6 operators affecting Higgs physics. The associated production information was vital in eliminating a blind direction, which can also be closed by including TGC measurements. These are most precisely measured by LEP, but it has been

[7] We note that larger marginalized ranges for $\bar{c}_R^e$ and $\bar{c}_{LL}^{(3)l}$ are found in [88], warranting further cross-checks.

JHEP03(2015)157

Operator	Coefficient	LHC Constraints	
		Individual	Marginalized
$\mathcal{O}_W = \frac{ig}{2}\left(H^\dagger\sigma^a \overleftrightarrow{D^\mu} H\right) D^\nu W^a_{\mu\nu}$ $\mathcal{O}_B = \frac{ig'}{2}\left(H^\dagger \overleftrightarrow{D^\mu} H\right)\partial^\nu B_{\mu\nu}$	$\frac{m_W^2}{\Lambda^2}(c_W - c_B)$	$(-0.022, 0.004)$	$(-0.035, 0.005)$
$\mathcal{O}_{HW} = ig(D^\mu H)^\dagger\sigma^a(D^\nu H)W^a_{\mu\nu}$	$\frac{m_W^2}{\Lambda^2}c_{HW}$	$(-0.042, 0.008)$	$(-0.035, 0.015)$
$\mathcal{O}_{HB} = ig'(D^\mu H)^\dagger(D^\nu H)B_{\mu\nu}$	$\frac{m_W^2}{\Lambda^2}c_{HB}$	$(-0.053, 0.044)$	$(-0.045, 0.075)$
$\mathcal{O}_{3W} = \frac{1}{3!}g\epsilon_{abc}W^{a\,\nu}_{\mu}W^b_{\nu\rho}W^{c\,\rho\mu}$	$\frac{m_W^2}{\Lambda^2}c_{3W}$	$(-0.083, 0.045)$	$(-0.083, 0.045)$
$\mathcal{O}_g = g_s^2\lvert H\rvert^2 G^A_{\mu\nu}G^{A\mu\nu}$	$\frac{m_W^2}{\Lambda^2}c_g$	$(0, 3.0)\times 10^{-5}$	$(-3.2, 1.1)\times 10^{-4}$
$\mathcal{O}_\gamma = g'^2\lvert H\rvert^2 B_{\mu\nu}B^{\mu\nu}$	$\frac{m_W^2}{\Lambda^2}c_\gamma$	$(-4.0, 2.3)\times 10^{-4}$	$(-11, 2.2)\times 10^{-4}$
$\mathcal{O}_H = \frac{1}{2}\left(\partial^\mu\lvert H\rvert^2\right)^2$	$\frac{v^2}{\Lambda^2}c_H$	$(-0.14, 0.194)$	$(-, -)$
$\mathcal{O}_f = y_f\lvert H\rvert^2\bar{F}_L H^{(c)} f_R + \text{h.c.}$	$\frac{v^2}{\Lambda^2}c_f$	$(-0.084, 0.155)(c_u)$ $(-0.198, 0.088)(c_d)$	$(-, -)$ $(-, -)$

Table 2. List of operators in our basis entering in LHC Higgs (including D0 associated production) and TGC physics, together with 95% CL bounds when individual coefficients are switched on one at a time, and marginalized in a simultaneous fit.

recently pointed out that the LEP TGC constraints[8] have a direction of limited sensitivity due to accidental partial cancellations [98]. Meanwhile, TGCs have been analysed at 8 TeV at the LHC by both the CMS and ATLAS experiments [95–97], and here we study their potential to complement Higgs physics in constraining a complete set of dimension-6 operators.

3.1 TGC constraints on dimension-6 operator coefficients

The operators affecting Higgs physics and TGCs in the basis we adopt are listed in table 2, with the Lagrangian given by

$$\mathcal{L}_{\text{dim-6}} \supset \frac{\bar{c}_W}{m_W^2}\mathcal{O}_W + \frac{\bar{c}_B}{m_W^2}\mathcal{O}_B + \frac{\bar{c}_{HW}}{m_W^2}\mathcal{O}_{HW} + \frac{\bar{c}_{HB}}{m_W^2}\mathcal{O}_{HB} + \frac{\bar{c}_\gamma}{m_W^2}\mathcal{O}_\gamma + \frac{\bar{c}_g}{m_W^2}\mathcal{O}_g + \frac{\bar{c}_{3W}}{m_W^2}\mathcal{O}_{3W} + \sum_{f=t,b,\tau}\frac{\bar{c}_f}{v^2}\mathcal{O}_f + \frac{\bar{c}_H}{v^2}\mathcal{O}_H + \frac{\bar{c}_6}{v^2}\mathcal{O}_6\,.$$

The constraint at the per-mille level on the combination $\bar{c}_W + \bar{c}_B$ obtained in the previous section allows us to set $\bar{c}_B = -\bar{c}_W$ (or equivalently to constrain the direction $\bar{c}_W - \bar{c}_B$). Ignoring the unconstrained operator $\mathcal{O}_6$ that affects the Higgs self-couplings and (for simplicity) setting $\bar{c}_b = \bar{c}_\tau \equiv \bar{c}_d$ then reduces the number of independent coefficients to nine. The coefficients $\bar{c}_W, \bar{c}_{HW}, \bar{c}_{HB}$ and $\bar{c}_{3W}$ affect TGCs, with $\bar{c}_{3W}$ being limited only by TGC measurements, since it does not affect Higgs physics.

[8] See also [119] for a recent discussion on the use of TGC observables as reported by LEP for constraining dimension-6 operators in different bases.

JHEP03(2015)157

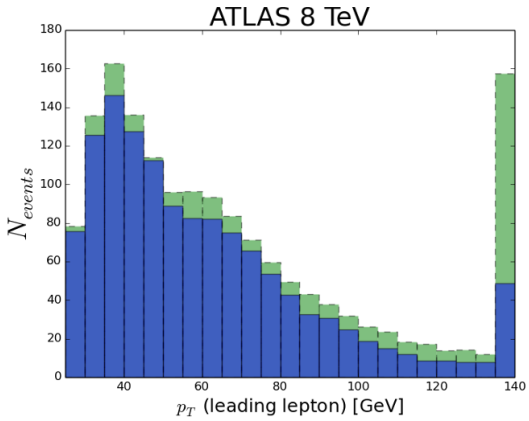

Figure 3. The same-flavour p_T distribution of the leading lepton after the TGC analysis cuts for ATLAS at 8 TeV. The Standard Model distribution is shown in blue with solid lines, and the effect of $\bar{c}_{HW} = 0.1$ is superimposed in green with dashed lines.

Note that our parametrization in terms of dimension-six effective operators are related to the *anomalous coupling* characterization [120–122], and the translation in written in the tables in ref. [118]. The kappa-formalism [123] can be linked to the EFT and AC characterization only at the level of total cross sections.

We calculate the TGCs in the presence of dimension-6 operators using the `FeynRules` implementation of [118] in `MadGraph v2.1.2` [124], interfaced with `Pythia` [125] and `Delphes` [126]. In the case of ATLAS, we implement the analysis given in [97]. This requires events that pass the selection cuts to have exactly 2 opposite-sign leptons with no jets, $p_T > 25(20)\,\text{GeV}$ for leading (sub-leading) leptons, $m_{ll} > 15(10)\,\text{GeV}$ and $E_T^{\text{miss}} > 45(15)\,\text{GeV}$ for same-flavour (different-flavour) lepton pairs, as well as $|m_{ll} - m_Z| > 15\,\text{GeV}$ for the same-flavour case. Similarly, following [95, 96], for the CMS cuts we require 2 opposite-sign leptons with $p_T > 20\,\text{GeV}$, total lepton $p_T > 45\,\text{GeV}$ and $75\,\text{GeV} < m_{ll} < 105\,\text{GeV}$, $E_T^{\text{miss}} > 37(20)\,\text{GeV}$ and $m_{ll} > 20(12)\,\text{GeV}$ for same-flavour (opposite-flavour) pairs, and no jets with $|\eta| < 5, E_T > 30\,\text{GeV}$.

The resulting p_T distribution of the leading lepton for the ATLAS 8 TeV analysis is shown in figure 3 including $\bar{c}_{HW} = 0.1$ as well as the Standard Model contribution.[9] We focus on the number of events in the last (overflow) bin, since this has the highest signal-to-background ratio and grows rapidly as a function of this and the other dimension-6 coefficients.[10] We prefer to keep only the linear dependences on the dimension-6 coefficients, considering that it is not consistent to keep terms that are quadratic in the dimension-6 coefficients if one does not have reason to expect that the coefficients of dimension-8 operators would be suppressed. As an example, we note that the signal-strength dependence of the overflow bin on $\bar{c}_{HW}$ for the ATLAS 8-TeV same-flavour distribution is found to be

$$\mu^{\text{ATLAS8}}_{\text{last-bin}} = 1 + 3.45\bar{c}_{HW} + 234\bar{c}^2_{HW}\,,$$

[9] The applicability of the effective field theory approach to this TGC analysis is discussed in the appendix.

[10] The validity of the effective field theory at such high p_T may be restricted only to certain models [127, 128], but the range of validity will increase as the current precision of LHC TGC measurements is improved.

JHEP03(2015)157

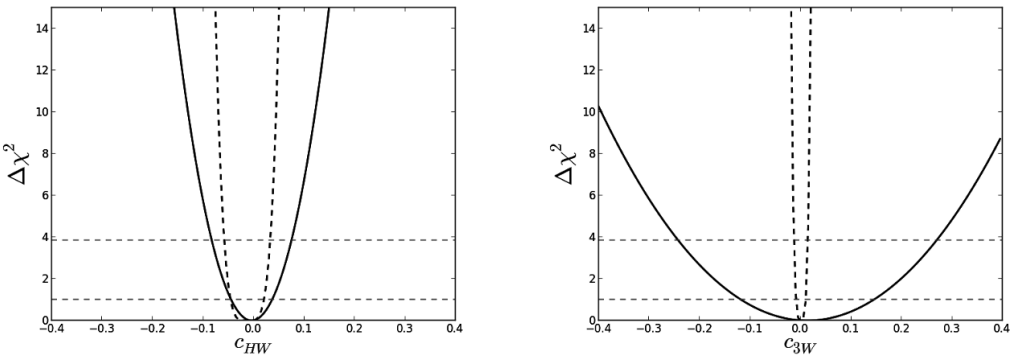

Figure 4. Comparisons between the χ^2 functions from fits to the same-flavour ATLAS distribution including only linear (solid lines) and also quadratic (dashed lines) dependences on the dimension-6 coefficients $\bar{c}_{HW}$ (left panel) and $\bar{c}_{3W}$ (right panel).

and we keep only the linear term in our global fits. The constraints obtained using this linear (quadratic) dependence on the dimension-6 coefficients are plotted as solid (dashed) lines in figure 4. The left panel is for $\bar{c}_{HW}$, and right panel is for $\bar{c}_{3W}$. When deriving constraints we use the background and Standard Model signal Monte-Carlo (MC) distributions of the leading lepton p_T provided by the experiments, and marginalize over the MC error. This is given along with the observed number of events and their errors in [97] for ATLAS and [95, 96] for CMS. We see that the quadratic and linear fits for $\bar{c}_{HW}$ are quite similar, whereas the constraint from the (preferred) linear fit for $\bar{c}_{3W}$ is significantly weaker than that from the (deprecated) quadratic fit.

For the full global fit we use the same-flavour and different-flavour distributions for ATLAS at 8 TeV and the CMS 7 and 8 TeV data. In figure 5 we compare the constraints from the combination of the ATLAS and CMS TGC measurements with the LHC Higgs signal-strength data on each of the dimension-6 coefficients $\bar{c}_W$, $\bar{c}_{HW}$ and $\bar{c}_{HB}$ (top row), $\bar{c}_g$, $\bar{c}_\gamma$ and $\bar{c}_{3W}$ (middle row), and $\bar{c}_b$, $\bar{c}_t$ and $\bar{c}_H$ (bottom row).[11] The purple line represents the combination of LHC signal-strength constraints with the ATLAS 8-TeV TGC measurements, the blue line the combination of CMS 7- and 8-TeV constraints, and the red line uses all the sets of LHC TGC constraints. We use the signal-strength information on the $W^+W^{-(*)}$, $ZZ^{(*)}$, $\gamma\gamma$, $Z\gamma$, and $\tau^+\tau^-$ final states, whose likelihoods are obtained as explained in [89]. We observe that the constraints on the coefficient $\bar{c}_{3W}$, which only affects TGCs, is at the same level as some of the other coefficients whose operators also affect Higgs physics.

The results in figure 5 are summarised in the marginalised 95% CL ranges displayed in figure 6. Again, the LHC signal-strength data are always included, in combination with the ATLAS 8-TeV data (purple bars), the CMS 7- and 8-TeV data (blue bars) and all the LHC TGC data (red bars). As already mentioned, the LHC TGC data enables a competitive model-independent bound on the coefficient $\bar{c}_{3W}$.

[11] We note that the constraints on the last three operators are relatively weak, but include them for information.

JHEP03(2015)157

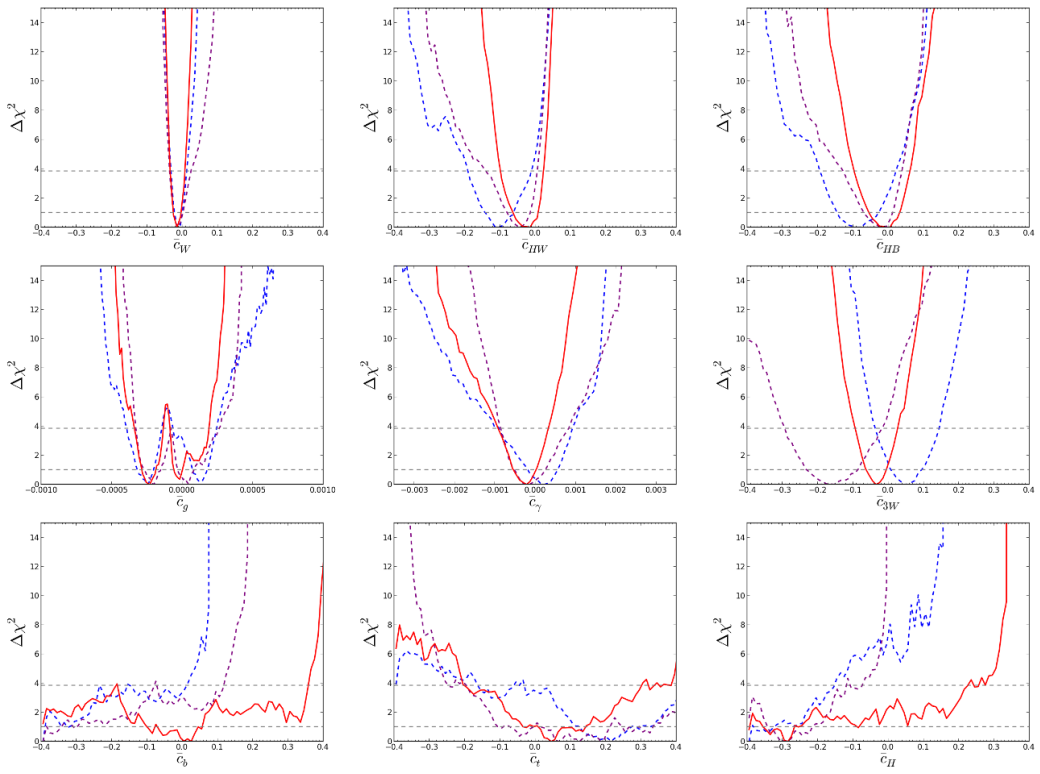

Figure 5. Comparisons of the constraints on the dimension-6 coefficients $\bar{c}_W$, $\bar{c}_{HW}$ and $\bar{c}_{HB}$ (top row), $\bar{c}_g$, $\bar{c}_\gamma$ and $\bar{c}_{3W}$ (middle row), and $\bar{c}_b$, $\bar{c}_t$ and $\bar{c}_H$ (bottom row) provided by the LHC signal-strength data together with the ATLAS 8-TeV (purple lines), the CMS 7- and 8-TeV TGC measurements (blue lines) and their combination (red lines).

3.2 Inclusion of Higgs associated production constraints

We now include in our analysis the constraints from the kinematics of associated Higgs production, following the analysis of [89].[12] Figure 7 displays the marginalised χ^2 distributions for each of the dimension-6 coefficients $\bar{c}_W$, $\bar{c}_{HW}$ and $\bar{c}_{HB}$ (top row), $\bar{c}_g$, $\bar{c}_\gamma$ and $\bar{c}_{3W}$ (middle row), and $\bar{c}_b$, $\bar{c}_t$ and $\bar{c}_H$ (bottom row).[13] In each panel, the dashed blue line includes the Higgs signal strengths measured at the LHC and the constraints from the kinematic distributions for associated $H + V$ production measured by ATLAS and D0, whereas the solid red line includes the signal strengths and the LHC TGC measurements. The solid black lines include all the constraints: the signal strengths, the kinematic distributions and the TGCs measured at the LHC. We see that the LHC TGC measurements are the strongest for $\bar{c}_W$ and $\bar{c}_{3W}$: in particular, they are necessary to obtain any meaningful constraint on $\bar{c}_{3W}$, which cannot be constrained at all by Higgs physics along as the marginalized

[12] The applicability of the effective field theory approach to this associated production analysis is discussed in the appendix.

[13] We note again that the constraints on the last three operators are relatively weak, but include them for information.

JHEP03(2015)157

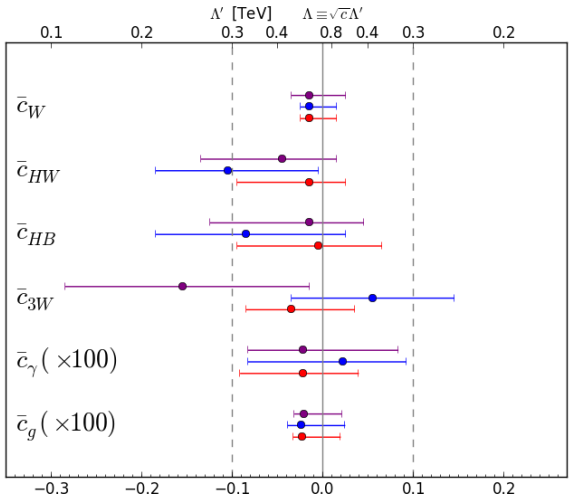

Figure 6. The marginalised 95% CL ranges for the dimension-6 operator coefficients obtained by combining the LHC signal-strength data with the ATLAS 8-TeV TGC data (purple bars), the CMS 7- and 8-TeV TGC measurements (blue bars), and their combination (red bars). Note that $\bar{c}_{\gamma,g}$ are shown $\times 100$, so for these coefficients the upper axis should therefore be read $\times 10$.

likelihood (shown as a dashed blue line) fluctuates stochastically over a range larger than that displayed. On the other hand, the Higgs constraints are more important for $\bar{c}_{HW}$, $\bar{c}_{HB}$ and $\bar{c}_g$, whereas the TGC and Higgs constraints are of comparable importance for the other coefficients.

The results of our fits are summarised in figure 8. The individual 95% CL constraints obtained by switching one coefficient on at a time are shown as green bars. The other lines are the marginalised 95% ranges obtained using the LHC signal-strength data in combination with the kinematic distributions for associated $H + V$ production measured by ATLAS and D0 (blue bars), in combination with the LHC TGC data (red lines), and in combination with both the associated production and TGC data (black bars). We see again that the LHC TGC constraints are the most important for $\bar{c}_W$ and $\bar{c}_{3W}$, whereas the Higgs constraints are more important for $\bar{c}_{HW}$, $\bar{c}_{HB}$ and $\bar{c}_g$. Our numerical results for the 95% CL ranges for these coefficients are shown alongside the operator definitions in table 2. Results for the coefficients c_b, c_t and c_H are shown in the case of one-by-one constraints, but once other Higgs-gauge bosons are included in the global fit the sensitivities to them is reduced to current limits on $h \to b\bar{b}$ in associated production and $t\bar{t}h$.

4 Application to the Two-Higgs Doublet Model

We now discuss an example of the application of our constraints to a specific ultra-violet (UV) completion of the effective field theory. The case of a singlet scalar and stops contributing to dimension-6 operators was recently considered in [129]. Here we briefly look at applying our constraints to the 2HDM scenario, which is worth further investigation [130].

JHEP03(2015)157

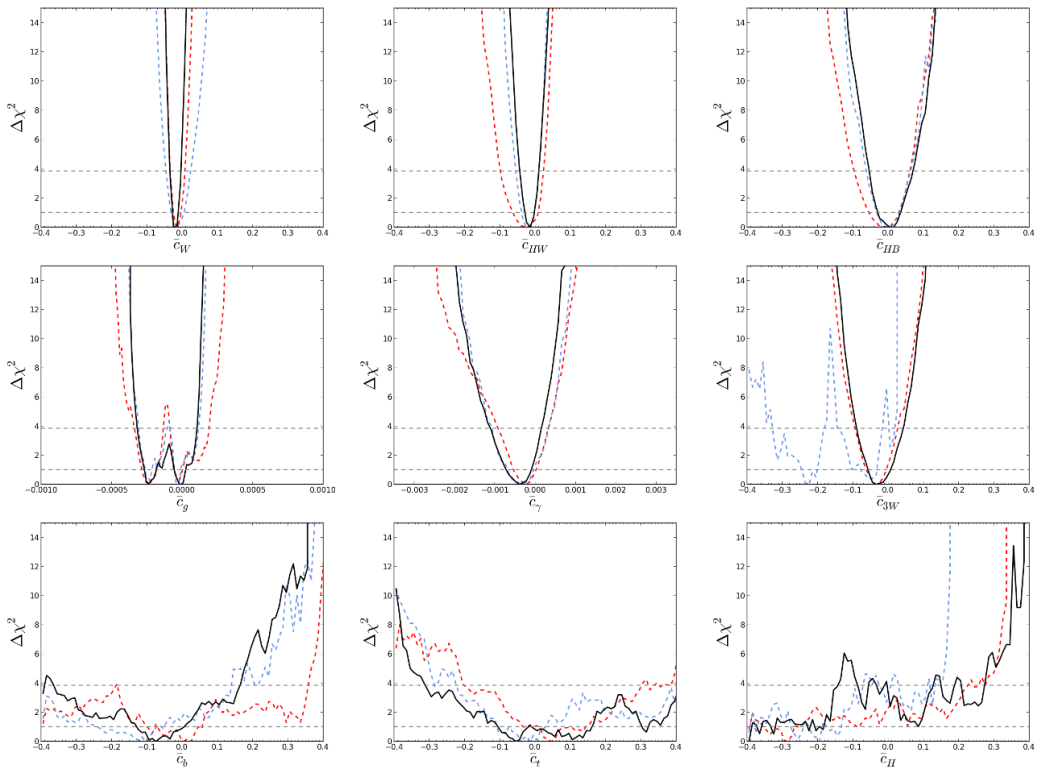

Figure 7. The marginalised χ^2 distributions for each of the dimension-6 coefficients $\bar{c}_W$, $\bar{c}_{HW}$ and $\bar{c}_{HB}$ (top row), $\bar{c}_g$, $\bar{c}_\gamma$ and $\bar{c}_{3W}$ (middle row), and $\bar{c}_b$, $\bar{c}_t$ and $\bar{c}_H$ (bottom row), including the signal strengths measured at the LHC and the constraints from the kinematic distributions for associated $H + V$ production measured by ATLAS and D0 (dashed blue lines), the signal strengths and the LHC TGC measurements (red lines), and all the constraints (black lines).

We will be interested in particular in the case of the 2HDM in the alignment limit [131, 132], where the light Higgs couples to fermions and gauge bosons as the SM-Higgs, and all new effects are then through loops of the heavy scalars in the 2HDM, as opposed to the usual limits coming from deviations of the Higgs couplings through mixing.

In a large range of models, including the 2HDM in this limit, the only coupling of the Higgs to massive vector bosons has the following Lorentz structure

$$hW_{\mu\nu}W^{\mu\nu} \,. \tag{4.1}$$

The translation between this Higgs anomalous coupling and the operators is given in [118] (see also [133]). The following constraints

$$\bar{c}_{HW} = -\bar{c}_W, \quad \bar{c}_{HB} = -\bar{c}_B \tag{4.2}$$

are then satisfied at the UV scale. We recall from section 2 that, in addition, the EWPTs impose the constraint $\bar{c}_W \simeq -\bar{c}_B$, implying that, to a good approximation

$$\bar{c}_W = -\bar{c}_B = -\bar{c}_{HW} = \bar{c}_{HB} \,, \tag{4.3}$$

JHEP03(2015)157

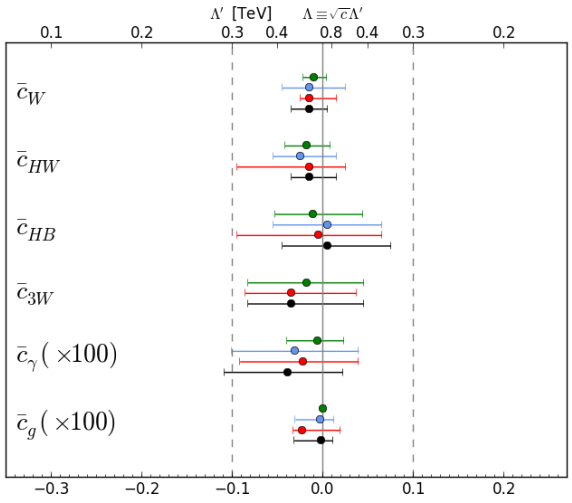

Figure 8. The 95% CL constraints obtained for single-coefficient fits (green bars), and the marginalised 95% ranges for the LHC signal-strength data combined with the kinematic distributions for associated $H + V$ production measured by ATLAS and D0 (blue bars), combined with the LHC TGC data (red lines), and the global combination with both the associated production and TGC data (black bars). Note that $\bar{c}_{\gamma,g}$ are shown $\times 100$, so for these coefficients the upper axis should therefore be read $\times 10$.

with corrections due to renormalization-group running effects that are negligible compared to the precision of the current LHC constraints. Moreover, in the 2DHM one also finds generically that $\bar{c}_{3W}$ is suppressed [130]

$$\bar{c}_{3W} \;\sim\; \mathcal{O}(0.1) g^2 \bar{c}_{HW}\,, \tag{4.4}$$

so that it can be an order of magnitude smaller. In our application to the 2HDM we set it to zero, as well as using the constraints (4.3). Note that in this case, the fit to electroweak data would be complementary to the LHC constraints, as the same operators involved in the Higgs data would be affecting TGCs, LEP and LHC [88]. Below we give the results of the fit using LHC diboson and Higgs data only, as with the combination of diboson ATLAS and CMS data, the inclusion of LEP data does not substantially affect our results.

Examples of models in this class include a general two-Higgs doublet model (2HDM) [130], supersymmetry with electroweakino/sfermion loops [134], and the exchange of a radion/dilaton particle [133]. In the former two models these operators are generated at loop level, whereas in the third case the operators appear at tree-level through the exchange of the radion/dilaton particle. In the loop-induced cases, the validity of the effective theory is typically $\sqrt{\hat{s}} \sim 2M$, where M is the mass scale of the heavy states. In 2HDMs one would usually finds modifications of the coupling of the H

Figure 9 shows the χ^2 distributions we find in a global fit to the three independent dimension-6 coefficients of the 2HDM, $\bar{c}_W$, $\bar{c}_g$ and $\bar{c}_\gamma$ obtained under these assumptions. These distributions have been obtained including all the constraints from the signal strengths measured at the LHC, the constraints from the kinematic distributions for asso-

JHEP03(2015)157

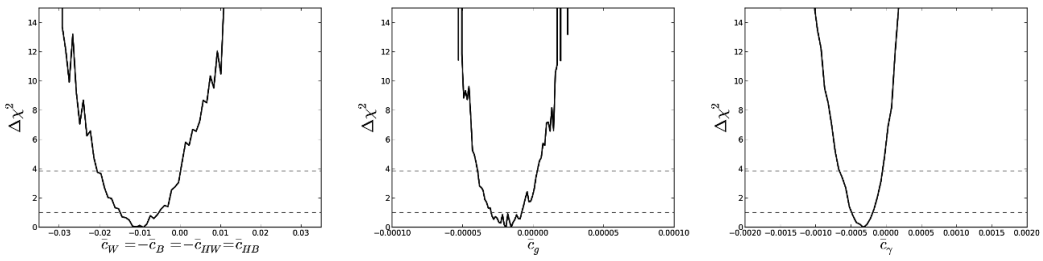

Figure 9. The marginalised χ^2 distributions for the coefficients $\bar{c}_W = -\bar{c}_B = -\bar{c}_{HW} = \bar{c}_{HB}$, $\bar{c}_g$, and $\bar{c}_\gamma$ of the three independent dimension-6 operators in the 2HDM under the assumptions stated in the text.

ciated $H + V$ production measured by ATLAS and D0, and the LHC TGC measurements. We find the following 95% CL ranges

$$\begin{aligned} \bar{c}_W &\in -(0.02, 0.0004) \\ \bar{c}_g &\in -(0.00004, 0.000003) \\ \bar{c}_\gamma &\in -(0.0006, -0.00003) \end{aligned} \tag{4.5}$$

in this particular class of models. The translation between the coefficients and the 2HDM will be presented in ref. [130], but let us comment here how these values relate to the validity of the effective theory. Roughly speaking, we find that $\bar{c} \simeq \frac{\lambda}{192\pi^2}\frac{v^2}{M^2}$, with λ a quartic coupling in the 2HDM scalar potential and M the mass of the heavy particles. Hence, a limit of the order of 10^{-4} would lead to a mass limit of 2 TeV for $\lambda = 4\pi$, and decrease as the the coupling becomes smaller.

5 Conclusions

The main lesson learned from Run I of the LHC is that, to a first approximation, we seem to have a Standard Model-like Higgs sector. Taken together with the fact that there is currently no clear evidence for any new physics beyond the Standard Model, it is natural to consider the Standard Model in its complete effective theory formulation. Such a (relatively) model-independent framework parameterises all the possible ways in which decoupled new physics may affect measurements at different experiments in a correlated and motivated way.

We have analysed in this paper the constraints imposed on the coefficients of dimension-6 operator extensions of the Standard Model by EWPTs and LHC data. We first analysed the EWPTs using the expansion formalism of [106], which is particularly appropriate for models where the dominant corrections to the Standard Model predictions are not necessarily present only in the vector-boson self-energies, as is the case for general dimension-6 extensions of the Standard Model. We confirm previous findings that the EWPTs provide particularly important constraints on some of the operator coefficients, as shown in figure 2 and table 1.

JHEP03(2015)157

We then analysed the TGC data now available from ATLAS at 8 TeV and from CMS at 7 and 8 TeV. We find that the most important aspects of the data are the highest-energy (overflow) bins in the lepton p_T distributions, as illustrated in figure 3, and use these together with Higgs signal strength measurements to obtain constraints on a set of nine operator coefficients, as shown in figures 5 and 6. We then combined these LHC TGC constraints with the constraints provided by measurements of the kinematics of Higgs production in association with massive vector bosons at the Tevatron and the LHC, obtaining the results shown in figures 7 and 8 and table 2. As seen there, we find that completing the Higgs signal strengths constraints on dimension-6 operators using the LHC TGCs provide the strongest LHC constraints on some of the coefficients, whereas the Higgs differential distributions in associated production are more important for some others, with both making important contributions in some cases. In particular, we obtain the first bounds on the coefficient $\bar{c}_{3W}$ for a complete basis in the effective Standard Model. It is only by combining the TGC and Higgs constraints that one can obtain a complete picture of the possible ranges of the dimension-6 operator coefficients after LHC Run 1.

It is to be expected that Run 2 of the LHC will provide important improvements in the sensitivity of LHC probes of possible dimension-6 operators. These improvements will come not only from the greater statistics, but also from the greater kinematic range that will strengthen the power of the associated Higgs production kinematics and the TGC constraints, in particular. At the moment we know that the Standard Model is very effective: LHC Run 2 data will give us a better idea just how effective it is, and perhaps provide some pointers to the nature of the new physics that surely lies beyond it at higher energies.

Acknowledgments

We thank Francesco Riva for useful conversations and Maxime Gouzevitch and Alexander Savin for helpful information about the CMS TGC distributions. The work of JE was supported partly by the London Centre for Terauniverse Studies (LCTS), using funding from the European Research Council via the Advanced Investigator Grant 26732, and partly by the STFC Grant ST/J002798/1. The work of VS was supported by the STFC Grant ST/J000477/1. The work of TY was supported by a Graduate Teaching Assistantship from King's College London.

A Kinematics and the validity of the effective field theory

We use in section 3 triple-gauge couplings and information on kinematic distributions in Higgs production in association with a vector boson production constraints, finding that typical 95% CL constraints on the dimension-6 coefficients are $\mathcal{O}(10^{-1}\text{–}10^{-2})$. For example, for the operator $\bar{c}_W$ our limits are

$$\bar{c}_W \in (-0.022, 0.004) \text{ [one-by-one] and } (-0.035, 0.005) \text{ [global]}\,. \tag{A.1}$$

JHEP03(2015)157

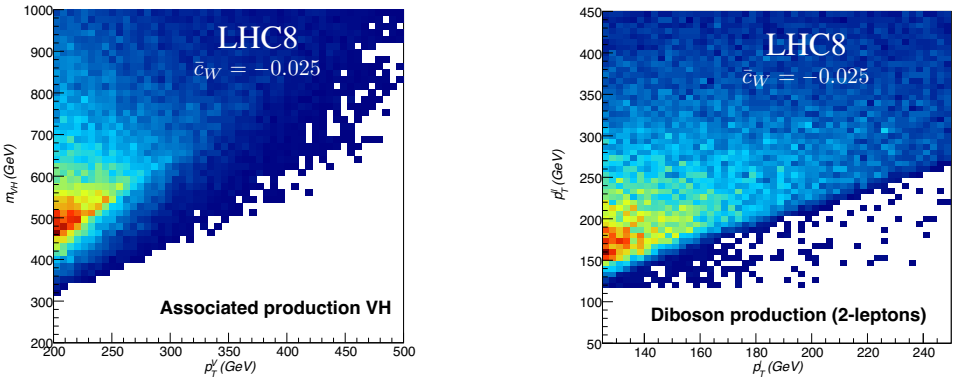

Figure 10. (Left) The kinematic distribution in the vector boson p_T^V vs m_{VH} plane for associated Higgs production at the LHC that would by induced by $\bar{c}_W = -0.025$. (Right) The kinematic distribution in the leading lepton p_T vs $p_T^{\ell\ell}$ plane for diboson production at the LHC that would by induced by $\bar{c}_W = -0.025$.

Recalling the definition of the barred coefficients in eq. (2.6), one can interpret these limits in terms of new physics at scale Λ coupled to the SM with strength $g_{\rm NP}$,

$$\frac{\bar{c}_W}{m_W^2} = \frac{g_{\rm NP}^2}{\Lambda^2}\,, \tag{A.2}$$

upto a factor g from the conventional definition of $\mathcal{O}_W$. The value of Λ corresponding to a value of $\bar{c}_W$ can be read off the upper x-axis in figure 8 assuming $g_{\rm NP}^2 = 1$, where we see that the marginalized range for $\bar{c}_W$ corresponds to $\Lambda \sim 400$–$800\,\text{GeV}$. However $g_{\rm NP}$ may vary to be less than 1 in weakly-coupled scenarios, in which case the new physics scale is lowered, or up to 4π for strongly-coupled new physics, which raises Λ. In general we have

$$\Lambda_{\bar{c}_W} \simeq \left(\frac{g_{\rm NP}}{4\pi}\right) 10\ \text{TeV}. \tag{A.3}$$

The question can be asked whether the effective Standard Model approach is justified.

In this appendix we address this question by considering the region where the most sensitivity is obtained, i.e., the last bin. First of all, it is important to note that the last bin is an overflow bin, containing all the events with p_T above a specified cut. For example, in the TGC analysis shown in figure 3 the last bin corresponds to $p_T > 135\,\text{GeV}$.

For a given value of Λ, one expects the effective theory to break down at parton energies $\sqrt{\hat{s}} \simeq \Lambda$, namely m_{VV} and m_{VH} in the diboson and VH production respectively. To illustrate this point, in figure 10 we show the kinematic distribution that would be induced by $\bar{c}_W = -0.025$ (our most conservative limit in $\bar{c}_W$) in the plane defined by the transverse momentum of the vector boson, p_T^V, and the invariant mass, m_{VH}, for associated Higgs production at the LHC in the 2-lepton channel. This plot corresponds to the last bin of the distribution, which has a cut $p_T^V > 200\,\text{GeV}$. We see that in this bin typically $p_T^V \lesssim 250\,\text{GeV}$, i.e., there is not a large spread of events at large values of the distribution, and $\sqrt{\hat{s}} = m_{VH} \lesssim 550\,\text{GeV}$.

JHEP03(2015)157

One can perform a similar analysis in the di-boson production case. For comparison, we show in the right panel of figure 10 the p_T distribution of the leading lepton in the $pp \to W^+W^- \to 2\ell + \not{E}_T$ production at LHC8 versus the transverse mass distribution of the two vector bosons, p_T^{ll}. For comparison with figure 3, we infer that the overflow bin of $p_T > 135\,\text{GeV}$ extends to about 160 GeV, and is correlated with $p_T\ell\ell < 250\,\text{GeV}$.

Thus, in both the associated production and TGC cases, for $g_{\text{NP}} = \mathcal{O}(1)$, equation (A.3) reassures us that the most important regions of the kinematical distributions are well within the ranges where one may expect the effective field theory to be a good enough approximation for our purposes.

JHEP03(2015)157

References

[1] ATLAS collaboration, *Observation of a new particle in the search for the Standard Model Higgs boson with the ATLAS detector at the LHC*, *Phys. Lett.* **B 716** (2012) 1 [arXiv:1207.7214] [INSPIRE].

[2] CMS collaboration, *Observation of a new boson at a mass of 125 GeV with the CMS experiment at the LHC*, *Phys. Lett.* **B 716** (2012) 30 [arXiv:1207.7235] [INSPIRE].

[3] M. Baak et al., *Updated Status of the Global Electroweak Fit and Constraints on New Physics*, *Eur. Phys. J.* **C 72** (2012) 2003 [arXiv:1107.0975] [INSPIRE].

[4] D. Carmi, A. Falkowski, E. Kuflik and T. Volansky, *Interpreting LHC Higgs Results from Natural New Physics Perspective*, *JHEP* **07** (2012) 136 [arXiv:1202.3144] [INSPIRE].

[5] A. Azatov, R. Contino and J. Galloway, *Model-Independent Bounds on a Light Higgs*, *JHEP* **04** (2012) 127 [*Erratum ibid.* **1304** (2013) 140] [arXiv:1202.3415] [INSPIRE].

[6] J.R. Espinosa, C. Grojean, M. Muhlleitner and M. Trott, *Fingerprinting Higgs Suspects at the LHC*, *JHEP* **05** (2012) 097 [arXiv:1202.3697] [INSPIRE].

[7] P.P. Giardino, K. Kannike, M. Raidal and A. Strumia, *Reconstructing Higgs boson properties from the LHC and Tevatron data*, *JHEP* **06** (2012) 117 [arXiv:1203.4254] [INSPIRE].

[8] T. Li, X. Wan, Y.-k. Wang and S.-h. Zhu, *Constraints on the Universal Varying Yukawa Couplings: from SM-like to Fermiophobic*, *JHEP* **09** (2012) 086 [arXiv:1203.5083] [INSPIRE].

[9] M. Rauch, *Determination of Higgs-boson couplings (SFitter)*, arXiv:1203.6826 [INSPIRE].

[10] J. Ellis and T. You, *Global Analysis of Experimental Constraints on a Possible Higgs-Like Particle with Mass* ~ 125 *GeV*, *JHEP* **06** (2012) 140 [arXiv:1204.0464] [INSPIRE].

[11] A. Azatov, R. Contino, D. Del Re, J. Galloway, M. Grassi and S. Rahatlou, *Determining Higgs couplings with a model-independent analysis of* $h \to \gamma\gamma$, *JHEP* **06** (2012) 134 [arXiv:1204.4817] [INSPIRE].

[12] M. Klute, R. Lafaye, T. Plehn, M. Rauch and D. Zerwas, *Measuring Higgs Couplings from LHC Data*, *Phys. Rev. Lett.* **109** (2012) 101801 [arXiv:1205.2699] [INSPIRE].

[13] L. Wang and X.-F. Han, *The recent Higgs boson data and Higgs triplet model with vector-like quark*, *Phys. Rev.* **D 86** (2012) 095007 [arXiv:1206.1673] [INSPIRE].

[14] D. Carmi, A. Falkowski, E. Kuflik and T. Volansky, *Interpreting the 125 GeV Higgs*, *Nuovo Cim.* **C 035** (2012) 315 [arXiv:1206.4201] [INSPIRE].

[15] M.J. Dolan, C. Englert and M. Spannowsky, *Higgs self-coupling measurements at the LHC*, *JHEP* **10** (2012) 112 [arXiv:1206.5001] [INSPIRE].

[16] J. Chang, K. Cheung, P.-Y. Tseng and T.-C. Yuan, *Distinguishing Various Models of the 125 GeV Boson in Vector Boson Fusion*, *JHEP* **12** (2012) 058 [arXiv:1206.5853] [INSPIRE].

[17] S. Chang, C.A. Newby, N. Raj and C. Wanotayaroj, *Revisiting Theories with Enhanced Higgs Couplings to Weak Gauge Bosons*, *Phys. Rev.* **D 86** (2012) 095015 [arXiv:1207.0493] [INSPIRE].

[18] I. Low, J. Lykken and G. Shaughnessy, *Have We Observed the Higgs (Imposter)?*, *Phys. Rev.* **D 86** (2012) 093012 [arXiv:1207.1093] [INSPIRE].

[19] J. Ellis and T. You, *Global Analysis of the Higgs Candidate with Mass* ~ 125 *GeV*, *JHEP* **09** (2012) 123 [arXiv:1207.1693] [INSPIRE].

[20] M. Montull and F. Riva, *Higgs discovery: the beginning or the end of natural EWSB?*, *JHEP* **11** (2012) 018 [arXiv:1207.1716] [INSPIRE].

[21] J.R. Espinosa, C. Grojean, M. Muhlleitner and M. Trott, *First Glimpses at Higgs' face*, *JHEP* **12** (2012) 045 [arXiv:1207.1717] [INSPIRE].

[22] D. Carmi, A. Falkowski, E. Kuflik, T. Volansky and J. Zupan, *Higgs After the Discovery: A Status Report*, *JHEP* **10** (2012) 196 [arXiv:1207.1718] [INSPIRE].

[23] S. Banerjee, S. Mukhopadhyay and B. Mukhopadhyaya, *New Higgs interactions and recent data from the LHC and the Tevatron*, *JHEP* **10** (2012) 062 [arXiv:1207.3588] [INSPIRE].

[24] F. Bonnet, T. Ota, M. Rauch and W. Winter, *Interpretation of precision tests in the Higgs sector in terms of physics beyond the Standard Model*, *Phys. Rev.* **D 86** (2012) 093014 [arXiv:1207.4599] [INSPIRE].

[25] T. Plehn and M. Rauch, *Higgs Couplings after the Discovery*, *Europhys. Lett.* **100** (2012) 11002 [arXiv:1207.6108] [INSPIRE].

[26] A. Djouadi, *Precision Higgs coupling measurements at the LHC through ratios of production cross sections*, *Eur. Phys. J.* **C 73** (2013) 2498 [arXiv:1208.3436] [INSPIRE].

[27] B. Batell, S. Gori and L.-T. Wang, *Higgs Couplings and Precision Electroweak Data*, *JHEP* **01** (2013) 139 [arXiv:1209.6382] [INSPIRE].

[28] G. Moreau, *Constraining extra-fermion(s) from the Higgs boson data*, *Phys. Rev.* **D 87** (2013) 015027 [arXiv:1210.3977] [INSPIRE].

[29] G. Cacciapaglia, A. Deandrea, G.D. La Rochelle and J.-B. Flament, *Higgs couplings beyond the Standard Model*, *JHEP* **03** (2013) 029 [arXiv:1210.8120] [INSPIRE].

[30] E. Massó and V. Sanz, *Limits on anomalous couplings of the Higgs boson to electroweak gauge bosons from LEP and the LHC*, *Phys. Rev.* **D 87** (2013) 033001 [arXiv:1211.1320] [INSPIRE].

[31] R.T. D'Agnolo, E. Kuflik and M. Zanetti, *Fitting the Higgs to Natural SUSY*, *JHEP* **03** (2013) 043 [arXiv:1212.1165] [INSPIRE].

JHEP03(2015)157

[32] A. Azatov and J. Galloway, *Electroweak Symmetry Breaking and the Higgs Boson: Confronting Theories at Colliders*, *Int. J. Mod. Phys.* **A 28** (2013) 1330004 [arXiv:1212.1380] [INSPIRE].

[33] G. Bhattacharyya, D. Das and P.B. Pal, *Modified Higgs couplings and unitarity violation*, *Phys. Rev.* **D 87** (2013) 011702 [arXiv:1212.4651] [INSPIRE].

[34] D. Choudhury, R. Islam and A. Kundu, *Anomalous Higgs Couplings as a Window to New Physics*, *Phys. Rev.* **D 88** (2013) 013014 [arXiv:1212.4652] [INSPIRE].

[35] R.S. Gupta, M. Montull and F. Riva, *SUSY Faces its Higgs Couplings*, *JHEP* **04** (2013) 132 [arXiv:1212.5240] [INSPIRE].

[36] G. Bélanger, B. Dumont, U. Ellwanger, J.F. Gunion and S. Kraml, *Higgs Couplings at the End of 2012*, *JHEP* **02** (2013) 053 [arXiv:1212.5244] [INSPIRE].

[37] K. Cheung, J.S. Lee and P.-Y. Tseng, *Higgs Precision (Higgcision) Era begins*, *JHEP* **05** (2013) 134 [arXiv:1302.3794] [INSPIRE].

[38] A. Falkowski, F. Riva and A. Urbano, *Higgs at last*, *JHEP* **11** (2013) 111 [arXiv:1303.1812] [INSPIRE].

[39] P.P. Giardino, K. Kannike, I. Masina, M. Raidal and A. Strumia, *The universal Higgs fit*, *JHEP* **05** (2014) 046 [arXiv:1303.3570] [INSPIRE].

[40] J. Ellis and T. You, *Updated Global Analysis of Higgs Couplings*, *JHEP* **06** (2013) 103 [arXiv:1303.3879] [INSPIRE].

[41] J. Bernon, B. Dumont and S. Kraml, *Status of Higgs couplings after run 1 of the LHC*, *Phys. Rev.* **D 90** (2014) 071301 [arXiv:1409.1588] [INSPIRE].

[42] T. Appelquist and J. Carazzone, *Infrared Singularities and Massive Fields*, *Phys. Rev.* **D 11** (1975) 2856 [INSPIRE].

[43] W. Buchmüller and D. Wyler, *Effective Lagrangian Analysis of New Interactions and Flavor Conservation*, *Nucl. Phys.* **B 268** (1986) 621 [INSPIRE].

[44] H.D. Politzer, *Power Corrections at Short Distances*, *Nucl. Phys.* **B 172** (1980) 349 [INSPIRE].

[45] H. Kluberg-Stern and J.B. Zuber, *Renormalization of Nonabelian Gauge Theories in a Background Field Gauge. 2. Gauge Invariant Operators*, *Phys. Rev.* **D 12** (1975) 3159 [INSPIRE].

[46] C. Grosse-Knetter, *Effective Lagrangians with higher derivatives and equations of motion*, *Phys. Rev.* **D 49** (1994) 6709 [hep-ph/9306321] [INSPIRE].

[47] C. Arzt, *Reduced effective Lagrangians*, *Phys. Lett.* **B 342** (1995) 189 [hep-ph/9304230] [INSPIRE].

[48] H. Simma, *Equations of motion for effective Lagrangians and penguins in rare B decays*, *Z. Phys.* **C 61** (1994) 67 [hep-ph/9307274] [INSPIRE].

[49] J. Wudka, *Electroweak effective Lagrangians*, *Int. J. Mod. Phys.* **A 9** (1994) 2301 [hep-ph/9406205] [INSPIRE].

[50] B. Grzadkowski, M. Iskrzynski, M. Misiak and J. Rosiek, *Dimension-Six Terms in the Standard Model Lagrangian*, *JHEP* **10** (2010) 085 [arXiv:1008.4884] [INSPIRE].

JHEP03(2015)157

[51] K. Hagiwara, S. Ishihara, R. Szalapski and D. Zeppenfeld, *Low-energy effects of new interactions in the electroweak boson sector*, *Phys. Rev.* **D 48** (1993) 2182 [INSPIRE].

[52] K. Hagiwara, R. Szalapski and D. Zeppenfeld, *Anomalous Higgs boson production and decay*, *Phys. Lett.* **B 318** (1993) 155 [hep-ph/9308347] [INSPIRE].

[53] F. Bonnet, M.B. Gavela, T. Ota and W. Winter, *Anomalous Higgs couplings at the LHC and their theoretical interpretation*, *Phys. Rev.* **D 85** (2012) 035016 [arXiv:1105.5140] [INSPIRE].

[54] T. Corbett, O.J.P. Eboli, J. Gonzalez-Fraile and M.C. Gonzalez-Garcia, *Constraining anomalous Higgs interactions*, *Phys. Rev.* **D 86** (2012) 075013 [arXiv:1207.1344] [INSPIRE].

[55] R. Contino, M. Ghezzi, C. Grojean, M. Muhlleitner and M. Spira, *Effective Lagrangian for a light Higgs-like scalar*, *JHEP* **07** (2013) 035 [arXiv:1303.3876] [INSPIRE].

[56] W.-F. Chang, W.-P. Pan and F. Xu, *Effective gauge-Higgs operators analysis of new physics associated with the Higgs boson*, *Phys. Rev.* **D 88** (2013) 033004 [arXiv:1303.7035] [INSPIRE].

[57] T. Corbett, O.J.P. Éboli, J. Gonzalez-Fraile and M.C. Gonzalez-Garcia, *Determining Triple Gauge Boson Couplings from Higgs Data*, *Phys. Rev. Lett.* **111** (2013) 011801 [arXiv:1304.1151] [INSPIRE].

[58] A. Hayreter and G. Valencia, *Constraints on anomalous color dipole operators from Higgs boson production at the LHC*, *Phys. Rev.* **D 88** (2013) 034033 [arXiv:1304.6976] [INSPIRE].

[59] H. Mebane, N. Greiner, C. Zhang and S. Willenbrock, *Constraints on Electroweak Effective Operators at One Loop*, *Phys. Rev.* **D 88** (2013) 015028 [arXiv:1306.3380] [INSPIRE].

[60] M.B. Einhorn and J. Wudka, *The Bases of Effective Field Theories*, *Nucl. Phys.* **B 876** (2013) 556 [arXiv:1307.0478] [INSPIRE].

[61] J. Elias-Miro, J.R. Espinosa, E. Masso and A. Pomarol, *Higgs windows to new physics through $D = 6$ operators: constraints and one-loop anomalous dimensions*, *JHEP* **11** (2013) 066 [arXiv:1308.1879] [INSPIRE].

[62] S. Banerjee, S. Mukhopadhyay and B. Mukhopadhyaya, *Higher dimensional operators and the LHC Higgs data: The role of modified kinematics*, *Phys. Rev.* **D 89** (2014) 053010 [arXiv:1308.4860] [INSPIRE].

[63] E. Boos, V. Bunichev, M. Dubinin and Y. Kurihara, *Higgs boson signal at complete tree level in the SM extension by dimension-six operators*, *Phys. Rev.* **D 89** (2014) 035001 [arXiv:1309.5410] [INSPIRE].

[64] B. Gripaios and D. Sutherland, *Searches for CP-violating dimension-6 electroweak gauge boson operators*, *Phys. Rev.* **D 89** (2014) 076004 [arXiv:1309.7822] [INSPIRE].

[65] C.-Y. Chen, S. Dawson and C. Zhang, *Electroweak Effective Operators and Higgs Physics*, *Phys. Rev.* **D 89** (2014) 015016 [arXiv:1311.3107] [INSPIRE].

[66] M. Dahiya, S. Dutta and R. Islam, *Unitarizing VV Scattering in Light Higgs Scenarios*, arXiv:1311.4523 [INSPIRE].

[67] C. Grojean, E. Salvioni, M. Schlaffer and A. Weiler, *Very boosted Higgs in gluon fusion*, *JHEP* **05** (2014) 022 [arXiv:1312.3317] [INSPIRE].

[68] J. Bramante, A. Delgado and A. Martin, *Cornering a hyper Higgs boson: Angular kinematics for boosted Higgs bosons with top pairs*, *Phys. Rev.* **D 89** (2014) 093006 [arXiv:1402.5985] [INSPIRE].

JHEP03(2015)157

[69] J.S. Gainer, J. Lykken, K.T. Matchev, S. Mrenna and M. Park, *Beyond Geolocating: Constraining Higher Dimensional Operators in $H \to 4\ell$ with Off-Shell Production and More*, *Phys. Rev.* **D 91** (2015) 035011 [arXiv:1403.4951] [INSPIRE].

[70] S. Bar-Shalom, A. Soni and J. Wudka, *EFT naturalness: an effective field theory analysis of Higgs naturalness*, arXiv:1405.2924 [INSPIRE].

[71] G. Amar et al., *Exploration of the tensor structure of the Higgs boson coupling to weak bosons in e^+ e^- collisions*, *JHEP* **02** (2015) 128 [arXiv:1405.3957] [INSPIRE].

[72] A. Azatov, C. Grojean, A. Paul and E. Salvioni, *Taming the off-shell Higgs boson*, *Zh. Eksp. Teor. Fiz.* **147** (2015) 410 [arXiv:1406.6338] [INSPIRE].

[73] E. Masso, *An Effective Guide to Beyond the Standard Model Physics*, *JHEP* **10** (2014) 128 [arXiv:1406.6376] [INSPIRE].

[74] R. Alonso, E.E. Jenkins and A.V. Manohar, *Holomorphy without Supersymmetry in the Standard Model Effective Field Theory*, *Phys. Lett.* **B 739** (2014) 95 [arXiv:1409.0868] [INSPIRE].

[75] R.M. Godbole, D.J. Miller, K.A. Mohan and C.D. White, *Jet substructure and probes of CP-violation in Vh production*, arXiv:1409.5449 [INSPIRE].

[76] F. Goertz, A. Papaefstathiou, L.L. Yang and J. Zurita, *Higgs boson pair production in the $D = 6$ extension of the SM*, arXiv:1410.3471 [INSPIRE].

[77] L. Lehman, *Extending the Standard Model Effective Field Theory with the Complete Set of Dimension-7 Operators*, *Phys. Rev.* **D 90** (2014) 125023 [arXiv:1410.4193] [INSPIRE].

[78] C. Englert, Y. Soreq and M. Spannowsky, *Off-Shell Higgs Coupling Measurements in BSM scenarios*, arXiv:1410.5440 [INSPIRE].

[79] A. Devastato, F. Lizzi, C.V. Flores and D. Vassilevich, *Unification of Coupling Constants, Dimension six Operators and the Spectral Action*, *Int. J. Mod. Phys.* **A 30** (2015) 1550033 [arXiv:1410.6624] [INSPIRE].

[80] S. Willenbrock and C. Zhang, *Effective Field Theory Beyond the Standard Model*, *Ann. Rev. Nucl. Part. Sci.* **64** (2014) 83 [arXiv:1401.0470] [INSPIRE].

[81] F. del Aguila and J. de Blas, *Electroweak constraints on new physics*, *Fortsch. Phys.* **59** (2011) 1036 [arXiv:1105.6103] [INSPIRE].

[82] J. de Blas, *Electroweak limits on physics beyond the Standard Model*, *EPJ Web Conf.* **60** (2013) 19008 [arXiv:1307.6173] [INSPIRE].

[83] J. de Blas et al., *Global Bayesian Analysis of the Higgs-boson Couplings*, arXiv:1410.4204 [INSPIRE].

[84] T. Corbett, O.J.P. Eboli, J. Gonzalez-Fraile and M.C. Gonzalez-Garcia, *Robust Determination of the Higgs Couplings: Power to the Data*, *Phys. Rev.* **D 87** (2013) 015022 [arXiv:1211.4580] [INSPIRE].

[85] B. Dumont, S. Fichet and G. von Gersdorff, *A Bayesian view of the Higgs sector with higher dimensional operators*, *JHEP* **07** (2013) 065 [arXiv:1304.3369] [INSPIRE].

[86] Z. Han and W. Skiba, *Effective theory analysis of precision electroweak data*, *Phys. Rev.* **D 71** (2005) 075009 [hep-ph/0412166] [INSPIRE].

JHEP03(2015)157

[87] M. Ciuchini, E. Franco, S. Mishima and L. Silvestrini, *Electroweak Precision Observables, New Physics and the Nature of a 126 GeV Higgs Boson*, *JHEP* **08** (2013) 106 [arXiv:1306.4644] [INSPIRE].

[88] A. Pomarol and F. Riva, *Towards the Ultimate SM Fit to Close in on Higgs Physics*, *JHEP* **01** (2014) 151 [arXiv:1308.2803] [INSPIRE].

[89] J. Ellis, V. Sanz and T. You, *Complete Higgs Sector Constraints on Dimension-6 Operators*, *JHEP* **07** (2014) 036 [arXiv:1404.3667] [INSPIRE].

[90] ALEPH, DELPHI, L3, OPAL, SLD collaborations, the LEP Electroweak Working Group, the SLD Electroweak Group, the SLD Heavy Flavour Group, S. Schael et al., *Precision electroweak measurements on the Z resonance*, *Phys. Rept.* **427** (2006) 257 [hep-ex/0509008] [INSPIRE].

[91] D0 collaboration, V.M. Abazov et al., *Combined search for the standard model Higgs boson decaying to $b\bar{b}$ using the D0 Run II data set*, *Phys. Rev. Lett.* **109** (2012) 121802 [arXiv:1207.6631] [INSPIRE].

[92] CMS collaboration, *Observation of a new boson with mass near 125 GeV in pp collisions at $\sqrt{s} = 7$ and 8 TeV*, *JHEP* **06** (2013) 081 [arXiv:1303.4571] [INSPIRE].

[93] ATLAS collaboration, *Constraints on New Phenomena via Higgs Coupling Measurements with the ATLAS Detector*, ATLAS-CONF-2014-010 (2014).

[94] ATLAS collaboration, *Search for the bb decay of the Standard Model Higgs boson in associated W/ZH production with the ATLAS detector*, ATLAS-CONF-2013-079 (2013).

[95] CMS collaboration, *Measurement of the W^+W^- Cross section in pp Collisions at $\sqrt{s} = 7$ TeV and Limits on Anomalous $WW\gamma$ and WWZ couplings*, *Eur. Phys. J.* **C 73** (2013) 2610 [arXiv:1306.1126] [INSPIRE].

[96] CMS collaboration, *Measurement of W^+W^- and ZZ production cross sections in pp collisions at $\sqrt{s} = 8$ TeV*, *Phys. Lett.* **B 721** (2013) 190 [arXiv:1301.4698] [INSPIRE].

[97] ATLAS collaboration, *Measurement of the W^+W^- production cross section in proton-proton collisions at $\sqrt{s} = 8$ TeV with the ATLAS detector*, ATLAS-CONF-2014-033 (2014).

[98] A. Falkowski, S. Fichet, K. Mohan, F. Riva and V. Sanz, *Triple gauge couplings revisited*, to appear.

[99] M.E. Peskin and T. Takeuchi, *A new constraint on a strongly interacting Higgs sector*, *Phys. Rev. Lett.* **65** (1990) 964 [INSPIRE].

[100] M.E. Peskin and T. Takeuchi, *Estimation of oblique electroweak corrections*, *Phys. Rev.* **D 46** (1992) 381 [INSPIRE].

[101] I. Maksymyk, C.P. Burgess and D. London, *Beyond S, T and U*, *Phys. Rev.* **D 50** (1994) 529 [hep-ph/9306267] [INSPIRE].

[102] R. Barbieri, A. Pomarol, R. Rattazzi and A. Strumia, *Electroweak symmetry breaking after LEP-1 and LEP-2*, *Nucl. Phys.* **B 703** (2004) 127 [hep-ph/0405040] [INSPIRE].

[103] G. Altarelli and R. Barbieri, *Vacuum polarization effects of new physics on electroweak processes*, *Phys. Lett.* **B 253** (1991) 161 [INSPIRE].

[104] R. Barbieri and A. Strumia, *What is the limit on the Higgs mass?*, *Phys. Lett.* **B 462** (1999) 144 [hep-ph/9905281] [INSPIRE].

JHEP03(2015)157

[105] R. Contino, M. Ghezzi, C. Grojean, M. Muhlleitner and M. Spira, *Effective Lagrangian for a light Higgs-like scalar*, *JHEP* **07** (2013) 035 [arXiv:1303.3876] [INSPIRE].

[106] J.D. Wells and Z. Zhang, *Precision Electroweak Analysis after the Higgs Boson Discovery*, *Phys. Rev.* **D 90** (2014) 033006 [arXiv:1406.6070] [INSPIRE].

[107] R.S. Gupta, A. Pomarol and F. Riva, *BSM Primary Effects*, *Phys. Rev.* **D 91** (2015) 035001 [arXiv:1405.0181] [INSPIRE].

[108] D.Y. Bardin et al., *ZFITTER v.6.21: A semianalytical program for fermion pair production in e^+e^- annihilation*, *Comput. Phys. Commun.* **133** (2001) 229 [hep-ph/9908433] [INSPIRE].

[109] M. Baak et al., *The Electroweak Fit of the Standard Model after the Discovery of a New Boson at the LHC*, *Eur. Phys. J.* **C 72** (2012) 2205 [arXiv:1209.2716] [INSPIRE].

[110] C. Grojean, E.E. Jenkins, A.V. Manohar and M. Trott, *Renormalization Group Scaling of Higgs Operators and $\Gamma(h \to \gamma\gamma)$*, *JHEP* **04** (2013) 016 [arXiv:1301.2588] [INSPIRE].

[111] J. Elias-Miró, J.R. Espinosa, E. Masso and A. Pomarol, *Renormalization of dimension-six operators relevant for the Higgs decays $h \to \gamma\gamma, \gamma Z$*, *JHEP* **08** (2013) 033 [arXiv:1302.5661] [INSPIRE].

[112] J. Elias-Miro, J.R. Espinosa, E. Masso and A. Pomarol, *Higgs windows to new physics through $D = 6$ operators: constraints and one-loop anomalous dimensions*, *JHEP* **11** (2013) 066 [arXiv:1308.1879] [INSPIRE].

[113] E.E. Jenkins, A.V. Manohar and M. Trott, *Renormalization Group Evolution of the Standard Model Dimension Six Operators I: Formalism and lambda Dependence*, *JHEP* **10** (2013) 087 [arXiv:1308.2627] [INSPIRE].

[114] E.E. Jenkins, A.V. Manohar and M. Trott, *Renormalization Group Evolution of the Standard Model Dimension Six Operators II: Yukawa Dependence*, *JHEP* **01** (2014) 035 [arXiv:1310.4838] [INSPIRE].

[115] R. Alonso, E.E. Jenkins, A.V. Manohar and M. Trott, *Renormalization Group Evolution of the Standard Model Dimension Six Operators III: Gauge Coupling Dependence and Phenomenology*, *JHEP* **04** (2014) 159 [arXiv:1312.2014] [INSPIRE].

[116] J. Elias-Miró, C. Grojean, R.S. Gupta and D. Marzocca, *Scaling and tuning of EW and Higgs observables*, *JHEP* **05** (2014) 019 [arXiv:1312.2928] [INSPIRE].

[117] R. Alonso, H.-M. Chang, E.E. Jenkins, A.V. Manohar and B. Shotwell, *Renormalization group evolution of dimension-six baryon number violating operators*, *Phys. Lett.* **B 734** (2014) 302 [arXiv:1405.0486] [INSPIRE].

[118] A. Alloul, B. Fuks and V. Sanz, *Phenomenology of the Higgs Effective Lagrangian via FeynRules*, *JHEP* **04** (2014) 110 [arXiv:1310.5150] [INSPIRE].

[119] M. Trott, *On the consistent use of Constructed Observables*, *JHEP* **02** (2015) 046 [arXiv:1409.7605] [INSPIRE].

[120] P. Artoisenet et al., *A framework for Higgs characterisation*, *JHEP* **11** (2013) 043 [arXiv:1306.6464] [INSPIRE].

[121] F. Demartin, F. Maltoni, K. Mawatari, B. Page and M. Zaro, *Higgs characterisation at NLO in QCD: CP properties of the top-quark Yukawa interaction*, *Eur. Phys. J.* **C 74** (2014) 3065 [arXiv:1407.5089] [INSPIRE].

JHEP03(2015)157

[122] F. Maltoni, K. Mawatari and M. Zaro, *Higgs characterisation via vector-boson fusion and associated production: NLO and parton-shower effects*, *Eur. Phys. J.* **C 74** (2014) 2710 [arXiv:1311.1829] [INSPIRE].

[123] LHC Higgs Cross section Working Group collaboration, A. David et al., *LHC HXSWG interim recommendations to explore the coupling structure of a Higgs-like particle*, arXiv:1209.0040 [INSPIRE].

[124] J. Alwall, M. Herquet, F. Maltoni, O. Mattelaer and T. Stelzer, *MadGraph 5: Going Beyond*, *JHEP* **06** (2011) 128 [arXiv:1106.0522] [INSPIRE].

[125] T. Sjöstrand, S. Mrenna and P.Z. Skands, *PYTHIA 6.4 Physics and Manual*, *JHEP* **05** (2006) 026 [hep-ph/0603175] [INSPIRE].

[126] DELPHES 3 collaboration, J. de Favereau et al., *DELPHES 3, A modular framework for fast simulation of a generic collider experiment*, *JHEP* **02** (2014) 057 [arXiv:1307.6346] [INSPIRE].

[127] A. Biekoetter, A. Knochel, M. Kraemer, D. Liu and F. Riva, *Vices and Virtues of Higgs EFTs at Large Energy*, arXiv:1406.7320 [INSPIRE].

[128] M. Beneke, D. Boito and Y.-M. Wang, *Anomalous Higgs couplings in angular asymmetries of $H \to Z\ell^+\ell^-$ and $e^+ e^- \to HZ$*, *JHEP* **11** (2014) 028 [arXiv:1406.1361] [INSPIRE].

[129] B. Henning, X. Lu and H. Murayama, *What do precision Higgs measurements buy us?*, arXiv:1404.1058 [INSPIRE].

[130] M. Gorbahn, J.M. No and V. Sanz, *Benchmarks for Higgs Effective Theory: Extended Higgs Sectors*, arXiv:1502.07352 [INSPIRE].

[131] J.F. Gunion and H.E. Haber, *The CP conserving two Higgs doublet model: The approach to the decoupling limit*, *Phys. Rev.* **D 67** (2003) 075019 [hep-ph/0207010] [INSPIRE].

[132] M. Carena, I. Low, N.R. Shah and C.E.M. Wagner, *Impersonating the Standard Model Higgs Boson: Alignment without Decoupling*, *JHEP* **04** (2014) 015 [arXiv:1310.2248] [INSPIRE].

[133] E. Massó and V. Sanz, *Limits on anomalous couplings of the Higgs boson to electroweak gauge bosons from LEP and the LHC*, *Phys. Rev.* **D 87** (2013) 033001 [arXiv:1211.1320] [INSPIRE].

[134] A. Djouadi, V. Driesen, W. Hollik and A. Kraft, *The Higgs photon-Z boson coupling revisited*, *Eur. Phys. J.* **C 1** (1998) 163 [hep-ph/9701342] [INSPIRE].

JHEP03(2015)157

6 Constraining EFT and Exact One-Loop Analyses of Non-Degenerate Stops

Published for SISSA by Springer

Received: *April 21, 2015*
Accepted: *May 14, 2015*
Published: *June 4, 2015*

Comparing EFT and exact one-loop analyses of non-degenerate stops

Aleksandra Drozd,[a] **John Ellis,**[a,b] **Jérémie Quevillon**[a] **and Tevong You**[a]

[a] *Theoretical Particle Physics and Cosmology Group, Physics Department, King's College London, London WC2R 2LS, U.K.*

[b] *TH Division, Physics Department, CERN, CH-1211 Geneva 23, Switzerland*

E-mail: aleksandra.drozd@kcl.ac.uk, john.ellis@kcl.ac.uk, jeremie.quevillon@kcl.ac.uk, tevong.you@kcl.ac.uk

Abstract: We develop a universal approach to the one-loop effective field theory (EFT) using the Covariant Derivative Expansion (CDE) method. We generalise previous results to include broader classes of UV models, showing how expressions previously obtained assuming degenerate heavy-particle masses can be extended to non-degenerate cases. We apply our method to the general MSSM with non-degenerate stop squarks, illustrating our approach with calculations of the coefficients of dimension-6 operators contributing to the hgg and $h\gamma\gamma$ couplings, and comparing with exact calculations of one-loop Feynman diagrams. We then use present and projected future sensitivities to these operator coefficients to obtain present and possible future indirect constraints on stop masses. The current sensitivity is already comparable to that of direct LHC searches, and future FCC-ee measurements could be sensitive to stop masses above a TeV. The universality of our one-loop EFT approach facilitates extending these constraints to a broader class of UV models.

Keywords: Supersymmetry Phenomenology, Phenomenology of Field Theories in Higher Dimensions

ArXiv ePrint: 1504.02409

doi:10.1007/JHEP06(2015)028

JHEP06(2015)028

Contents

JHEP06(2015)028

1 Introduction

In view of the overall consistency between the current measurements of particle properties and predictions in the Standard Model (SM), a common approach to the analysis of present and prospective future data is to describe them via an effective field theory (EFT) in which the renormalizable SM $d = 4$ Lagrangian is supplemented with higher-dimensional terms composed from SM fields [1–7]. To the extent that this new physics has a mass scale that is substantially higher than the energy scale of the available measurements [8], the EFT approach is a powerful way to constrain possible new physics beyond the SM (BSM) that is model-independent [9–18]. The $d = 6$ operators in this Effective SM (ESM) were first classified in [1],[1] with a complete basis using equations of motion to eliminate redundancies [2–7] being first presented in [21]. There have been many studies of various aspects of these dimension-6 operators,[2] and a short review can be found in [76].

The EFT approach may well be a good approximation if the new physics affects precision observables at the tree level, or if it is strongly-interacting. In these cases the new physics mass scale is likely to be relatively high, and considering the lowest-dimensional

[1]This EFT approach that we follow, in which the $SU(2)_L \times U(1)_Y$ electroweak symmetry is linearly realized, is to be distinguished from a non-linear EFT based on the chiral electroweak Lagrangian [19] and the more general anomalous coupling framework of a $U(1)_{EM}$ effective Lagrangian [20].

[2]See [1–7, 22–27] for some examples of earlier work and [9–18, 21, 28–75] for a sampling of more recent studies.

EFT operators may well be sufficient. However, the EFT approach may have limitations if the new physics has effects only at the loop level, or is weakly interacting. In these cases, the EFT approach may be sensitive only to new physics at some relatively low mass scale, and the new physics effects may not be characterised well by considering simply the lowest-dimensional EFT operators.

Examples in the first, 'safer' category may include certain models with extended Higgs sectors [75], such as two-Higgs-doublet models, or some composite models. Examples in the second category may include the loop effects of supersymmetric models. However, even in this case it is possible that precision electroweak and Higgs data may provide interesting constraints on the possible masses of stop squarks, which have relatively large Yukawa couplings to the SM Higgs field. In particular, the EFT approach may be useful in the framework of 'natural' supersymmetric models with stops that have masses above 100 GeV but still relatively light compared to other supersymmetric particles.

Important steps towards the calculation of loop effects and the simplification of their matching with EFT coefficients have been taken recently by Henning, Lu and Murayama (HLM) [72, 73]. In particular, they use a covariant-derivative expansion (CDE) [77, 78] to characterise new-physics effects via the evaluation of the one-loop effective action. They apply these techniques to derive universal results and also study some explicit models including electroweak triplet scalars, an extra electroweak scalar doublet, and light stops within the minimal supersymmetric extension of the SM (MSSM), as well as some other models. They also discuss electroweak precision observables, triple-gauge couplings and Higgs decay widths and production cross sections [73], and have used their results to derive indicative constraints on the basis of present and future data [72].

In this paper we discuss aspects of the applicability of the EFT approach to models with relatively light stops, exploring in more depth some issues arising from the work of HLM [72, 73]. As they discuss, using the CDE and the one-loop effective action is more elegant and less time-consuming than a complete one-loop Feynman diagram computation. On the other hand, they applied their approach to models with degenerate soft supersymmetry-breaking terms for the stop squarks, and we show how to extend their approach to the non-degenerate case, with specific applications to the dimension-6 operators that contribute to the hgg and $h\gamma\gamma$ couplings. Our extension of the CDE approach would also permit applications to a wider class of ultra-violet (UV) extensions of the SM and other EFT operators.

Another important aspect of our work is a comparison of the EFT results with the corresponding full one-loop Feynman diagram calculations also in the non-degenerate case, so as to assess the accuracy of the EFT approach for analysing present and future data.

In a recent paper, together with Sanz, two of us (JE and TY) made a global fit to dimension-6 EFT operator coefficients including electroweak precision data, LHC measurements of triple-gauge couplings, Higgs rates and production kinematics [18]. Here we use this global fit to constrain the stop mass $m_{\tilde{t}}$ and the mixing parameter X_t, comparing results obtained using the EFT with those using the full one-loop diagrammatic calculation. The bounds on $m_{\tilde{t}}$ and X_t are strongly correlated, and we find that the EFT approach may yield quite accurate constraints for the limits of larger $m_{\tilde{t}}$ and X_t. However, there

JHEP06(2015)028

are substantial differences from the full diagrammatic result for smaller $m_{\tilde{t}}$ and X_t. In this case the diagrammatic approach gives indirect constraints on the stop squark that are quite competitive with direct experimental searches at the LHC. We also explore the possible accuracy of the EFT for possible future data sets, including those obtainable from the LHC and possible e^+e^- colliders.[3] For example, possible FCC-ee measurements [83] may be sensitive indirectly to stop masses $\gtrsim 1\,\text{TeV}$.

The layout of this paper is as follows. In section 2 we introduce the covariant derivative expansion (CDE) and discuss its application to the one-loop effective action, highlighting how the HLM approach [72, 73] may be extended to the case of non-degenerate squarks. As we discuss, one way to achieve this is to use the Baker-Campbell-Hausdorff (BCH) theorem to rearrange the one-loop effective action, and another is to introduce an auxiliary expansion variable. Results obtained by these two methods agree, and are also consistent with the full one-loop Feynman diagram result presented in section 3. Analyses of the current data in the frameworks of the EFT and the diagrammatic approach are presented in section 4, and their results compared. Studies of the possible sensitivities of future measurements at the ILC and FCC-ee are presented in section 5, and section 6 discusses our conclusions and possible directions for future work.

2 The covariant derivative expansion and the one-loop effective action

The one-loop effective action may be obtained by integrating out directly the heavy particles in the path integral using the saddle-point approximation of the functional integral. The contributions to operators involving only light fields can be evaluated by various expansion methods for the application of the path integral. Here we follow the Covariant Derivative Expansion (CDE), a manifestly gauge-invariant method first introduced in the 1980s by Gaillard [77] and Cheyette [78], and recently applied to the Effective SM (ESM) by Henning, Lu and Murayama (HLM) [73].[4] The latter provide, in particular, universal results for operators up to dimension-6 in the form of a one-loop effective Lagrangian with coefficients evaluated via momentum integrals. This approach applies generally, and greatly simplifies the matching to UV models, since it avoids the necessity of recalculating one-loop Feynman diagrams for every model. However, HLM assume a degenerate mass matrix, which may not be the case in general, as for example in the 'natural' MSSM with light stops. We show here how their results may be extended to the non-degenerate case for the one-loop effective Lagrangian terms involved in the dimension-6 operators affecting the hgg and $h\gamma\gamma$ couplings, with application to the case of non-degenerate stops and sbottoms.

2.1 The non-degenerate one-loop effective Lagrangian

We consider a generic Lagrangian consisting of the SM part with complex heavy scalar fields arranged in a multiplet Φ,

$$\mathcal{L}_{\text{UV}} = \mathcal{L}_{\text{SM}} + (\Phi^\dagger F(x) + \text{h.c.}) + \Phi^\dagger(P^2 - M^2 - U(x))\Phi + \mathcal{O}(\Phi^3)\,, \tag{2.1}$$

[3] For previous analyses, see [72, 79–81].

[4] We thank Hermès Bélusca-Maïto for pointing out to us another recent paper that computes the one-loop effective action for certain dimension-6 QCD operators [82].

JHEP06(2015)028

where $P \equiv iD_\mu$, with D_μ the gauge-covariant derivative, $F(x)$ and $U(x)$ are combinations of SM fields coupling linearly and quadratically respectively to Φ, and M is a diagonal mass matrix. The path integral over Φ may be computed by expanding the action around the minimum with respect to Φ, so that the linear terms give the tree-level effective Lagrangian upon substituting the equation of motion for Φ:

$$\mathcal{L}^{\text{eff}}_{\text{tree}} = \sum_{n=0} F^\dagger M^{-2}[(P^2 - U)M^{-2}]^n F + \mathcal{O}(\Phi^3)\,,$$

whereas the quadratic terms are responsible for the one-loop part of the effective Lagrangian. After evaluating the functional integral and Fourier transforming to momentum space, this can be written in the form

$$\mathcal{L}^{\text{eff}}_{\text{1-loop}} = i\int \frac{d^4q}{(2\pi)^4}\text{Tr}\ln(-(P_\mu - q_\mu)^2 + M^2 + U)\,.$$

It is convenient, before expanding the logarithm, to shift the momentum using the covariant derivative, by inserting factors of $e^{\pm P_\mu \partial/\partial q_\mu}$:

$$\mathcal{L}^{\text{eff}}_{\text{1-loop}} = i\int \frac{d^4q}{(2\pi)^4}\text{Tr}\ln[e^{P_\mu \partial/\partial q_\mu}(-(P_\mu - q_\mu)^2 + M^2 + U)e^{-P_\mu \partial/\partial q_\mu}]\,.$$

This choice ensures a convergent expansion while the calculation of operators remains manifestly gauge-invariant throughout.[5] The result is a series involving gauge field strengths, covariant derivatives and SM fields encoded in the matrix $U(x)$:

$$\mathcal{L}^{\text{eff}}_{\text{1-loop}} = i\int \frac{d^4q}{(2\pi)^4}\text{Tr}\ln[-(\tilde{G}_{\nu\mu}\partial/\partial q_\mu + q_\mu)^2 + M^2 + \tilde{U}]\,,$$

where

$$\tilde{G}_{\nu\mu} \equiv \sum_{n=0}\frac{n+1}{(n+2)!}[P_{\alpha_1},[\ldots[P_{\alpha_n},G'_{\nu\mu}]]]\frac{\partial^n}{\partial q_{\alpha_1}\ldots q_{\alpha_n}}\,,$$
$$\tilde{U} = \sum_{n=0}\frac{1}{n!}[P_{\alpha_1},[\ldots[P_{\alpha_n},U]]]\frac{\partial^n}{\partial q_{\alpha_1}\ldots q_{\alpha_n}}$$

Here we defined $G'_{\nu\mu} \equiv -iG_{\nu\mu}$ with the field strength given by $[P_\nu, P_\mu] = -G'_{\nu\mu}$. It is convenient to group together the terms involving momentum derivatives:

$$\mathcal{L}^{\text{eff}}_{\text{1-loop}} = i\int \frac{d^4q}{(2\pi)^4}\text{Tr}\ln(A+B)\,,$$

where

$$A \equiv -\{q_\mu, \tilde{G}_{\nu\mu}\}\frac{\partial}{\partial q_\nu} - \tilde{G}_{\nu\mu}\tilde{G}_{\alpha\mu}\frac{\partial^2}{\partial q_\nu q_\alpha} + \delta\tilde{U}\,, \tag{2.2}$$
$$B \equiv -q^2 + M^2 + U\,,$$

and we have separated $\tilde{U} = U + \delta\tilde{U}$.

[5] We refer the reader to [73, 77, 78] for technical details and discussions of the CDE method.

JHEP06(2015)028

Expanding the logarithm using the Baker-Campbell-Hausdorff (BCH) formula gives

$$\ln(A+B)=\ln(B)+\ln(1+B^{-1}A)+\frac{1}{2}[\ln B,\ln(1+B^{-1}A)]+\frac{1}{12}[\ln B,[\ln B,\ln(1+B^{-1}A)]]+\dots$$

and, using the identity $[\ln X, Y]=\sum_{n=1}\frac{1}{n}X^{-n}L_X^n Y$, where $L_X Y\equiv[X,Y]$, we see that all possible gauge-invariant operators are obtained by evaluating commutators of A and B.

As an example, we compute the term contributing to the dimension-6 operator affecting Higgs production by gluon fusion:

$$\mathcal{O}_g = g_3^2|H^2|G^a_{\mu\nu}G^{a\mu\nu}\,.$$

The calculation can be organised by writing A as a series in momentum derivatives,

$$A=\sum_{n=1}A_n^{\alpha_1\dots\alpha_n}\frac{\partial^n}{\partial q_{\alpha_1}\dots\partial q_{\alpha_n}}=A_1^{\alpha_1}\frac{\partial}{\partial q_{\alpha_1}}+A_2^{\alpha_1\alpha_2}\frac{\partial^2}{\partial q_{\alpha_1 q_{\alpha_2}}}+\dots\,,$$

where each term is obtained by substituting $\tilde{G}$ and $\tilde{U}$ in eq. (2.2). Here we require only the part $A_2^{\alpha_1\alpha_2}\supset-\frac{1}{4}G'_{\alpha_1\mu}G'_{\alpha_2\mu}$, together with the following commutators:

$$i\int\frac{d^4q}{(2\pi)^4}\mathrm{Tr}\ln(A+B)\supset i\int\frac{d^4q}{(2\pi)^4}\mathrm{Tr}\left(\frac{1}{2}B^{-2}[B,A]+\frac{1}{3}B^{-3}[B,[B,A]]\right)\,.$$

We note that M and U are $n\times n$ matrices that do not commute in general, which motivates the use of the BCH expansion, first applied to the CDE in [78]. Evaluating the commutators we find

$$\mathcal{L}^{\text{eff}}_{\text{1-loop}}\supset i\int\frac{d^4q}{(2\pi)^4}\mathrm{Tr}\left\{B^{-2}\left(-\frac{1}{4}G'_{\nu\mu}G'^{\nu\mu}\right)+\frac{8}{3}q_\alpha q_\nu B^{-3}\left(-\frac{1}{4}G'^{\alpha}{}_{\mu}G'^{\nu\mu}\right)\right\}$$

and using $B^{-1}=-\Delta\sum_{n=0}(\Delta U)^n$, where $\Delta\equiv1/(q^2-M^2)$, we see that to obtain operators up to dimension 6 requires retaining up to two powers of U, so that we have traces of the form

$$\mathrm{Tr}(\Delta^a U G'^{\alpha}{}_{\mu}G'^{\nu\mu})=\sum_{i=1}^{n}\left(\Delta_i^a U_{ii}G_i'^{\alpha}{}_{\mu}G_i'^{\nu\mu}\right)\,,$$

$$\mathrm{Tr}(\Delta^a U\Delta^b U\Delta^c G'^{\alpha}{}_{\mu}G'^{\nu\mu})=\sum_{i=1}^{n}\sum_{j=1}^{n}\left(\Delta_i^{a+c}\Delta_j^b U_{ij}U_{ji}G_i'^{\alpha}{}_{\mu}G_i'^{\nu\mu}\right)\,.$$

Here we assume $G'=\mathrm{diag}(G'_1,\dots,G'_n)$ and $\Delta=\mathrm{diag}(\Delta_1,\dots,\Delta_n)$, where $\Delta_i\equiv1/(q^2-m_i^2)$, and U is a general $n\times n$ matrix. To evaluate the momentum integrals of arbitrary powers of mixed propagators we need to combine them using Feynman parameters:

$$\int\frac{d^4q}{(2\pi)^4}q^l\Delta_i^a\Delta_j^b=\frac{(a+b+1)!}{(a-1)!(b-1)!}\int_0^1 dz_i dz_j\left[z_i^{a-1}z_j^{b-1}\left(\int\frac{d^4q}{(2\pi)^4}q^l\Delta_{ij}^{a+b}\right)\delta(1-z_i-z_j)\right]\,,$$

where $\Delta_{ij}\equiv1/(q^2-m_i^2z_i-m_j^2z_j)$. Taking care in applying the $\delta-$function in the summation over the matrix indices, we finally obtain the following expression valid in the case of a non-degenerate mass matrix:

$$\mathcal{L}^{\text{eff}}_{\text{1-loop}}\supset\frac{1}{(4\pi)^2}\left[-\frac{1}{12}\sum_{i=1}^{n}\left(\frac{U_{ii}}{m_i^2}G'_{i\mu\nu}G_i'^{\mu\nu}\right)+\frac{1}{24}\sum_{i=1}^{n}\sum_{j=1}^{n}\left(\frac{U_{ij}U_{ji}}{m_i^2m_j^2}G'_{i\mu\nu}G_i'^{\mu\nu}\right)\right]\,. \qquad (2.3)$$

JHEP06(2015)028

We have checked this result by extending the log-expansion method of [73] to the non-degenerate case by introducing an auxiliary parameter ξ and then differentiating under the integral sign:

$$\begin{aligned}\mathcal{L}^{\text{eff}}_{\text{1-loop}} &= i\int\frac{d^4q}{(2\pi)^4}\text{Tr}\ln[-(\tilde{G}_{\nu\mu}\partial/\partial q_\mu + q_\mu)^2 + \xi M^2 + \tilde{U}] \\ &= i\int\frac{d^4q}{(2\pi)^4}\int d\xi\text{Tr}\left(\frac{1}{A+U-\Delta_\xi^{-1}}M^2\right),\end{aligned}$$

where $\Delta^\xi \equiv 1/(q^2-\xi M^2)$ and ξ is set to 1 at the end of the calculation. The expansion then reads

$$\mathcal{L}^{\text{eff}}_{\text{1-loop}} = i\int\frac{d^4q}{(2\pi)^4}\int d\xi\text{Tr}\left\{\sum_{n=0}^{\infty}\left[-\Delta^\xi(A+U)\right]^n\Delta^\xi M^2\right\},$$

and yields the same result as in (2.3), demonstrating the consistency of our approach.

In general the field strength matrix $G_{\mu\nu}$ may not be diagonal, as for example when the Φ multiplet contains an $\text{SU}(2)_L$ doublet and singlet, so that we have a 2×2 non-diagonal sub-matrix $W^a_{\mu\nu}\tau^a$ involving the weak gauge bosons W^a_μ. The relevant non-degenerate one-loop effective Lagrangian terms then generalise to the universal expression

$$\mathcal{L}^{\text{eff}}_{\text{1-loop}} \supset \frac{1}{(4\pi)^2}\left\{-\frac{1}{12}\text{Tr}\left(\bar{U}G'_{\mu\nu}G'^{\mu\nu}\right)+\frac{1}{24}\text{Tr}\left(\bar{U}^2G'_{\mu\nu}G'^{\mu\nu}\right)+\frac{1}{240}\text{Tr}\left(\left[\bar{U},G'_{\mu\nu}\right]\left[\bar{U},G'^{\mu\nu}\right]\right)\right\}, \tag{2.4}$$

where $\bar{U}_{ij} \equiv \frac{U_{ij}}{m_i m_j}$, which is sufficient for computing the one-loop coefficients in the hgg and $h\gamma\gamma$ couplings.[6]

2.2 A light stop in the hgg and $h\gamma\gamma$ couplings

The result (2.4) is universal in the sense that all the UV information is encapsulated in the U, M matrices and the P_μ covariant derivative, while the operator coefficients are determined by integrals over momenta that are performed once and for all. The simplicity of this approach is illustrated by integrating out stops in the MSSM, whose leading-order contribution necessarily appears at one-loop due to R-parity. Since gluon fusion in the SM also occurs at one-loop and currently provides the strongest constraint on any dimension-6 operator in the Higgs sector, we first calculate its Wilson coefficient within the EFT framework. Later we extend the calculation to the the dimension-6 operators contributing to the $h\gamma\gamma$ coupling, and comment on the extension to other dimension-6 operators.

The M and U matrices are given by the quadratic stop term in the MSSM Lagrangian,

$$\mathcal{L}_{\text{MSSM}} \supset \Phi^\dagger(M^2+U(x))\Phi\,,$$

[6] We provide more details on obtaining this and the rest of the non-degenerate universal one-loop effective Lagrangian in a forthcoming work in preparation [84].

JHEP06(2015)028

where $\Phi = (\tilde{Q}\,, \tilde{t}_R^*)$, and

$$M^2 = \begin{pmatrix} m_{\tilde{Q}}^2 & 0 \\ 0 & m_{\tilde{t}_R}^2 \end{pmatrix},$$
$$U = \begin{pmatrix} (h_t^2 + \frac{1}{2}g_2^2 c_\beta^2)\tilde{H}\tilde{H}^\dagger + \frac{1}{2}g_2^2 s_\beta^2 H H^\dagger - \frac{1}{2}(g_1^2 Y_{\tilde{Q}} c_{2\beta} + \frac{1}{2}g_2^2)|H|^2 & h_t X_t \tilde{H} \\ h_t X_t \tilde{H}^\dagger & (h_t^2 - \frac{1}{2}g_1^2 Y_{\tilde{t}_R} c_{2\beta})|H|^2 \end{pmatrix}.$$

Here we have defined $\tilde{H} \equiv i\sigma^2 H^*$, $h_t \equiv y_t s_\beta$, $X_t \equiv A_t - \mu \cot\beta$, and the hypercharges are $Y_{\tilde{Q}} = 1/6, Y_{\tilde{t}_R} = -2/3$. The mass matrix entries $m_{\tilde{Q}}$ and $m_{\tilde{t}_R}$ are the soft supersymmetry-breaking masses in the MSSM Lagrangian. We note that $\tilde{Q} = (\tilde{t}_L\,, \tilde{b}_L)$ is an $\mathrm{SU}(2)_L$ doublet, so U is implicitly a 3×3 matrix, and there will be an additional trace over color. Substituting this into (2.4) with $G_{\mu\nu}$ the gluon field strength, we extract from the universal one-loop effective action the term

$$\mathcal{L}^{\text{eff}}_{\text{1-loop}} \supset \frac{1}{(4\pi)^2}\frac{1}{24}\left(\frac{h_t^2 - \frac{1}{6}g_1^2 c_{2\beta}}{m_{\tilde{Q}}^2} + \frac{h_t^2 + \frac{1}{3}g_1^2 c_{2\beta}}{m_{\tilde{t}_R}^2} - \frac{h_t^2 X_t^2}{m_{\tilde{Q}}^2 m_{\tilde{t}_R}^2}\right) g_3^2 |H|^2 G^a_{\mu\nu} G^{a\mu\nu}\,.$$

This yields the dimension-6 operator $\mathcal{O}_g$ in the ESM:

$$\mathcal{L}_{\text{dim-6}} \supset \frac{\bar{c}_g}{m_W^2}\mathcal{O}_g\,,$$

with the Wilson coefficient given in this normalisation[7] by

$$\bar{c}_g = \frac{m_W^2}{(4\pi)^2}\frac{1}{24}\left(\frac{h_t^2 - \frac{1}{6}g_1^2 c_{2\beta}}{m_{\tilde{Q}}^2} + \frac{h_t^2 + \frac{1}{3}g_1^2 c_{2\beta}}{m_{\tilde{t}_R}^2} - \frac{h_t^2 X_t^2}{m_{\tilde{Q}}^2 m_{\tilde{t}_R}^2}\right).$$

This example demonstrates the relative ease with which one may obtain a Wilson coefficient at the one-loop level without having to compute Feynman diagrams in both the UV model and the EFT that then have to be matched, a process that must be redone every time one adds a new particle to integrate out. Here we may add a right-handed sbottom simply by enlarging the U matrix for $\Phi = (\tilde{Q}\,, \tilde{t}_R^*\,, \tilde{b}_R^*)$ and plugging it back into (2.4), giving the result

$$\bar{c}_g = \frac{m_W^2}{(4\pi)^2}\frac{1}{24}\left(\frac{h_b^2 + h_t^2 - \frac{1}{6}g_1^2 c_{2\beta}}{m_{\tilde{Q}^2}} + \frac{h_t^2 + \frac{1}{3}g_1^2 c_{2\beta}}{m_{\tilde{t}_R^2}} + \frac{h_b^2 - \frac{1}{6}g_1^2 c_{2\beta}}{m_{\tilde{b}_R^2}} - \frac{h_t^2 \tilde{X}_t^2}{m_{\tilde{Q}^2} m_{\tilde{t}_R^2}} - \frac{h_b^2 \tilde{X}_b^2}{m_{\tilde{Q}^2} m_{\tilde{b}_R^2}}\right). \tag{2.5}$$

We compute similarly the dimension-6 operators affecting the $h\gamma\gamma$ coupling, with the field strength matrix given in this case by

$$G'_{\mu\nu} = \begin{pmatrix} W'^a_{\mu\nu}\tau^a + Y_{\tilde{Q}} B'_{\mu\nu}\mathbb{1} & 0 \\ 0 & -Y_{\tilde{t}_R} B'_{\mu\nu} \end{pmatrix}.$$

[7] In general, barred coefficients are related to unbarred ones by $\bar{c} \equiv c\frac{M^2}{\Lambda^2}$ where $M = v, m_W$ depending on the operator normalisation in the Lagrangian.

JHEP06(2015)028

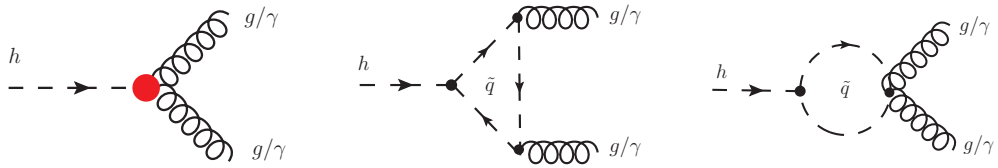

Figure 1. Leading order tree-level Feynman diagram for the EFT (left) and one-loop diagrams for the squark contributions (middle and right) to the $h \to gg/\gamma\gamma$ amplitude.

Evaluating (2.4) then yields directly

$$\mathcal{L}_{\text{dim-6}} \supset \frac{\bar{c}_{BB}}{m_W^2}\mathcal{O}_{BB} + \frac{\bar{c}_{WW}}{m_W^2}\mathcal{O}_{WW} + \frac{\bar{c}_{WB}}{m_W^2}\mathcal{O}_{WB}\,,$$

where

$$\mathcal{O}_{BB} = g_1^2|H|^2 B_{\mu\nu}B^{\mu\nu}\,, \quad \mathcal{O}_{WW} = g_2^2|H|^2 W^a_{\mu\nu}W^{a\mu\nu}\,, \quad \mathcal{O}_{WB} = 2g_1g_2H^\dagger\tau^a H W^a_{\mu\nu}B^{\mu\nu}\,,$$

and

$$\bar{c}_{BB} = \frac{m_W^2}{(4\pi)^2}\left(\frac{1}{144}\frac{(h_t^2 - \frac{1}{6}g_1^2c_{2\beta})}{m_{\tilde{Q}}^2} + \frac{1}{9}\frac{(h_t^2 + \frac{1}{3}g_1^2c_{2\beta})}{m_{\tilde{t}_R}^2} + \frac{1}{36}\frac{(h_t^2 - \frac{1}{6}g_1^2c_{2\beta})}{m_{\tilde{b}_R}^2} - \frac{19}{360}\frac{h_t^2X_t^2}{m_{\tilde{Q}}^2m_{\tilde{t}_R}^2} - \frac{1}{90}\frac{h_b^2X_b^2}{m_{\tilde{Q}}^2m_{\tilde{b}_R}^2}\right), \tag{2.6}$$

$$\bar{c}_{WW} = \frac{m_W^2}{(4\pi)^2}\left(\frac{1}{16}\frac{(h_t^2 - \frac{1}{6}g_1^2c_{2\beta})}{m_{\tilde{Q}}^2} - \frac{1}{40}\frac{h_t^2X_t^2}{m_{\tilde{Q}}^2m_{\tilde{t}_R}^2} - \frac{1}{40}\frac{h_b^2X_b^2}{m_{\tilde{Q}}^2m_{\tilde{b}_R}^2}\right), \tag{2.7}$$

$$\bar{c}_{WB} = \frac{m_W^2}{(4\pi)^2}\left(-\frac{1}{48}\frac{(2h_t^2 + g_2^2c_{2\beta})}{m_{\tilde{Q}}^2} + \frac{1}{30}\frac{h_t^2X_t^2}{m_{\tilde{Q}}^2m_{\tilde{t}_R}^2} + \frac{1}{120}\frac{h_b^2X_b^2}{m_{\tilde{Q}}^2m_{\tilde{b}_R}^2}\right). \tag{2.8}$$

In the basis used in [18], the operators $\mathcal{O}_{WW}$ and $\mathcal{O}_{WB}$ are eliminated and constraints are placed on $\mathcal{O}_\gamma \equiv \mathcal{O}_{BB}$. The coefficients are related by $\bar{c}_\gamma = \bar{c}_{BB} + \bar{c}_{WW} - \bar{c}_{WB}$.

To summarise, one may calculate $\bar{c}_g$ and $\bar{c}_\gamma$ from integrating out a heavy complex scalar Φ in an arbitrary UV model by substituting the SM field matrix, $U(x)$, and field strength matrix, $G_{\mu\nu}$, into the universal one-loop effective Lagrangian of eq. (2.4). The computation of one-loop Wilson coefficients is thus reduced to evaluating the trace of a few matrices. These universal results are extendable to all dimension-6 operators and apply also when integrating out heavy fermions and massive or massless gauge bosons [73, 84].

3 Feynman diagram calculations and comparison

To estimate quantitatively the validity of the dimension-6 EFT we compare the coefficients obtained above with results from an exact one-loop calculation in the MSSM. This is achieved by calculating the Feynman diagrams in figure 1 then matching the $h \to gg$ and $h \to \gamma\gamma$ amplitudes in the EFT with the equivalent MSSM amplitude. In the EFT

JHEP06(2015)028

the operators $\mathcal{O}_g$ and $\mathcal{O}_\gamma$ can be expanded after electroweak symmetry breaking (EWSB) around the vacuum expectation value $v \sim 174\,\text{GeV}$ in order to get the Lagrangian

$$\mathcal{L}_{hVV} = g_3^2\sqrt{2}v\frac{\bar{c}_g}{m_W^2}hG^a_{\mu\nu}G^{a,\mu\nu} + g_1^2\sqrt{2}v\frac{\bar{c}_\gamma}{m_W^2}hB_{\mu\nu}B^{\mu\nu}\,,$$

corresponding to the following Feynman rules for the hgg and $h\gamma\gamma$ vertices:

$$iV^{\mu\nu}_{hgg}(p_2,p_3) = -4ig_3^2\sqrt{2}v\frac{\bar{c}_g}{m_W^2}\left(p_2p_3g^{\mu\nu} - p_2^\nu p_3^\mu\right),$$
$$iV^{\mu\nu}_{h\gamma\gamma}(p_2,p_3) = -4ie^2\sqrt{2}v\frac{\bar{c}_\gamma}{m_W^2}\left(p_2p_3g^{\mu\nu} - p_2^\nu p_3^\mu\right).$$

Thus the $h \to gg$ and $h \to \gamma\gamma$ amplitudes for on-shell external particles are

$$\mathcal{A}^{hgg}_{EFT} = -16g_s^2\sqrt{2}v\frac{\bar{c}_g}{m_W^2}\left(\xi_2^*.\xi_3^*M_h^2 - 2(\xi_2^*.p_1)(\xi_3^*.p_1)\right), \tag{3.1}$$

$$\mathcal{A}^{h\gamma\gamma}_{EFT} = -2g_1^2\cos^2\theta_W\sqrt{2}v\frac{\bar{c}_\gamma}{m_W^2}\left(\xi_2^*.\xi_3^*M_h^2 - 2(\xi_2^*.p_1)(\xi_3^*.p_1)\right), \tag{3.2}$$

where the ξ_i are the polarization vectors of the gauge bosons.

We computed the one-loop diagrams in figure 1 in the MSSM and checked our results using the `FeynArts` package [89]. The CP-even Higgs bosons are rotated to their physical basis by a mixing angle α which we set to be $\alpha = \beta - \pi/2$ corresponding to the decoupling limit when the pseudo-scalar Higgs mass is much heavier than the mass of the Z gauge boson, as indicated by the experimental data [86, 87] and appropriate to our scenario of light stops.[8]

When comparing the EFT and MSSM amplitudes we may choose the momenta of the external particles to be on-shell for convenience. The result of this procedure for the $h \to gg$ amplitude yields the same expression as (3.1) with the replacement $\bar{c}_g \to \bar{c}_g^{\text{MSSM}}$, where

$$\bar{c}_g^{\text{MSSM}} = (\bar{c}_g^{\text{MSSM}})^{\tilde{t}} + (\bar{c}_g^{\text{MSSM}})^{\tilde{b}}\,, \tag{3.3}$$

where the part due to stops is given by

$$(\bar{c}_g^{\text{MSSM}})^{\tilde{t}} = \frac{m_W^2}{6(4\pi)^2}\frac{N_g^{\tilde{t}}}{D_g^{\tilde{t}}},$$
$$N_g^{\tilde{t}} = \frac{c_{2\beta}g_1^2}{s_W^2}\left[v^2c_{2\beta}g_1^2\left(2c_{2W}+1\right) + 3\left(3v^2h_t^2 + 2\left(m^2_{\tilde{t}_R} - m^2_{\tilde{Q}}\right)c_{2W} + 2m^2_{\tilde{Q}} + m^2_{\tilde{t}_R}\right)\right]$$
$$+ 36h_t^2\left(v^2h_t^2 + m^2_{\tilde{Q}} + m^2_{\tilde{t}_R} - X_t^2\right),$$
$$D_g^{\tilde{t}} = \frac{v^2c_{2\beta}g_1^2}{s_W^2}\left[v^2c_{2\beta}g_1^2\left(2c_{2W}+1\right) + 3\left(3v^2h_t^2 + 4\left(m^2_{\tilde{t}_R} - m^2_{\tilde{Q}}\right)c_{2W} + 4m^2_{\tilde{Q}} + 2m^2_{\tilde{t}_R}\right)\right]$$
$$+ 36\left(v^2h_t^2 + 2m^2_{\tilde{Q}}\right)\left(v^2h_t^2 + 2m^2_{\tilde{t}_R}\right) - 72v^2h_t^2X_t^2\,,$$

[8] The case of relatively heavy stops has been demonstrated to be described in a very compact and convenient way, depending only on the two parameters $\tan\beta$ and the pseudo-scalar Higgs mass, when the observed Higgs mass is taken into account [86, 87].

JHEP06(2015)028

and the sbottom contribution reads,

$$(\bar{c}_g^{\rm MSSM})^{\tilde{b}} = \frac{m_W^2}{6(4\pi)^2} \frac{c_{2\beta} g_1^2 \left\{ 6 \left[\left(m_{\tilde{b}_R}^2 - m_{\tilde{Q}}^2 \right) c_{2W} + m_{\tilde{Q}}^2 + 2 m_{\tilde{b}_R}^2 \right] - v^2 c_{2\beta} g_1^2 \left(c_{2W} + 2 \right) \right\}}{\left(12 m_{\tilde{b}_R}^2 - v^2 c_{2\beta} g_1^2 \right) \left[v^2 c_{2\beta} g_1^2 \left(c_{2W} + 2 \right) - 24 m_{\tilde{Q}}^2 s_W^2 \right]} \,.$$

For $\bar{c}_\gamma$ we simply have

$$\bar{c}_\gamma^{\rm MSSM} = \frac{8}{3} (\bar{c}_g^{\rm MSSM})^{\tilde{t}} + \frac{3}{2} (\bar{c}_g^{\rm MSSM})^{\tilde{b}} \,. \tag{3.4}$$

In the limit $v \to 0$ we obtain the same expressions as $\bar{c}_g$ and $\bar{c}_\gamma$ in (2.5) and (2.8), respectively. Since $\bar{c}_g$ and $\bar{c}_\gamma$ correspond to a truncation of the full theory at the dimension-6 level, they contain only the leading-order terms in an expansion in inverse powers of the stop mass, whereas the MSSM result is exact and include higher-order terms in $v/m_{\tilde{t},\tilde{b}}$ that would be generated by higher-dimensional operators in the EFT approach. Therefore, we expect the discrepancy between the two approaches to scale with the ratio $v/m_{\tilde{t},\tilde{b}}$ for $m_{\tilde{t},\tilde{b}}$, and the differences between the EFT and exact MSSM results gives insight into the potential importance of such higher-dimensional operators. We note that a large value of X_t in terms like $v^2 m_W^2 X_t^2 / m_{\tilde{t}}^6$ could potentially affect the validity of the EFT even for large stop masses, but the positivity of the lightest physical mass eigenvalue imposes an upper limit $X_t \simeq m_{\tilde{t}}^2 / m_t$.

The physical mass eigenstates are obtained by diagonalizing the squark mass matrices [85]

$$\mathcal{M}_{\tilde{q}}^2 = \begin{pmatrix} m_q^2 + m_{LL}^2 & m_q X_q \\ m_q X_q & m_q^2 + m_{RR}^2 \end{pmatrix} \tag{3.5}$$

with the various entries defined by

$$m_{LL}^2 = m_{\tilde{Q}}^2 + (I_q^{3L} - Q_q s_W^2) M_Z^2 c_{2\beta} \,, \tag{3.6}$$

$$m_{RR}^2 = m_{\tilde{q}_R}^2 + Q_q s_W^2 M_Z^2 c_{2\beta} \,, \tag{3.7}$$

$$X_q = A_q - \mu (\tan\beta)^{-2 I_q^{3L}} \,. \tag{3.8}$$

Q_q and I_q^{3L} is the electromagnetic charge and the weak doublet isospin respectively. After rotating the 2×2 matrices by an angle θ_q, which transforms the interaction eigenstates $\tilde{q}_L$ and $\tilde{q}_R$ into the mass eigenstates $\tilde{q}_1$ and $\tilde{q}_2$, the mixing angle and physical squark masses are given by

$$s_{2\theta_q} = \frac{2 m_q X_q}{m_{\tilde{q}_1}^2 - m_{\tilde{q}_2}^2} \,, \qquad c_{2\theta_q} = \frac{m_{LL}^2 - m_{RR}^2}{m_{\tilde{q}_1}^2 - m_{\tilde{q}_2}^2} \tag{3.9}$$

$$m_{\tilde{q}_{1,2}}^2 = m_q^2 + \frac{1}{2} \left[m_{LL}^2 + m_{RR}^2 \mp \sqrt{(m_{LL}^2 - m_{RR}^2)^2 + 4 m_q^2 X_q^2} \, \right] \,. \tag{3.10}$$

We see that in the stop sector the mixing is strong for large values of the parameter $X_t = A_t - \mu \cot\beta$, which generates a large mass splitting between the two physical mass eigenstates and makes $\tilde{q}_1$ much lighter than the other sparticle $\tilde{q}_2$.

JHEP06(2015)028

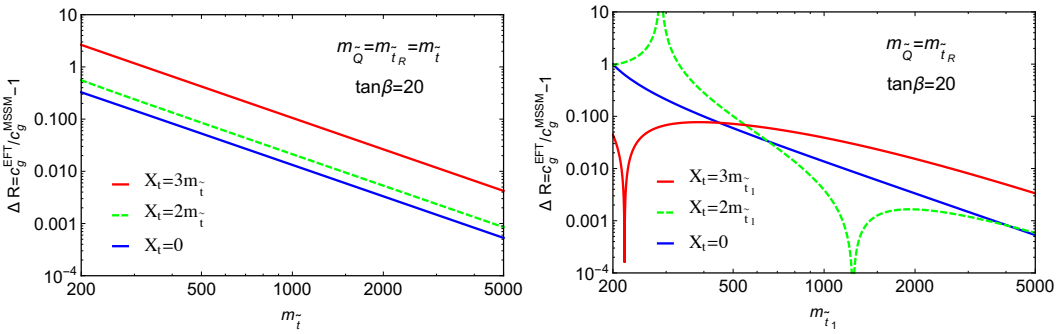

Figure 2. Values of ΔR, defined in (3.11), in the degenerate case $m_{\tilde{Q}} = m_{\tilde{t}_R} \equiv m_{\tilde{t}}$ for $\tan\beta = 20$ and the indicated values of X_t, as a function of $m_{\tilde{t}}$ (left panel), and as functions of $m_{\tilde{t}_1}$ (right panel).

We now compare the values of the $\bar{c}_g$ coefficients calculated in the MSSM and the EFT:[9]

$$\Delta R \equiv \frac{\bar{c}_g^{\rm EFT}}{\bar{c}_g^{\rm MSSM}} - 1\,. \tag{3.11}$$

Figure 2 displays values of ΔR for the degenerate case $m_{\tilde{Q}} = m_{\tilde{t}_R} \equiv m_{\tilde{t}}$, three different values of X_t and the representative choice $\tan\beta = 20$. In the left panel we plot ΔR as functions of $m_{\tilde{t}}$, and the right panel shows ΔR as functions of the lighter stop mass, $m_{\tilde{t}_1}$. We see that in both cases $\Delta R \lesssim 0.1$ for $m_{\tilde{t}}(m_{\tilde{t}_1}) \gtrsim 500\,\text{GeV}$, with a couple of exceptions. One is for the relatively large value $X_t = 3m_{\tilde{t}}$ in the left panel, for which $\Delta R \gtrsim 0.1$ for $m_{\tilde{t}} \lesssim 1000\,\text{GeV}$, and the other is for $X_t = 2m_{\tilde{t}_1}$ and $m_{\tilde{t}_1} \sim 290\,\text{GeV}$ in the right panel, which is due to a node in $\bar{c}_g^{\rm MSSM}$. These results serve as a warning that, although the EFT approach is in general quite reliable for stop mass parameters $\gtrsim 500\,\text{GeV}$, care should always be exercised for masses $\lesssim 1000\,\text{GeV}$.

A similar message is conveyed by figure 3, which uses colour-coding to display values of the differences $|\bar{c}_g^{\rm EFT} - \bar{c}_g^{\rm MSSM}|$ (left panel) and $|\bar{c}_\gamma^{\rm EFT} - \bar{c}_\gamma^{\rm MSSM}|$ (right panel) in $(X_t/m_{\tilde{t}}, m_{\tilde{t}})$ planes for the degenerate case $m_{\tilde{Q}} = m_{\tilde{t}_R} \equiv m_{\tilde{t}}$ with $\tan\beta = 20$. Also shown are contours of $m_{\tilde{t}_1} = 200\,\text{GeV}$ (red), $500\,\text{GeV}$ (green) and $1\,\text{TeV}$ (yellow) and regions where the $\tilde{t}_1$ becomes tachyonic (shaded grey). We see that the differences are generally $< 2.5 \times 10^{-6}$ for $|\bar{c}_g^{\rm EFT} - \bar{c}_g^{\rm MSSM}|$ and $< 10^{-5}$ for $|\bar{c}_\gamma^{\rm EFT} - \bar{c}_\gamma^{\rm MSSM}|$ when $m_{\tilde{t}_1} > 500\,\text{GeV}$, even for large values of X_t, but that much larger differences are possible for $m_{\tilde{t}_1} < 200\,\text{GeV}$, even for small values of X_t.

4 Constraints on light stops from a global fit

We now discuss the constraints on the lighter stop mass that are imposed by the current experimental constraints on the coefficients $\bar{c}_g$ and $\bar{c}_\gamma$, comparing them with the constraints imposed by electroweak precision observables via the oblique parameters S and T [104–107],

[9] We omit RGE effects that mix the coefficients in the running [90–97], as they would be higher-order corrections beyond the one-loop level of our analysis.

JHEP06(2015)028

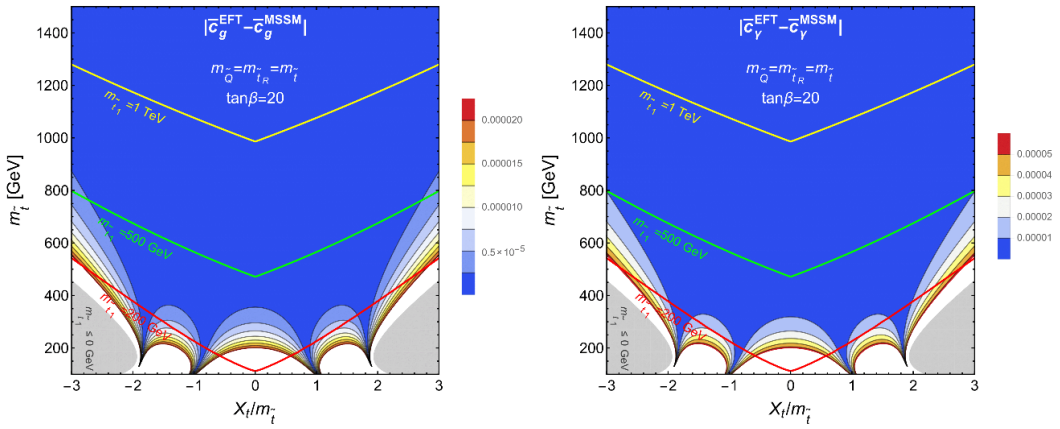

Figure 3. Contours of the differences $|\bar{c}_g^{\rm EFT} - \bar{c}_g^{\rm MSSM}|$ (left panel) and $|\bar{c}_\gamma^{\rm EFT} - \bar{c}_\gamma^{\rm MSSM}|$ (right panel) in $(X_t/m_{\tilde{t}}, m_{\tilde{t}})$ planes for the degenerate case $m_{\tilde{Q}} = m_{\tilde{t}_R} \equiv m_{\tilde{t}}$ with $\tan\beta = 20$. Also shown are contours of $m_{\tilde{t}_1} = 200\,\text{GeV}$, 500 GeV and 1 TeV and regions where the $\tilde{t}_1$ becomes tachyonic.

as well as the ranges favoured by measurements of the Higgs mass M_h and direct searches at the LHC. We note that the S and T parameters are related to the dimension-6 operator coefficients $\bar{c}_W$, $\bar{c}_B$ and $\bar{c}_T$, as defined in the basis of [18],[10] through

$$S = \frac{4\sin^2\theta_W}{\alpha(m_Z)}(\bar{c}_W + \bar{c}_B) \approx 119(\bar{c}_W + \bar{c}_B)\,,$$
$$T = \frac{1}{\alpha(m_Z)}\bar{c}_T \approx 129\bar{c}_T\,.$$

We shall quote the electroweak precision constraints on $\bar{c}_W + \bar{c}_B$ and $\bar{c}_T$ instead of S and T, in keeping with the EFT approach. The stop contributions to these coefficients were given in [72, 73], and table 1 displays the current experimental constraints on $\bar{c}_g, \bar{c}_\gamma, \bar{c}_T$ and $\bar{c}_W + \bar{c}_B$ that we apply.

The constraints on the coefficients in the penultimate column of table 1 are taken from a recent global analysis [18] of LEP, LHC and Tevatron data on Higgs production and triple-gauge couplings. For $\bar{c}_g$ and $\bar{c}_\gamma$ we list the current 95% CL ranges after marginalising a two-parameter fit in which both $\bar{c}_g$ and $\bar{c}_\gamma$ are allowed to vary,[11] as well as considering the more restrictive ranges found when only $\bar{c}_g$ or $\bar{c}_\gamma \neq 0$ individually, with the other operator coefficients set to zero. Similar marginalized and individual 95% CL limits on $\bar{c}_T$ and $\bar{c}_W + \bar{c}_B$ are displayed, where the two-parameter fit varying $\bar{c}_T$ and $\bar{c}_W + \bar{c}_B$ simultaneously is equivalent to the S, T ellipse, as reproduced in [18]. We note that the stop contributions to the coefficients of the other relevant operators are far smaller than the ranges of these coefficients that were found in the global fit. This indicates that one is justified in setting

[10] In other bases $\bar{c}_W$ and $\bar{c}_B$ may be eliminated in favour of $\bar{c}_{WB}$.

[11] In any specific model there may be model-dependent correlations between operator coefficients. In the case with only light stops and nothing else one expects the relation between $\bar{c}_g$ and $\bar{c}_\gamma$ shown in (3.4) to hold, as studied in [88]. Here we use the more conservative marginalized ranges shown in the middle and right panels of figure 4, thereby allowing for additional loop contributions to $\bar{c}_g$ or $\bar{c}_\gamma$.

JHEP06(2015)028

Coeff.	Experimental constraints		95 % CL limit	deg. $m_{\tilde{t}_1}$, $X_t = 0$
$\bar{c}_g$	LHC	marginalized	$[-4.5, 2.2] \times 10^{-5}$	$\sim 410\,\text{GeV}$
		individual	$[-3.0, 2.5] \times 10^{-5}$	$\sim 390\,\text{GeV}$
$\bar{c}_\gamma$	LHC	marginalized	$[-6.5, 2.7] \times 10^{-4}$	$\sim 215\,\text{GeV}$
		individual	$[-4.0, 2.3] \times 10^{-4}$	$\sim 230\,\text{GeV}$
$\bar{c}_T$	LEP	marginalized	$[-10, 10] \times 10^{-4}$	$\sim 290\,\text{GeV}$
		individual	$[-5, 5] \times 10^{-4}$	$\sim 380\,\text{GeV}$
$\bar{c}_W + \bar{c}_B$	LEP	marginalized	$[-7, 7] \times 10^{-4}$	$\sim 185\,\text{GeV}$
		individual	$[-5, 5] \times 10^{-4}$	$\sim 195\,\text{GeV}$

Table 1. List of the experimental 95% CL bounds on coefficients used in setting current limits on stops, which are taken from [18]. The marginalized LHC limits are for a two-parameter fit allowing $\bar{c}_g$ and $\bar{c}_\gamma$ to vary, and the marginalized LEP limits are for a two-parameter fit of $\bar{c}_T$ and $\bar{c}_W + \bar{c}_B$. The corresponding lightest stop mass limits shown are for degenerate soft-supersymmetry breaking masses $m_{\tilde{Q}} = m_{\tilde{t}_R} = m_{\tilde{t}}$ with $X_t = 0$.

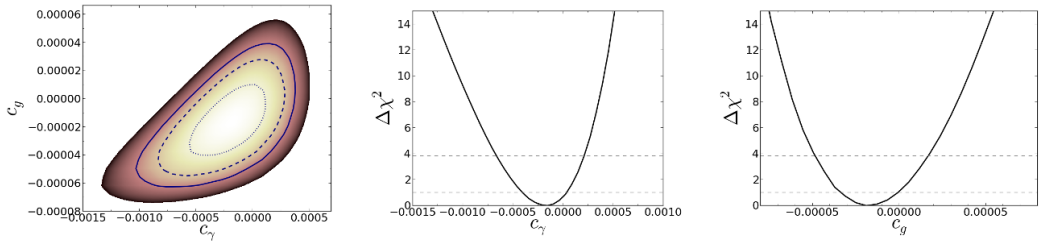

Figure 4. Results based on the global fit in [18], varying $\bar{c}_g$ and $\bar{c}_\gamma$ simultaneously but setting to zero the coefficients of the other dimension-6 operators contributing to the Higgs sector. The dotted, dashed and solid contours on the left denote the allowed 68%, 95% and 99% CL regions respectively. The middle and right figures show the marginalized χ^2 functions for $\bar{c}_\gamma$ and $\bar{c}_g$ respectively.

these other operator coefficients to zero when considering bounds on the stop sector, if one assumes that there are no important contributions from other possible new physics.

4.1 Degenerate stop masses

Figure 5 displays the current constraints in the case of degenerate soft masses $m_{\tilde{Q}} = m_{\tilde{t}_R} \equiv m_{\tilde{t}}$ with decoupled sbottoms, in the upper panels for $m_{\tilde{t}}$ as functions of $X_t/m_{\tilde{t}}$ and in the lower panels for $m_{\tilde{t}_2}$ as functions of $m_{\tilde{t}_1}$, in both cases for $\tan\beta = 20$. The left panels show the stop constraints from the current marginalized 95% bounds on $\bar{c}_g$ (red lines) and $\bar{c}_\gamma$ (blue lines), and the right panels show the corresponding bounds from the current marginalized 95% bounds. The solid (dashed) lines are obtained from an exact one-loop MSSM analysis and the EFT approach, respectively. The purple lines show the individual bound from $\bar{c}_T$ in the EFT approach. The bounds from $\bar{c}_W + \bar{c}_B$ corresponding to the S parameter are negligible and omitted here. The grey shaded regions are excluded

JHEP06(2015)028

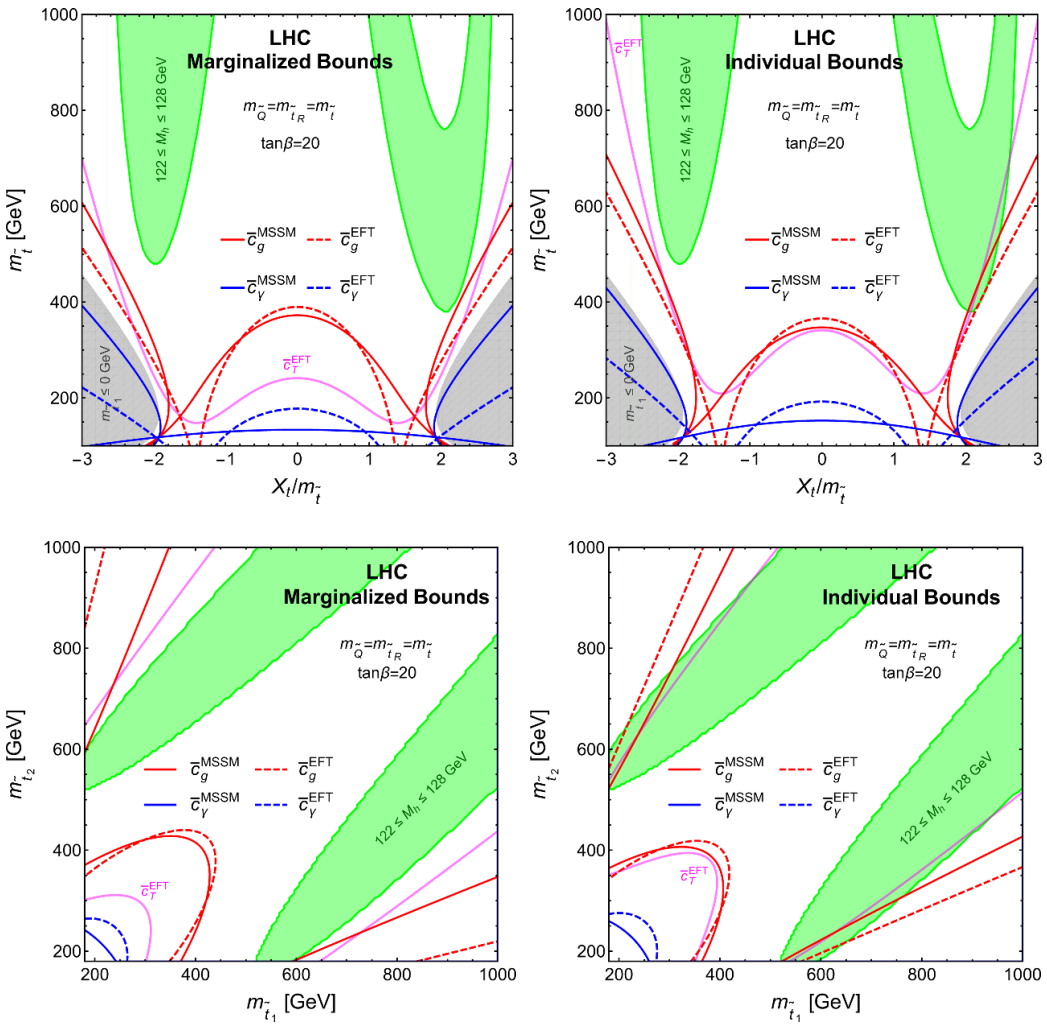

Figure 5. Compilation of the constraints in (upper panels) the $(X_t/m_{\tilde{t}_1}, m_{\tilde{t}})$ plane and (lower panels) the $(m_{\tilde{t}}, m_{\tilde{t}_2})$ plane from (left panels) the marginalized bounds on $\bar{c}_g$ (red lines) and $\bar{c}_\gamma$ (blue lines), and from (right panels) the individual bounds on $\bar{c}_g$ and $\bar{c}_\gamma$. Also shown are the EFT bounds on $\bar{c}_T$ (purple lines), the constraint that the lighter stop should not be tachyonic (grey shading) and the region where $M_h \in (122, 128)$ GeV according to a `FeynHiggs 2.10.3` [98–102] calculation assuming no other significant contributions from outside the stop sector (green shading).

because the lighter stop becomes tachyonic, and the green shaded regions correspond to 122 GeV$< M_h <$128 GeV, as calculated using `FeynHiggs 2.10.3` [98–102], allowing for a theoretical uncertainty of ± 3 GeV and assuming that there are no other important MSSM contributions to M_h.

We see in the upper panels of figure 5 that the $\bar{c}_g$ constraints on $m_{\tilde{t}_1}$ are generally the strongest, except for large $|X_t/m_{\tilde{t}}|$. We also observe that the MSSM and EFT evaluations give rather similar bounds on $m_{\tilde{t}_1}$ for $|X_t/m_{\tilde{t}}| \lesssim 1$ and $\gtrsim 2$. However, there are

JHEP06(2015)028

significant differences for $1 \lesssim |X_t/m_{\tilde{t}}| \lesssim 2$, due to the fact that the two evaluations have zeroes at different values of $X_t/m_{\tilde{t}}$. The next most sensitive constraints are those from T, parametrised here by the coefficient $\bar{c}_T$, which become competitive with the $\bar{c}_g$ constraints at large $|X_t/m_{\tilde{t}}|$, but are significantly weaker for small values of $X_t/m_{\tilde{t}}$. The constraints from $\bar{c}_\gamma$ are weaker still for all values of $X_t/m_{\tilde{t}}$, as might have been expected because the global fit in [18] gave constraints on $\bar{c}_\gamma$ that are weaker than those on $\bar{c}_g$. Indeed, the $\bar{c}_\gamma$ constraint is not significantly stronger than the constraint that the $\tilde{t}_1$ not be tachyonic, as shown by the grey shading in the upper panels of figure 5. We also note that the LHC measurement of M_h favours $|X_t/m_{\tilde{t}}| \gtrsim 2$ and values of $m_{\tilde{t}}$ that are consistent with the EFT bounds.

These results are reflected in the lower panels of figure 5, where we present the $(m_{\tilde{t}_1}, m_{\tilde{t}_2})$ planes with the marginalized constraints (left panel) and the individual constraints (right panel). The MSSM and EFT implementations of the $\bar{c}_g$ constraint give qualitatively similar results, and (except for extreme values of $m_{\tilde{t}_1}/m_{\tilde{t}_2}$) are generally stronger than the constraints from $\bar{c}_T$, which are in turn stronger than the $\bar{c}_\gamma$ constraint. We also note that the LHC measurement of M_h favours moderate values of $m_{\tilde{t}_1}/m_{\tilde{t}_2}$ and values of $m_{\tilde{t}_1}$ or $m_{\tilde{t}_2} \gtrsim 520\,\text{GeV}$.

The limits on the lightest stop mass for degenerate soft-supersymmetry breaking masses $m_{\tilde{Q}} = m_{\tilde{t}_R} = m_{\tilde{t}}$ with $X_t = 0$ are shown in the last column of table 1.

4.2 Non-degenerate stop masses

We consider now cases with non-degenerate stop soft mass parameters, allowing also for the possibility that the lighter sbottom squark plays a rôle. We show in figure 6 various planes under the hypotheses $m_{\tilde{b}_1} = m_{\tilde{t}_1}$ and $\tan\beta = 20$, considering several possibilities for X_t. In all panels, the constraints from the individual 95% bound on $\bar{c}_g$ are indicated by red lines and those from $\bar{c}_\gamma$ are indicated by blue lines (solid for the exact MSSM evaluation and dashed for the EFT approach), and the region allowed by the exact calculation is shaded pink.

The upper left panel is for $X_t = 0$: we see that in the limit $m_{\tilde{t}_2} \gg m_{\tilde{t}_1}$ the $\bar{c}_g$ constraint imposes $m_{\tilde{t}_1} \gtrsim 300\,\text{GeV}$, with a difference of $\sim 20\,\text{GeV}$ between the exact and EFT calculations. On the other hand, if $m_{\tilde{t}_2} = m_{\tilde{t}_1}$ we find $m_{\tilde{t}_1} \gtrsim 380\,\text{GeV}$, again with the EFT calculation giving a bound $\sim 20\,\text{GeV}$ stronger than the exact MSSM calculation. The corresponding bounds from the individual 95% constraint on $\bar{c}_\gamma$ are $\simeq 100\,\text{GeV}$ weaker. However, we note that the LHC constraint on M_h is not respected anywhere in this plane.

Turning now to the case $X_t = 1\,\text{TeV}$ shown in the upper right panel of figure 6, we see a grey shaded band around the $m_{\tilde{t}_1} = m_{\tilde{t}_2}$ line that is disallowed by $\tilde{t}_1 - \tilde{t}_2$ mixing, and other grey shaded regions where $m_{\tilde{t}_1} \ll m_{\tilde{t}_2}$ (or vice versa) and the lighter stop is tachyonic. In this case the M_h constraint (green shaded band) can be satisfied, with small strips of the parameter space ruled out by the $\bar{c}_g$ constraint. The $\bar{c}_\gamma$ constraint is unimportant in this case.

When X_t is increased to 3 TeV, as shown in the lower left panel of figure 6, the diagonal band forbidden by mixing expands considerably, and the $\bar{c}_\gamma$ constraint disappears. In this case the $\bar{c}_g$ constraint would allow $(m_{\tilde{t}_1}, m_{\tilde{t}_2}) \gtrsim (400, 1100)\,\text{GeV}$ on the boundary of the

JHEP06(2015)028

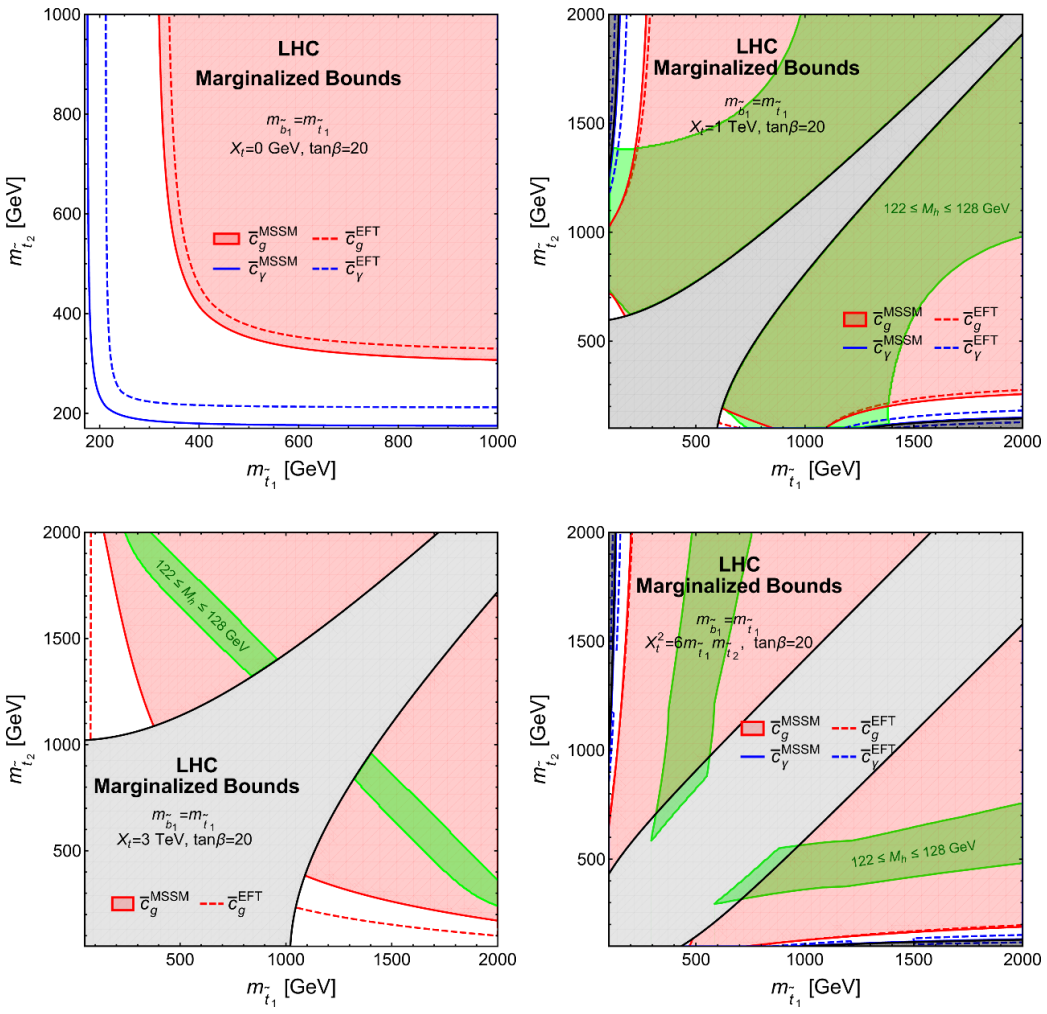

Figure 6. Compilation of the constraints in the case of non-degenerate soft mass parameters, including also sbottom squarks and assuming $m_{\tilde{b}_1} = m_{\tilde{t}_1}$ under the hypotheses $\tan\beta = 20$ and $X_t = 0$ (upper left panel), $X_t = 1\,\text{TeV}$ (upper right panel), $X_t = 3\,\text{TeV}$ (lower left panel) and $X_t = \sqrt{6 m_{\tilde{t}_1} m_{\tilde{t}_2}}$ (lower right panel). The red (blue) lines show the current individual 95% CL constraints from $\bar{c}_g$ ($\bar{c}_\gamma$) as evaluated exactly in the MSSM (solid lines) and in the EFT approach. Additionally, the region compatible with $\bar{c}_g$ is shaded pink, the band compatible with M_h is shaded green, and regions disallowed by the mixing hypothesis or the appearance of a tachyonic stop are shaded grey.

band forbidden by the mixing hypothesis, but the M_h constraint is stronger, enforcing $(m_{\tilde{t}_1}, m_{\tilde{t}_2}) \gtrsim (800, 1300)\,\text{GeV}$ along this boundary.

Finally, we consider in the lower right panel of figure 6 the so-called maximal-mixing hypothesis $X_t = \sqrt{6 m_{\tilde{t}_1} m_{\tilde{t}_2}}$. In this case, almost the entire $(m_{\tilde{t}_1}, m_{\tilde{t}_2})$ plane is allowed by the $\bar{c}_g$ constraint, whereas a triangular region at small $m_{\tilde{t}_1}$ and/or $m_{\tilde{t}_2}$ is forbidden by the M_h constraint.

JHEP06(2015)028

It is interesting to compare the limits on $m_{\tilde{t}_1}$ that we find with those found in a recent global fit to the pMSSM [103] in which universal third-generation squark masses were assumed at the renormalisation scale $\sqrt{m_{\tilde{t}_1} m_{\tilde{t}_2}}$, the first- and second-generation squark masses were assumed to be equal, but allowed to differ from the third-generation mass as were the slepton masses, arbitrary non-universal gaugino masses $M_{1,2,3}$ were allowed, and the trilinear soft supersymmetry-breaking parameter A was assumed to be universal but otherwise free. That analysis included LHC, dark matter and flavour constraints, as well as electroweak precision observables and Higgs measurements, and found $m_{\tilde{t}_1} \gtrsim 400\,\text{GeV}$. The analysis of this paper uses somewhat different assumptions and hence is not directly comparable, but it is interesting that the one-loop sensitivity of $\bar{c}_g$ to the stop mass parameters is quite comparable.

5 Sensitivities of possible future precision measurements

We saw in the previous section that the precision of current measurements does not exclude in a model-independent way most of the parameter space for a stop below the TeV scale, and barely reaches into the region required for a 125 GeV Higgs mass in the MSSM. However, future colliders will increase significantly the precision of electroweak and Higgs measurements to the level required to challenge seriously the naturalness paradigm and test the MSSM calculations of M_h.

In this section we assess the potential improvements for constraints on a light stop possible with future e^+e^- colliders. As previously, we perform an analysis in the EFT framework via the corresponding bounds on the relevant dimension-6 coefficients, and compare it with the exact one-loop MSSM calculation. As representative examples of future e^+e^- colliders, we focus on the ILC [110] and FCC-ee [108, 109] (formerly known as TLEP) proposals. The scenarios considered here for the ILC and FCC-ee postulate centre-of-mass energies of 250 and 240 GeV with luminosities of 1150 fb^{-1} and 10000 fb^{-1}, respectively.

Table 2 lists the prospective 95% CL limits obtained on $\bar{c}_g, \bar{c}_\gamma, \bar{c}_T$, and $\bar{c}_W + \bar{c}_B$ from a χ^2 analysis, with the marginalized constraints on $\bar{c}_g$ and $\bar{c}_\gamma$ obtained in a two-parameter fit to just these coefficients, and similarly for $\bar{c}_T$ and $\bar{c}_W + \bar{c}_B$, corresponding to the T and S parameters respectively, as well as the constraints obtained when each operator coefficient is allowed individually to be non-zero. The target precisions on experimental errors for the electroweak precision observables m_W, Γ_Z, R_l and A_l at the ILC are given in [110], and those at FCC-ee were taken from [108, 109], and include important systematic uncertainties. The errors on the Higgs associated production cross-section times branching ratio are from [111] for the ILC and from [83] for FCC-ee. The numbers quoted in table 2 neglect theoretical uncertainties, in order to reflect the possible performances of the experiments.[12] The treatment of the dimension-6 coefficients in the observables follows a procedure similar to that of the global fit performed in [18], and we use the results of [74] to rescale the constraint from associated Higgs production.

[12] We also show as dashed purple lines in the FCC-ee panels the weaker constraints obtained using the estimates of theoretical uncertainties in [112], while noting that these have not been studied in detail.

JHEP06(2015)028

Coeff.	Experimental constraints		95 % CL limit	deg. $m_{\tilde{t}_1}$	
				$X_t = 0$	$X_t = m_{\tilde{t}}/2$
$\bar{c}_g$	$\text{ILC}^{1150\text{fb}^{-1}}_{250\text{GeV}}$	marginalized	$[-7.7, 7.7] \times 10^{-6}$	$\sim 675\,\text{GeV}$	$\sim 520\,\text{GeV}$
		individual	$[-7.5, 7.5] \times 10^{-6}$	$\sim 680\,\text{GeV}$	$\sim 545\,\text{GeV}$
	FCC-ee	marginalized	$[-3.0, 3.0] \times 10^{-6}$	$\sim 1065\,\text{GeV}$	$\sim 920\,\text{GeV}$
		individual	$[-3.0, 3.0] \times 10^{-6}$	$\sim 1065\,\text{GeV}$	$\sim 915\,\text{GeV}$
$\bar{c}_\gamma$	$\text{ILC}^{1150\text{fb}^{-1}}_{250\text{GeV}}$	marginalized	$[-3.4, 3.4] \times 10^{-4}$	$\sim 200\,\text{GeV}$	$\sim 40\,\text{GeV}$
		individual	$[-3.3, 3.3] \times 10^{-4}$	$\sim 200\,\text{GeV}$	$\sim 35\,\text{GeV}$
	FCC-ee	marginalized	$[-6.4, 6.4] \times 10^{-5}$	$\sim 385\,\text{GeV}$	$\sim 250\,\text{GeV}$
		individual	$[-6.3, 6.3] \times 10^{-5}$	$\sim 390\,\text{GeV}$	$\sim 260\,\text{GeV}$
$\bar{c}_T$	$\text{ILC}^{1150\text{fb}^{-1}}_{250\text{GeV}}$	marginalized	$[-3, 3] \times 10^{-4}$	$\sim 480\,\text{GeV}$	$\sim 285\,\text{GeV}$
		individual	$[-7, 7] \times 10^{-5}$	$\sim 930\,\text{GeV}$	$\sim 780\,\text{GeV}$
	FCC-ee	marginalized	$[-3, 3] \times 10^{-5}$	$\sim 1410\,\text{GeV}$	$\sim 1285\,\text{GeV}$
		individual	$[-0.9, 0.9] \times 10^{-5}$	$\sim 2555\,\text{GeV}$	$\sim 2460\,\text{GeV}$
$\bar{c}_W + \bar{c}_B$	$\text{ILC}^{1150\text{fb}^{-1}}_{250\text{GeV}}$	marginalized	$[-2, 2] \times 10^{-4}$	$\sim 230\,\text{GeV}$	$\sim 170\,\text{GeV}$
		individual	$[-6, 6] \times 10^{-5}$	$\sim 340\,\text{GeV}$	$\sim 470\,\text{GeV}$
	FCC-ee	marginalized	$[-2, 2] \times 10^{-5}$	$\sim 545\,\text{GeV}$	$\sim 960\,\text{GeV}$
		individual	$[-0.8, 0.8] \times 10^{-5}$	$\sim 830\,\text{GeV}$	$\sim 1590\,\text{GeV}$

Table 2. List of the 95% CL bounds on EFT operator coefficients from projected constraints on Higgs couplings and electroweak precision observables at the future e^+e^- colliders ILC and FCC-ee. The marginalized limits on $\bar{c}_g$ or $\bar{c}_\gamma$ ($\bar{c}_T$ or $\bar{c}_W + \bar{c}_B$) are for a two-parameter fit allowing $\bar{c}_g$ and $\bar{c}_\gamma$ ($\bar{c}_T$ and $\bar{c}_W + \bar{c}_B$) to vary simultaneously but setting other operator coefficients to zero. The corresponding lightest stop mass limits shown are for degenerate soft-supersymmetry breaking masses $m_{\tilde{Q}} = m_{\tilde{t}_R} = m_{\tilde{t}}$ with $X_t = 0$ and $X_t/m_{\tilde{t}} = 2$.

5.1 Degenerate stop masses

Contours from possible future constraints on $\bar{c}_g$, $\bar{c}_\gamma$ and $\bar{c}_T$ for the case of degenerate soft masses $m_{\tilde{Q}} = m_{\tilde{t}_R} \equiv m_{\tilde{t}}$ are plotted in figure 7, using again the value $\tan\beta = 20$. The upper panels show results for the ILC, the lower panels for FCC-ee, the left panels show the marginalized constraints and the right panels show the individual constraints. The grey and green shaded regions are the same as in figure 7. We see that the marginal and individual sensitivities to $m_{\tilde{t}}$ from $\bar{c}_g$ and $\bar{c}_\gamma$ are very similar, whereas the individual sensitivity of $\bar{c}_T$ are much stronger, particularly at FCC-ee. We see that ILC is indirectly sensitive to $m_{\tilde{t}} \sim 600\,\text{GeV}$, and that FCC-ee is indirectly sensitive to stops in the TeV range. The measurement of the $\bar{c}_T$ coefficient at FCC-ee has the highest potential reach, though this will be highly dependent on future improvements in reducing theory uncertainties [83, 112].

The limits on the lightest stop mass for degenerate soft-supersymmetry breaking masses $m_{\tilde{Q}} = m_{\tilde{t}_R} = m_{\tilde{t}}$ with $X_t = 0$ and $X_t/m_{\tilde{t}} = 2$ are shown in the two last columns of table 2.

JHEP06(2015)028

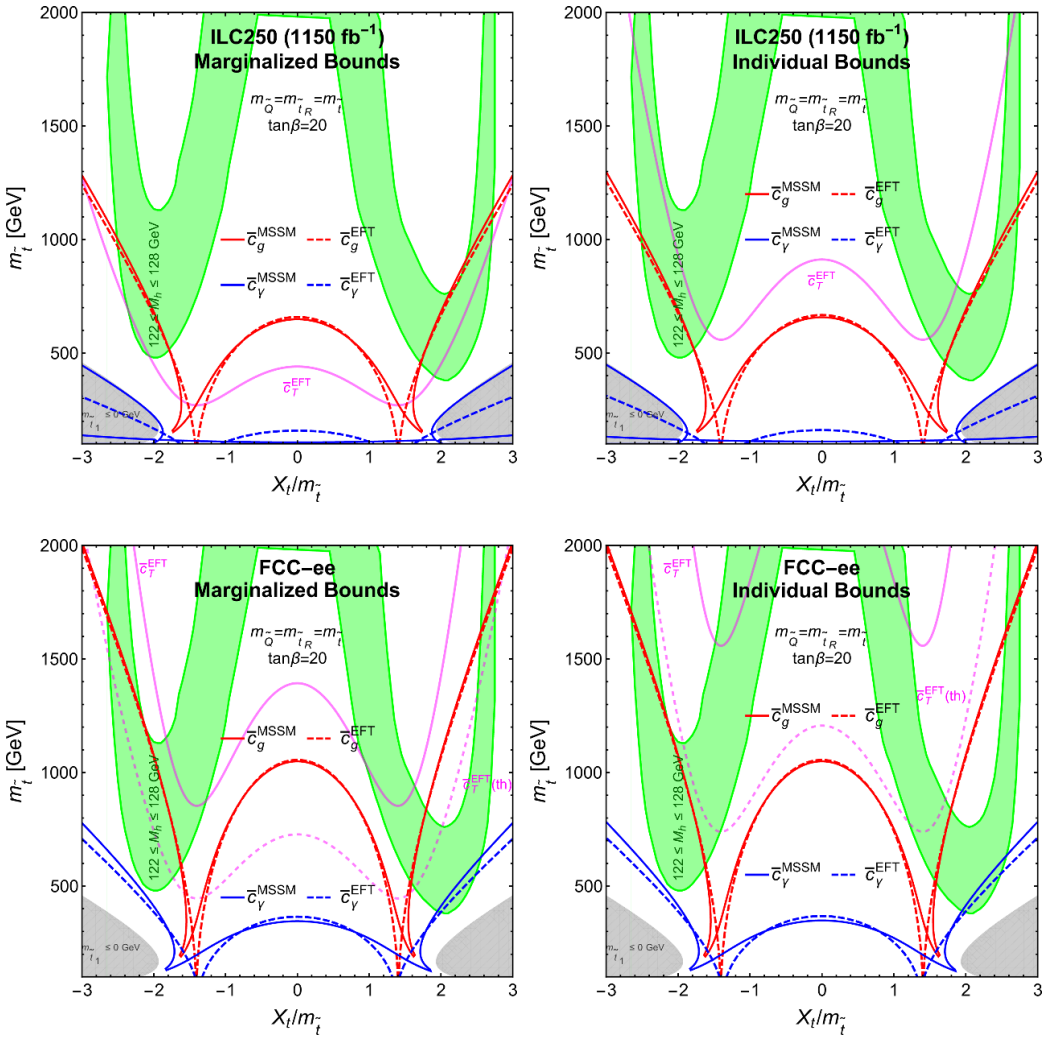

Figure 7. The $(X_t/m_{\tilde{t}}, m_{\tilde{t}})$ planes, analogous to those in the upper panels of figure 5, showing prospective marginalized bounds (left panels) and individual bounds (right panels) from the ILC [110] with 1150 fb^{-1} of luminosity at 250 GeV (upper panels) and from FCC-ee [108, 109] with 10^4 fb^{-1} of luminosity at 240 GeV (lower panels). In the latter case, the solid purple lines are the 95% CL contours for electroweak precision measurements from FCC-ee incorporating the projected statistical and systematic experimental errors alone, and the dashed purple lines also include theory errors from [112].

5.2 Non-degenerate stop masses

Moving on to the non-degenerate case, the $\bar{c}_g$ and $\bar{c}_\gamma$ 95% CL limits for ILC and FCC-ee are plotted in the $m_{\tilde{t}_1}$ vs $m_{\tilde{t}_2}$ plane for various X_t values in figure 8 and 9 respectively. The top left, top right, and bottom left plots correspond to $X_t = 0, 1$ and 3 TeV respectively, while the bottom right plot is for the maximal-mixing hypothesis $X_t = \sqrt{6 m_{\tilde{t}_1} m_{\tilde{t}_2}}$. We see

JHEP06(2015)028

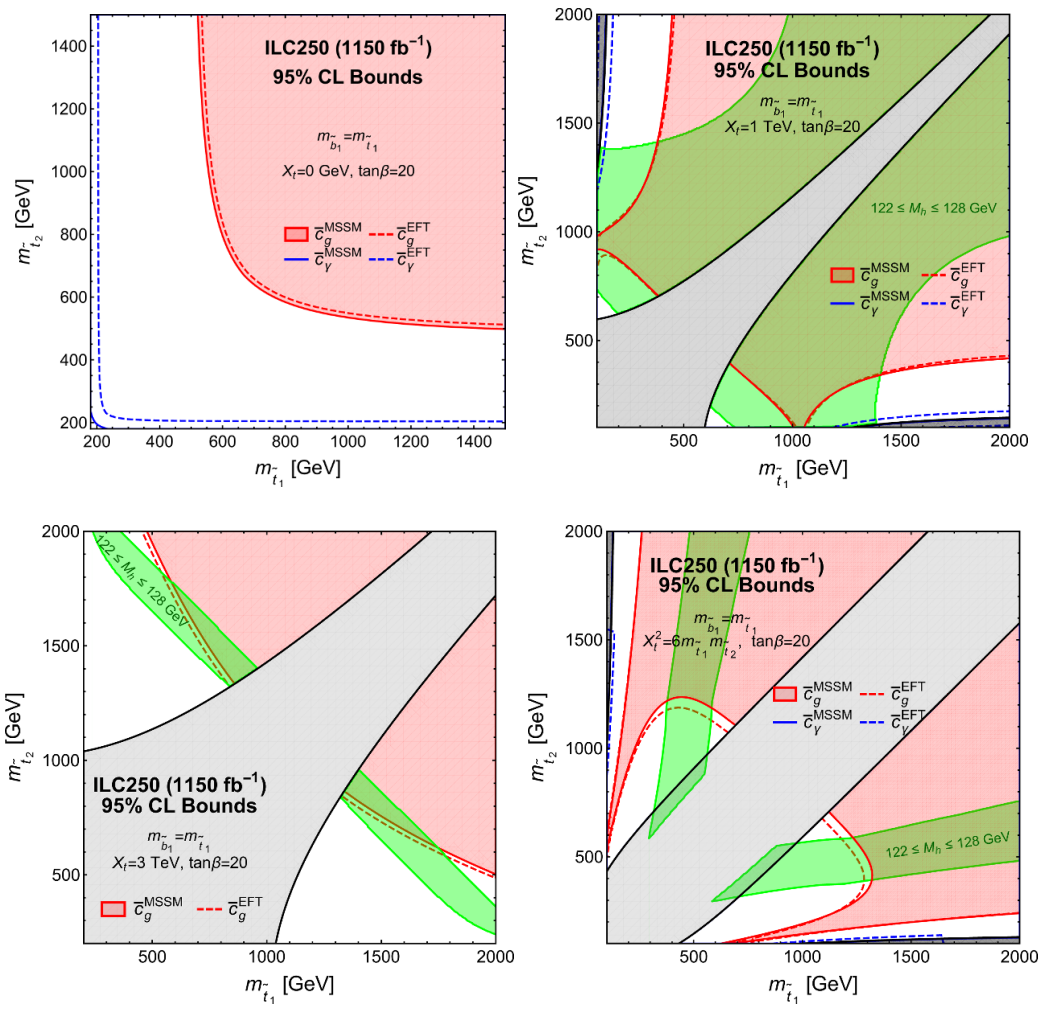

Figure 8. Compilation of projected ILC 95 % CL bounds from $\bar{c}_g$ ($\bar{c}_\gamma$) given by red (blue) lines in the $m_{\tilde{t}_1}$ vs $m_{\tilde{t}_2}$ plane, analogous to figure 6, with $m_{\tilde{b}_1} = m_{\tilde{t}_1}$ and $\tan\beta = 20$. Values of $X_t = 0, 1, 3, \sqrt{6 m_{\tilde{t}_1} m_{\tilde{t}_2}}$ TeV are shown clockwise from top left. The marginalized limits are displayed and the individual bounds are very similar.

that the ILC sensitivity to $\bar{c}_g$ begins to probe and potentially exclude parts of the green shaded region compatible with the measured M_h, while FCC-ee would push the sensitivity of $\bar{c}_g$ constraints into the TeV scale. In particular, it could eliminate the entire allowed M_h region for $X_t = 3\,\text{TeV}$.

6 Conclusions and prospects

In light of the SM-like Higgs sector and the current lack of direct evidence for additional degrees of freedom beyond the SM, the framework of the Effective SM (ESM) is gaining increasing attention as a general framework for characterising the indirect effects of possible

JHEP06(2015)028

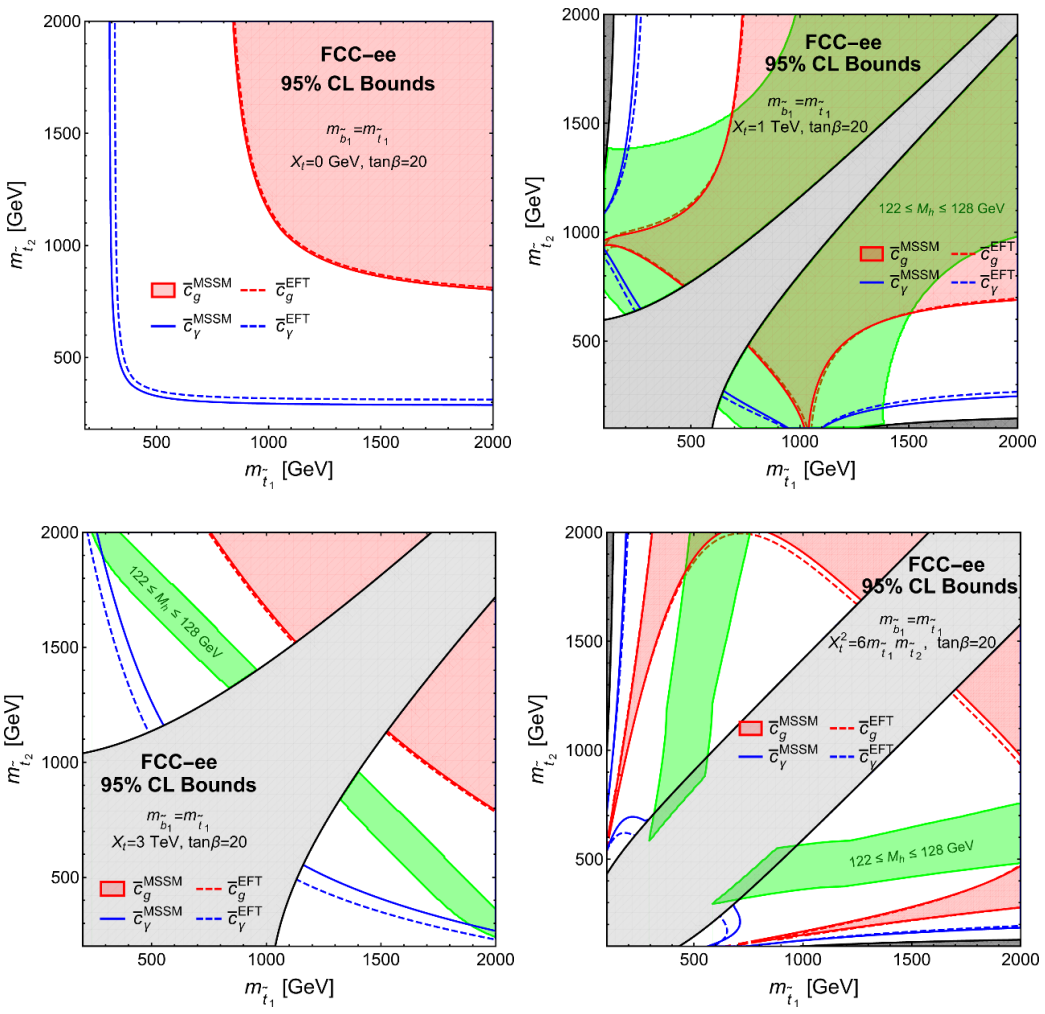

Figure 9. Compilation of projected FCC-ee 95 % CL bounds from $\bar{c}_g$ ($\bar{c}_\gamma$) given by red (blue) lines in the $m_{\tilde{t}_1}$ vs $m_{\tilde{t}_2}$ plane, analogous to figure 6, with $m_{\tilde{b}_1} = m_{\tilde{t}_1}$ and $\tan\beta = 20$. Values of $X_t = 0, 1, 3, \sqrt{6 m_{\tilde{t}_1} m_{\tilde{t}_2}}$ TeV is shown clockwise from top left. The marginalized limits are displayed and the individual bounds are very similar.

new physics in a model-independent way. The ESM is simply the SM extended in the way it has always been regarded: as an effective field theory supplemented by higher-dimensional operators suppressed by the scale of new physics. The leading lepton-number-conserving effects are parametrised by dimension-6 operators, whose coefficients are determined by matching to a UV model and constrained through their effects on experimental observables. In this paper we have illustrated all these steps in the EFT approach for light stops in the MSSM.

In particular, we employed the CDE method to compute the one-loop effective Lagrangian, showing how certain results derived previously under the assumption of a degener-

JHEP06(2015)028

ate mass matrix can be generalised to the non-degenerate case. The universal one-loop effective Lagrangian can then be used without caveats to obtain directly one-loop Wilson coefficients. The advantage of this was demonstrated here in the calculation of the $\bar{c}_g$ and $\bar{c}_\gamma$ coefficients. One simply takes the mass and U matrices from the quadratic term of the heavy field being integrated out, as defined in (2.1), and substitutes it with the corresponding field strength matrix into the universal expression in (2.4) to get the desired operators, without having to evaluate any loop integrals or match separate calculations in the UV and EFT.

Since the hgg and $h\gamma\gamma$ couplings are loop-induced in the SM, the $\bar{c}_g$ and $\bar{c}_\gamma$ coefficients are currently the most sensitive to light stops. The stop contribution to these coefficients is also loop-suppressed, thus lowering the EFT cut-off scale, and it is natural to ask at what point the EFT breaks down and the effects of higher-dimensional operators are no longer negligible. We addressed this question by comparing the EFT coefficients with a full calculation in the MSSM, finding that the disagreement is generally $\lesssim 10\%$ for a lightest stop mass $m_{\tilde{t}_1} \gtrsim 500\,\text{GeV}$, with the exception of a large $|X_t| \geq 3m_{\tilde{t}_1}$ or accidental cancellations in the Higgs-stop couplings.

The constraints on $\bar{c}_g$ and $\bar{c}_\gamma$ from a global fit to the current LHC and Tevatron data, and the constraints on $\bar{c}_T$ and $\bar{c}_W + \bar{c}_B$ from LEP electroweak precision observables, were then translated into the corresponding constraints on the stop masses and X_t. The coefficient $\bar{c}_g$ is the most sensitive, followed by $\bar{c}_T$, which is equivalent to the oblique T parameter. In the case of degenerate soft masses, this analysis requires $m_{\tilde{t}_1} \gtrsim 410\,\text{GeV}$ for $X_t = 0$, and $m_{\tilde{t}_1} \gtrsim 200\,\text{GeV}$ if we also apply the Higgs mass constraint. This is competitive with direct searches and is complimentary in the sense that it does not depend on how the stop decays. The limits in the non-degenerate case are generally weaker than the Higgs mass requirement, though a few strips in the parameter space compatible with M_H can still be excluded.

The sensitivity of future colliders can greatly improve the reach of indirect constraints into the region of parameter space compatible with the observed Higgs mass. The most promising measurements will be the hgg coupling and the T parameter, with FCC-ee capable of reaching a sensitivity to stop masses above 1 TeV. Thus, FCC-ee measurements will be able to challenge the naturalness paradigm in a rather model-independent way.

As LHC Run 2 gets under way, the question how to interpret any new physics or lack thereof will be aided by the systematic approach of the ESM. We have demonstrated this for the case of light stops in the MSSM, showing how the EFT framework can simplify both the calculation of relevant observables and the application of experimental constraints on these observables, giving results similar to exact one-loop calculations in the MSSM.

Acknowledgments

The work of AD was supported by the STFC Grant ST/J002798/1. The work of JE was supported partly by the London Centre for Terauniverse Studies (LCTS), using funding from the European Research Council via the Advanced Investigator Grant 26732, and partly by the STFC Grants ST/J002798/1 and ST/L000326/1. The work of JQ was supported by the STFC Grant ST/L000326/1. The work of TY was supported by a Graduate Teaching Assistantship from King's College London.

JHEP06(2015)028

References

[1] W. Buchmüller and D. Wyler, *Effective Lagrangian Analysis of New Interactions and Flavor Conservation*, *Nucl. Phys.* **B 268** (1986) 621 [INSPIRE].

[2] H.D. Politzer, *Power Corrections at Short Distances*, *Nucl. Phys.* **B 172** (1980) 349 [INSPIRE].

[3] H. Kluberg-Stern and J.B. Zuber, *Renormalization of Nonabelian Gauge Theories in a Background Field Gauge. 2. Gauge Invariant Operators*, *Phys. Rev.* **D 12** (1975) 3159 [INSPIRE].

[4] C. Grosse-Knetter, *Effective Lagrangians with higher derivatives and equations of motion*, *Phys. Rev.* **D 49** (1994) 6709 [hep-ph/9306321] [INSPIRE].

[5] C. Arzt, *Reduced effective Lagrangians*, *Phys. Lett.* **B 342** (1995) 189 [hep-ph/9304230] [INSPIRE].

[6] H. Simma, *Equations of motion for effective Lagrangians and penguins in rare B decays*, *Z. Phys.* **C 61** (1994) 67 [hep-ph/9307274] [INSPIRE].

[7] J. Wudka, *Electroweak effective Lagrangians*, *Int. J. Mod. Phys.* **A 9** (1994) 2301 [hep-ph/9406205] [INSPIRE].

[8] T. Appelquist and J. Carazzone, *Infrared singularities and massive fields*, *Phys. Rev.* **D 11** (1975) 2856.

[9] Z. Han and W. Skiba, *Effective theory analysis of precision electroweak data*, *Phys. Rev.* **D 71** (2005) 075009 [hep-ph/0412166] [INSPIRE].

[10] T. Corbett, O.J.P. Eboli, J. Gonzalez-Fraile and M.C. Gonzalez-Garcia, *Robust Determination of the Higgs Couplings: Power to the Data*, *Phys. Rev.* **D 87** (2013) 015022 [arXiv:1211.4580] [INSPIRE].

[11] B. Dumont, S. Fichet and G. von Gersdorff, *A Bayesian view of the Higgs sector with higher dimensional operators*, *JHEP* **07** (2013) 065 [arXiv:1304.3369] [INSPIRE].

[12] M. Ciuchini, E. Franco, S. Mishima and L. Silvestrini, *Electroweak Precision Observables, New Physics and the Nature of a 126 GeV Higgs Boson*, *JHEP* **08** (2013) 106 [arXiv:1306.4644] [INSPIRE].

[13] A. Pomarol and F. Riva, *Towards the Ultimate SM Fit to Close in on Higgs Physics*, *JHEP* **01** (2014) 151 [arXiv:1308.2803] [INSPIRE].

[14] J. de Blas et al., *Global Bayesian Analysis of the Higgs-boson Couplings*, arXiv:1410.4204 [INSPIRE].

[15] A. Falkowski and F. Riva, *Model-independent precision constraints on dimension-6 operators*, *JHEP* **02** (2015) 039 [arXiv:1411.0669] [INSPIRE].

[16] A. Efrati, A. Falkowski and Y. Soreq, *Electroweak constraints on flavorful effective theories*, arXiv:1503.07872 [INSPIRE].

[17] J. Ellis, V. Sanz and T. You, *Complete Higgs Sector Constraints on Dimension-6 Operators*, *JHEP* **07** (2014) 036 [arXiv:1404.3667] [INSPIRE].

JHEP06(2015)028

[18] J. Ellis, V. Sanz and T. You, *The Effective Standard Model after LHC Run I*, *JHEP* **03** (2015) 157 [arXiv:1410.7703] [INSPIRE].

[19] G. Buchalla, O. Catà, A. Celis and C. Krause, *Note on Anomalous Higgs-Boson Couplings in Effective Field Theory*, arXiv:1504.01707 [INSPIRE].

[20] P. Artoisenet et al., *A framework for Higgs characterisation*, *JHEP* **11** (2013) 043 [arXiv:1306.6464] [INSPIRE].

[21] B. Grzadkowski, M. Iskrzynski, M. Misiak and J. Rosiek, *Dimension-Six Terms in the Standard Model Lagrangian*, *JHEP* **10** (2010) 085 [arXiv:1008.4884] [INSPIRE].

[22] K. Hagiwara, S. Ishihara, R. Szalapski and D. Zeppenfeld, *Low-energy effects of new interactions in the electroweak boson sector*, *Phys. Rev.* **D 48** (1993) 2182 [INSPIRE].

[23] K. Hagiwara, R. Szalapski and D. Zeppenfeld, *Anomalous Higgs boson production and decay*, *Phys. Lett.* **B 318** (1993) 155 [hep-ph/9308347] [INSPIRE].

[24] G.J. Gounaris, J. Layssac, J.E. Paschalis and F.M. Renard, *Unitarity constraints for new physics induced by dim-6 operators*, *Z. Phys.* **C 66** (1995) 619 [hep-ph/9409260] [INSPIRE].

[25] S. Alam, S. Dawson and R. Szalapski, *Low-energy constraints on new physics revisited*, *Phys. Rev.* **D 57** (1998) 1577 [hep-ph/9706542] [INSPIRE].

[26] R. Barbieri and A. Strumia, *What is the limit on the Higgs mass?*, *Phys. Lett.* **B 462** (1999) 144 [hep-ph/9905281] [INSPIRE].

[27] V. Barger, T. Han, P. Langacker, B. McElrath and P. Zerwas, *Effects of genuine dimension-six Higgs operators*, *Phys. Rev.* **D 67** (2003) 115001 [hep-ph/0301097] [INSPIRE].

[28] G.F. Giudice, C. Grojean, A. Pomarol and R. Rattazzi, *The Strongly-Interacting Light Higgs*, *JHEP* **06** (2007) 045 [hep-ph/0703164] [INSPIRE].

[29] F. Bonnet, M.B. Gavela, T. Ota and W. Winter, *Anomalous Higgs couplings at the LHC and their theoretical interpretation*, *Phys. Rev.* **D 85** (2012) 035016 [arXiv:1105.5140] [INSPIRE].

[30] T. Corbett, O.J.P. Eboli, J. Gonzalez-Fraile and M.C. Gonzalez-Garcia, *Constraining anomalous Higgs interactions*, *Phys. Rev.* **D 86** (2012) 075013 [arXiv:1207.1344] [INSPIRE].

[31] R. Contino, M. Ghezzi, C. Grojean, M. Muhlleitner and M. Spira, *Effective Lagrangian for a light Higgs-like scalar*, *JHEP* **07** (2013) 035 [arXiv:1303.3876] [INSPIRE].

[32] W.-F. Chang, W.-P. Pan and F. Xu, *Effective gauge-Higgs operators analysis of new physics associated with the Higgs boson*, *Phys. Rev.* **D 88** (2013) 033004 [arXiv:1303.7035] [INSPIRE].

[33] J. Ellis, V. Sanz and T. You, *Associated Production Evidence against Higgs Impostors and Anomalous Couplings*, *Eur. Phys. J.* **C 73** (2013) 2507 [arXiv:1303.0208] [INSPIRE].

[34] T. Corbett, O.J.P. Éboli, J. Gonzalez-Fraile and M.C. Gonzalez-Garcia, *Determining Triple Gauge Boson Couplings from Higgs Data*, *Phys. Rev. Lett.* **111** (2013) 011801 [arXiv:1304.1151] [INSPIRE].

[35] A. Hayreter and G. Valencia, *Constraints on anomalous color dipole operators from Higgs boson production at the LHC*, *Phys. Rev.* **D 88** (2013) 034033 [arXiv:1304.6976] [INSPIRE].

[36] H. Mebane, N. Greiner, C. Zhang and S. Willenbrock, *Constraints on Electroweak Effective Operators at One Loop*, *Phys. Rev.* **D 88** (2013) 015028 [arXiv:1306.3380] [INSPIRE].

[37] M.B. Einhorn and J. Wudka, *The Bases of Effective Field Theories*, *Nucl. Phys.* **B 876** (2013) 556 [arXiv:1307.0478] [INSPIRE].

JHEP06(2015)028

[38] J. Elias-Miro, J.R. Espinosa, E. Masso and A. Pomarol, *Higgs windows to new physics through $D = 6$ operators: constraints and one-loop anomalous dimensions*, *JHEP* **11** (2013) 066 [arXiv:1308.1879] [INSPIRE].

[39] S. Banerjee, S. Mukhopadhyay and B. Mukhopadhyaya, *Higher dimensional operators and the LHC Higgs data: The role of modified kinematics*, *Phys. Rev.* **D 89** (2014) 053010 [arXiv:1308.4860] [INSPIRE].

[40] E. Boos, V. Bunichev, M. Dubinin and Y. Kurihara, *Higgs boson signal at complete tree level in the SM extension by dimension-six operators*, *Phys. Rev.* **D 89** (2014) 035001 [arXiv:1309.5410] [INSPIRE].

[41] B. Gripaios and D. Sutherland, *Searches for CP-violating dimension-6 electroweak gauge boson operators*, *Phys. Rev.* **D 89** (2014) 076004 [arXiv:1309.7822] [INSPIRE].

[42] A. Alloul, B. Fuks and V. Sanz, *Phenomenology of the Higgs Effective Lagrangian via FEYNRULES*, *JHEP* **04** (2014) 110 [arXiv:1310.5150] [INSPIRE].

[43] C.-Y. Chen, S. Dawson and C. Zhang, *Electroweak Effective Operators and Higgs Physics*, *Phys. Rev.* **D 89** (2014) 015016 [arXiv:1311.3107] [INSPIRE].

[44] M. Dahiya, S. Dutta and R. Islam, *Unitarizing VV Scattering in Light Higgs Scenarios*, arXiv:1311.4523 [INSPIRE].

[45] C. Grojean, E. Salvioni, M. Schlaffer and A. Weiler, *Very boosted Higgs in gluon fusion*, *JHEP* **05** (2014) 022 [arXiv:1312.3317] [INSPIRE].

[46] J. Bramante, A. Delgado and A. Martin, *Cornering a hyper Higgs boson: Angular kinematics for boosted Higgs bosons with top pairs*, *Phys. Rev.* **D 89** (2014) 093006 [arXiv:1402.5985] [INSPIRE].

[47] R.S. Gupta, A. Pomarol and F. Riva, *BSM Primary Effects*, *Phys. Rev.* **D 91** (2015) 035001 [arXiv:1405.0181] [INSPIRE].

[48] J.S. Gainer, J. Lykken, K.T. Matchev, S. Mrenna and M. Park, *Beyond Geolocating: Constraining Higher Dimensional Operators in $H \to 4\ell$ with Off-Shell Production and More*, *Phys. Rev.* **D 91** (2015) 035011 [arXiv:1403.4951] [INSPIRE].

[49] S. Bar-Shalom, A. Soni and J. Wudka, *EFT naturalness: an effective field theory analysis of Higgs naturalness*, arXiv:1405.2924 [INSPIRE].

[50] G. Amar et al., *Exploration of the tensor structure of the Higgs boson coupling to weak bosons in e^+ e^- collisions*, *JHEP* **02** (2015) 128 [arXiv:1405.3957] [INSPIRE].

[51] A. Azatov, C. Grojean, A. Paul and E. Salvioni, *Taming the off-shell Higgs boson*, *Zh. Eksp. Teor. Fiz.* **147** (2015) 410 [arXiv:1406.6338] [INSPIRE].

[52] E. Masso, *An Effective Guide to Beyond the Standard Model Physics*, *JHEP* **10** (2014) 128 [arXiv:1406.6376] [INSPIRE].

[53] A. Biekötter, A. Knochel, M. Krämer, D. Liu and F. Riva, *Vices and virtues of Higgs effective field theories at large energy*, *Phys. Rev.* **D 91** (2015) 055029 [arXiv:1406.7320] [INSPIRE].

[54] C. Englert and M. Spannowsky, *Effective Theories and Measurements at Colliders*, *Phys. Lett.* **B 740** (2015) 8 [arXiv:1408.5147] [INSPIRE].

[55] R. Alonso, E.E. Jenkins and A.V. Manohar, *Holomorphy without Supersymmetry in the Standard Model Effective Field Theory*, *Phys. Lett.* **B 739** (2014) 95 [arXiv:1409.0868] [INSPIRE].

JHEP06(2015)028

[56] R.M. Godbole, D.J. Miller, K.A. Mohan and C.D. White, *Jet substructure and probes of CP-violation in Vh production*, *JHEP* **04** (2015) 103 [arXiv:1409.5449] [INSPIRE].

[57] M. Trott, *On the consistent use of Constructed Observables*, *JHEP* **02** (2015) 046 [arXiv:1409.7605] [INSPIRE].

[58] F. Goertz, A. Papaefstathiou, L.L. Yang and J. Zurita, *Higgs boson pair production in the $D = 6$ extension of the SM*, *JHEP* **04** (2015) 167 [arXiv:1410.3471] [INSPIRE].

[59] L. Lehman, *Extending the Standard Model Effective Field Theory with the Complete Set of Dimension-7 Operators*, *Phys. Rev.* **D 90** (2014) 125023 [arXiv:1410.4193] [INSPIRE].

[60] C. Englert, Y. Soreq and M. Spannowsky, *Off-Shell Higgs Coupling Measurements in BSM scenarios*, arXiv:1410.5440 [INSPIRE].

[61] A. Devastato, F. Lizzi, C.V. Flores and D. Vassilevich, *Unification of coupling constants, dimension 6 operators and the spectral action*, *Int. J. Mod. Phys.* **A 30** (2015) 1550033 [arXiv:1410.6624] [INSPIRE].

[62] D. Ghosh and M. Wiebusch, *Dimension-six triple gluon operator in Higgs+jet observables*, *Phys. Rev.* **D 91** (2015) 031701 [arXiv:1411.2029] [INSPIRE].

[63] T. Corbett, O. Éboli and M. Gonzalez-Garcia, *Unitarity Constraints on Dimension-Six Operators*, *Phys. Rev.* **D 91** (2015) 035014 [arXiv:1411.5026] [INSPIRE].

[64] M. Gonzalez-Alonso, A. Greljo, G. Isidori and D. Marzocca, *Pseudo-observables in Higgs decays*, *Eur. Phys. J.* **C 75** (2015) 128 [arXiv:1412.6038] [INSPIRE].

[65] R. Edezhath, *Dimension-6 Operator Constraints from Boosted VBF Higgs*, arXiv:1501.00992 [INSPIRE].

[66] A. Eichhorn et al., *The Higgs Mass and the Scale of New Physics*, *JHEP* **04** (2015) 022 [arXiv:1501.02812] [INSPIRE].

[67] S. Dawson, I.M. Lewis and M. Zeng, *Usefulness of effective field theory for boosted Higgs production*, *Phys. Rev.* **D 91** (2015) 074012 [arXiv:1501.04103] [INSPIRE].

[68] A. Azatov, R. Contino, G. Panico and M. Son, *Effective field theory analysis of double Higgs production via gluon fusion*, arXiv:1502.00539 [INSPIRE].

[69] L. Berthier and M. Trott, *Towards consistent Electroweak Precision Data constraints in the SMEFT*, *JHEP* **05** (2015) 024 [arXiv:1502.02570] [INSPIRE].

[70] C. Bobeth and U. Haisch, *Anomalous triple gauge couplings from B-meson and kaon observables*, arXiv:1503.04829 [INSPIRE].

[71] T. Han, Z. Liu, Z. Qian and J. Sayre, *Improving Higgs coupling measurements through ZZ Fusion at the ILC*, arXiv:1504.01399 [INSPIRE].

[72] B. Henning, X. Lu and H. Murayama, *What do precision Higgs measurements buy us?*, arXiv:1404.1058 [INSPIRE].

[73] B. Henning, X. Lu and H. Murayama, *How to use the Standard Model effective field theory*, arXiv:1412.1837 [INSPIRE].

[74] N. Craig, M. Farina, M. McCullough and M. Perelstein, *Precision Higgsstrahlung as a Probe of New Physics*, *JHEP* **03** (2015) 146 [arXiv:1411.0676] [INSPIRE].

[75] M. Gorbahn, J.M. No and V. Sanz, *Benchmarks for Higgs Effective Theory: Extended Higgs Sectors*, arXiv:1502.07352 [INSPIRE].

JHEP06(2015)028

[76] S. Willenbrock and C. Zhang, *Effective Field Theory Beyond the Standard Model*, *Ann. Rev. Nucl. Part. Sci.* **64** (2014) 83 [arXiv:1401.0470] [INSPIRE].

[77] M.K. Gaillard, *The Effective One Loop Lagrangian With Derivative Couplings*, *Nucl. Phys.* **B 268** (1986) 669 [INSPIRE].

[78] O. Cheyette, *Effective Action for the Standard Model With Large Higgs Mass*, *Nucl. Phys.* **B 297** (1988) 183 [INSPIRE].

[79] J. Fan and M. Reece, *A New Look at Higgs Constraints on Stops*, *JHEP* **06** (2014) 031 [arXiv:1401.7671] [INSPIRE].

[80] J. Fan, M. Reece and L.-T. Wang, *Possible Futures of Electroweak Precision: ILC, FCC-ee and CEPC*, arXiv:1411.1054 [INSPIRE].

[81] J. Fan, M. Reece and L.-T. Wang, *Precision Natural SUSY at CEPC, FCC-ee and ILC*, arXiv:1412.3107 [INSPIRE].

[82] N. Haba, K. Kaneta, S. Matsumoto and T. Nabeshima, *A Simple Method of Calculating Effective Operators*, *Acta Phys. Polon.* **B 43** (2012) 405 [arXiv:1106.6106] [INSPIRE].

[83] TLEP Design Study Working Group collaboration, M. Bicer et al., *First Look at the Physics Case of TLEP*, *JHEP* **01** (2014) 164 [arXiv:1308.6176] [INSPIRE].

[84] A. Drozd, J. Ellis, J. Quevillon and T. You, *niversal One Loop Effective Action for Dimension Six Operators*, work in preparation.

[85] A. Djouadi, *The Anatomy of electro-weak symmetry breaking. II. The Higgs bosons in the minimal supersymmetric model*, *Phys. Rept.* **459** (2008) 1 [hep-ph/0503173] [INSPIRE].

[86] A. Djouadi et al., *The post-Higgs MSSM scenario: Habemus MSSM?*, *Eur. Phys. J.* **C 73** (2013) 2650 [arXiv:1307.5205] [INSPIRE].

[87] A. Djouadi, L. Maiani, A. Polosa, J. Quevillon and V. Riquer, *Fully covering the MSSM Higgs sector at the LHC*, arXiv:1502.05653 [INSPIRE].

[88] J.R. Espinosa, C. Grojean, V. Sanz and M. Trott, *NSUSY fits*, *JHEP* **12** (2012) 077 [arXiv:1207.7355] [INSPIRE].

[89] T. Hahn, *Generating Feynman diagrams and amplitudes with FeynArts 3*, *Comput. Phys. Commun.* **140** (2001) 418 [hep-ph/0012260] [INSPIRE].

[90] C. Grojean, E.E. Jenkins, A.V. Manohar and M. Trott, *Renormalization Group Scaling of Higgs Operators and* $\Gamma(h \to \gamma\gamma)$, *JHEP* **04** (2013) 016 [arXiv:1301.2588] [INSPIRE].

[91] J. Elias-Miró, J.R. Espinosa, E. Masso and A. Pomarol, *Renormalization of dimension-six operators relevant for the Higgs decays* $h \to \gamma\gamma, \gamma Z$, *JHEP* **08** (2013) 033 [arXiv:1302.5661] [INSPIRE].

[92] J. Elias-Miro, J.R. Espinosa, E. Masso and A. Pomarol, *Higgs windows to new physics through* $d = 6$ *operators: constraints and one-loop anomalous dimensions*, *JHEP* **11** (2013) 066 [arXiv:1308.1879] [INSPIRE].

[93] E.E. Jenkins, A.V. Manohar and M. Trott, *Renormalization Group Evolution of the Standard Model Dimension Six Operators I: Formalism and lambda Dependence*, *JHEP* **10** (2013) 087 [arXiv:1308.2627] [INSPIRE].

[94] E.E. Jenkins, A.V. Manohar and M. Trott, *Renormalization Group Evolution of the Standard Model Dimension Six Operators II: Yukawa Dependence*, *JHEP* **01** (2014) 035 [arXiv:1310.4838] [INSPIRE].

JHEP06(2015)028

[95] R. Alonso, E.E. Jenkins, A.V. Manohar and M. Trott, *Renormalization Group Evolution of the Standard Model Dimension Six Operators III: Gauge Coupling Dependence and Phenomenology*, *JHEP* **04** (2014) 159 [arXiv:1312.2014] [INSPIRE].

[96] J. Elias-Miró, C. Grojean, R.S. Gupta and D. Marzocca, *Scaling and tuning of EW and Higgs observables*, *JHEP* **05** (2014) 019 [arXiv:1312.2928] [INSPIRE].

[97] R. Alonso, H.-M. Chang, E.E. Jenkins, A.V. Manohar and B. Shotwell, *Renormalization group evolution of dimension-six baryon number violating operators*, *Phys. Lett.* **B 734** (2014) 302 [arXiv:1405.0486] [INSPIRE].

[98] G. Degrassi, S. Heinemeyer, W. Hollik, P. Slavich and G. Weiglein, *Towards high precision predictions for the MSSM Higgs sector*, *Eur. Phys. J.* **C 28** (2003) 133 [hep-ph/0212020] [INSPIRE].

[99] S. Heinemeyer, W. Hollik and G. Weiglein, *The Masses of the neutral CP-even Higgs bosons in the MSSM: Accurate analysis at the two loop level*, *Eur. Phys. J.* **C 9** (1999) 343 [hep-ph/9812472] [INSPIRE].

[100] S. Heinemeyer, W. Hollik and G. Weiglein, *FeynHiggs: A Program for the calculation of the masses of the neutral CP even Higgs bosons in the MSSM*, *Comput. Phys. Commun.* **124** (2000) 76 [hep-ph/9812320] [INSPIRE].

[101] M. Frank et al., *The Higgs Boson Masses and Mixings of the Complex MSSM in the Feynman-Diagrammatic Approach*, *JHEP* **02** (2007) 047 [hep-ph/0611326] [INSPIRE].

[102] http://www.feynhiggs.de.

[103] MasterCode collaboration, K.J. de Vries et al., , KCL-PH-TH/2015-15, LCTS/2015-07, CERN-PH-TH/2015-066 [arXiv:1504.03260] [INSPIRE].

[104] M.E. Peskin and T. Takeuchi, *A New constraint on a strongly interacting Higgs sector*, *Phys. Rev. Lett.* **65** (1990) 964 [INSPIRE].

[105] M.E. Peskin and T. Takeuchi, *Estimation of oblique electroweak corrections*, *Phys. Rev.* **D 46** (1992) 381 [INSPIRE].

[106] G. Altarelli and R. Barbieri, *Vacuum polarization effects of new physics on electroweak processes*, *Phys. Lett.* **B 253** (1991) 161 [INSPIRE].

[107] G. Altarelli, R. Barbieri and S. Jadach, *Toward a model independent analysis of electroweak data*, *Nucl. Phys.* **B 369** (1992) 3 [*Erratum ibid.* **B 376** (1992) 444] [INSPIRE].

[108] TLEP Design Study Working Group collaboration, M. Bicer et al., *First Look at the Physics Case of TLEP*, *JHEP* **01** (2014) 164 [arXiv:1308.6176] [INSPIRE].

[109] A. Blondel, *Search for heavy right handed neutrinos at circular e^+e^- colliders*, at *Exploring the Physics Frontier with Circular Colliders*, Aspen Colorado U.S.A., 31 January 2015, http://indico.cern.ch/event/336571/other-view?view=standard.

[110] A. Freitas et al., *Exploring Quantum Physics at the ILC*, arXiv:1307.3962 [INSPIRE].

[111] D.M. Asner et al., *ILC Higgs White Paper*, arXiv:1310.0763 [INSPIRE].

[112] S. Mishima, *Sensitivity to new physics from TLEP precision measurements*, at *6th TLEP workshop*, CERN, Geneva Switzerland, 16 October 2013, http://indico.cern.ch/event/257713/session/1/contribution/30.

JHEP06(2015)028

7 Conclusion

The Standard Model of particle physics is the frontier of our current experimental understanding of the fundamentals underlying the universe. The theory has been remarkably successful in predicting every outcome of measurements designed to test it. Following the direct discovery of each elementary particle of the Standard Model, precise measurements of their interactions have stood in quantitative agreement with calculations, and the Higgs boson is so far no exception.

The discovery of a Higgs boson was announced on July 2012 and the task was then to characterise its properties. We analysed its couplings within the framework of a non-linear effective Lagrangian, placing limits on non-standard Higgs sectors and proposing a test of its defining characteristic as a scalar whose coupling strength is proportional to mass. We pointed out that the associated production channel of the Higgs is a particularly sensitive way of gaining information about its spin-parity property or other new physics that modify the Lorentz structure of its interactions.

The Higgs boson completes the set of fundamental particles in the Standard Model and the absence of other BSM resonances motivates the assumption that new physics may be decoupled at higher energies. The Standard Model is then considered as an effective field theory supplemented by higher-dimensional operators whose effects on observables constrains the UV cut-off scale. We bounded the operator coefficients using electroweak precision tests, Higgs physics and triple-gauge couplings, emphasising the complementarity between the different measurements.

The Wilson coefficients of the Standard Model effective field theory (SM EFT) may be elegantly calculated at one-loop using path integral methods. We showed how the covariant derivative method can yield a universal result for the specific case of operators contributing to the Higgs-gluon-gluon and Higgs-photon-photon couplings under more general assumptions than previously assumed. This is demonstrated in the case of stop squarks in the MSSM. We placed limits on the lightest stop mass from the corresponding SM EFT constraint. We also investigated the potential prospects for improvements from more precise measurements at future colliders.

Until the clear discovery of new BSM particles or interactions the SM EFT will represent the boundary of our microscopic knowledge of the world as supported by exper-

imental data. It is also the point at which we transition to a purely theoretical understanding of what we expect to lie beyond based on empirical evidence or arguments such as naturalness or aesthetics. We therefore advocate fully exploring this phenomenological framework from both a top-down and bottom-up perspective. Even when the decoupling assumption breaks down and the EFT is no longer valid we have a self-consistent way of saying where this happens, so that constraints must instead be placed on non-decoupled hidden particles until the sensitivity of the relevant measurements are improved.

As Run 2 of the LHC gets under way anticipation is high that new BSM particles may yet be found. The high-luminosity phase of the LHC and future colliders can also probe higher energy scales and see indirect signs of new physics by improving precision measurements. The naturalness problem will be seriously challenged as we fully explore the Higgs sector and go beyond the weak scale. Before us lies the exciting prospect of answering decades-old questions about the nature of electroweak symmetry breaking.